Characterization of iron acquisition catalyzed by Fiu

by

Taihao Yang

B.S., Dalian Medical University, 2014
M.S., Emporia State University, 2016

AN ABSTRACT OF A DISSERTATION

submitted in partial fulfillment of the requirements for the degree

DOCTOR OF PHILOSOPHY

Biochemistry and Molecular Biophysics Graduate Group

KANSAS STATE UNIVERSITY

Manhattan, Kansas

2022

Abstract

Under iron deficient conditions, Gram-negative bacteria like *Escherichia coli* secrete enterobactin, a catecholate siderophore that complexes and solubilizes iron in the extracellular environment. Ferric enterobactin (FeEnt) is the most avid natural or synthetic iron complex. It may be glucosylated (FeGEnt), and it is subject to chemical degradation and oxidation (FeEnt*). *E. coli* Fiu is an outer membrane protein that transports monomeric catecholate iron complexes. Using siderophore nutrition tests and radioisotope accumulation experiments, we found that Fiu preferentially recognized and transported FeEnt*. To further analyze the specificity of Fiu-mediated FeEnt* uptake, we engineered fluorescent sensors by creating Cys substitutions in the external loops of Fiu and labeled them with fluorescein maleimide. Upon binding of ferric siderophores, the surface loops of siderophore receptors undergo conformational motion that may quench attached fluorophores, allowing quantitative determinations of affinity and specificity. We screened potential ligands for Fiu and determined its binding affinities to the ferric catecholates FeEnt*, FeEnt, FeGEnt, FeDHBA, FeDHBS, and two siderophore antibiotics FeFDC and FeMB-1. To gain more insight into these binding reactions we performed computational docking experiments and molecular dynamic (MD) simulations with Fiu. The modeling studies found two potential binding sites for FeEnt* and identified residues that might participate in interactions with the iron complex. We tested these predictions by site-directed alanine scanning mutagenesis. Ala substitutions at F105, E108, D124, R142 and K739 impaired ligand binding. FeEnt* uptake by those mutants was reduced or abolished in siderophore nutrition tests. In summary, Fiu manifests specificity for the degradation products of FeEnt, but also recognizes FeEnt, FeGEnt, FeDHBS, FeDHBA,, FeFDC and Fe MB-1, confirming its importance in Gram-negative bacterial iron acquisition systems that function in colonization or

pathogenesis of humans and animals. Insight into the binding and transport mechanisms of Fiu is essential to the understanding of next-generation antibiotics targeting TonB-dependent receptors like Fiu, including the recently licensed compound cefidericol (FeTroja).

Characterization of iron acquisition catalyzed by Fiu

by

Taihao Yang

B.S., Dalian Medical University, 2014
M.S., Emporia State University, 2016

A DISSERTATION

submitted in partial fulfillment of the requirements for the degree

DOCTOR OF PHILOSOPHY

Biochemistry and Molecular Biophysics Graduate Group

KANSAS STATE UNIVERSITY

Manhattan, Kansas

2022

Approved by:

Major Professor

Dr. Phillip Klebba

Copyright

© Taihao Yang

Abstract

Under iron deficient conditions, Gram-negative bacteria like *Escherichia coli* secrete enterobactin, a catecholate siderophore that complexes and solubilizes iron in the extracellular environment. Ferric enterobactin (FeEnt) is the most avid natural or synthetic iron complex. It may be glucosylated (FeGEnt), and it is subject to chemical degradation and oxidation (FeEnt*). *E. coli* Fiu is an outer membrane protein that transports monomeric catecholate iron complexes. Using siderophore nutrition tests and radioisotope accumulation experiments, we found that Fiu preferentially recognized and transported FeEnt*. To further analyze the specificity of Fiu-mediated FeEnt* uptake, we engineered fluorescent sensors by creating Cys substitutions in the external loops of Fiu and labeled them with fluorescein maleimide. Upon binding ferric siderophores, the surface loops of siderophore receptors undergo conformational motion that may quench attached fluorophores, allowing quantitative determinations of affinity and specificity. We screened potential ligands for Fiu and determined its binding affinities for the ferric catecholates FeEnt*, FeEnt, FeGEnt, FeDHBA, FeDHBS, and two siderophore antibiotics FeFDC and FeMB-1. To gain more insight into these binding reactions we performed computational docking experiments and molecular dynamic (MD) simulations with Fiu. The modeling studies found two potential binding sites for FeEnt* and identified residues that might participate in interactions with the iron complex. We tested these predictions by site-directed alanine scanning mutagenesis. Ala substitutions at F105, E108, D124, R142 and K739 impaired ligand binding. FeEnt* uptake by those mutants was reduced or abolished in siderophore nutrition tests. In summary, Fiu manifests specificity for the degradation products of FeEnt, but also recognizes FeEnt, FeGEnt, FeDHBS, FeDHBA,, FeFDC and Fe MB-1, confirming its importance in Gram-negative bacterial iron acquisition systems that function in colonization or

pathogenesis of humans and animals. Insight into the binding and transport mechanisms of Fiu is essential to the understanding of next-generation antibiotics targeting TonB-dependent receptors like Fiu, including the recently licensed compound cefidericol (FeTroja).

Table of Contents

List of Figures x
List of Tables xi
Acknowledgements xii
Dedication xiv
Chapter 1 Introduction 1
Bacterial Infections 1
Iron and Siderophore 2
TonB-Dependent Iron Transport 6
Iron Acquisition in *Y. pestis* 9
Reference 13
Chapter 2 Experimental Approaches 20
Bacterial Strains and Plasmids 20
Site-Directed Mutagenesis 20
Culture Conditions 20
Purification of Siderophores 21
Siderophore Nutrition Tests 21
Preparation of OM Fractions 22
Site-Directed Fluorescence Labeling with FM 22
SDS-PAGE Electrophoresis 23
Radioisotopic Ferric Siderophore Transport Assays 23
Fluorescence Determinations of Ligand Binding 23
In silico Docking and Molecular Dynamics Simulation 24
Reference 27
Chapter 3 Characterization of Iron Acquisition Catalyzed by Fiu 29
Introduction 29
Results 31
Characterization of FeEnt-Related Catechols 31
Screening of Catecholate Ligands for Fiu 37
Fluorescent Determination of Binding Affinity 42

Determination of Binding Sites by *in silico* Docking and MD Simulation 49
Analysis of Binding Sites by Site-directed Mutagenesis 57
Discussion 65
Reference 71
Supplementary Materials 77
Chapter 4 Fluorescent Sensors of Siderophores Produced by Bacterial Pathogens 79
Introduction 79
Results 80
Engineering of Decoy Sensors for Siderophores 80
Binding Promiscuity of LGPs 81
Exclusivity of LGP binding 92
Measurement of Ferric Siderophores in Samples 96
Measurement of Siderophore Transport 100
Discussion 103
Reference 106
Supplementary Materials 115
Chapter 5 Other Studies 119
Universal fluorescent sensors of high-affinity iron transport, applied to ESKAPE pathogens 119
Conformational rearrangements in the N-domain of *Escherichia coli* FepA during ferric enterobactin transport 122
Reference 125
Appendix A – Copyright Permissions 126
Appendix B – Published Studies 128

List of Figures

Figure 1-1 TonB-dependent iron transport pathway in Gram-negative bacteria. 8
Figure 3-1 Characterization of Ferric Siderophores 36
Figure 3-2 Characterization of siderophore transport by siderophore nutrition test. 39
Figure 3-3 [^{59}Fe] siderophore accumulation assay 41
Figure 3-4 Fluorescence quenching assay for affinity determination. 45
Figure 3-5 Determination of binding affinities by fluorescence quenching assay. 48
Figure 3-6 Molecular docking and molecular dynamic (MD) simulation. 56
Figure 3-7 Characterization of ligand binding and transport by site-directed mutagenesis. 64
Figure 3-8 Superimposed structure of two ligand binding models. 70
Figure 4-1 Ligand recognition by Fluorescent EcoFiu Sensor. 87
Figure 4-2 Ligand recognition by Fluorescent EcoCir Sensor. 89
Figure 4-3 Ligand recognition by Fluorescent AbaPirA Sensor. 91
Figure 4-4 Ligand recognition by Fluorescent PaeFpvA Sensor. 94
Figure 4-5 Ligand recognition by Fluorescent KpnFyuA Sensor. 95
Figure 4-6 Determination of siderophore in culture supernatants by fluorescent sensor. 99
Figure 4-7 Transport Assay by fluorescent decoy sensor. 102
Figure 5-1 Elution profile of ferric siderophores by Sephadex DE52 anion chromatography. .. 121
Figure 5-2 Siderophore nutrition test in the presence or absence of βME 124

List of Tables

Table 1-1 Structure of siderophore and siderophore antibiotics 5
Table 2-1 List of bacterial strains 26
Table 3-1 Siderophore nutrition test with catecholate siderophores. 40
Table 3-2 Binding Affinity of Fiu Mutants to FeEnt* (μM) 60
Table 3-3 Siderophore nutrition test of Fiu mutants with FeEnt* 61
Table 4-1 Binding affinities of LGP sensors for apo or ferric siderophores 84

Acknowledgements

I would like to express my deepest appreciation to my major advisor Dr. Phillip Klebba and Dr. Salete Newton for their support, encouragement, and suggestions during my Ph. D study at K-state. I learned not only scientific skills but also a positive life attitude from them. Dr. Klebba always came up with great ideas to solve complicated problems in both research and in real life. He can also fix a variety of instruments all by himself just like playing magic. In addition to science, Sally is also an expert in baking. I will never forget her amazing cookies every Monday and birthday biscuits or cakes every year. I am also thankful to my committee members Dr. Michael Kanost, who always responded quickly to my question or appointment; Dr. Ho Ng, who provided generous help and suggestions on simulation experiment and job application; and Dr. Katsura Asano, who shared a lot of great insights into the structure analysis of protein and RNA.

I would like to thank our previous lab member and my good friend Dr. Ashish Kumar, and my teaching partner Dr. Lynn Schrag. I will never forget their help and encouragement in the teaching lab in the first year of my Ph. D life. I also want to thank our previous lab members Dr. Somnath Chakravorty, Dr. Yan Shipelskiy and Dr. Aritri Majumdar for their help and supervision on research and experimental skills. I want to thank Susan Whitaker for her help with the mass spectrometry.

I would like to thank my good friend Ye Zou and Yu song. Ye gave me solid support in MD simulation of Fiu project, which brought this project to another level. She is always willing to help people whenever she can. Yu is a great basketball teammate with a tough defense, which pushed me to improve my offense skills all the time. We three stayed together and had a happy time every holiday in the last five years and we encouraged and helped each other during the

hard time. I would also want to thank Miao Li for her friendship, help and encouragement. She had such great cooking skills and made a lot of delicious dishes during holiday parties. I am extremely grateful to Qi Jiang, who was always staying around whenever I am happy or sad, up and down in the last ten years.

Dedication

I dedicate this dissertation to my mother Lianhua Quan and my farther Wei Yang, who stand behind me all the time with their unconditional love. It is my fortune to be born in this family.

Chapter 1 Introduction

Bacterial Infections

Bacterial infections are a threat to human health, with historical documented pandemics such as Plague of Athens in 430 B.C.E, Bubonic Plagues from 541 to 750 C.E, and the Black Death from1346 to 136, etc. All these bacteria-caused pandemics resulted in hundreds of millions deaths over the word. (1,2) Bacterial infectious is still one of the leading causes of mortality in the 21st century with antibiotic-resistant pathogens as the emerging threat. Gram-negative pathogens, especially carbapenem-resistant *Enterobacterales* (CRE) (3-5) and the group of *Enterococcus*, *Staphylococcus*, *Klebsiella*, *Acinetobacter*, *Pseudomonas*, and *Enterobacter* (ESKAPE) (6,7) pathogens, caused two thirds of bacteria-associated death in U.S. (8) In 2019, CDC released "Antibiotics Resistance Threat in United States ", which reported over 2.8 million infections caused by CRE/ESKAPE and other antibiotic- resistant pathogens each year, with over 35000 deaths in U.S. (9) The report suggested over 223,900 cases and 12,800 deaths from *Clostridioides difficile*. Mutations that alter the selective permeability of cell membrane make those pathogens resistant to novel antibiotics (10-12) by occluding or actively exporting antibiotics. (13,14) Multidrug-resistant pathogens, including CRE/ESKAPE members and other Gram-negative bacteria, have been identified as urgent threat (*Enterobacterales, Neisseria gonorrhoeae, Acinetobacter*) or serious threat (*Staphylococcus, Enterococcus, Enterobacterales, Pseudomonas, Salmonella, Shigella, Campylobacter*) by CDC. (9) Development of new antibiotics has been an urgent need. Iron acquisition is tightly associated with bacterial pathogenesis and infections. (15-18) Thus, understanding how TonB-dependent receptors bind and capture siderophore ligands is essential to develop new antibiotics targeting iron acquisition system of Gram-negative pathogens.

Iron and Siderophore

Iron is an essential element for both prokaryotic and eukaryotic organisms, playing a central role in various metabolic pathways. Over 100 enzymes require iron-containing co-factors to function properly in the processes of primary and secondary metabolisms, including Krebs cycle (succinate dehydrogenase and aconitase), electron transport chain (proton-pumping oxidoreductases), de novo DNA synthesis (class Ia ribonucleotide reductases), gene expression involved in protection of reactive oxygen species and iron acquisition. (19-21) The most physically relevant iron species are ferrous iron Fe [II] and ferric iron Fe [III], which can be acquired through cellular uptake. As a soluble iron species, Fe [II] can be transported into cells through metal uptake transporters. Fe [II] is converted into Fe [III] through spontaneous oxidation or enzyme-catalyzed oxidation, in the form of $Fe_2O_3 \cdot nH_2O$ at neutral to basic pH, and thus restricted the concentration of free Fe [III] in aqueous solution to $10^{-9} \sim 10^{-18}$ M. (22) Mammalian hosts further limit the concentration of free iron by producing various iron binding proteins including ferritin, hemoglobin, transferrin, lactoferrin and hemoglobin. Hemoglobin and ferritin, two iron storage proteins, store about 90% of body iron. Transferrin, the iron transport protein in plasma, and lactoferrin, the innate defense protein in body fluids, bind and carry the circulating exchangeable iron. In the presence of those iron binding proteins, the concentration of serum iron is restricted to about to about 10^{-24} M (23-25) , making iron acquisition a determinant for the infection of pathogenic bacteria.

Pathogens acquire iron from hosts by developing both direct and indirect mechanisms. Direct uptake of iron sources like transferrin, ferritin, heme and lactoferrin requires the development of specific receptors, which limits the iron acquisition upon composition changes on those iron sources. (22) The indirect strategies were found to be more broadly applied by

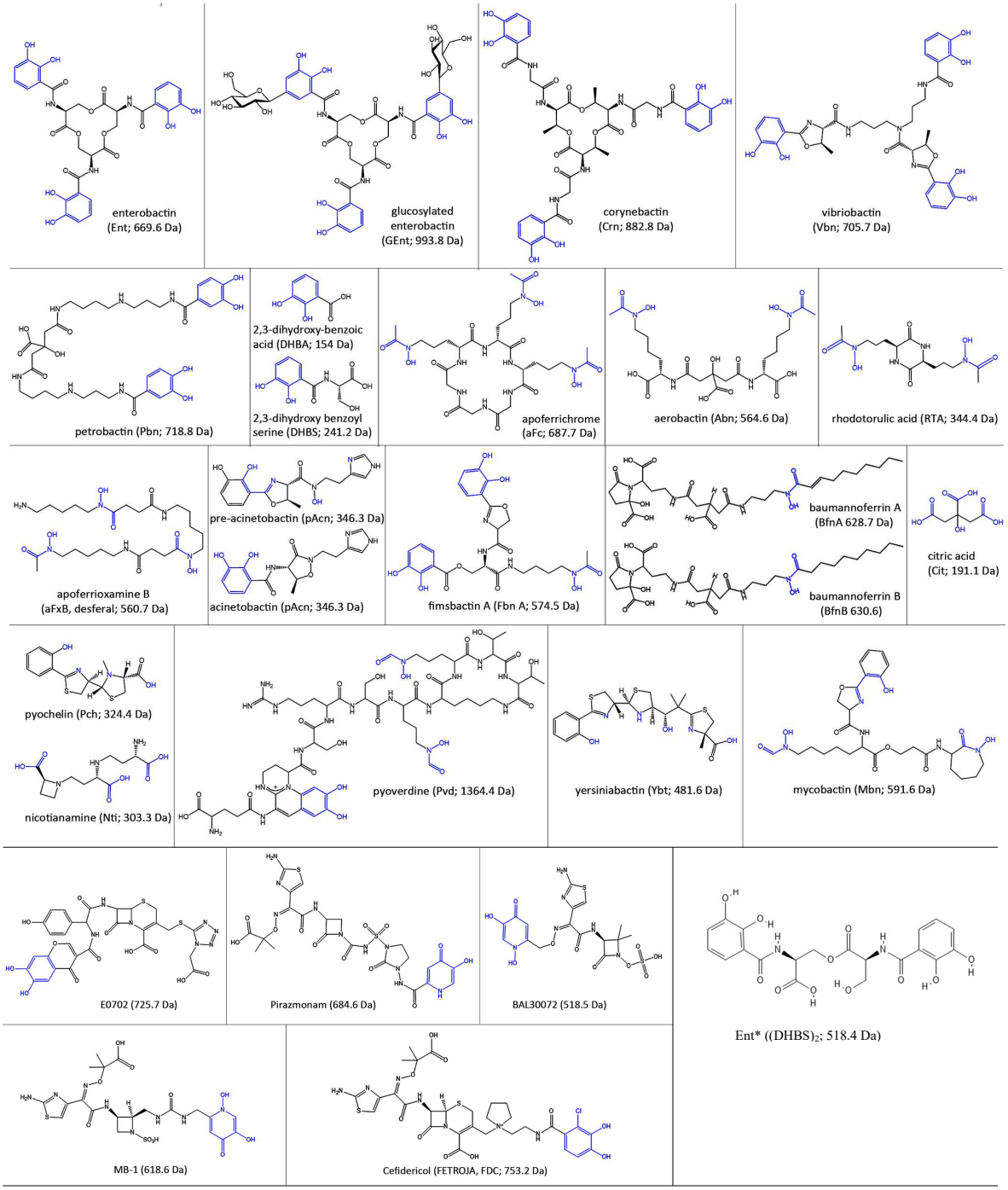
pathogens, especially Gram-negative bacteria. Under iron deficient conditions, Gram-negative bacteria secrete small organic molecules with a molecular weight lower than 1 kD, siderophores, to complex and solubilize Fe [III] in the solution with extremely high binding affinity (~10^{52} M^{-1} for enterobactin). (26-29) The ferric siderophore is then captured and internalized into cells through the action of particular outer membrane receptors.

More than 500 siderophores were found and characterized. They can be divided into three main categories: catecholate, hydroxamate, and mixed types. (Table 1-1) (27-31) Enterobactin and ferrichrome are prototypic catecholate and hydroxamate siderophores, respectively. Enterobactin (Ent) is usually produced by the Gram-negative Enterobacterales family, consisting of three 2,3-dihydroxybezoyl serine molecules connected by ester linkages. Spontaneous chemical decay of enterobactin, the hydrolysis of the cyclic lactone backbone and the oxidation of catecholate to quinones, produces natural degradation products including monomer, dimer, and linearized trimer of catecholate siderophores. (32) In addition, enterobactin could be modified to produce glucosylated enterobactin by adding glucose groups to two of catechol groups. Glucosylated enterobactin is secreted and utilized by *Salmonella* and pathogenic *E. coli* strains and is critical for those pathogens to escape from the host immune system. (33-35) Other catecholate siderophores include monomeric siderophores dihydroxybenzyl serine (DHBS) and dihydroxybenzoic acid (DHBA), corynebactin (Crn) (36), and virbriobactin (37) .

Ferric ion is a hard Lewis acid and favors the formation of hexacoordinated $Fe(H_2O)_6^{3+}$ complex with octahedral geometry in aqueous solution. (22) Ferric ion was found to be complexed by ligand oxygen favorably over sulfur or nitrogen, regardless that siderophores with distinct characteristics have different binding affinities to ferric ion. (21) Upon iron complexation with siderophores, water molecules surrounding the ferric ion will be replaced by

six donor oxygen atoms of siderophore, and the process is driven by gain of entropy. Ent and GEnt contain three catechol groups, which chelate ferric ions in the center through the interaction with six donor oxygens. The stable hexacoordinated conformation explains why the chelate effect results in a much higher binding affinity than that of monomeric and dimeric catecholate siderophore. Trimer catecholate siderophore like ENT and GEnt also resist dissociation after forming complex with ferric iron. Complexation of ferric iron with monomeric catecholate siderophore like DHBA and DHBS requires three separate interactions with each monomeric molecule, and thus, form hexacoordinated complex. Once one monomer dissociates from the complex, it would be lost in the solution, and its position will be occupied by water molecules. (21) For trimeric siderophores like ENT and GEnt, iron complexation is achieved by the initial attachment of first catechol group, followed by attachment of the second and then the third catechol groups. If one catechol group dissociates from the complex, it will reattach to the ferric iron as long as other catechol groups remain attached. (21) These ensure the stabilization of ferric siderophore with ENT or GEnt, compared to that with DHBA, DHBS, and the dimeric degraded Ent (Ent*) (21)

Table 1-1 Structure of siderophore and siderophore antibiotics. (21)



TonB-Dependent Iron Transport

Gram-negative bacteria acquire ferric siderophore though a family of outer membrane receptors, known as TonB-dependent receptors (TBDT). (Figure 1-1) (38) Those surface receptors were also described as ligand-gated porin (LGP). (39-41) Ligand binding to LGP induces the activation of TonB, which then triggers a series of conformational changes in the LGP driven by electrochemical proton motive force (PMF). The conformational changes drive the internalization of bound ferric siderophore across the outer membrane into the periplasm. (42-44) All Gram-negative infectious bacteria acquire iron through TonB-dependent systems, making TonB an attractive target for drug development. The transport system includes multi-proteins that participate cooperatively in ligand recognition, signal transduction across the cell envelope, protein-protein interactions and conformational rearrangement drive by energy transmission, and active transport across OM and IM driven by both electrochemical proton motive force (PMF) and ATP hydrolysis, respectively. (22) The complete mechanism of iron transport through has not been fully illustrated, and further research is required for the development of antimicrobial treatment targeting TonB-dependent iron transport. (45-47)

The first crystal structure of a porin was resolved in 1990 by Weiss et al, then the crystal structure of EcoOmpF, EcoFepA, and EcoFhuA were reported. (48-52) Detailed crystal structures of another 18 LGPs were resolved since then. (22) All the TonB-dependent LGPs adopt 22-stranded transmembrane beta sheets, with a 150- amino acids globular domain in the center, which regulates the transport of molecules through the pore. The crystal structures are important to completely understand the mechanism of iron transport through these LGPs.

N-terminus of LGPs contains a conserved short sequence “TonB-box”, which is usually 7 ~11 residues in length. (3,53) TonB-box serves as the bridge in the signal transduction between

TonB energy transduction system and LGPs. Ligand binding to corresponding LGP is the molecular signal that induces a series of conformational changes in the loops. As a result, the position of TonB-box in the periplasm will be altered, favoring its interaction with TonB, which is anchored to the inner membrane (IM), The direct physical interaction between TonB C-terminal domain and TonB box has been experimentally demonstrated in several LGPs including FepA, BtuB, FecA,and FhuA, via designated disulfide cross link and site-directed mutagenesis in TonB box. (54-60) The activated TonB energy transduction system (TonB/ExbB/ExbD) in IM then transduces the energy derived from PMF in IM to LGP in OM, driving the transport of bound siderophore ligand across OM. (53,61,62) A rotational surveillance and energy transfer (ROSET) model and other evidence suggests that TonB transduces energy in a rotary motion, with the involvement of ExbB and ExbD, driven by the electrochemical gradient across the IM. (63-68) TonB-dependent transport allows the cellular accumulation of iron from hosts against concentration gradient, which is critical for bacterial pathogenesis. Thus, TonB-dependent transport system is considered a virulence factor of Gram-negative pathogens. (16,69-74)

Gram-negative bacteria encode different LGPs in OM for the acquisition of various iron sources. K-12 *E. coli* strains encode eight LGPs: FepA, CirA, and Fiu for ferric catecholate siderophores; (52,75,76) FhuA, FhuE, and IutA for ferric hydroxymate siderophore; (50,51,77,78) FecA for ferric citrate; (79) BtuB for cyanocobalamin (vitamin B12). (80) *P. aeruginosa* PAO1 strain encodes FyuA (termed Psn in *Y. pestis*), which mediate the transport of ferric yersiniabactin (FeYbt); FpvA and FptA in *P. aeruginosa* mediates the transport of ferric pyoverdine (FePvd) and ferric pyocheilin (FePch), respectively. (81-86)

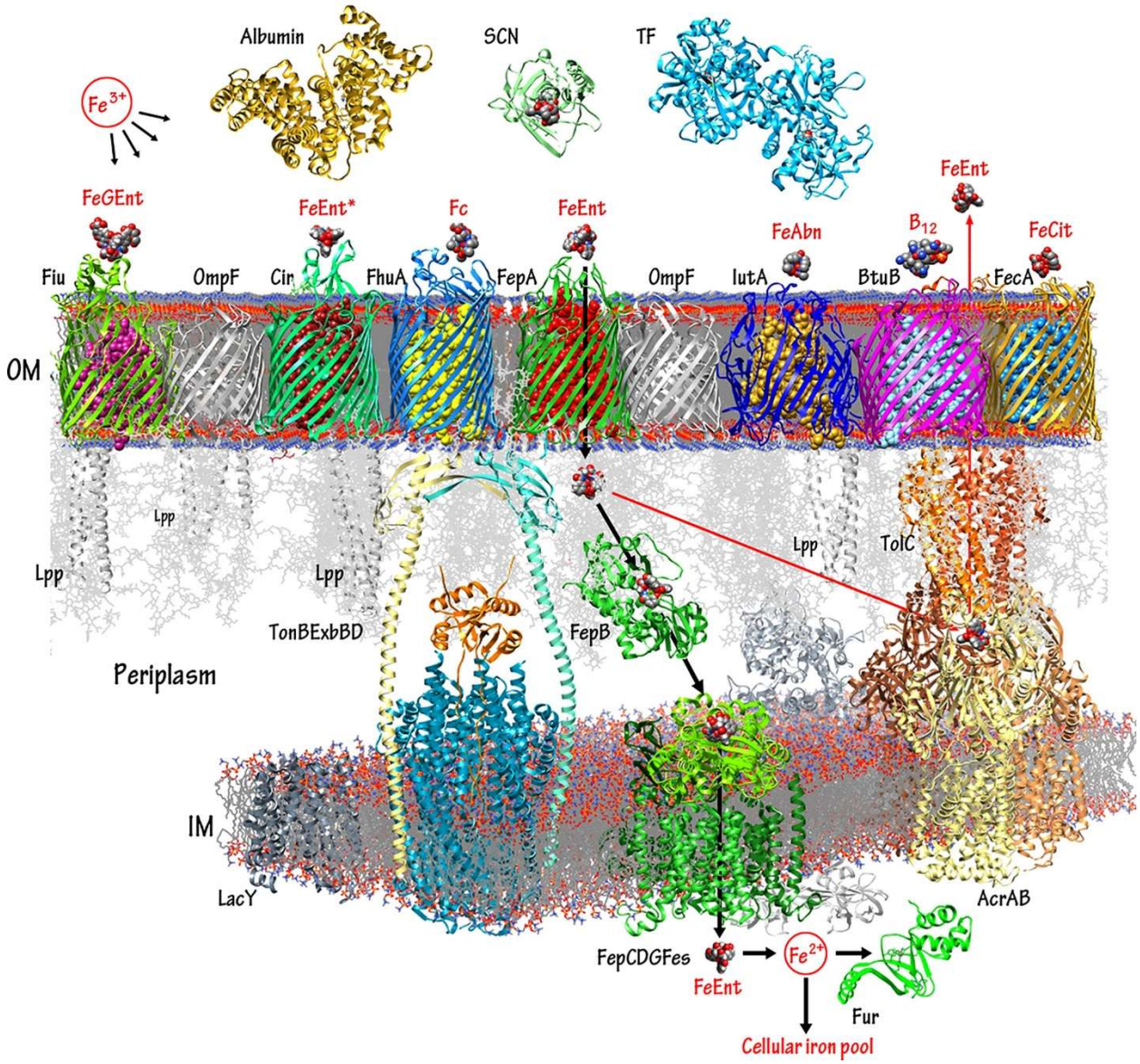


Figure 1-1 TonB-dependent iron transport pathway in Gram-negative bacteria.

TonB-dependent iron transport of selected OM receptor in *E. coli,* including FepA, Cir, Fiu, FhuA, IutA, BtuB and FecA. The transport of ferric siderophore across OM by these receptors depends on IM-anchored protein TonB for energization. (21)

Iron Acquisition in *Y. pestis*

Iron acquisition system in *Y. pestis* was reviewed in detail in *Klebba et al 2021*, as part of the publication.

Yersinia pestis is a Gram-negative pathogenic bacterium, which causes fatal diseases, including septicemic, bubonic, and pneumonic plague. (1,2,87,88) The ability of pathogens to infect hosts relies on the activation of various virulent pathways, some of which are essential for nutrient acquisition from mammalian host. Iron acquisition systems are important for intracellular growth and colonization of *Yersinia pestis*, and thus, is tightly related to its virulence. (43,89-91) Multiple iron-transport mechanisms and transporters have been characterized in *Yersinia pestis*, including siderophore dependent systems, ABC transporters, non-ABC transporters, as well as hemin transporters. *Yersinia* ironomic studies have identified 16 iron transport systems, while only Ybt siderophore-dependent system and Yfe iron-transport system were demonstrated to be essential for its virulence. (90,92-100)

Yersiniabactin (Ybt) TonB-dependent siderophore transport system is encoded on a high pathogenicity island termed *pgm,* including *psn* locus*, ybtPQXS* loci*,* and *irp12ybtUTE* loci. (101) The *pgm* locus is often deleted via genome recombination, generating the *pgm* deficient strain with attenuated virulence. (102-105) Yersiniabactin has a binding affinity of 4×10^{36} M^{-1} for Fe^{3+} and can remove iron from lactoferrin and transferrin. (88,106) The synthesis of Ybt requires HMWP proteins encoded by *irp* gene, and YbtU, YbtS, YbtT, YbtE proteins. (101) After Ybt is secreted to extracellular environment and acquires iron from the host, it is internalized into the bacterial cell via the outer membrane (OM) receptor Psn (termed FyuA in *E. coli*), and a permease-ATPase complex consisting of two inner membrane (IM) proteins YbtP and YbtQ.(107-109) YbtX is not required for iron uptake through Ybt system: YbtX deficient strain

did not show significant alteration on Ybt secretion as well as iron-deficient growth. But YbtX was found essential for Zn uptake via Ybt system. (109)

Ybt system is one of the virulence factors of *Y. pestis* for the early stage of bubonic plague progression: Ybt deficient strains, either Ybt biosynthetic or transport mutants are avirulent in mice model when inoculated subcutaneously but remain fully virulent when inoculated intravenously. (88,110) In pneumonic plague model, *irp*- strain (biosynthetic mutant) showed a greater loss of virulence than that of *psn*- strain (transport mutant), suggesting a signaling function of Ybt siderophore in the pathogenesis of pneumonic plague in addition to iron acquisition. (88,110) In a model proposed by Fetherston et al, Ybt could serve as a signal molecule that activates the transcription of regulated genes, probably other virulence factors, through Ybt/YbtA pathway in *Y.pestis*, but further work is required to elucidate the underlying mechanism. (88) Besides, *irp2* and *fyuA* are important to the virulence of *avian pathogenic E. coli*: knock-out of *irp2* and *fyuA* genes located on HPI led to a reduced cell adhesion, inhibited transcription of other virulence genes, and a reduced pathogenicity. (111)

The crystal structures of inner membrane protein YbtPQ of uropathogenic *E. coli* was determined recently using cryo-electron microscopy. (112) Known as an ABC importer, YbtPQ was surprisingly found to adopt a type IV exporter conformation. Besides, a transmembrane helix of YbtP unwinds upon releasing substrate. The nucleotide binding domain remains tightly packed even without nucleotide binding. These findings suggest a different transport mechanism of YbtPQ transporter to transport iron-complexed siderophore, which needs to be further investigated. (112)

FyuA (termed Psn in *Y. pestis*) is a TonB-dependent transporter, adopting a beta-barrel

conformation consisting of 22 beta strands. A hybrid toxin has been engineered to target FyuA and was able to kill pathogenic *E. coli* and *Yersinia*. This hybrid toxin consists of a FyuA binding domain from pesticin, and the N terminus of T4 lysozyme that degrades peptidoglycan of target pathogens. The hybrid toxin crosses the outer membrane, and remains unaffected by Pim, an inhibitor of peptidoglycan degrading enzyme secreted by some *Yersinia* pathogens. Using hybrid toxin or modified siderophore could be a potential method to specifically target pathogens expressing particular transporters that are associated with their virulence.(113)

Another iron acquisition system critical for the virulence of *Y. pestis* is Yfe system. Yfe loci are located on a 5.6 kb region of the *Y. pestis* genome, consisting of two different operons: *yfeABCD* and *yfeE* operon. *yfeABCD* operon encodes an ABC iron-transport system: YfeA, a periplasmic binding protein; YfeB, a ATP-binding protein; YfeC and YfeD, a heterodimeric IM permease. YfeE is not essential for iron transport via this system, its exact function has not been identified. Yfe system is TonB-independent, and no corresponding OM receptor was found. *yfeABCD* operon is regulated by iron and Fur, while *yfeE* operon is not.(94,96,106)

Yfe system plays a critical role in the pathogenesis of bubonic plague. (94,114) The ybt-yfe- mutant showed no virulence when inoculated intravenously in mice compared to ybt-yfe+ strain, suggesting that Yfe system is essential for its virulence during the latter stage. When inoculated subcutaneously, ybt+yfe- strains showed a reduced virulence compared to ybt+yfe+ strains, indicating that Yfe system participates in the early stage of bubonic plague progression, but is not essential. (94) Ybt system was not essential in the later stage but is essential for the virulence in the early stage of bubonic stage. Hence, Ybt and Yfe system may drive the progression of bubonic plague through different stages. (94,114,115)

In Yfe system, YfeA is the substrate binding protein (SBP), and its crystal structures under different conditions have been determined. (116) YfeA was classified as cluster A-1 SBP, which directly bound to metal ions like Zn, Mn, and Fe. Two metal binding sites in YfeA were characterized: Site 1 shows polyspecificity to Zn, Mn and Fe, and is able to alter its substrate binding specificity in response to different environmental conditions. Besides, YfeA bind metal ions tightly in site 1, as incubation with EDTA cannot remove metals ions from site 1 in the absence of its downstream metal-exchanging partners, suggesting conformational changes are required for the metal exchange. Site 2 was found only to bind Zn and Mn, but not Fe, its biological function remains to be determined. (117)

TonB-dependent system plays a central role for critical Gram-negative pathogens including CRE/ESKAPE strains, which allows the pathogens to acquire iron in the host to for bacterial growth and pathogenesis. Given the importance of iron and TonB-dependent iron acquisition system, OM receptors that mediate siderophore transport could be the potential targets for new antibiotics. Thus, it is important to understand the binding preference, specificity, and the mechanism behind of these TonB-dependent OM receptors.

Reference

1. Pollitzer, R. (1954) Plague. *Geneva: WHO*, 409-482
2. Perry, R. D., and Fetherston, J. D. (1997) Yersinia pestis--etiologic agent of plague. *Clinical microbiology reviews* 10, 35-66
3. Guterman, S., and Dann, L. (1973) Excretion of enterochelin by exbA and exbB mutants of Escherichia coli. *Journal of Bacteriology* 114, 1225-1230
4. Perez, F., and Van Duin, D. (2013) Carbapenem-resistant Enterobacteriaceae: a menace to our most vulnerable patients. *Cleveland Clinic journal of medicine* 80, 225
5. Smith, H. Z., and Kendall, B. (2021) Carbapenem Resistant Enterobacteriaceae. in *StatPearls [Internet]*, StatPearls Publishing. pp
6. Rice, L. B. (2008) Federal funding for the study of antimicrobial resistance in nosocomial pathogens: no ESKAPE. The University of Chicago Press
7. Boucher, H. W., Talbot, G. H., Bradley, J. S., Edwards, J. E., Gilbert, D., Rice, L. B., Scheld, M., Spellberg, B., and Bartlett, J. (2009) Bad bugs, no drugs: no ESKAPE! An update from the Infectious Diseases Society of America. *Clinical infectious diseases* 48, 1-12
8. Elemam, A., Rahimian, J., and Mandell, W. (2009) Infection with panresistant Klebsiella pneumoniae: a report of 2 cases and a brief review of the literature. *Clinical infectious diseases* 49, 271-274
9. Control, C. f. D., and Prevention. (2020) Antibiotic resistance threats in the United States. US Department of Health and Human Services., 2019.
10. Nikaido, H., and Vaara, M. (1985) Molecular basis of bacterial outer membrane permeability. *Microbiological reviews* 49, 1-32
11. Nikaido, H. (1998) Multiple antibiotic resistance and efflux. *Current opinion in microbiology* 1, 516-523
12. Nikaido, H. (2003) Molecular basis of bacterial outer membrane permeability revisited. *Microbiology and molecular biology reviews* 67, 593-656
13. Zgurskaya, H. I., and Nikaido, H. (1999) Bypassing the periplasm: reconstitution of the AcrAB multidrug efflux pump of Escherichia coli. *Proceedings of the National Academy of Sciences* 96, 7190-7195
14. Yu, E. W., McDermott, G., Zgurskaya, H. I., Nikaido, H., and Koshland Jr, D. E. (2003) Structural basis of multiple drug-binding capacity of the AcrB multidrug efflux pump. *Science* 300, 976-980
15. Griffiths, E., Rogers, H. J., and Bullen, J. (1980) Iron, plasmids and infection. *Nature* 284, 508-509
16. Bullen, J. (1981) The significance of iron in infection. *Reviews of infectious diseases* 3, 1127-1138
17. Bullen, J. (1985) Iron and infection. Springer
18. Bullen, J., Griffiths, E., Rogers, H., and Ward, G. (2000) Sepsis: the critical role of iron. *Microbes and infection* 2, 409-415
19. Klausner, R. D., Rouault, T. A., and Harford, J. B. (1993) Regulating the fate of mRNA: the control of cellular iron metabolism. *Cell* 72, 19-28
20. Hantke, K. (2001) Iron and metal regulation in bacteria. *Current opinion in microbiology* 4, 172-177

21. Klebba, P. E., Newton, S. M., Six, D. A., Kumar, A., Yang, T., Nairn, B. L., Munger, C., and Chakravorty, S. (2021) Iron acquisition systems of gram-negative bacterial pathogens define TonB-dependent pathways to novel antibiotics. *Chemical reviews* 121, 5193-5239
22. Miethke, M., and Marahiel, M. A. (2007) Siderophore-based iron acquisition and pathogen control. *Microbiology and molecular biology reviews* 71, 413-451
23. Anderson, C. P., Shen, M., Eisenstein, R. S., and Leibold, E. A. (2012) Mammalian iron metabolism and its control by iron regulatory proteins. *Biochimica et Biophysica Acta (BBA)-Molecular Cell Research* 1823, 1468-1483
24. Anderson, G. J., and Frazer, D. M. (2017) Current understanding of iron homeostasis. *The American journal of clinical nutrition* 106, 1559S-1566S
25. Cronin, S. J., Woolf, C. J., Weiss, G., and Penninger, J. M. (2019) The role of iron regulation in immunometabolism and immune-related disease. *Frontiers in molecular biosciences* 6, 116
26. Neilands, J. (1952) A crystalline organo-iron pigment from a rust fungus (Ustilago sphaerogena). *Journal of the American Chemical Society* 74, 4846-4847
27. Harris, W. R., Carrano, C. J., and Raymond, K. N. (1979) Spectrophotometric determination of the proton-dependent stability constant of ferric enterobactin. *Journal of the American Chemical Society* 101, 2213-2214
28. Neilands, J. B. (1981) Microbial iron compounds.
29. Neilands, J. (1995) Siderophores: structure and function of microbial iron transport compounds. *Journal of Biological Chemistry* 270, 26723-26726
30. Raymond, K. N., Dertz, E. A., and Kim, S. S. (2003) Enterobactin: an archetype for microbial iron transport. *Proceedings of the national academy of sciences* 100, 3584-3588
31. Hider, R. C., and Kong, X. (2010) Chemistry and biology of siderophores. *Natural product reports* 27, 637-657
32. Holden, V. I., Breen, P., Houle, S., Dozois, C. M., and Bachman, M. A. (2016) Klebsiella pneumoniae siderophores induce inflammation, bacterial dissemination, and HIF-1α stabilization during pneumonia. *MBio* 7, e01397-01316
33. Hantke, K., Nicholson, G., Rabsch, W., and Winkelmann, G. (2003) Salmochelins, siderophores of Salmonella enterica and uropathogenic Escherichia coli strains, are recognized by the outer membrane receptor IroN. *Proceedings of the National Academy of Sciences* 100, 3677-3682
34. Bister, B., Bischoff, D., Nicholson, G. J., Valdebenito, M., Schneider, K., Winkelmann, G., Hantke, K., and Süssmuth, R. D. (2004) The structure of salmochelins: C-glucosylated enterobactins of Salmonella enterica §. *Biometals* 17, 471-481
35. Valdebenito, M., Bister, B., Reissbrodt, R., Hantke, K., and Winkelmann, G. (2005) The detection of salmochelin and yersiniabactin in uropathogenic Escherichia coli strains by a novel hydrolysis-fluorescence-detection (HFD) method. *International journal of medical microbiology* 295, 99-107
36. May, J. r. J., Wendrich, T. M., and Marahiel, M. A. (2001) The dhb operon of bacillus subtilisEncodes the biosynthetic template for the catecholic siderophore 2, 3-dihydroxybenzoate-glycine-threonine trimeric ester bacillibactin. *Journal of Biological Chemistry* 276, 7209-7217
37. Griffiths, G., Sigel, S., Payne, S., and Neilands, J. (1984) Vibriobactin, a siderophore from Vibrio cholerae. *Journal of Biological Chemistry* 259, 383-385

38. Schauer, K., Rodionov, D. A., and de Reuse, H. (2008) New substrates for TonB-dependent transport: do we only see the 'tip of the iceberg'? *Trends in biochemical sciences* 33, 330-338
39. Moreira, C., Calixto, A. R., Richard, J. P., and Kamerlin, S. C. L. (2019) The role of ligand-gated conformational changes in enzyme catalysis. *Biochemical Society Transactions* 47, 1449-1460
40. Abbott, G. W. (2020) KCNQs: ligand-and voltage-gated potassium channels. *Frontiers in Physiology* 11, 583
41. Vetter, I., Carter, D., Bassett, J., Deuis, J. R., Tay, B., Jami, S., and Robinson, S. D. (2020) High-throughput fluorescence assays for ion channels and GPCRs. *Calcium Signaling*, 27-72
42. Cornelissen, C. N., and Sparling, P. F. (1994) Iron piracy: acquisition of transferrin-bound iron by bacterial pathogens. *Molecular microbiology* 14, 843-850
43. Guerinot, M. L. (1994) Microbial iron transport. *Annual review of microbiology* 48, 743-772
44. Cornelis, P. (2010) Iron uptake and metabolism in pseudomonads. *Applied microbiology and biotechnology* 86, 1637-1645
45. Anderson, J. E., Sparling, P. F., and Cornelissen, C. N. (1994) Gonococcal transferrin-binding protein 2 facilitates but is not essential for transferrin utilization. *Journal of bacteriology* 176, 3162-3170
46. Klebba, P. E. (2003) Three paradoxes of ferric enterobactin uptake. *Frontiers in Bioscience-Landmark* 8, 1422-1436
47. Klebba, P. E. (2004) Transport biochemistry of FepA. *Iron transport in bacteria*, 147-157
48. Weiss, M., Wacker, T., Weckesser, J., Weite, W., and Schulz, G. (1990) The three-dimensional structure of porin from Rhodobacter capsulatus at 3 Å resolution. *Febs letters* 267, 268-272
49. Cowan, S., Schirmer, T., Rummel, G., Steiert, M., Ghosh, R., Pauptit, R., Jansonius, J., and Rosenbusch, J. (1992) Crystal structures explain functional properties of two E. coli porins. *Nature* 358, 727-733
50. Ferguson, A. D., Hofmann, E., Coulton, J. W., Diederichs, K., and Welte, W. (1998) Siderophore-mediated iron transport: crystal structure of FhuA with bound lipopolysaccharide. *science* 282, 2215-2220
51. Locher, K. P., Rees, B., Koebnik, R., Mitschler, A., Moulinier, L., Rosenbusch, J. P., and Moras, D. (1998) Transmembrane signaling across the ligand-gated FhuA receptor: crystal structures of free and ferrichrome-bound states reveal allosteric changes. *Cell* 95, 771-778
52. Buchanan, S. K., Smith, B. S., Venkatramani, L., Xia, D., Esser, L., Palnitkar, M., Chakraborty, R., Van Der Helm, D., and Deisenhofer, J. (1999) Crystal structure of the outer membrane active transporter FepA from Escherichia coli. *Nature structural biology* 6, 56-63
53. Kadner, R. (1990) Vitamin B12 transport in Escherichia coli: energy coupling between membranes. *Molecular microbiology* 4, 2027-2033
54. Skare, J., Ahmer, B., Seachord, C., Darveau, R. P., and Postle, K. (1993) Energy transduction between membranes. TonB, a cytoplasmic membrane protein, can be chemically cross-linked in vivo to the outer membrane receptor FepA. *Journal of Biological Chemistry* 268, 16302-16308

55. Larsen, R. A., Foster-Hartnett, D., McIntosh, M. A., and Postle, K. (1997) Regions of Escherichia coli TonB and FepA proteins essential for in vivo physical interactions. *Journal of bacteriology* 179, 3213-3221
56. Moeck, G. S., Coulton, J. W., and Postle, K. (1997) Cell envelope signaling in Escherichia coli: Ligand binding to the ferrichrome-iron receptor FhuA promotes interaction with the energy-transducing protein TonB. *Journal of Biological Chemistry* 272, 28391-28397
57. Cadieux, N., and Kadner, R. J. (1999) Site-directed disulfide bonding reveals an interaction site between energy-coupling protein TonB and BtuB, the outer membrane cobalamin transporter. *Proceedings of the National Academy of Sciences* 96, 10673-10678
58. Moeck, G. S., and Letellier, L. (2001) Characterization of in vitro interactions between a truncated TonB protein from Escherichia coli and the outer membrane receptors FhuA and FepA. *Journal of Bacteriology* 183, 2755-2764
59. Pawelek, P. D., Croteau, N., Ng-Thow-Hing, C., Khursigara, C. M., Moiseeva, N., Allaire, M., and Coulton, J. W. (2006) Structure of TonB in complex with FhuA, E. coli outer membrane receptor. *Science* 312, 1399-1402
60. Shultis, D. D., Purdy, M. D., Banchs, C. N., and Wiener, M. C. (2006) Outer membrane active transport: structure of the BtuB: TonB complex. *Science* 312, 1396-1399
61. Postle, K. (1993) TonB protein and energy transduction between membranes. *Journal of bioenergetics and biomembranes* 25, 591-601
62. Larsen, R. A., Myers, P. S., Skare, J. T., Seachord, C. L., Darveau, R. P., and Postle, K. (1996) Identification of TonB homologs in the family Enterobacteriaceae and evidence for conservation of TonB-dependent energy transduction complexes. *Journal of bacteriology* 178, 1363-1373
63. Chang, C., Mooser, A., Plückthun, A., and Wlodawer, A. (2001) Crystal structure of the dimeric C-terminal domain of TonB reveals a novel fold. *Journal of biological chemistry* 276, 27535-27540
64. Zhai, Y. F., Heijne, W., and Saier Jr, M. H. (2003) Molecular modeling of the bacterial outer membrane receptor energizer, ExbBD/TonB, based on homology with the flagellar motor, MotAB. *Biochimica et Biophysica Acta (BBA)-Biomembranes* 1614, 201-210
65. Kaserer, W. A., Jiang, X., Xiao, Q., Scott, D. C., Bauler, M., Copeland, D., Newton, S. M., and Klebba, P. E. (2008) Insight from TonB hybrid proteins into the mechanism of iron transport through the outer membrane. *Journal of Bacteriology* 190, 4001-4016
66. Ollis, A. A., Manning, M., Held, K. G., and Postle, K. (2009) Cytoplasmic membrane protonmotive force energizes periplasmic interactions between ExbD and TonB. *Molecular microbiology* 73, 466-481
67. Jordan, L. D., Zhou, Y., Smallwood, C. R., Lill, Y., Ritchie, K., Yip, W. T., Newton, S. M., and Klebba, P. E. (2013) Energy-dependent motion of TonB in the Gram-negative bacterial inner membrane. *Proceedings of the National Academy of Sciences* 110, 11553-11558
68. Klebba, P. E. (2016) ROSET model of TonB action in Gram-negative bacterial iron acquisition. *Journal of bacteriology* 198, 1013-1021
69. Wang, C. C., and Newton, A. (1969) Iron transport in Escherichia coli: relationship between chromium sensitivity and high iron requirement in mutants of Escherichia coli. *Journal of Bacteriology* 98, 1135-1141
70. Wang, C., and Newton, A. (1971) An additional step in the transport of iron defined by the tonB locus of Escherichia coli. *Journal of Biological Chemistry* 246, 2147-2151

71. Bullen, J. (1974) Proceedings: iron and infection. *British journal of haematology* 28, 139-140
72. Bradbeer, C., and Woodrow, M. L. (1976) Transport of vitamin B12 in Escherichia coli: energy dependence. *Journal of Bacteriology* 128, 99-104
73. Bullen, J., Rogers, H. J., and Griffiths, E. (1978) Role of iron in bacterial infection. *Current topics in microbiology and immunology*, 1-35
74. Newton, S. M., Trinh, V., Pi, H., and Klebba, P. E. (2010) Direct measurements of the outer membrane stage of ferric enterobactin transport: postuptake binding. *Journal of Biological Chemistry* 285, 17488-17497
75. Nikaido, H., and Rosenberg, E. Y. (1990) Cir and Fiu proteins in the outer membrane of Escherichia coli catalyze transport of monomeric catechols: study with beta-lactam antibiotics containing catechol and analogous groups. *Journal of bacteriology* 172, 1361-1367
76. Buchanan, S. K., Lukacik, P., Grizot, S., Ghirlando, R., Ali, M. M., Barnard, T. J., Jakes, K. S., Kienker, P. K., and Esser, L. (2007) Structure of colicin I receptor bound to the R-domain of colicin Ia: implications for protein import. *The EMBO journal* 26, 2594-2604
77. Bindereif, A., and Neilands, J. (1983) Cloning of the aerobactin-mediated iron assimilation system of plasmid ColV. *Journal of Bacteriology* 153, 1111-1113
78. Hantke, K. (1983) Identification of an iron uptake system specific for coprogen and rhodotorulic acid in Escherichia coli K12. *Molecular and General Genetics MGG* 191, 301-306
79. Ferguson, A. D., Chakraborty, R., Smith, B. S., Esser, L., Van Der Helm, D., and Deisenhofer, J. (2002) Structural basis of gating by the outer membrane transporter FecA. *Science* 295, 1715-1719
80. Chimento, D. P., Mohanty, A. K., Kadner, R. J., and Wiener, M. C. (2003) Substrate-induced transmembrane signaling in the cobalamin transporter BtuB. *Nature Structural & Molecular Biology* 10, 394-401
81. Elliott, R. (1958) Some properties of pyoverdine, the water-soluble fluorescent pigment of the pseudomonads. *Applied microbiology* 6, 241-246
82. Liu, P. V., and Shokrani, F. (1978) Biological activities of pyochelins: iron-chelating agents of Pseudomonas aeruginosa. *Infection and immunity* 22, 878-890
83. Cox, C. D. (1980) Iron uptake with ferripyochelin and ferric citrate by Pseudomonas aeruginosa. *Journal of bacteriology* 142, 581-587
84. Philson, S., and Llinas, M. (1982) Siderochromes from Pseudomonas fluorescens. I. Isolation and characterization. *Journal of Biological Chemistry* 257, 8081-8085
85. Cobessi, D., Celia, H., Folschweiller, N., Schalk, I. J., Abdallah, M. A., and Pattus, F. (2005) The crystal structure of the pyoverdine outer membrane receptor FpvA from Pseudomonas aeruginosa at 3.6 Å resolution. *Journal of molecular biology* 347, 121-134
86. Cobessi, D., Celia, H., and Pattus, F. (2005) Crystal structure at high resolution of ferric-pyochelin and its membrane receptor FptA from Pseudomonas aeruginosa. *Journal of molecular biology* 352, 893-904
87. Hinnebusch, B., and Erickson, D. (2008) Yersinia pestis biofilm in the flea vector and its role in the transmission of plague. in *Bacterial biofilms*, Springer. pp 229-248
88. Fetherston, J. D., Kirillina, O., Bobrov, A. G., Paulley, J. T., and Perry, R. D. (2010) The yersiniabactin transport system is critical for the pathogenesis of bubonic and pneumonic plague. *Infection and immunity* 78, 2045-2052

89. Mietzner, T. A., and Morse, S. A. (1994) The role of iron-binding proteins in the survival of pathogenic bacteria. *Annual review of nutrition* 14, 471-493
90. Crosa, J. H., Mey, A. R., and Payne, S. M. (2004) *Iron transport in bacteria*, ASM press Washington, DC
91. Payne, S. M., and Mey, A. R. (2004) Pathogenic Escherichia coli, Shigella, and Salmonella. *Iron transport in bacteria*, 197-218
92. Bearden, S. W., Fetherston, J. D., and Perry, R. D. (1997) Genetic organization of the yersiniabactin biosynthetic region and construction of avirulent mutants in Yersinia pestis. *Infection and immunity* 65, 1659-1668
93. Bearden, S. W., Staggs, T. M., and Perry, R. D. (1998) An ABC Transporter System of Yersinia pestis Allows Utilization of Chelated Iron by Escherichia coliSAB11. *Journal of bacteriology* 180, 1135-1147
94. Bearden, S. W., and Perry, R. D. (1999) The Yfe system of Yersinia pestis transports iron and manganese and is required for full virulence of plague. *Molecular microbiology* 32, 403-414
95. Gong, S., Bearden, S. W., Geoffroy, V. A., Fetherston, J. D., and Perry, R. D. (2001) Characterization of the Yersinia pestisYfu ABC Inorganic Iron Transport System. *Infection and immunity* 69, 2829-2837
96. Perry, R. D., Abney, J., Mier, I., Lee, Y., Bearden, S. W., and Fetherston, J. D. (2004) Regulation of the Yersinia pestis Yfe and Ybt iron transport systems. in *The Genus Yersinia*, Springer. pp 275-283
97. Kirillina, O., Bobrov, A. G., Fetherston, J. D., and Perry, R. D. (2006) Hierarchy of iron uptake systems: Yfu and Yiu are functional in Yersinia pestis. *Infection and immunity* 74, 6171-6178
98. Perry, R. D., Mier, I., and Fetherston, J. D. (2007) Roles of the Yfe and Feo transporters of Yersinia pestis in iron uptake and intracellular growth. *Biometals* 20, 699
99. Forman, S., Paulley, J. T., Fetherston, J. D., Cheng, Y.-Q., and Perry, R. D. (2010) Yersinia ironomics: comparison of iron transporters among Yersiniapestis biotypes and its nearest neighbor, Yersinia pseudotuberculosis. *Biometals* 23, 275-294
100. Pieper, R., Huang, S.-T., Parmar, P. P., Clark, D. J., Alami, H., Fleischmann, R. D., Perry, R. D., and Peterson, S. N. (2010) Proteomic analysis of iron acquisition, metabolic and regulatory responses of Yersinia pestis to iron starvation. *BMC microbiology* 10, 30
101. Perry, R., and Fetherston, J. (2004) Iron and heme uptake systems. *Yersinia Molecular and Cellular Biology*, 257-283
102. Iteman, I., Guiyoule, A., de Almeida, A., Guilvout, I., Baranton, G., and Carniel, E. (1993) Relationship between loss of pigmentation and deletion of the chromosomal iron-regulated irp2 gene in Yersinia pestis: evidence for separate but related events. *Infection and immunity* 61, 2717-2722
103. Carniel, E., Guilvout, I., and Prentice, M. (1996) Characterization of a large chromosomal" high-pathogenicity island" in biotype 1B Yersinia enterocolitica. *Journal of bacteriology* 178, 6743-6751
104. Rakin, A., Noelting, C., Schubert, S., and Heesemann, J. (1999) Common and specific characteristics of the high-pathogenicity island of Yersinia enterocolitica. *Infection and immunity* 67, 5265-5274

105. Lesic, B., and Carniel, E. (2004) The high pathogenicity island: a broad-host-range pathogenicity island. *Yersinia molecular and cellular biology. Horizon Bioscience, Norfolk, United Kingdom*, 285-306
106. Perry, R. D., Balbo, P. B., Jones, H. A., Fetherston, J. D., and DeMoll, E. (1999) Yersiniabactin from Yersinia pestis: biochemical characterization of the siderophore and its role in iron transport and regulation. *Microbiology* 145, 1181-1190
107. Rakin, A., Saken, E., Harmsen, D., and Heesemann, J. (1994) The pesticin receptor of Yersinia enterocolitica: a novel virulence factor with dual function. *Molecular microbiology* 13, 253-263
108. Fetherston, J. D., Lillard, J., and Perry, R. D. (1995) Analysis of the pesticin receptor from Yersinia pestis: role in iron-deficient growth and possible regulation by its siderophore. *Journal of Bacteriology* 177, 1824-1833
109. Fetherston, J. D., Bertolino, V. J., and Perry, R. D. (1999) YbtP and YbtQ: two ABC transporters required for iron uptake in Yersinia pestis. *Molecular microbiology* 32, 289-299
110. Sebbane, F., Jarrett, C., Gardner, D., Long, D., and Hinnebusch, B. J. (2010) Role of the Yersinia pestis yersiniabactin iron acquisition system in the incidence of flea-borne plague. *PLoS One* 5, e14379
111. Tu, J., Hue, T., Qi, K., Shao, Y., Huang, B., Wang, X., and Zhou, X. (2016) The irp2 and fyuA genes in High Pathogenicity Islands are involved in the pathogenesis of infections caused by avian pathogenic Escherichia coli (APEC). *Polish journal of veterinary sciences* 19
112. Wang, Z., Hu, W., and Zheng, H. (2020) Pathogenic siderophore ABC importer YbtPQ adopts a surprising fold of exporter. *Science advances* 6, eaay7997
113. Lukacik, P., Barnard, T. J., Keller, P. W., Chaturvedi, K. S., Seddiki, N., Fairman, J. W., Noinaj, N., Kirby, T. L., Henderson, J. P., and Steven, A. C. (2012) Structural engineering of a phage lysin that targets Gram-negative pathogens. *Proceedings of the National Academy of Sciences* 109, 9857-9862
114. Fetherston, J. D., Mier, I., Truszczynska, H., and Perry, R. D. (2012) The Yfe and Feo transporters are involved in microaerobic growth and virulence of Yersinia pestis in bubonic plague. *Infection and immunity* 80, 3880-3891
115. Une, T., and Brubaker, R. R. (1984) In vivo comparison of avirulent Vwa-and Pgm-or Pstr phenotypes of yersiniae. *Infection and immunity* 43, 895-900
116. Skare, J. T., Ahmer, B., Seachord, C. L., Darveau, R. P., and Postle, K. (1993) Energy transduction between membranes. TonB, a cytoplasmic membrane protein, can be chemically cross-linked in vivo to the outer membrane receptor FepA. *Journal of Biological Chemistry* 268, 16302-16308
117. Radka, C. D., DeLucas, L. J., Wilson, L. S., Lawrenz, M. B., Perry, R. D., and Aller, S. G. (2017) Crystal structure of Yersinia pestis virulence factor YfeA reveals two polyspecific metal-binding sites. *Acta Crystallographica Section D: Structural Biology* 73, 557-572

Chapter 2 Experimental Approaches

Bacterial Strains and Plasmids

We generated site-directed deletions in derivatives of *E. coli* strain BN1071 (1): OKN1(ΔtonB), OKN359 (ΔfepA/Δcir/Δfiu) and OKN1359 (ΔtonB/ΔfepA/Δcir/Δfiu). MG1655 (2) CP9, an extraintestinal pathogenic *E. coli* (ExPEC), was isolated from a patient with sepsis (3-5); courtesy of Dr. Thomas A. Russo (University of Buffalo School of Medicine). *fiu* was PCR amplified from *E. coli* MG1655, and cloned into the low-copy plasmid pHSG575, under control of *fepA* fur-regulated promoter, designated as pITS42. (6) pITS42 was transformed into OKN359 for transport analysis and into OKN1359 for binding analysis.

Site-Directed Mutagenesis

We performed site-directed substitutions using QuickChange (Stratagene) in pITS42 that carries *fiu*. Cys or Ala residue were introduced into specific sites. *fiu* sequence was amplified using a pair of complementary primers that flank the mutation. WT template was digested by restriction enzyme DpnI. We sequenced the plasmid encoding mutant *fiu* to confirm Cys or Ala substitutions.

Culture Conditions

OKN359 or OKN1359 cells carrying pITS42 encoding WT or mutant *fiu* were grown in Luria-Bertani (LB) broth at 37 °C overnight to stationary phase. Chloramphenicol (20 μg/mL) and streptomycin (100 μg/mL) were added to the medium for plasmid selection. LB cultures at stationary phase were sub-cultured at 0.5 % into MOPS iron-deficient medium (7) to induce the expression of fur-regulated *fiu*, and were shaken at 200 rpm for 20 hours at 37 °C, reaching a cell density of $1.5x10^9$ cells/mL.

Purification of Siderophores

Enterobactin (Ent) was isolated from *E. coli* and incubated with ^{56}Fe or ^{59}Fe to form ferric-siderophore. (8,9) FeEnt was then passed through LH20 hydrophobic column to separate FeEnt* and FeEnt. (9) Glucosylated FeEnt (Salmochelin S4) was purified from ExPEC CP9 following the procedure described in Hantke et al 2003. (10) We grew cells in LB medium to stationary phase, and sub-cultured into TY medium at 1%. After 30 hours incubation, cells were sedimented and removed, and $FeSO_4$ was added to 5 mM to form ferric siderophore complex. Supernatant was passed through Sephadex DE52 cellulose chromatography, allowing negatively charged ferric siderophore to bind. The column was washed with 5 column volumes of Tris-HCl pH7, and ferric-siderophores were eluted with H_2O/2 M ammonium chloride gradient. The dark red fraction was concentrated by evaporation and further purified by Sephadex G-10 chromatography. The concentrated FeGEnt fraction was then analyzed by mass spectrometry. We also spectroscopically analyzed solutions of FeEnt, FeEnt* and FeGEnt to obtain their absorption spectra.

Siderophore Nutrition Tests

We qualitatively analyzed the uptake of Ferric siderophores by siderophore nutrition tests. Cells expressing WT or mutant Fiu were grown in LB broth for 12 hours to stationary phase and sub-inoculated into nutrient broth at 1%. We added chloramphenicol (20 ug/mL) and streptomycin (100 ug/mL) for the selection of cells expressing target LGP. Cells were analyzed after 8 hours growth. We mixed 100 µL of cells with 3 mL of NB top agar containing 30 µL of apofecA and 100 µg/mL of streptomycin and plated the mixture onto a six-well plate. We placed a piece of paper disc on the center of each well and added 5 µL of 100 µM ferric siderophore onto the paper disc. Cells were incubated at 37 °C for 24 hours, and growth halo around paper

disc was measured. The ability of WT or mutant Fiu to transport ferric siderophore was expressed as the diameter of growth halo around the paper disc.

Preparation of OM Fractions

We inoculated LB culture in stationary phase into 10 mL of MOPS iron-deficient media at 1% and incubated with shaking at 200 rpm for 20 hours at 37 °C. Cells were collected by centrifugation at 7500 rpm for 20 minutes and were re-suspended in 4 mL of PBS buffer containing trace amounts of RNase and DNase. Cells were lysed by passing through a French press cell at 8000 p.s.i, and cell lysate was removed by centrifugation at 6000 rpm for 30 minutes. We centrifuged the supernatant at 13000 rpm for 1 h to sediment cell envelope fraction and resuspended it in 200 □L of 50 mM Tris-HCl pH 7.4. An equal volume of 1% sarcosyl was added to solubilize inner membrane fraction. The OM fraction was sedimented by centrifugation at 13000 rpm for 1 hour and was resuspended in 200 µL of 50 mM PBS pH 7.4.

Site-Directed Fluorescence Labeling with FM

We grew cells expressing WT or mutant Fiu in 10 mL of MOPS iron deficient media for 20 hours, reaching a density of 10^9 cells/mL. We pelleted and collected cells by centrifugation at 7500 rpm for 10 mins and washed and resuspended cells with 10 mL of labeling buffer (50 mM Na_2HPO4 pH6.7). Cells were then exposed to 5 µM fluorescein-5-maleimide in labeling buffer and were incubated at 37 °C for 30 mins. We added 10 µL of 130 mM β-mercaptoethanol to stop the labeling reaction. Cells were pelleted by centrifugation and were washed and resuspended in 10 mL of PBS pH 7.0. The FM-labeled cells were analyzed in a fluorescence spectrometer (SLM AMINCO 8000) with an OLIS operating system.

SDS-PAGE Electrophoresis

We analyzed protein expression and cell labeling with SDS-PAGE (11,12). To analyze protein expression, we mixed 50 μg of OM fraction, as determined by absorbance at 280 nm SDS sample buffer containing 1% SDS and 3% βME; We incubated the sample in boiling water bath for 5 mins, resolved sample by running SDS-polyacrylamide gel (12% acrylamide /0.3% bis acrylamide) at 30 mA, until the tracking dye ran out of the gel. We stained the gel and compared the expression of Fiu with other LGPs. To analyze FM-labeling of cells, we mixed $1x10^8$ labeled cells with SDS sample buffer, boiled the sample, and run SDS-polyacrylamide gel as described above. We observed the gel under UV light, and compared the labeling of Cys-modified Fiu with WT.

Radioisotopic Ferric Siderophore Transport Assays

LB overnight cultures were sub-inoculated into MOPS iron-deficient medium at 1% and were shaken at 37 ° C for 5.5 h. Appropriate antibiotics were supplied (100 ug/mL streptomycin for BN1071, OKN35, and OKN359, and 20 ug/mL for OKN359/pITS42(*fiu*)). 3 mL aliquots of cell cultures were incubated with 10 μM of [^{59}Fe] Ent or [^{59}Fe] Ent* at 37 ° C. We collected 100 μL of cell cultures at 5 min, 10 mins, 15 min, 30 min, 45 min for isotope determination: Cells were filtered through 0.45 um membrane and were washed with 10 mL of 0.9 % LiCl; the amounts of [^{59}Fe] of cells on the filter membrane were analyzed in Packard gamma counter. In each time point, we collected triplicate samples for isotope determination.

Fluorescence Determinations of Ligand Binding

We performed fluorescent determinations of ligand binding in an SLM AMINCO 8100 fluorescence spectrometer with OLIS operating system (OLIS Inc., Bogart, GA). We added 1.5 $x10^8$ FM-labeled cells harboring WT or mutant Fiu to 2 mL of PBS buffer containing 0.2%

glucose in a quartz cuvette with stirring. FM-labeled cells were excited at 494 nm, and emission fluorescence at 520 nm were recoded. We measured the initial fluorescence (F_0), titrated labeled cells with ferric siderophore to increasing concentrations, and recorded corresponding fluorescence as F. We collected data in triplicates, normalized the average values as 1-F/F0 at each concentration of ligand. We analyzed the binding by plotting 1-F/F0 *vs* [Ligand], and analyzing data using Grafit 6.0.12 (Erithacus Ltd. West Sussex, UK). We calculated a fitting curve using the 1-site binding with background model, which plots [bound ligand] as a function of [free ligand].

$$[Bound\ ] = \frac{Capacity\ .[Free\ ]}{K_d + [Free\ ]} + Background$$

K_D values with standard errors were determined using the saturation fitting curve described above.

In silico Docking and Molecular Dynamics Simulation

In silico Docking

The crystal structure of Fiu was obtained from the Protein Data Bank (PDB ID 6BPM) and the structure of FeEnt* was modified by ferric salmochelin S1 (PubChem CID 135398071) by removing the glucose group followed by energy minimization using VEGA ZZ 3.2.1. Autodock Vina (v1.2.1) was used to dock FeEnt* to Fiu. Ligand and receptor were processed following the standard procedure in the user manual. We ran the docking experiment using the following searching box: box 1 (size x= 50 , y= 78, z = 78; center x= -55 , y= 45, z = 20) for whole receptor search, box 2 (size x= 40 , y= 30, z = 30; center x= -60, y= 47, z = 16) for surface binding sites, and box 3 (size x= 38 , y= 26, z = 32; center x= -59 , y= 39, z = 29) for binding site 3. And the top 9 ligand poses were listed for each docking run and were analyzed using Autodock Tool and Chimera.

Molecular Dynamics Simulation

The docked models were obtained from the ligand docking study. The protein models were prepared by Schrödinger Protein Preparation Wizard (13). Each Fiu complex system was embedded into the 1-palmitoyl-2-oleoyl-sn-glycero-3-phosphocholine (POPC) lipid bilayer which was perpendicular to the z-axis. The TIP3P water molecules were added into the system and the size of orthorhombic buffer box was 10Å x 10Å x10Å. The systems were built by Desmond system builder (Schrödinger Release 2021-4). Sodium chloride (0.15 M) was used to neutralize the system. OPLS4 was used for the force field (14,15). Simulation conditions in the isothermal-isobaric (NPT) ensemble were as follows: 1.01325 bar of pressure, 310 K of temperature. The systems were minimized in 100 ps. The temperature was controlled using a Langevin thermostat. The time step of these simulations was 0.002ps, the total production time was 1.0 μs. All data was processed with Schrödinger Desmond. The MD simulations movie was generated by Schrödinger Maestro (Schrödinger Release 2021-4).

Table 2-1 List of bacterial strains

E. coli Strains	Genotype
MG1655	WT
BN1071	F-, rpsL trp, B1, entA
OKN3	ΔfepA
OKN35	ΔfepAΔcir
OKN9	Δfiu
OKN359	ΔfepAΔcirΔfiu
OKN1359	ΔtonBΔfepAΔcirΔfiu

Reference

1. Montgomerie, J., Bindereif, A., Neilands, J., Kalmanson, G., and Guze, L. (1984) Association of hydroxamate siderophore (aerobactin) with Escherichia coli isolated from patients with bacteremia. *Infection and Immunity* **46**, 835-838
2. Blattner, F. R., Plunkett III, G., Bloch, C. A., Perna, N. T., Burland, V., Riley, M., Collado-Vides, J., Glasner, J. D., Rode, C. K., and Mayhew, G. F. (1997) The complete genome sequence of Escherichia coli K-12. *science* **277**, 1453-1462
3. Nazareth, H., Genagon, S. A., and Russo, T. A. (2007) Extraintestinal pathogenic Escherichia coli survives within neutrophils. *Infection and immunity* **75**, 2776-2785
4. Russo, T. A., Guenther, J. E., Wenderoth, S., and Frank, M. M. (1993) Generation of isogenic K54 capsule-deficient Escherichia coli strains through TnphoA-mediated gene disruption. *Molecular microbiology* **9**, 357-364
5. Johnson, J. R., Russo, T. A., Scheutz, F., Brown, J. J., Zhang, L., Palin, K., Rode, C., Bloch, C., Marrs, C. F., and Foxman, B. (1997) Discovery of disseminated J96-like strains of uropathogenic Escherichia coli O4: H5 containing genes for both PapGJ96 (class I) and PrsGJ96 (class III) gal (α1-4) gal-binding adhesins. *Journal of Infectious Diseases* **175**, 983-988
6. Takeshita, S., Sato, M., Toba, M., Masahashi, W., and Hashimoto-Gotoh, T. (1987) High-copy-number and low-copy-number plasmid vectors for lacZα-complementation and chloramphenicol-or kanamycin-resistance selection. *Gene* **61**, 63-74
7. Neidhardt, F. C., Bloch, P. L., and Smith, D. F. (1974) Culture medium for enterobacteria. *Journal of bacteriology* **119**, 736-747
8. Wayne, R., Frick, K., and Neilands, J. (1976) Siderophore protection against colicins M, B, V, and Ia in Escherichia coli. *Journal of bacteriology* **126**, 7-12
9. Newton, S. M., Trinh, V., Pi, H., and Klebba, P. E. (2010) Direct measurements of the outer membrane stage of ferric enterobactin transport: postuptake binding. *Journal of Biological Chemistry* **285**, 17488-17497
10. Hantke, K., Nicholson, G., Rabsch, W., and Winkelmann, G. (2003) Salmochelins, siderophores of Salmonella enterica and uropathogenic Escherichia coli strains, are recognized by the outer membrane receptor IroN. *Proceedings of the National Academy of Sciences* **100**, 3677-3682
11. Lugtenberg, B., Meijers, J., Peters, R., van der Hoek, P., and van Alphen, L. (1975) Electrophoretic resolution of the 'major outer membrane protein'of Escherichia coli K12 into four bands. *FEBS letters* **58**, 254-258
12. Hancock, R. E., and Braun, V. (1976) The colicin I receptor of Escherichia coli K-12 has a role in enterochelin-mediated iron transport. *FEBS letters* **65**, 208-210
13. Sastry, G. M., Adzhigirey, M., Day, T., Annabhimoju, R., and Sherman, W. (2013) Protein and ligand preparation: parameters, protocols, and influence on virtual screening enrichments. *Journal of computer-aided molecular design* **27**, 221-234

14. Jorgensen, W. L., and Tirado-Rives, J. (1988) The OPLS [optimized potentials for liquid simulations] potential functions for proteins, energy minimizations for crystals of cyclic peptides and crambin. *Journal of the American Chemical Society* **110**, 1657-1666
15. Lu, C., Wu, C., Ghoreishi, D., Chen, W., Wang, L., Damm, W., Ross, G. A., Dahlgren, M. K., Russell, E., and Von Bargen, C. D. (2021) OPLS4: Improving force field accuracy on challenging regimes of chemical space. *Journal of chemical theory and computation* **17**, 4291-4300

Chapter 3 Characterization of Iron Acquisition Catalyzed by Fiu

Introduction

Iron is essential for bacteria to survive in the host. On the one hand, Fe^{3+} exists as $Fe(OH)_3$ in aqueous solution with extremely low solubility ($K_{SP} = 2.79 \times 10^{-39}$) (2), which makes it hard to be utilized by bacteria. On the other hand, hosts like humans produce iron binding proteins, including ferritin and transferrin, that can capture iron from the solution. Iron is restricted to a low level of concentration in serum upon bacterial infection. (3) To obtain iron and survive in host, bacteria secrete organic metal binding molecules with low molecular weight, siderophores, to complex and solubilize iron in the extracellular environment. The resulting iron-siderophore complex, a ferric siderophore, is then internalized and utilized by bacteria. (4) Enterobactin (Ent) binds iron with an extremely high binding affinity ($K_D = 10^{52}$ M^{-1}) and forms a hexacoordinate-conformation with six hydroxyl groups. (5) In Gram-negative bacteria, transport of ferric siderophores is mediated by TonB-dependent transport systems. (4) Under iron deficient conditions, Gram-negative bacteria trigger the expression of outer-membrane (OM) receptors, which recognize and transport particular ferric siderophores.(6) These OM receptors adopt a transmembrane β-barrel conformation consisting of 22 β-strands and rely on TonB for energization. Thus they are referred to as TonB-dependent transporters (TBDT), or ligand-gated porin (LGP). (7,8) Ligand binding induces a conformational change in LGPs, which activates TonB for its energized motion. The activated TonB then drives LGPs to transport ferric siderophore across OM. (9,10)

Ferric iron uptake (Fiu) transporter is a TonB-dependent receptor not only found in commensal *E. coli*, but also in pathogenic *E. coli*, *K.pneumoniae* and *A. baumannii*. (11) Other catechol transporters include FeEnt receptor FepA, and colicin Ia receptor Cir. Early studies

suggested that Fiu and Cir participated in the transport of mono-catecholate siderophores, including ferric dihydroxybenzolyserine (DHBS) and ferric dihydroxybenzoic acid (DHBA). (12) Other studies found that Fiu catalyzed the uptake of catechol-containing antibiotics. (13,14) But no further research about Fiu was published afterwards, until Grinter *et al* solved its crystal structure. (15) None of those studies clearly identified the ligand of Fiu by determining its binding affinity. Further research, which I performed herein, was required to identify its ligand, and to understand how Fiu captures and internalizes its catecholate ligand from the environment.

In this study, we for the first time isolated and identified the natural ligand of Fiu, which is the degradation product of FeEnt. Mass spectrometry analysis identified it as Fe-$(DHBS)_2 \cdot 2H_2O$. We engineered fluorescent Fiu sensors to screen its target ligands among catecholate ferric siderophores. Our results showed that Fiu can recognize FeGEnt, FeEnt, FeEnt*, DHBS, DHBA, but it can only catalyze the uptake of FeEnt* in *E. coli*. We determined the binding affinity of each candidate ligand to Fiu senor and found that FeDHBS (K_D = 0.092 μM) had the strongest binding among the selected catecholate ligands, followed by FeGEnt (K_D = 0.34 μM), FeEnt* (K_D = 0.69 μM), FeDHBA (K_D = 0.68 μM), and FeEnt (K_D = 0.96 μM). Moreover, Fiu also bound two siderophore antibiotics ferric cefidericol (FDC, K_D = 0.44 μM) and ferric MB-1 (K_D = 4.2 μM). We then performed *in silico* docking combined with molecular dynamic (16) simulation to explore potential binding sites in Fiu. Results showed that Fiu had two binding sites that can recognize and hold the ligand, with several residues that participated in the ligand-receptor interaction. The binding sites and important residues were experimentally verified by site-directed mutagenesis. Mutation to alanine at these sites not only significantly impaired binding affinity, but also affected the uptake of FeEnt*.

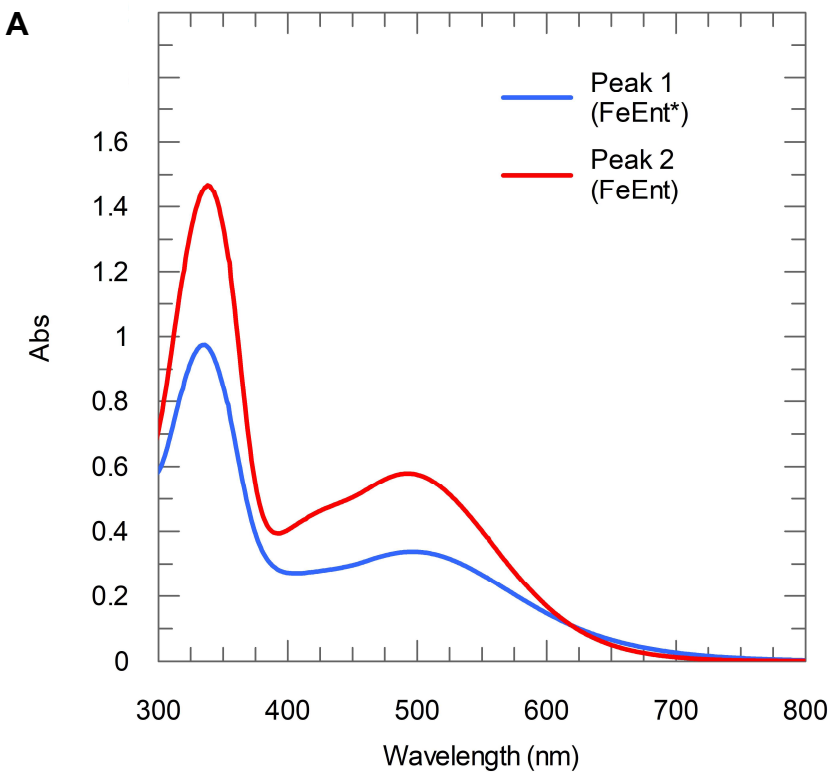
Results

Characterization of FeEnt-Related Catechols

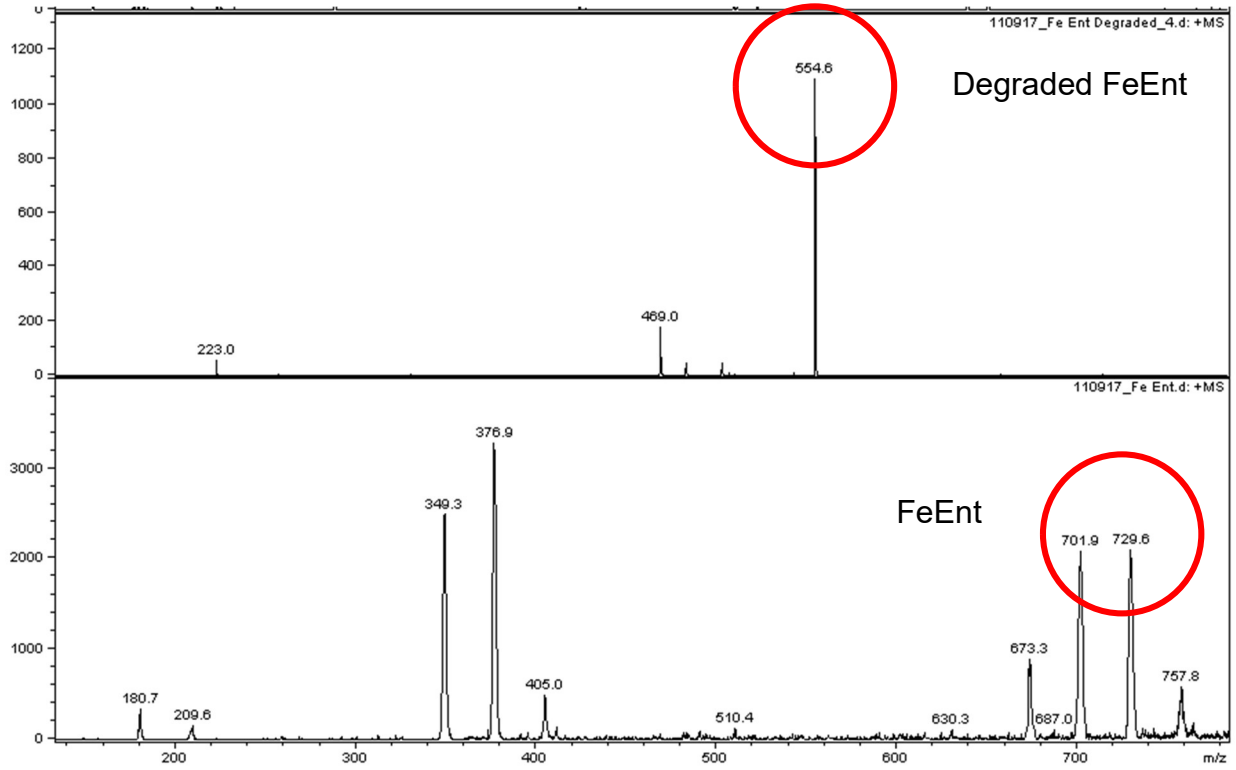
Ferric enterobactin (FeEnt) is prone to degradation. The cyclic lactone backbone that connects three catechol groups can be cleaved by esterase or hydrolyzed under acidic or basic conditions. After being stored at 4 ℃ for a period, ferric enterobactin was purified by hydrophobic chromatography and two fractions were eluted from the column. (Figure 3-1 A) The absorption spectrum indicated that the second fraction was ferric enterobactin, with an absorption maximum at 495 nm. (Figure 3-1 A) Another fraction showed a shift of the absorption peak (505 nm) and we considered it as degradation product of FeEnt (FeEnt*). (Figure 3-1 A) To identify FeEnt*, we analyzed the fraction using electrospray mass spectrometry with FeEnt as the control. (Figure 3-1 B) FeEnt fraction showed a peak at 729.6 m/z that corresponds to ferric enterobactin (Mw=725.4), while FeEnt* fraction showed a peak at 554.6 m/z, which was close to the molecular weight of $Fe(DHBS)_2$ (Mw=518.4). (Figure 3-1 B) Given ferric iron must be hexa-coordinated, another two oxygen atoms would come from two water molecules. Thus, we concluded that FeEnt* was $Fe(DHBS)_2 \cdot 2H_2O$, whose molecular weight (Mw = 554.4) exactly matched the peak at 554.6 m/z detected by mass spectrometry.

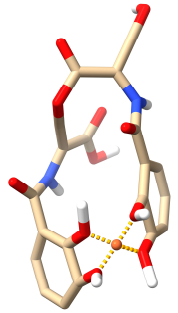
Salmochelin S4 is the glucosylated form of FeEnt (FeGEnt). The host immune system secretes siderophore binding proteins, such as lipocalin, to prevent pathogenic bacteria from acquiring iron by binding to ferric siderophores secreted by pathogens. To escape from the host immune system, some pathogenic bacteria secrete FeGEnt for iron acquisition, which cannot be recognized and bound by lipocalin. (17-21) To purify FeGEnt, we grew pathogenic *E. coli* CP9 in iron-deficient MOPS media and added $FeCl_3$ to the supernatant to form ferric siderophores. FeGEnt was purified by Sephadex DE52 ion-exchange chromatography, followed by Sephadex

G10 gel filtration chromatography for desalting. We then identified it as FeGEnt with mass spectrometry. (Figure 3-1 C)


A
Peak 1
(FeEnt*)
Peak 2
(FeEnt)
Abs
1.6
1.4
1.2
1
0.8
0.6
0.4
0.2
0
300
400
500
600
700
800
Wavelength (nm)

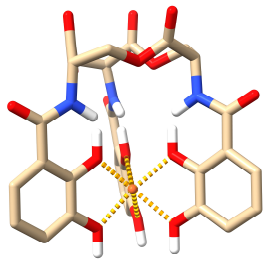
B





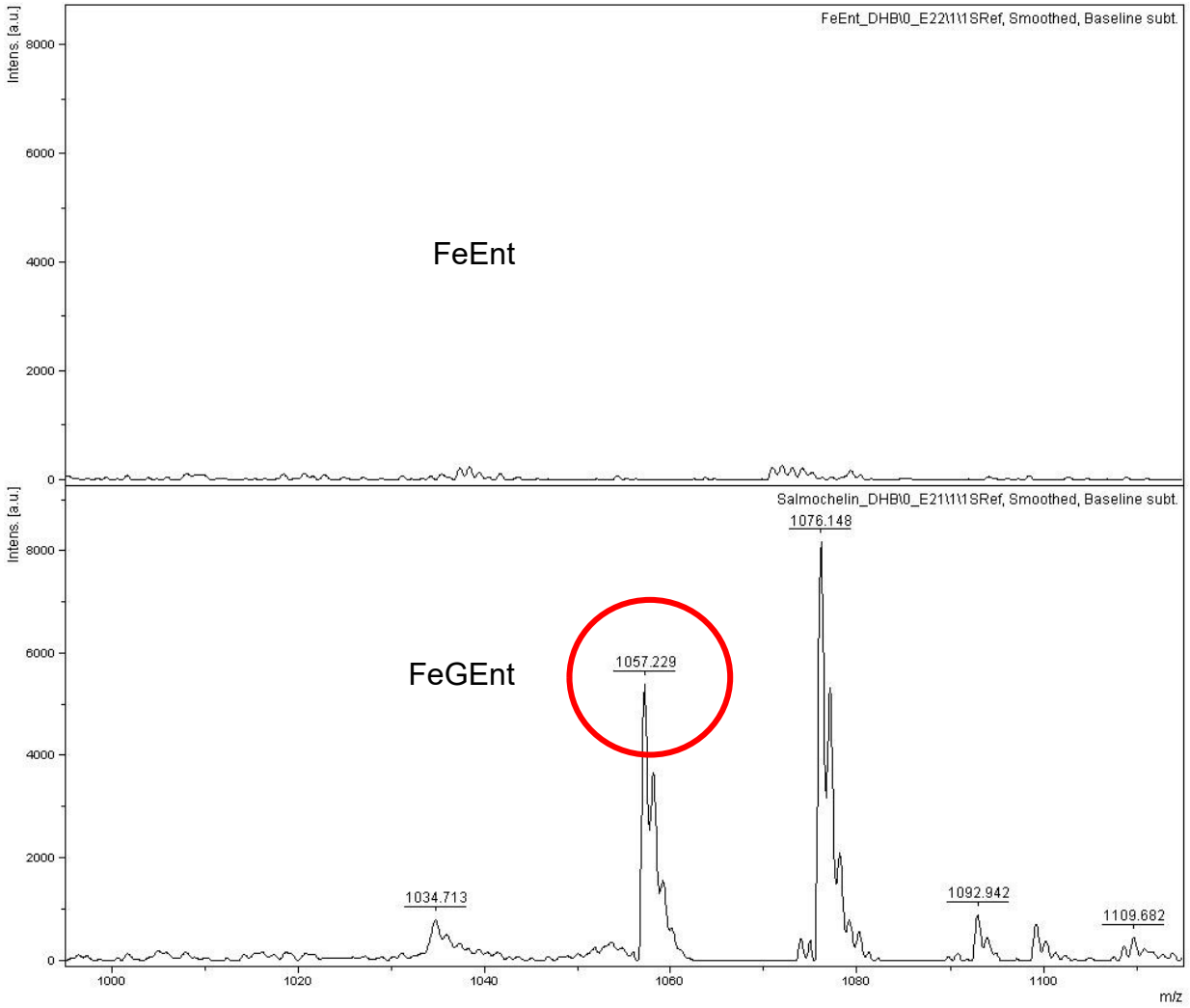
FeEnt*

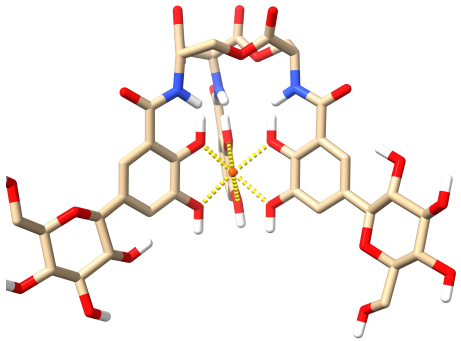
$(Fe(DHBS)_2)$



FeEnt

c





FeGEnt

(Salmochelin S4)

Figure 3-1 Characterization of Ferric Siderophores

(A) We purified the degraded product from FeEnt sample by LH20 hydrophobic chromatography, collected two colored fractions and scanned their absorbance spectra. FeEnt showed an absorption peak at 495 nm while FeEnt* showed an absorption peak at 505nm. (B) We then determined the Mw of FeEnt and FeEnt* by mass spectrometry. (C) FeGEnt was purified from the culture supernatant of pathogenic *E. coli* CP9. We passed the ferrated supernatant sample through Sephadex DE52 ion-exchange chromatography, washed it with Tris-HCl pH7 buffer and eluted ferric siderophores with gradient ammonia chloride followed by gel filtration chromatography for desalting. We determined the Mw of purified fractions by mass spectrometry and verified it as the FeGEnt.

Screening of Catecholate Ligands for Fiu

In the past, Fiu was proposed as the transporter of monomeric catechols, and perhaps the receptor for a degradation product of FeEnt. (12,22) We cloned *Ecofiu* into pHSG575 vector and expressed it in *E. coli* OKN359 (Δ*fepA*/Δ*cirA*/Δ*fiu*) cell. To screen ferric siderophores that are transported by Fiu, we performed siderophore nutrition test on OKN359 cells or OKN359 expressing Fiu with addition of desired catechol, including FeEnt, FeEnt*, FeGEnt. (Figure 3-2) The transport was evaluated by the diameters of growth halo, which were listed in Table 3-1. Fiu only transported FeEnt*, as suggested by growth halo, but not FeEnt. Faint growth halos were observed in the group exposed to FeGEnt, but this was found to be non-specific transport, as the negative control OKN359 showed the same halo. Besides, we further validated the transport of FeEnt* by Fiu with isotope accumulation assay. (Figure 3-3) Cells expressing Fiu or not were exposed to [^{59}Fe]Ent or [^{59}Fe]Ent* and aliquots were collected at sequential times. Radioactivity was measured to evaluate the uptake of FeEnt or FeEnt*. BN1071 (WT) expressed all three receptors (FepA, Cir, Fiu) and can transport both FeEnt and FeEnt*. (Figure 3-3) OKN359 (Δ*fepA*/Δ*cirA*/Δ*fiu*), the negative control, showed no transport for FeEnt nor FeEnt*. Two Fiu expressing strains, OKN35 ((Δ*fepA*/Δ*cirA)* and OKN359 expressing Fiu, transported only degraded FeEnt but not FeEnt. (Figure 3-3) Thus, we verified that Fiu mediated the transport of FeEnt* under *E. coli* background.

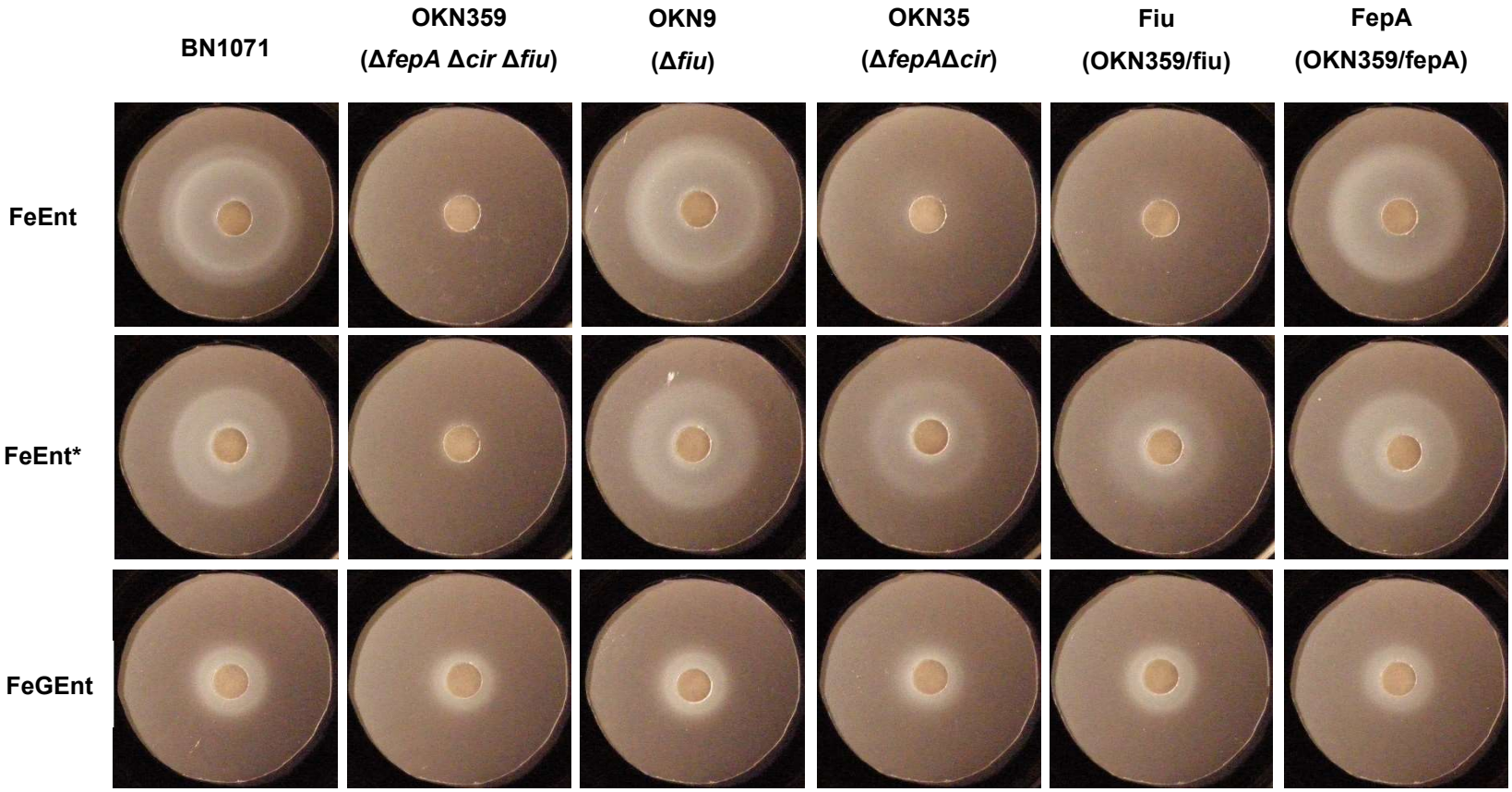

BN1071
OKN359
(Δ*fepA* Δ*cir* Δ*fiu*)
OKN9
(Δ*fiu*)
OKN35
(Δ*fepA*Δ*cir*)
Fiu
(OKN359/fiu)
FepA
(OKN359/fepA)
FeEnt
FeEnt*
FeGEnt

Figure 3-2 Characterization of siderophore transport by siderophore nutrition test.
We cloned EcofepA and Ecofiu gene into pHSG575 vector, expressed them in OKN359 cells grew them in nutrient broth (NB) media to induce the expression of fur-regulated OM receptor. BN1071, OKN359, OKN35, OKN9 were used as positive or negative control. We mixed cell culture in NB soft agar (0.7% agar) with addition of antibiotics and iron-chelating compound apoFcA, plated them onto the petri dish plate and add 10 μL of 100 mM ferric siderophore onto the paper disc. We incubated them at 37 °C for 24 hours and evaluated the transport by measuring the growth halo around the paper disc

Table 3-1 Siderophore nutrition test with catecholate siderophores.

Diameter (nm)	BN1071	OKN359 (ΔfepAΔcir Δfiu)	OKN9 (ΔfepAΔcir)	OKN35 (Δfiu)	Fiu (OKN359/fiu)	FepA (OKN359/fepA)
FeEnt	21.40 ± 0.55	0	21.20 ± 1.30	8.00 ± 0.71 (faint halo)	7.20 ± 0.45 (faint halo)	19.80 ± 1.79
FeEnt*	16.50 ± 0.87	0	16.80 ± 0.84	18.40 ± 1.82	18.60 ± 2.51	18.40 ± 0.89
FeGEnt	2.50 ± 0.10	2.50 ± 0.10	2.50 ± 0.10	2.50 ± 0.10	2.50 ± 0.10	2.50 ± 0.10

The table listed the diameters of growth halo around the paper disc containing 100 μM of catecholate ferric siderophores, after incubation at 37 °C for 24 hours.

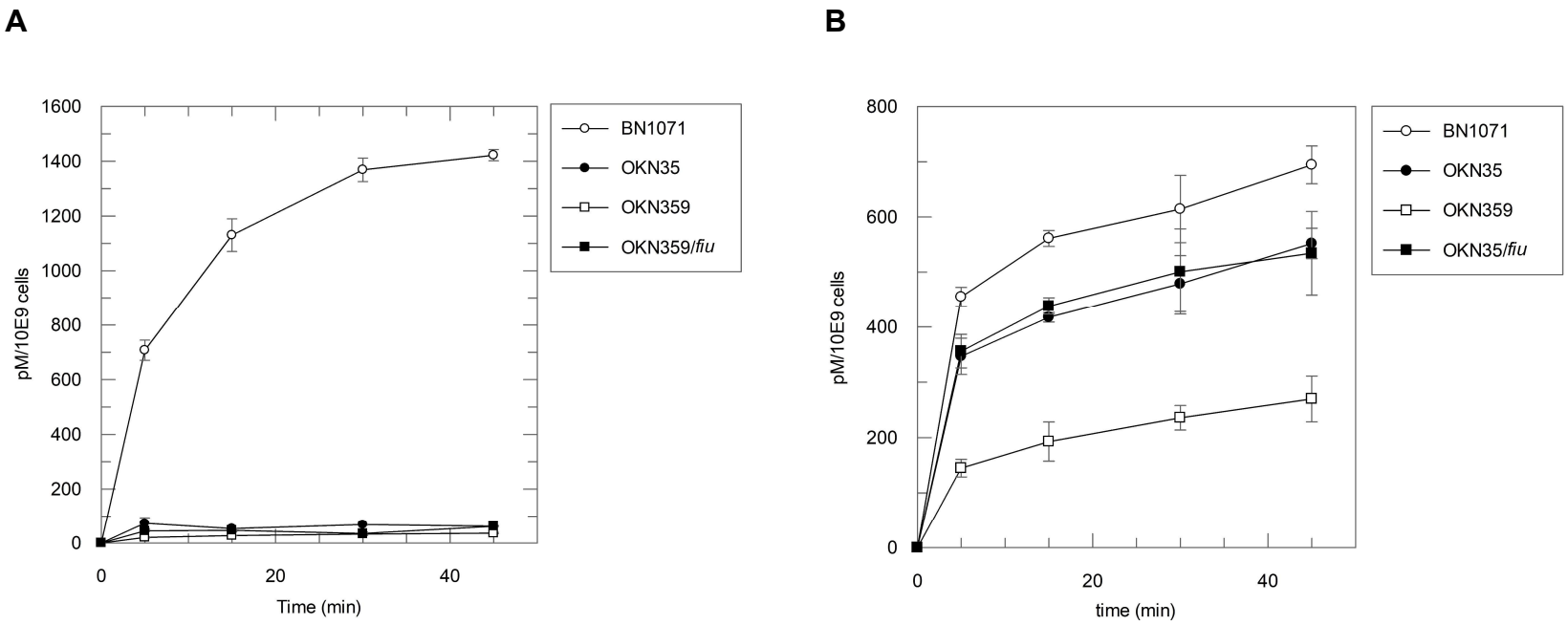


Figure 3-3 [^{59}Fe] siderophore accumulation assay

We grew cells in nutrient broth, exposed them exposed to (A) [^{59}Fe]Ent or (B) [^{59}Fe]Ent, collected aliquots samples at sequential times and measured corresponding radioactivity to evaluate the uptake of ferric siderophores.

Fluorescent Determination of Binding Affinity

To quantitively analyze the binding of ferric siderophores to Fiu, we engineered Fiu fluorescent sensor. We introduced cysteine residues into the external loop, which was then labeled specifically with fluorescein-maleimide (FM). Upon binding to ligand, the external loop will undergo conformational change, leading to the quenching of adjacent fluorophore. Binding affinity can be determined by analyzing the fluorescence quenching against corresponding concentration of siderophore. We selected several positions to introduce cysteine mutation (S347C, T414C, S555C, A694C) (Figure 3-4 A) and compared their fluorescence labeling with fluorescein maleimide. (Figure 3-4 B, C) FiuA694C showed the highest fluorescence and was selected for the determination of binding affinity to different siderophores. (Figure 3-4 B, C) We titrated FM-FiuA694C cells with ferric siderophores to increasing concentrations and read corresponding fluorescence. (Figure 3-4 D) K_D value was calculated by plotting the normalized fluorescence against siderophore concentration. Using this method, we tested catecholate siderophores including FeEnt, FeEnt*, FeGEnt, FeCrn, FeDHBA, FeDHBS, FeFDC, FeMB-1, FePvD. FiuA694C was found to recognize DHBS (K_D = 0.1 μM) at the highest binding affinity, followed by FeGEnt (K_D = 0.34 μM), FeEnt* (K_D = 0.69 μM), FeEnt (K_D = 0.96 μM). (Figure 3-5 A-G) Besides, Fiu also bound two siderophore antibiotics ferric cefidericol (FDC, K_D = 0.44 μM) and ferric MB-1 (K_D = 4.2 μM). (Figure 3-5 F, G) No binding was observed to FeDHBA using FiuA694C sensor, which is inconsistent with previous study. To study the binding of Fiu to FeDHBA, we introduced cysteine to the site (N554) that is closer to the binding pocket as computed by docking study (see following part). We performed siderophore nutrition test to check its functionality and found that cysteine mutation at this site did not affect ligand transport. Cells were labeled fluorescently, and we analyzed its binding to FeDHBA by titration as

described previously, with FeDHBS as the control. FiuN554C bound both FeDHBA and FeDHBS, as indicated by fluorescent quenching upon addition of ligand. By analyzing fluorescence quenching at increasing concentrations, we determined a K_D of 0.68 μM for FeDHBA, (Figure 3-5 E) FeDHBS showed similar binding affinity (K_D = 0.092 μM) to the one determined using sensor Fiu A694C (K_D = 0.1 μM). (Figure 3-5 D)

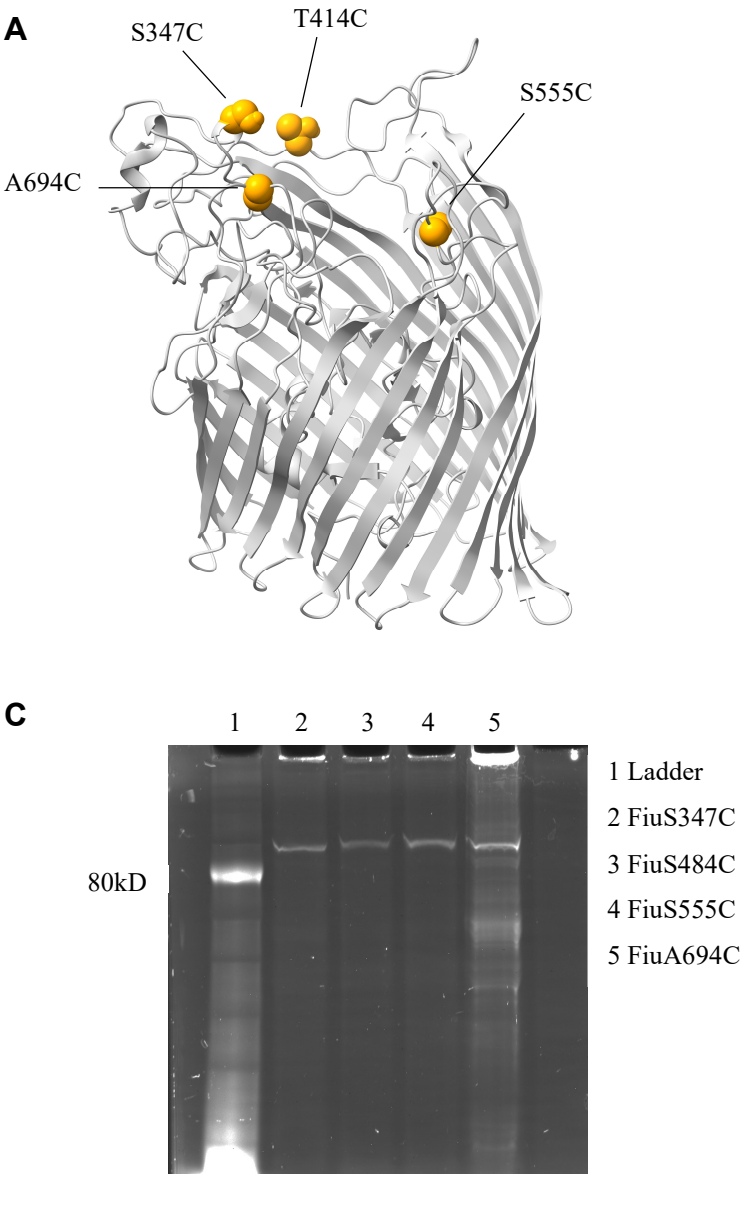
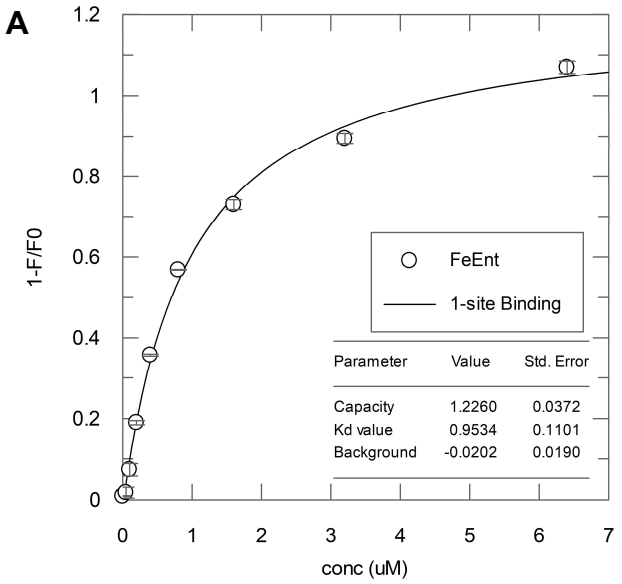
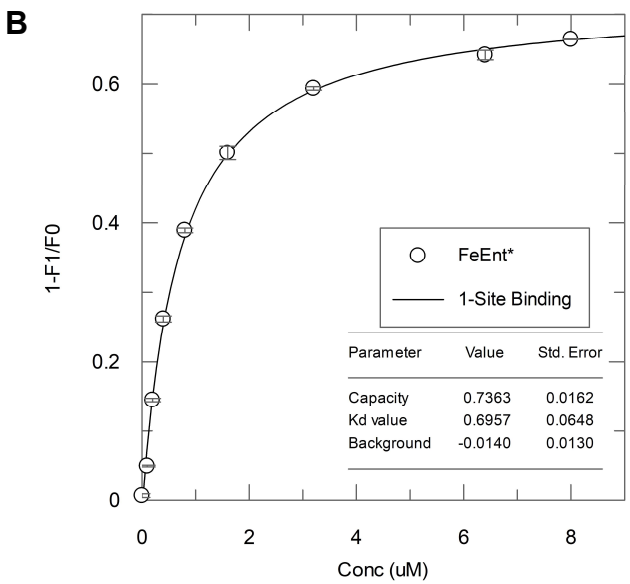
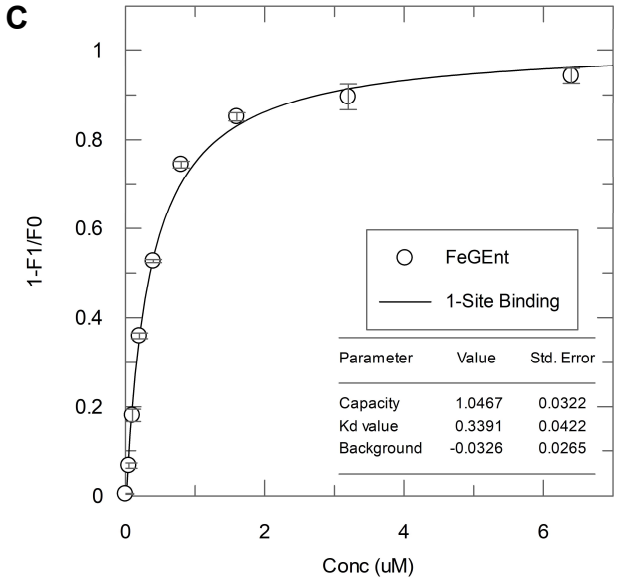

A
S347C
T414C
S555C
A694C
B
FiuS347C
FiuS484C
FiuS555C
FiuA694C
F
0.6
0.4
0.2
0
200
400
Time (s)
C
1 2 3 4 5
80kD
1 Ladder
2 FiuS347C
3 FiuS484C
4 FiuS555C
5 FiuA694C
D
FiuA694C
F1/F0
1.2
1
0.8
0.6
0.4
0.2
0
0
200
400
600
800
Time (s)

Figure 3-4 Fluorescence quenching assay for affinity determination.

(A) We selected several residues in the external loops for cysteine mutagenesis, labeled them with fluorescein maleimide and (B) checked their labeling and quenching by adding FeEnt* to 0.69 μM. Fiu A649C showed the highest fluorescence labeling and the most sensitive quenching upon ligand binding, so we selected this mutant for the determination of binding affinities of siderophore ligands. (C) The expression and labeling of cysteine mutants were also confirmed by running a fluorescent SDS polyacrylamide gel. (D) We put $5x10^7$ cells/mL of FM-labeled cells in quartz cuvette, titrated them with increasing concentration of ferric siderophore and read corresponding fluorescence.


A
1-F/F0
conc (uM)
FeEnt
1-site Binding
Parameter Value Std. Error
Capacity 1.2260 0.0372
Kd value 0.9534 0.1101
Background -0.0202 0.0190


B
1-F1/F0
Conc (uM)
FeEnt*
1-Site Binding
Parameter Value Std. Error
Capacity 0.7363 0.0162
Kd value 0.6957 0.0648
Background -0.0140 0.0130


C
1-F1/F0
Conc (uM)
FeGEnt
1-Site Binding
Parameter Value Std. Error
Capacity 1.0467 0.0322
Kd value 0.3391 0.0422
Background -0.0326 0.0265

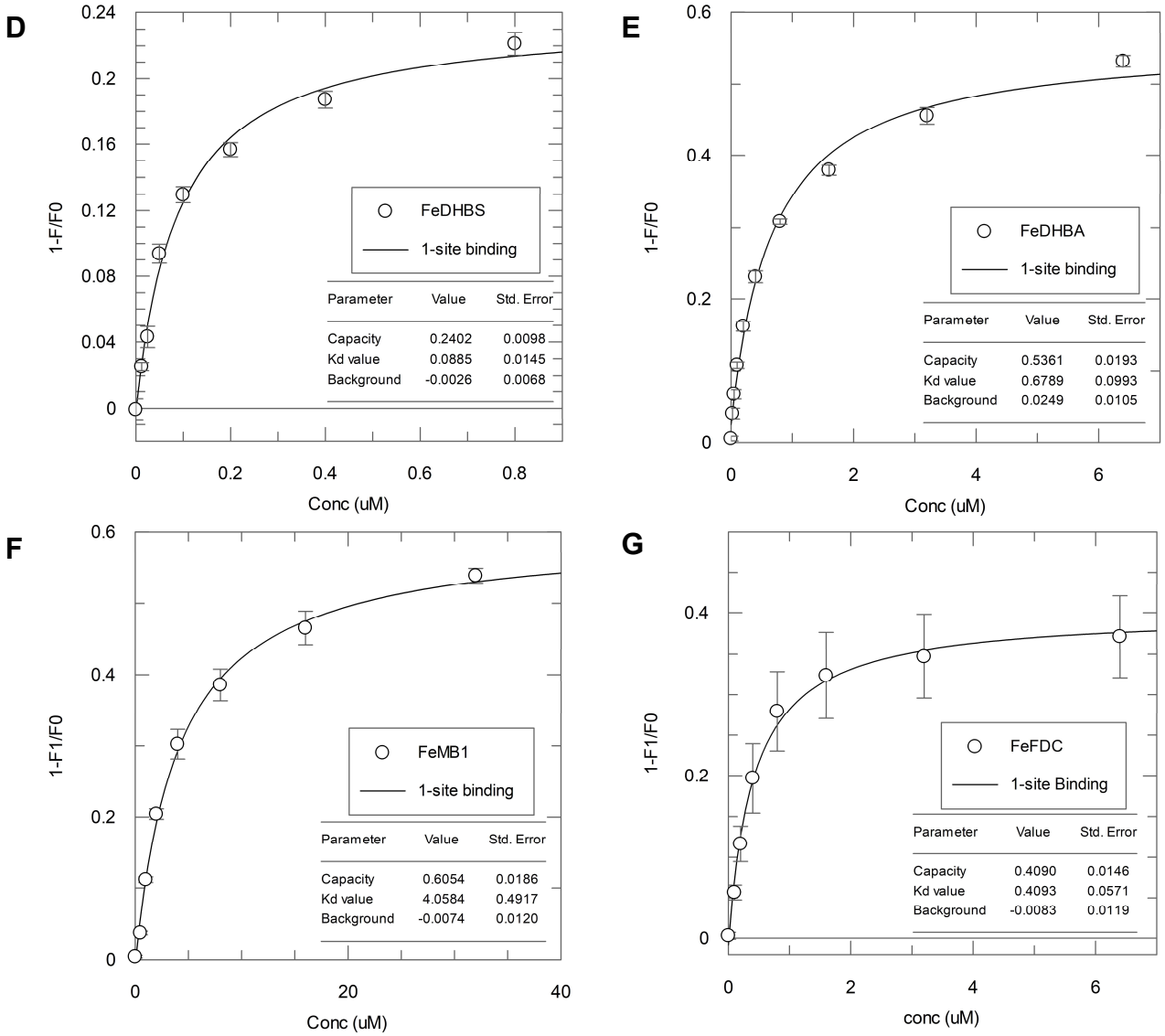

D
1-F/F0
Conc (uM)
FeDHBS
1-site binding
Parameter Value Std. Error
Capacity 0.2402 0.0098
Kd value 0.0885 0.0145
Background -0.0026 0.0068
E
1-F/F0
Conc (uM)
FeDHBA
1-site binding
Parameter Value Std. Error
Capacity 0.5361 0.0193
Kd value 0.6789 0.0993
Background 0.0249 0.0105
F
1-F1/F0
Conc (uM)
FeMB1
1-site binding
Parameter Value Std. Error
Capacity 0.6054 0.0186
Kd value 4.0584 0.4917
Background -0.0074 0.0120
G
1-F1/F0
conc (uM)
FeFDC
1-site Binding
Parameter Value Std. Error
Capacity 0.4090 0.0146
Kd value 0.4093 0.0571
Background -0.0083 0.0119

Figure 3-5 Determination of binding affinities by fluorescence quenching assay.

We performed fluorescence quenching assay as described in the previous figure. We titrated FM-labeled sensor with siderophore ligand and calculated binding affinity by analyzing normalized fluorescence against ligand concentration. Each data point was calculated by three determinations. We plotted the average value of normalized fluorescence against corresponding ligand concentration, created non-linear fit using 1-site binding model (Grafit6.0.12) and calculated the binding affinities based on the fitting curve. The KD values and associated standard errors were listed in figure (A) FeEnt, (B) FeEnt*, (C) FeGEnt, (D) FeDHBS, (E) FeDHBA, (F) FeMB-1, (G) FeFDC

Determination of Binding Sites by *in silico* Docking and MD Simulation

We performed *in silico* docking to calculate potential binding sites in Fiu (PDB 6BPM) to accommodate FeEnt* using AutoDock Vina. We restricted the search box from middle to surface of the Fiu and found three potential binding sites: site 1 and site 2 were in the surface area and site 3 was in the middle of the beta-barrel. (Figure 3-6 A) To validate binding sites predicted by docking and to narrow down residues that participate in the ligand-receptor interaction, we performed molecular dynamic (MD) simulation. (Figure 3-6 B-E) In this case, we only focused on the surface binding sites (site 1 and site 2), which are important for ligand recognition and binding. This also allowed us to perform further characterization using fluorescent sensor with chemical modification on the surface loop, which is sensitive to the surface interactions of OM receptor. We allowed the docked FeEnt* to interact with the receptor for 1 microsecond. when they reach a stable state, we analyzed ligand position as well as important amino acid residues involved in ligand-receptor interaction.

Two binding sites were determined and validated by docking and MD simulation: Binding site 1 was in the upper region of the beta barrel, closed to loop 8 and loop 9. (Figure 3-6 B) In this binding site, we found that ligand interacted with residue F105, E108, D124, K739: ferric iron was coordinated by four hydroxy groups from the siderophore and two molecules of H_2O, and thus, forming a hexacoordinated conformation; F105 provided hydrophobic contact for the ligand, making the binding pocket more fit to FeEnt*; E108 and Asp124 formed both hydrogen bond and salt bridge with the ligand; A hydrogen bond was also observed between the side chain of K739 and the ligand. (Figure 3-6 D)

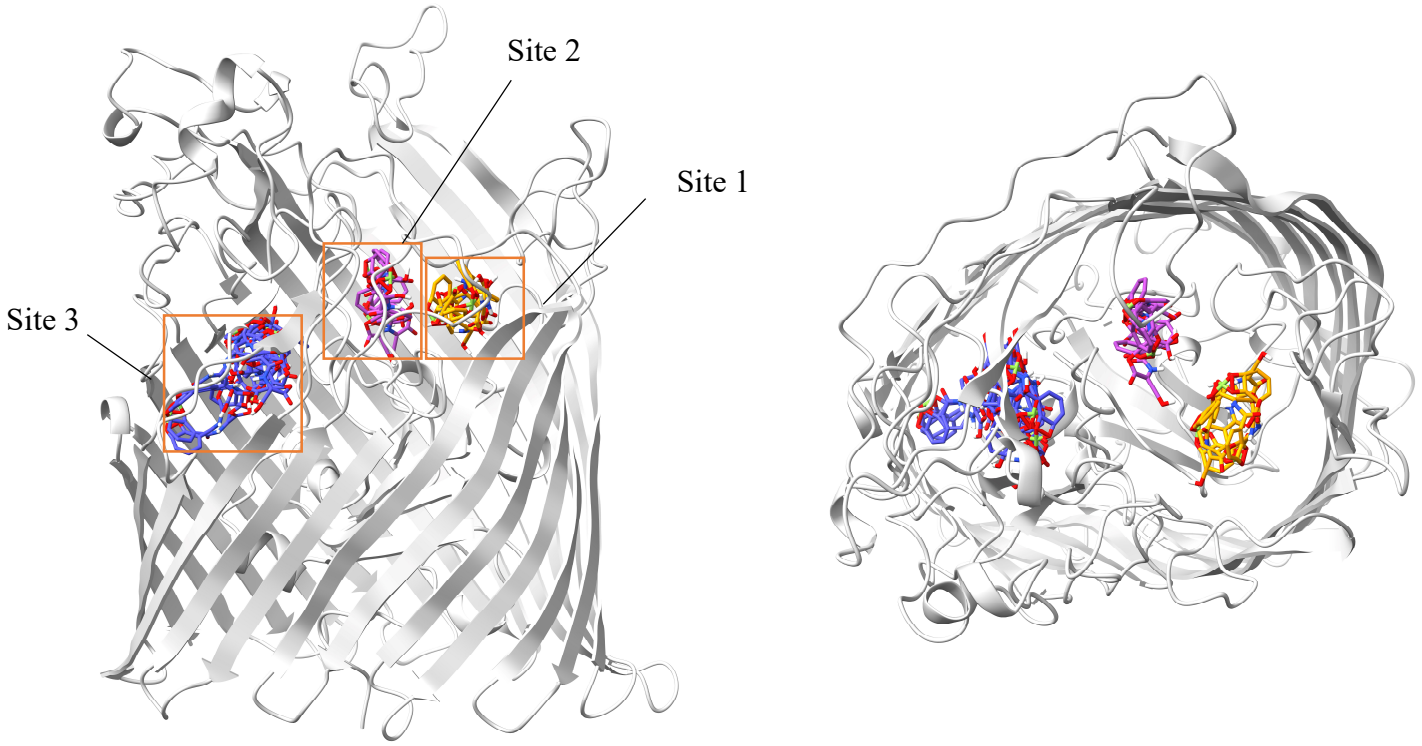
Binding site 2 was in the lower area to binding site 1, closed to plug loop and loop 7. (Figure 3-6 C) S126, N127, G138, S139, R142, and Q335 were found to participate in the

interaction with ligand. (Figure 3-6 E) Ferric iron formed coordination bond with two hydroxy groups from G138 and S139. Along with another four hydroxy groups from the ligand, ferric ion formed a stable hexacoordinated conformation. (Figure 3-6 E) FeEnt* formed hydrogen bonds with S126 and N127, which helped to stabilize its binding in the binding pocket. (Figure 3-6 E) The most important interactions we observed in this binding site were from Arg142: The positively charged side chain of R142 interacted with the surface of electron-rich phenol ring of the siderophore, forming a strong perpendicular cation-π bond; Arg142 also formed a salt-bridge with ligand, which further strengthen its interaction with ligand. (Figure 3-6 E) The interaction between ligand and Q335 was not stable, it occasionally formed hydrogen bond with ligand. But at the end of the MD simulation, it moved away from ligand. (Figure 3-6 E) Thus, Q335 was not considered as an important residue for ligand-receptor interaction in this binding site.

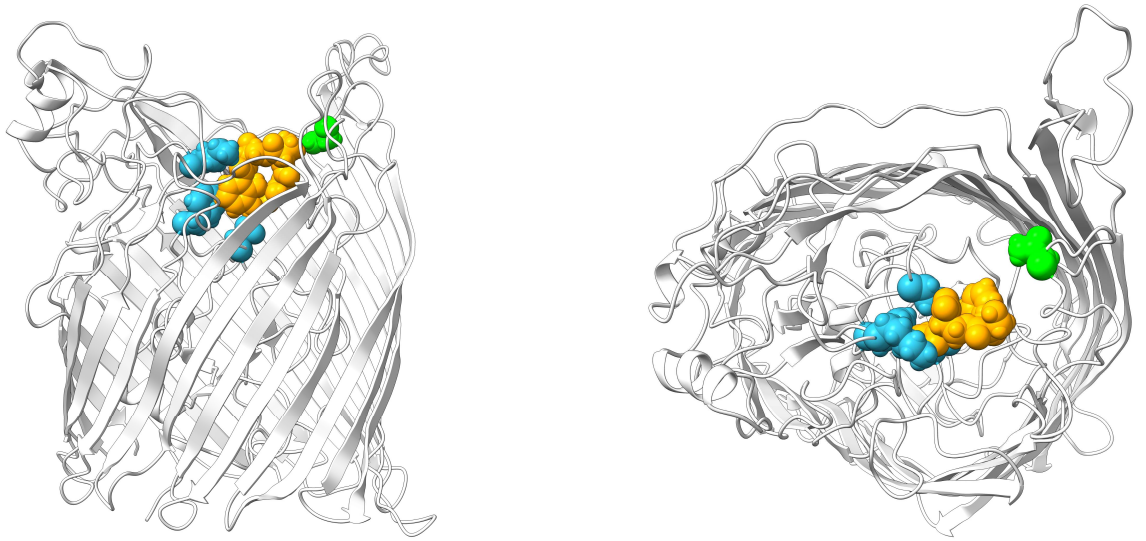
In addition to amino acid residues that participate in the ligand binding, we also observed different conformations of external loops corresponding to each binding state. (Figure 3-6 F, G) Upon the Initial ligand binding to site 1, external loops including loop 7, loop 8 and loop 9 adopted an opened conformation, which allowed the receptor to better capture ligand in the extracellular environment; (Figure 3-6 F) Ligand binding to site 2 resulted in a more closed loop conformation compared to that of site 1. (Figure 3-6 G) This observation led us to believe Fiu adopted a two-step binding model: The opened external loops make it easy for Fiu to capture ligand in environment under iron-deficient condition; Ligand captured in site 1 was then transfer to a deeper region of the beta-barrel, site 2, and was stabilized there via interactions with several amino acid residues, mainly through the cation-pi interaction and hydrogen bond with R142; At this time, the external loops closed up, making site 2 isolated from external environment. The closed loop conformation created an isolated environment for the ligand to be further transferred

across OM and then into cytoplasm without taking non-specific macromolecules. (Figure 3-6 B-C)

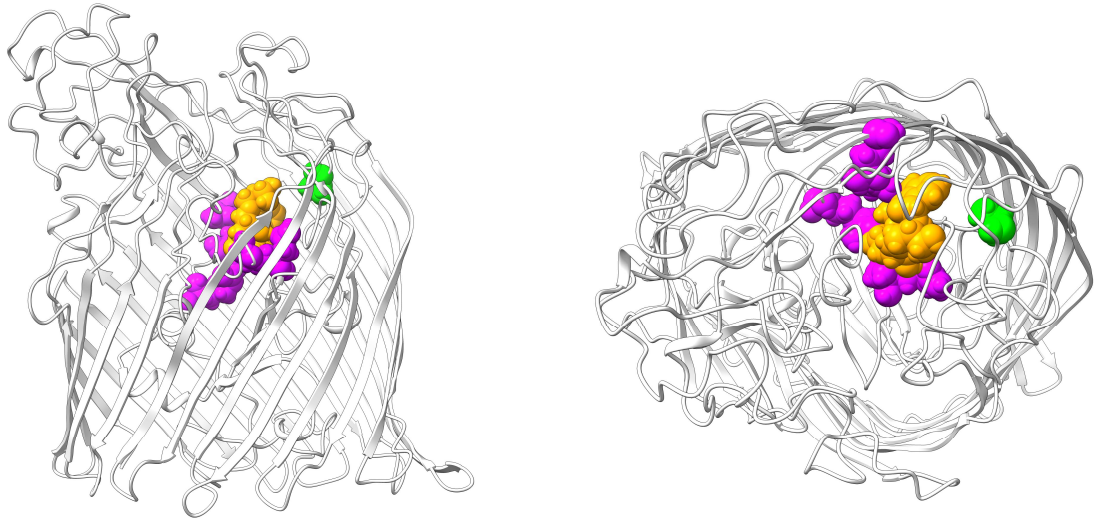
A



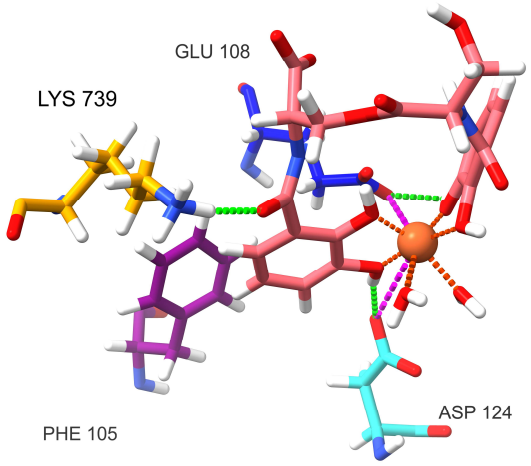
B

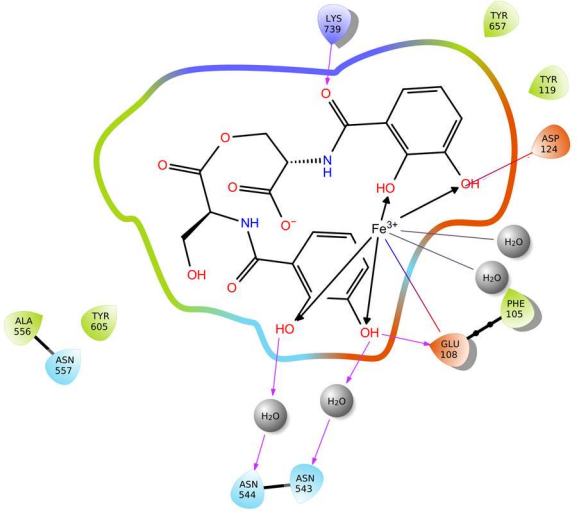


C

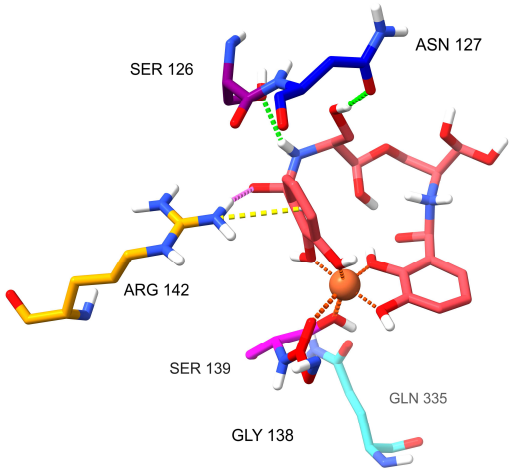


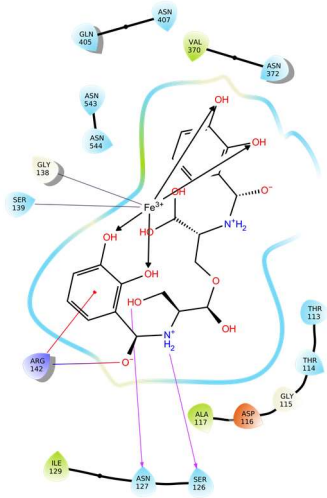
D


GLU 108
LYS 739
ASP 124
PHE 105


LYS 739
TYR 657
TYR 119
ASP 124
PHE 105
GLU 108
ALA 556
TYR 605
ASN 557
ASN 544
ASN 543

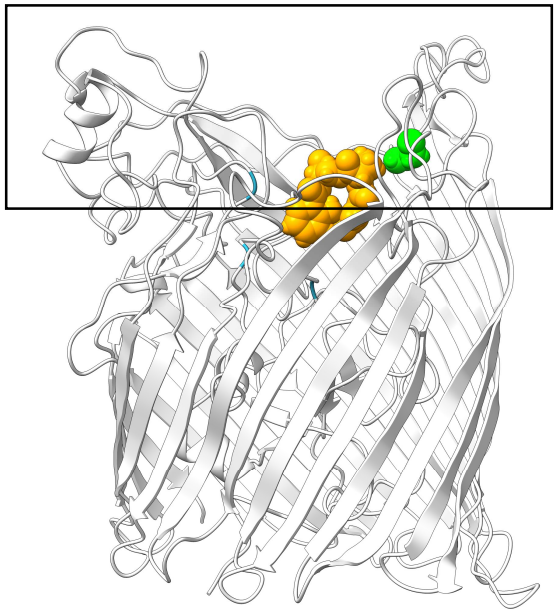
E


SER 126
ASN 127
ARG 142
SER 139
GLN 335
GLY 138


ASN 407
GLN 405
VAL 370
ASN 372
ASN 543
ASN 544
GLY 138
SER 139
THR 113
THR 114
ARG 142
GLY 115
ALA 117
ASP 116
ILE 129
ASN 127
SER 126

F

Opened loop conformation



G

Closed loop conformation

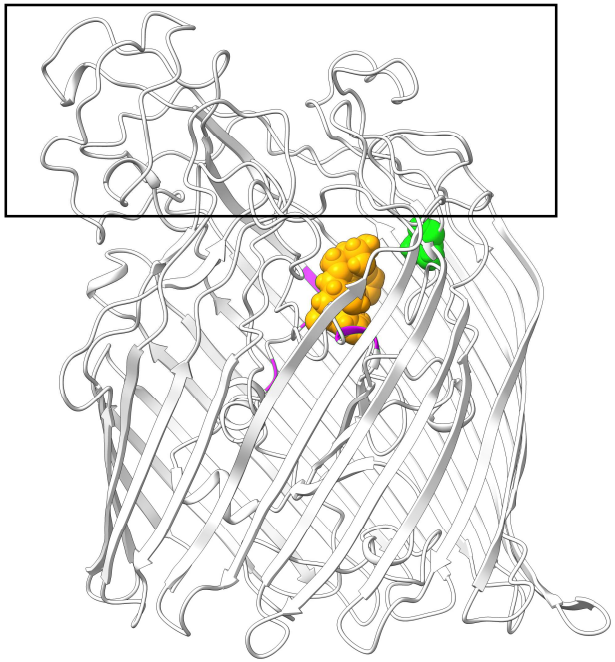


Figure 3-6 Molecular docking and molecular dynamic (MD) simulation.

(A) we performed in silico docking study using AutoDock Vina. The ligand (FeEnt*) and receptor (Fiu PDB 6BPM) files were processed using AutoDock Tool 1.5.6. The program calculated and listed the top 10 binding poses in each search box. We identified two surface binding sites, site 1 (orange) and site 2 (magenta), and site 3 (blue) in the middle of the beta-barrel. (B-C) We performed MD simulation study on the docked models of two surface binding sites using Schrödinger. After 1 microsecond experiment time, FeEnt* was found to be stabilized in both binding site 1 (B) and site 2 (C). Ligand was shown in orange; and cysteine residue in green was used to analyze the binding reaction in each binding site in the following experiment. (D-E) Detailed interactions in binding site 1(D) and site 2 (E) and their corresponding 2D diagrams. (F-G) Different loop conformation observed in different binding states: (F) Opened loop conformation during ligand binding to site 1; (G) Closed loop conformation during ligand binding to site 2.

Analysis of Binding Sites by Site-directed Mutagenesis

To experimentally verify the binding sites assigned via docking and MD simulation, we selected residues in close contact with ligand for site-directed mutagenesis. Residues were selected based on the interactions determined by docking and MD simulation and were mutated to alanine.

To investigate the effect of these single mutations on the binding to ferric siderophores, we engineered fluorescent Fiu sensor by introducing cysteine mutation to the site close to each binding pocket. Cysteine mutation should not affect the binding nor the transport, so selected cysteine residue should not be too close nor too far from each binding site. N554C was engineered to detect the binding reaction in site 1 and A546C was created for site 2. (Figure 3-6 B, C) Cells expressing each mutant were grown in MOPS iron-deficient media. After labeling with fluorescein maleimide, we checked the labelling and expression by running a fluorescent gel. (Figure S3-1) All the mutants were expressed and labeled properly. The binding affinity of each mutant was determined by titration with FeEnt* to increasing concentrations and corresponding fluorescence quenching was measured as described above. Our results revealed that in binding site 1, R142A showed the most weakened binding to FeEnt* (K_D = 2.70 μM), in comparison to the positive control A546C (K_D = 1.02 μM). (Table 3-2; Figure 3-7 A) Other single mutations in binding site 1 had less effect on ligand binding, including S126A (K_D = 1.88 μM), N127A (K_D = 1.58 μM), S139A (K_D = 1.71 μM) and Q335A (K_D = 1.91 μM). (Table 3-2; Figure 3-7 A) In binding site 2, the positive control N554C had a K_D of 0. 90 μM. All the other alanine mutation created in this site showed impaired ligand binding: F105A (K_D = 1.24 μM), E108A (K_D = 1.68 μM), D124A (K_D = 2.46 μM) and K739A (K_D = 1.79 μM). (Figure 3-7 A; Table 3-2)

We then analyzed the effect of these mutations on ligand transport, with OKN359 and OKN359 expressing FiuWT as negative and positive control, respectively. (Figure 3-7 B) The transport was evaluated by the diameter of the growth halo around the paper disc. In binding site 1, R142A abolished the transport and no growth halo was observed with exposure of FeEnt*. Neither S126A, N127A, S139A nor Q335A affected FeEnt* transport, as indicated by similar growth halo to that of FiuWT. (Figure 3-7 B) In binding site 2, every single mutation including F105A, E108A, D124A and K739A significantly affected or abolished the ligand transport. (Figure 3-7 B) F105A significantly impaired the transport as suggested by a much smaller growth halo compared to that of FiuWT, while E108A, D124A and K739CA completely abolished the transport and no growth was observed. (Figure 3-7 B) The diameters of growth halo were listed in Table 3-3.

These results were consistent with MD results: In binding site 1, ferric ion formed initial interactions with F105, E108, D124 and K739 and was coordinated by four oxygen atoms from the siderophore and another two oxygens from water molecules. Siderophore was bound by E108 and D124 via hydrogen bond and a salt bridge, respectively. Mutation of those two residues abolished the transport. (Figure 3-6 D; Figure 3-7 B) Ligand-receptor interaction was further strengthened by K739, and the transport was abolished when the sidechain was mutated; F105 did not form any specific interaction with ligand but non-specific hydrophobic contact, so F105A still reserved some transport. (Figure 3-6 D; Figure 3-7 B) In site 2, two water molecules that coordinating ferric iron in site 1 were replaced by G138 and S139, which could be driven by the conformation change of induced fit; S126 and N127 stabilized the ligand with hydrogen bond; No stable interaction was observed between Q335 and ligand. (Figure 3-6 E; Figure 3-7 B) But the presence of R142 in this binding site renders those interactions nonessential. Mutation of

R142 to alanine completely abolished the transport of the FeEnt*, while other single mutations including S126A, N127A, S139A and Q335A, did not affect transport at all. (Figure 3-7 B) R142A also showed the most weakened binding to the ligand (K_D= 2.70 μM) compared to the positive control N554C (K_D= 0.86 μM) while other mutants showed comparable binding affinities. (Table 3-2; Figure 3-7 A) These results suggested a critical role of R142 in ligand binding and transport. Considering the formation of the most stable T-shape cation-π interaction and a hydrogen bond with siderophore, R142 rendered other residues in this binding site dispensable for ligand binding and uptake. (Figure 3-6 E; Figure 3-7)

To further validate the binding sites, we generated Fiu mutants carrying double mutations, with one in each binding site. According to previous results, F105A, E108A, D124A and K739A in site 1 and R142A in site 2 significantly affected both ligand binding and transport. Thus, we created Fiu mutants with four mutation pairs: R142A-F105A, R142A-E108A, R142A-D124A and R142A-K739A. After checking the expression and fluorescence labeling, we determined their binding affinities by fluorescence quenching assay and characterized the transport by siderophore nutrition test as described previously. All four double mutants significantly impaired binding compared to positive control and single mutants, with a 7 to 22 folds increase in K_D. (Table 3-2; Figure 3-7 A) Besides, no growth halo was observed for those four double mutants, suggested that transport was abolished. (Table 3-2; Figure 3-7 A) Thus, we confirmed those two binding sites via single and double mutagenesis, along with fluorescence quenching and siderophore nutrition test. Those residues played a critical role in ligand recognition, binding and uptake.

Table 3-2 Binding Affinity of Fiu Mutants to FeEnt* (μM)

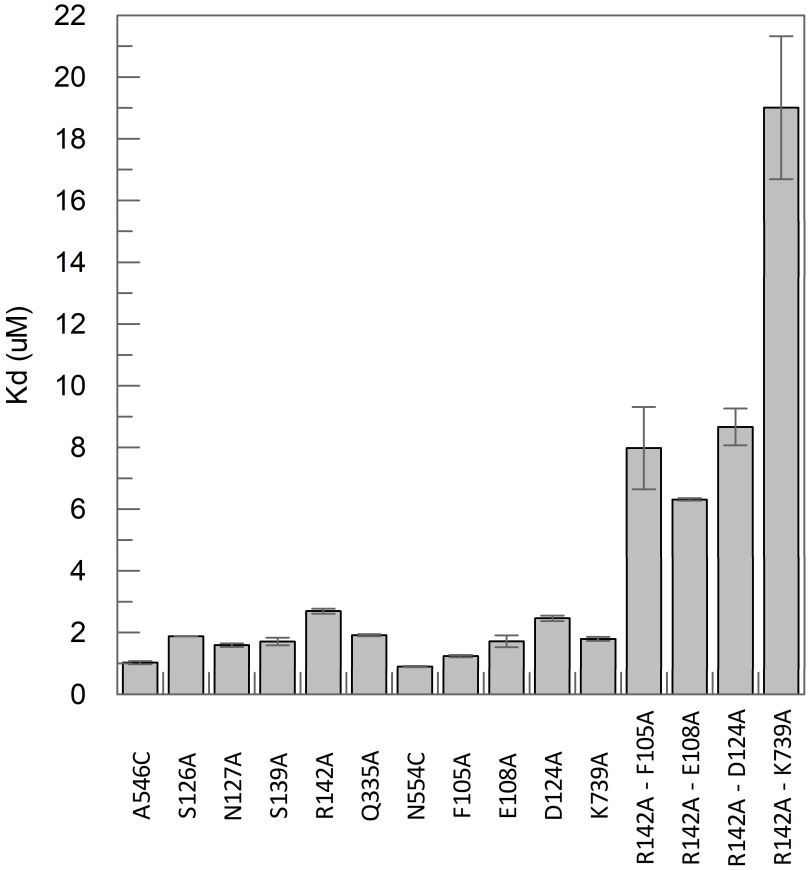
Binding site 1						
Mutation	N554C (+)	F105A	E108A	D124A	K739A	
Affinity K_D (μM)	0.90 ± 0.02	1.24 ± 0.04	1.71 ± 0.19	2.46 ± 0.09	1.80 ± 0.07	
Binding site 2						
Mutation	A546C (+)	S126A	N127A	S139A	R142A	Q335A
Affinity K_D (μM)	1.03 ± 0.05	1.88 ± 0.01	1.59 ± 0.06	1.71 ± 0.12	2.70 ± 0.08	1.91 ± 0.03
Double mutagenesis						
Mutation	A546C (+)	F105A-R142A	E108A-R142A	D124A-R142A	K739A-R142A	
Affinity K_D (μM)	1.03 ± 0.05	7.98 ± 1.33	6.31 ± 0.04	8.66 ± 0.59	19.00 ± 2.32	

Table 3-3 Siderophore nutrition test of Fiu mutants with FeEnt*

Binding site 1							
Mutation	N554C (+)	F105A	E108A	D124A	K739A		
Diameter (nm)	21.00 ± 1.41	9.50 ± 0.71	0	0	0		
Binding site 2							
Mutation	A546C (+)	S126A	N127A	S139A	R142A	Q335A	
Diameter (nm)	20.00 ± 0.50	19.50 ± 0.71	20.50 ± 0.71	19.50 ± 0.71	2.00 ± 0.1 (faint halo)	18.50 ± 0.71	
Double mutagenesis and Control							
Mutation	OKN359 (-)	WT (+)	A546C (+)	F105A-R142A	E108A-R142A	D124A-R142A	K739A-R142A
Diameter (nm)	0.90 ± 0.02	21.50 ± 0.71	20.00 ± 0.50	0	0	0	0

The table listed the diameters of growth halo around the paper disc containing 100 μM of FeEnt*, after incubation at 37 °C for 24 hours.

A


Kd (uM)
0
2
4
6
8
10
12
14
16
18
20
22
A546C
S126A
N127A
S139A
R142A
Q335A
N554C
F105A
E108A
D124A
K739A
R142A - F105A
R142A - E108A
R142A - D124A
R142A - K739A

B

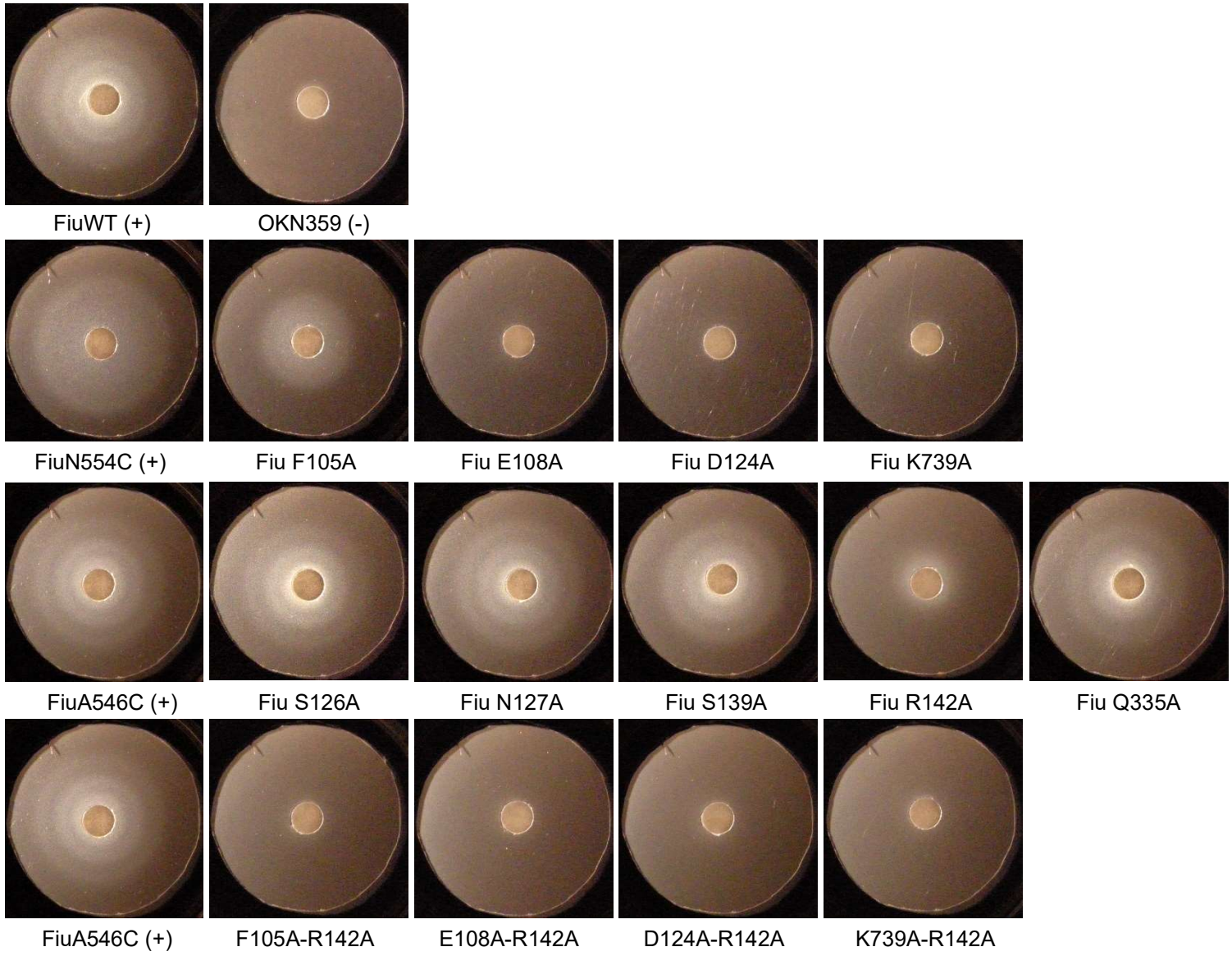

Control
FiuWT (+)
OKN359 (-)
Site-1
FiuN554C (+)
Fiu F105A
Fiu E108A
Fiu D124A
Fiu K739A
Site-2
FiuA546C (+)
Fiu S126A
Fiu N127A
Fiu S139A
Fiu R142A
Fiu Q335A
Double Mutations
FiuA546C (+)
F105A-R142A
E108A-R142A
D124A-R142A
K739A-R142A

Figure 3-7 Characterization of ligand binding and transport by site-directed mutagenesis. We selected residues that participated in the ligand-receptor interactions in MD simulation for alanine mutagenesis. N554 and A546 were mutated to cysteine for the analysis of binding reaction in site 1 site 2, respectively. We expressed Fiu mutants carrying alanine single or double mutation and corresponding cysteine mutation in OKN359 (for transport) or OKN1359 (for binding) cells. (A) We determined the binding affinity of Fiu mutants by fluorescence quenching assay as described previously with FiuN554C and FiuA546C as positive control. (B) We analyzed the transport of FeEnt* catalyzed by Fiu mutants by siderophore nutrition test as described previously, with FiuWT, FiuN554C, FiuA546C as the positive control and OKN359 as the negative control.

Discussion

Bacterial infections have been a long-standing threat to human health. In the 21st century antibiotic-resistant pathogens have been an urgent threat, which is one of the leading cause of deaths. Gram-negative pathogens, especially carbapenem-resistant *Enterobacterales* (CRE) (23,24) and the group of *Enterococcus, Staphylococcus, Klebsiella, Acinetobacter, Pseudomonas,* and *Enterobacter* (ESKAPE) (25,26) pathogens, caused two thirds of bacteria-associated death in U.S. (27) In 2019, CDC reported over 2.8 million infections caused by CRE/ESKAPE and other antibiotic-resistant pathogens each year, with over 35000 deaths in U.S. (1) Iron acquisition has been found to be tightly associated with bacterial pathogenesis and infections. (28-31) Thus, understanding how TonB-dependent receptors bind and capture siderophore ligands is essential to develop new antibiotics targeting iron acquisition system of Gram-negative pathogens.

The natural ligand for Fiu has been unknown for a long time. Fiu was suggested to be the receptor for monomeric catecholate siderophores in early studies, but none of them clearly identified the ligand nor determined its binding affinity (12,14). Few scientific articles about this TonB-dependent LGP were-published since 1990s, until its crystal structure was resolved in 2020 by Grinter *et al* (15). Our study screened and identified for the first time the ligands for Fiu using a fluorescence quenching assay. We engineered FM-labeled Fiu sensors by introducing cysteine to the external loops and labeled them with fluorescein maleimide. Fluorescence quenching resulting from ligand binding allowed us to quantitively analyze the binding reaction of potential ligands to Fiu. Fiu showed binding to several catecholate siderophores, but with different affinities: FeEnt (K_D = 0.95 μM), FeEnt* (K_D = 0.69 μM), FeGEnt (K_D = 0.34 μM), FeDHBA (K_D = 0.68 μM) and FeDHBS with a K_D of 0.1 μM. We are unable to detect binding of

FeDHBA using Fiu A694C sensor, while it showed ligand binding using another sensor FiuN554C, which is closer to the binding site 1. Even though Fiu showed binding to several catecholates, it can only transport FeEnt* under *E. coli* background as suggested by siderophore nutrition test. FeEnt or FeGEnt showed similar binding affinities to that of FeEnt*, but no transport was observed in the siderophore nutrition test. (Figure 3-2) FeEnt* contains two catechol groups, while both FeEnt and FeGEnt consist of three catechol groups. The difference in size and the resulting structure configuration could explain the inconsistent results of binding assay and transport assay: Smaller size and the unique structure configuration made FeEnt* fit to binding sites better, and allowed it to be further transported through the narrow receptor channel; while the large sizes and different structure configurations prevented the transport of FeEnt and FeGEnt through Fiu. Besides, the transport of FeGEnt requires not only a surface OM receptor, but also a periplasmic hydrolase IroE and perhaps the Fes-like IroD, which are absent in *E. coli*. (17) As a result, we only observed the non-specific transport of FeGEnt, which could be mediated by an uncharacterized receptor in *E. coli.*

Understanding the binding mechanism is critical for development of siderophore antibiotics. To determine potential ligand binding sites in Fiu, we performed rigid docking with the FeEnt*. Two binding sites were found in the surface of beta-barrel (binding site 1 and 2). We performed MD simulation with these two docked binding models, which allowed the ligand to interact with the receptor for 1 microsecond. We analyzed ligand-receptor interactions after the system was stable and found ligand was stabilized in both binding sites via interactions with several critical amino acid residues. The MD simulation results were analyzed in combination with site-directed mutagenesis: all the single mutations to alanine at binding site 1 both weakened the binding affinity and the uptake of FeEnt*; The story in binding site 2 is interesting,

single mutations impaired the binding affinity to some extent, while only R142A abolished ligand uptake. According to the results of MD simulation, in addition to hydrogen bond and salt bridge, R142 also formed cation-π interaction through its positively charged side chain with the electron-rich phenol ring. Cation-π interaction is considered as one of the strongest interactions in biological complexation process, especially when the bond angle is closed to 90 °. (32-35) Strong interactions between R142 and ligand make other residues dispensable in binding site 2, which may just provide some support interactions for ligand stabilization. Double mutagenesis further confirmed those two binding sites: combined alanine mutation in each binding site significantly weakened the binding affinity (as much as 23 folds) and completely abolished ligand transport. F105A, E108A, D124A, K739A and R142A played important roles in the recognition and transport of ligand, which may serve as potential targets for the development of antibiotics targeting Fiu.

We also observed Fiu adopted different loop conformations in different binding states: Upon ligand binding to site 1, Fiu adopts an opened loop conformation, including loop 7, loop 8 and loop 9; while when ligand binds to site 2, the overall loop conformation is closed, creating an isolated environment. The closed loop conformation (29-31) allowed the ligand to be further transferred inside the beta-barrel without internalizing non-specific large molecules.

Those results revealed a two-step binding model of Fiu to capture ligand from environment: the open loop conformation allows Fiu to capture siderophore ligand more easily, via the interactions with F105, E108, D124 and K739; at this binding state, ferric iron of FeEnt* was still coordinated with two water molecules to form hexa-coordinated conformation, indicating the initial binding state. When the ligand is stabilized in binding site 1, it is then further relocated inside the beta-barrel to binding site 2. At this binding state, external loops start

to close, occluding other large molecules from the binding site during the transport of ligand across OM through its channel. We noticed Grinter *et al* also mentioned a two-step binding model of Fiu which is different than what we proposed here. They identified two binding sites based on their docking results: one was located in the top region, corresponding to binding site 2 in our study, another was in the middle of the beta-barrel, corresponding to binding site 3 that we identified. In addition to Fiu, FepA was also suggested to adopt a two-step ligand binding in an early study. (81) Using a fluorescent derivative, they found that FepA bound to FeEnt and Colicin B with biphasic kinetics, an initial rapid binding followed by a slower secondary binding, corresponding to ligand binding to site 1 and site 2 in Fiu, respectively. (81) Using a different method, our study showed that TonB-dependent receptor could adopt a two-step model for ligand binding, which agreed with the previous study of FepA. Last, our research only focused on the initial surface binding, which was critical for ligand recognition and thus drug development. We were also able to analyze the interactions in the surface binding sites quantitively using FM-labeled sensor we engineered.

Iron acquisition has been found critical for bacterial pathogenesis (29-31): pathogens develop biosynthetic and transport systems to obtain iron from the host, which is essential for their survival and infections in the host (36-49); Disruption of iron acquisition system in the pathogens leads to reduced virulence (50-58) Siderophore antibiotics have been developed soon after researchers realized their clinical potential (59-72). Cefiderocol (FDC) the catecholate-cephalosporin conjugate, is the first antibiotic conjugate (Trojan Horse antibiotic) licensed by FDA, for the treatment of infections caused by antibiotic-resistant Gram-negative bacteria like carbapenem-resistant *A.baumannii* and *P. aeruginosa* (73-78). The approval of Cefiderocol showed the clinical potential of antibiotics targeting iron acquisition pathway and understanding

the binding mechanism is critical for drug design. Research has shown that the uptake of FDC is mediated by combination of Fiu-Cir or PiuA-PirA (75,79,80). Our research filled out the blank of one of the major OM iron receptors in Gram-negative bacteria, but also gained insight into the binding mechanisms, which provides molecular basis for the development of siderophore antibiotics targeting Fiu

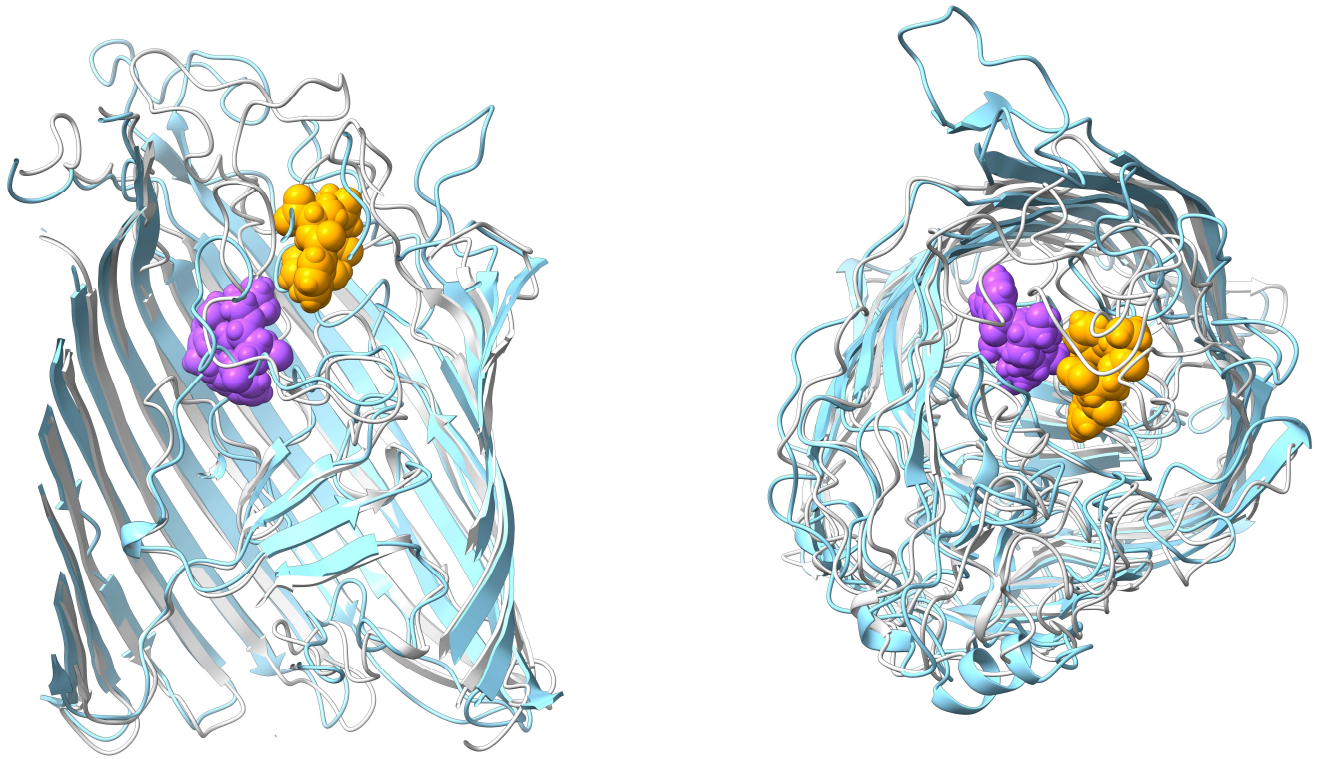


Figure 3-8 Superimposed structure of two ligand binding models.

We superimposed the structure of two ligand binding model calculated by MD simulation using ChimeraX 1.3. Structure of binding model 1 is shown in light blue with binding site 1 in orange. Structure of binding model 2 is shown in silver with binding site two in purple. We proposed a two-step binding model for Fiu to capture ligand from extracellular environment: ligand was captured and stabilized in site 1 with opened loop conformation; Ligand was transferred to and stabilized in site 2 with a closed loop conformation.

Reference

1. Control, C. f. D., and Prevention. (2020) Antibiotic resistance threats in the United States. US Department of Health and Human Services., 2019.
2. Neilands, J. (1974) Iron and its role in microbial physiology. in *Microbial iron metabolism*, Elsevier. pp 3-34
3. Wish, J. B. (2006) Assessing iron status: beyond serum ferritin and transferrin saturation. *Clinical Journal of the American Society of Nephrology* **1**, S4-S8
4. Noinaj, N., Guillier, M., Barnard, T. J., and Buchanan, S. K. (2010) TonB-dependent transporters: regulation, structure, and function. *Annual review of microbiology* **64**, 43-60
5. Harris, W. R., Carrano, C. J., Cooper, S. R., Sofen, S. R., Avdeef, A. E., McArdle, J. V., and Raymond, K. N. (1979) Coordination chemistry of microbial iron transport compounds. 19. Stability constants and electrochemical behavior of ferric enterobactin and model complexes. *Journal of the American Chemical Society* **101**, 6097-6104
6. Neilands, J. B. (1995) Siderophores: structure and function of microbial iron transport compounds. *J Biol Chem* **270**, 26723-26726
7. Rutz, J. M., Liu, J., Lyons, J. A., Goranson, J., Armstrong, S. K., McIntosh, M. A., Feix, J. B., and Klebba, P. E. (1992) Formation of a gated channel by a ligand-specific transport protein in the bacterial outer membrane. *Science* **258**, 471-475
8. Schauer, K., Rodionov, D. A., and de Reuse, H. (2008) New substrates for TonB-dependent transport: do we only see the 'tip of the iceberg'? *Trends in biochemical sciences* **33**, 330-338
9. Guerinot, M. L. (1994) Microbial iron transport. *Annual review of microbiology* **48**, 743-772
10. Cornelis, P. (2010) Iron uptake and metabolism in pseudomonads. *Appl Microbiol Biotechnol* **86**, 1637-1645
11. Klebba, P. E., Newton, S. M., Six, D. A., Kumar, A., Yang, T., Nairn, B. L., Munger, C., and Chakravorty, S. (2021) Iron acquisition systems of gram-negative bacterial pathogens define TonB-dependent pathways to novel antibiotics. *Chemical reviews* **121**, 5193-5239
12. Hantke, K. (1990) Dihydroxybenzolyserine—a siderophore for E. coli. *FEMS Microbiology Letters* **67**, 5-8
13. Curtis, N., Eisenstadt, R. L., East, S. J., Cornford, R. J., Walker, L. A., and White, A. J. (1988) Iron-regulated outer membrane proteins of Escherichia coli K-12 and mechanism of action of catechol-substituted cephalosporins. *Antimicrobial agents and chemotherapy* **32**, 1879-1886
14. Nikaido, H., and Rosenberg, E. Y. (1990) Cir and Fiu proteins in the outer membrane of Escherichia coli catalyze transport of monomeric catechols: study with beta-lactam antibiotics containing catechol and analogous groups. *J Bacteriol* **172**, 1361-1367

15. Grinter, R., and Lithgow, T. (2019) The structure of the bacterial iron–catecholate transporter Fiu suggests that it imports substrates via a two-step mechanism. *Journal of Biological Chemistry* **294**, 19523-19534
16. Majumdar, A., Trinh, V., Moore, K. J., Smallwood, C. R., Kumar, A., Yang, T., Scott, D. C., Long, N. J., Newton, S. M., and Klebba, P. E. (2020) Conformational rearrangements in the N-domain of Escherichia coli FepA during ferric enterobactin transport. *Journal of Biological Chemistry* **295**, 4974-4984
17. Hantke, K., Nicholson, G., Rabsch, W., and Winkelmann, G. (2003) Salmochelins, siderophores of Salmonella enterica and uropathogenic Escherichia coli strains, are recognized by the outer membrane receptor IroN. *Proceedings of the National Academy of Sciences* **100**, 3677-3682
18. Williams, P., Rabsch, W., Methner, U., Voigt, W., Tschäpe, H., and Reissbrodt, R. (2006) Catecholate receptor proteins in Salmonella enterica: role in virulence and implications for vaccine development. *Vaccine* **24**, 3840-3844
19. Caza, M., Lépine, F., Milot, S., and Dozois, C. M. (2008) Specific roles of the iroBCDEN genes in virulence of an avian pathogenic Escherichia coli O78 strain and in production of salmochelins. *Infection and immunity* **76**, 3539-3549
20. Bachman, M. A., Lenio, S., Schmidt, L., Oyler, J. E., and Weiser, J. N. (2012) Interaction of lipocalin 2, transferrin, and siderophores determines the replicative niche of Klebsiella pneumoniae during pneumonia. *MBio* **3**, e00224-00211
21. Lee, I. R., Molton, J. S., Wyres, K. L., Gorrie, C., Wong, J., Hoh, C. H., Teo, J., Kalimuddin, S., Lye, D. C., and Archuleta, S. (2016) Differential host susceptibility and bacterial virulence factors driving Klebsiella liver abscess in an ethnically diverse population. *Scientific reports* **6**, 1-12
22. Nikaido, H., and Rosenberg, E. Y. (1990) Cir and Fiu proteins in the outer membrane of Escherichia coli catalyze transport of monomeric catechols: study with beta-lactam antibiotics containing catechol and analogous groups. *Journal of bacteriology* **172**, 1361-1367
23. Perez, F., and Van Duin, D. (2013) Carbapenem-resistant Enterobacteriaceae: a menace to our most vulnerable patients. *Cleveland Clinic journal of medicine* **80**, 225
24. Smith, H. Z., and Kendall, B. (2021) Carbapenem Resistant Enterobacteriaceae. in *StatPearls [Internet]*, StatPearls Publishing. pp
25. Rice, L. B. (2008) Federal funding for the study of antimicrobial resistance in nosocomial pathogens: no ESKAPE. The University of Chicago Press
26. Boucher, H. W., Talbot, G. H., Bradley, J. S., Edwards, J. E., Gilbert, D., Rice, L. B., Scheld, M., Spellberg, B., and Bartlett, J. (2009) Bad bugs, no drugs: no ESKAPE! An update from the Infectious Diseases Society of America. *Clinical infectious diseases* **48**, 1-12

27. Elemam, A., Rahimian, J., and Mandell, W. (2009) Infection with panresistant Klebsiella pneumoniae: a report of 2 cases and a brief review of the literature. *Clinical infectious diseases* **49**, 271-274
28. Griffiths, E., Rogers, H. J., and Bullen, J. (1980) Iron, plasmids and infection. *Nature* **284**, 508-509
29. Bullen, J. (1981) The significance of iron in infection. *Reviews of infectious diseases* **3**, 1127-1138
30. Bullen, J. (1985) Iron and infection. Springer
31. Bullen, J., Griffiths, E., Rogers, H., and Ward, G. (2000) Sepsis: the critical role of iron. *Microbes and infection* **2**, 409-415
32. Nishio, M., Hirota, M., and Umezawa, Y. (1998) *The CH/π interaction: evidence, nature, and consequences*, John Wiley & Sons
33. Anslyn, E. V., and Dougherty, D. A. (2006) *Modern physical organic chemistry*, University science books
34. Doonan, C. J., Morris, W., Furukawa, H., and Yaghi, O. M. (2009) Isoreticular metalation of metal− organic frameworks. *Journal of the American Chemical Society* **131**, 9492-9493
35. Marshall, M. S., Steele, R. P., Thanthiriwatte, K. S., and Sherrill, C. D. (2009) Potential energy curves for cation− π interactions: off-axis configurations are also attractive. *The Journal of Physical Chemistry A* **113**, 13628-13632
36. Williams, P. H. (1979) Novel iron uptake system specified by ColV plasmids: an important component in the virulence of invasive strains of Escherichia coli. *Infection and Immunity* **26**, 925-932
37. Payne, S. M., and Neilands, I. (1988) Iron and virulence in the family Enterobacteriaceae. *CRC Critical reviews in microbiology* **16**, 81-111
38. Payne, S. (1989) Iron and virulence in Shigella. *Molecular microbiology* **3**, 1301-1306
39. Payne, S. M. (1993) Iron acquisition in microbial pathogenesis. *Trends in microbiology* **1**, 66-69
40. Stojijkovic, I., Hwa, V., de Saint Martin, L., O'Gaora, P., Nassif, X., Heffron, F., and So, M. (1995) The Neisseria meningitidis haemoglobin receptor: its role in iron utilization and virulence. *Molecular microbiology* **15**, 531-541
41. Dhople, A. M., Ibanez, M. A., and Poirier, T. C. (1996) Role of iron in the pathogenesis of Mycobacterium avium infection in mice. *Microbios* **87**, 77-87
42. Wong, H.-c., Liu, C.-C., Yu, C.-M., and Lee, Y.-S. (1996) Utilization of iron sources and its possible roles in the pathogenesis of Vibrio parahaemolyticus. *Microbiology and immunology* **40**, 791-798
43. STURM, W. A. (1997) Iron and Virulence ofHaemophilus ducreyiin a Primate Model. *Sexually transmitted diseases* **24**, 64-68
44. Zhou, D., Hardt, W.-D., and Galán, J. E. (1999) Salmonella typhimurium encodes a putative iron transport system within the centisome 63 pathogenicity island. *Infection and immunity* **67**, 1974-1981

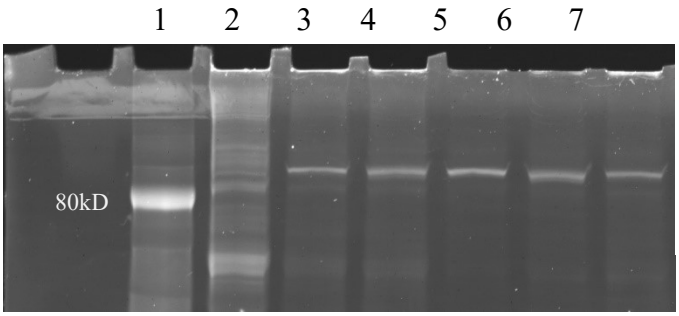
45. Torres, A. G., Redford, P., Welch, R. A., and Payne, S. M. (2001) TonB-dependent systems of uropathogenic Escherichia coli: aerobactin and heme transport and TonB are required for virulence in the mouse. *Infection and immunity* **69**, 6179-6185
46. Schoolnik, G. K. (2002) Microarray analysis of bacterial pathogenicity.
47. Snyder, J. A., Haugen, B. J., Buckles, E. L., Lockatell, C. V., Johnson, D. E., Donnenberg, M. S., Welch, R. A., and Mobley, H. L. (2004) Transcriptome of uropathogenic Escherichia coli during urinary tract infection. *Infection and immunity* **72**, 6373-6381
48. Buckling, A., Harrison, F., Vos, M., Brockhurst, M. A., Gardner, A., West, S. A., and Griffin, A. (2007) Siderophore-mediated cooperation and virulence in Pseudomonas aeruginosa. *FEMS microbiology ecology* **62**, 135-141
49. Smith, K. D. (2007) Iron metabolism at the host pathogen interface: lipocalin 2 and the pathogen-associated iroA gene cluster. *The international journal of biochemistry & cell biology* **39**, 1776-1780
50. Gregory, E. M., Yost Jr, F. J., and Fridovich, I. (1973) Superoxide dismutases of Escherichia coli: intracellular localization and functions. *Journal of Bacteriology* **115**, 987-991
51. Tai, S. S., Lee, C.-J., and Winter, R. (1993) Hemin utilization is related to virulence of Streptococcus pneumoniae. *Infection and immunity* **61**, 5401-5405
52. Cornelissen, C. N., and Sparling, P. F. (1994) Iron piracy: acquisition of transferrin-bound iron by bacterial pathogens. *Molecular microbiology* **14**, 843-850
53. Furman, M., Fica, A., Saxena, M., Di Fabio, J. L., and Cabello, F. C. (1994) Salmonella typhi iron uptake mutants are attenuated in mice. *Infection and immunity* **62**, 4091-4094
54. Rouquette, C., Bolla, J.-m., and Berche, P. (1995) An iron-dependent mutant of Listeria monocytogenes of attenuated virulence. *FEMS microbiology letters* **133**, 77-83
55. Conte, M. P., Longhi, C., Polidoro, M., Petrone, G., Buonfiglio, V., Di Santo, S., Papi, E., Seganti, L., Visca, P., and Valenti, P. (1996) Iron availability affects entry of Listeria monocytogenes into the enterocytelike cell line Caco-2. *Infection and immunity* **64**, 3925-3929
56. Tsolis, R. M., Bäumler, A. J., Heffron, F., and Stojiljkovic, I. (1996) Contribution of TonB- and Feo-mediated iron uptake to growth of Salmonella typhimurium in the mouse. *Infection and immunity* **64**, 4549-4556
57. Ward, C. G., Bullen, J., and Rogers, H. J. (1996) Iron and infection: New development and their implications. *Journal of Trauma and Acute Care Surgery* **41**, 356-364
58. Rozalska, B., Lisiecki, P., Sadowska, B., Mikucki, J., and Rudnicka, W. (1998) The virulence of Staphylococcus aureus isolates differing by siderophore production. *Acta Microbiologica Polonica* **47**, 185-194
59. Heilmeyer, L., and Woehler, F. (1962) Modern problems of hemochromatosis with special reference to desferrioxamine treatment. *Deutsche medizinische Wochenschrift (1946)* **87**, 2661-2667

60. Risell, E., and Schnack, H. (1962) Experiences with a new iron compound, desferrioxamine. *Wiener klinische Wochenschrift* **74**, 577-580
61. Tripod, J., and Keberle, H. (1962) Biological assay with desferrioxamine. *Helvetica physiologica et pharmacologica acta* **20**, 291-293
62. COULTON, J. W., NAEGELI, H. U., and BRAUN, V. (1979) Iron Supply of Escherichia coli with Polymer-Bound Ferricrocin. *European Journal of Biochemistry* **99**, 39-47
63. Rogers, H. J., Synge, C., and Woods, V. E. (1980) Antibacterial effect of scandium and indium complexes of enterochelin on Klebsiella pneumoniae. *Antimicrobial Agents and Chemotherapy* **18**, 63-68
64. PLAHA, D. S., ROGERS, H. J., and WILLIAMS, G. W. (1984) Studies of the antibacterial effect of the scandium complex of enterochelin. *The Journal of antibiotics* **37**, 588-595
65. BASKER, M. J., BRANCH, C. L., FINCH, S. C., Guest, A. W., MILNER, P. H., PEARSON, M. J., PONSFORD, R. J., and SMALE, T. C. (1986) STUDIES ON SEMI-SYNTHETIC 7α-FORMAMIDOCEPHALOSPORINS I. STRUCTURE-ACTIVITY RELATIONSHIPS IN SOME SEMI-SYNTHETIC 7α-FORMAMIDOCEPHALOSPORINS. *The Journal of Antibiotics* **39**, 1788-1791
66. BURTON, G., BEST, D. J., DIXON, R. A., KENYON, R. F., and LASHFORD, A. G. (1986) STUDIES ON 6α-SUBSTITUTED PENICILLINS II. SYNTHESIS AND STRUCTURE-ACTIVITY RELATIONSHIPS OF 6β-(2-ARYL-2-SULFOACETAMIDO)-6α-METHOXY PENICILLANIC ACIDS. *The Journal of Antibiotics* **39**, 1419-1429
67. OHI, N., AOKI, B., SHINOZAKI, T., MORO, K., NOTO, T., NEHASHI, T., OKAZAKI, H., and MATSUNAGA, I. (1986) Semisynthetic β-lactam antibiotics I. Synthesis and antibacterial activity of new ureidopenicillin derivatives having catechol moieties. *The Journal of Antibiotics* **39**, 230-241
68. Labott, S. M., and Martin, R. B. (1987) The stress-moderating effects of weeping and humor. *Journal of Human Stress* **13**, 159-164
69. Nakagawa, S., Sanada, M., Matsuda, K., Hazumi, N., and Tanaka, N. (1987) Biological activity of BO-1236, a new antipseudomonal cephalosporin. *Antimicrobial agents and chemotherapy* **31**, 1100-1105
70. Watanabe, N., Nagasu, T., Katsu, K., and Kitoh, K. (1987) E-0702, a new cephalosporin, is incorporated into Escherichia coli cells via the tonB-dependent iron transport system. *Antimicrobial agents and chemotherapy* **31**, 497-504
71. Miller, M. J., McKee, J. A., Minnick, A. A., and Dolence, E. K. (1991) The design, synthesis and study of siderophore-antibiotic conjugates Siderophore mediated drug transport. *Biology of metals* **4**, 62-69
72. Carpenter, C., and Payne, S. M. (2014) Regulation of iron transport systems in Enterobacteriaceae in response to oxygen and iron availability. *Journal of inorganic biochemistry* **133**, 110-117

73. Lugtenberg, B., Meijers, J., Peters, R., van der Hoek, P., and van Alphen, L. (1975) Electrophoretic resolution of the 'major outer membrane protein'of Escherichia coli K12 into four bands. *FEBS letters* **58**, 254-258
74. Ito, A., Nishikawa, T., Matsumoto, S., Yoshizawa, H., Sato, T., Nakamura, R., Tsuji, M., and Yamano, Y. (2016) Siderophore cephalosporin cefiderocol utilizes ferric iron transporter systems for antibacterial activity against Pseudomonas aeruginosa. *Antimicrobial agents and chemotherapy* **60**, 7396-7401
75. Ito, A., Sato, T., Ota, M., Takemura, M., Nishikawa, T., Toba, S., Kohira, N., Miyagawa, S., Ishibashi, N., and Matsumoto, S. (2018) In vitro antibacterial properties of cefiderocol, a novel siderophore cephalosporin, against Gram-negative bacteria. *Antimicrobial agents and chemotherapy* **62**, e01454-01417
76. Yamano, Y. (2019) In vitro activity of cefiderocol against a broad range of clinically important Gram-negative bacteria. *Clinical Infectious Diseases* **69**, S544-S551
77. Shields, R. K. (2020) Case commentary: the need for cefiderocol is clear, but are the supporting clinical data? *Antimicrobial Agents and Chemotherapy* **64**, e00059-00020
78. Wu, J. Y., Srinivas, P., and Pogue, J. M. (2020) Cefiderocol: a novel agent for the management of multidrug-resistant Gram-negative organisms. *Infectious diseases and therapy* **9**, 17-40
79. Kim, A., Kutschke, A., Ehmann, D. E., Patey, S. A., Crandon, J. L., Gorseth, E., Miller, A. A., McLaughlin, R. E., Blinn, C. M., and Chen, A. (2015) Pharmacodynamic profiling of a siderophore-conjugated monocarbam in Pseudomonas aeruginosa: assessing the risk for resistance and attenuated efficacy. *Antimicrobial agents and chemotherapy* **59**, 7743-7752
80. Luscher, A., Moynié, L., Auguste, P. S., Bumann, D., Mazza, L., Pletzer, D., Naismith, J. H., and Köhler, T. (2018) TonB-dependent receptor repertoire of Pseudomonas aeruginosa for uptake of siderophore-drug conjugates. *Antimicrobial agents and chemotherapy* **62**, e00097-00018
81. Payne, M. A., Igo, J. D., Cao, Z., Foster, S. B., Newton, S. M., and Klebba, P. E. (1997) Biphasic binding kinetics between FepA and its ligands. *Journal of Biological Chemistry* 272, 21950-21955

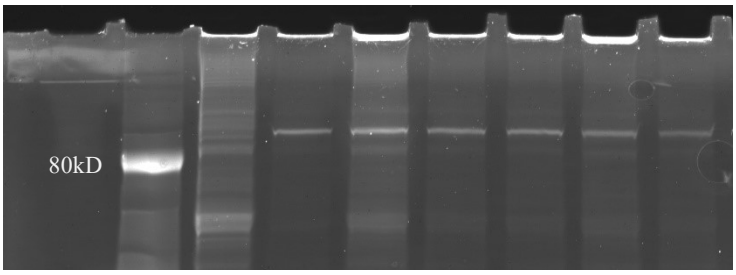
Supplementary Materials

A



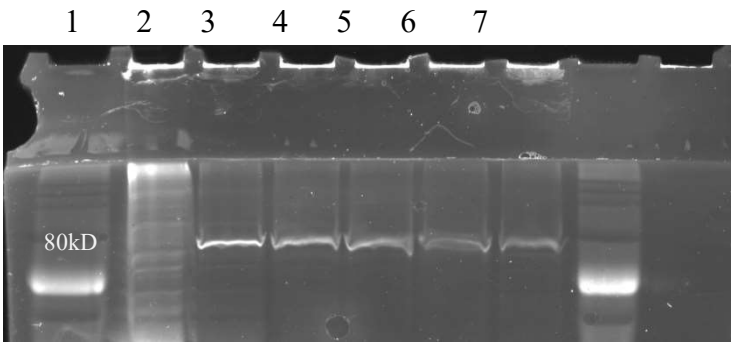
1 Ladder
2 OKN1359/pFiuWT
3 ‘’ /pFiuN554C
4 ‘’ /pFiuF105A
5 ‘’ /pFiuE108A
6 ‘’ /pFiuD124A
7 ‘’ /pFiuK739A

B



1 Ladder
2 OKN1359/pFiuWT
3 ‘’ /pFiuA546C
4 ‘’ /pFiuS126A
5 ‘’ /pFiuN127A
6 ‘’ /pFiuS139A
7 ‘’ /pFiuR142A
8 ‘’ /pFiuQ335A

C



1 Ladder
2 OKN1359/pFiuWT
3 ‘’ /pFiuA546C
4 ‘’ /pFiuF105A-R142A
5 ‘’ /pFiuE108A-R142A
6 ‘’ /pFiuD124A-R142A
7 ‘’ /pFiuK739A-R142A

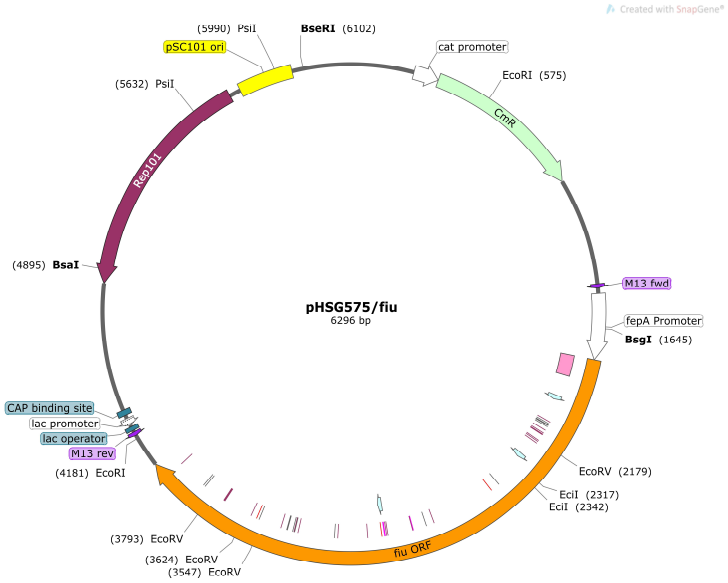


Figure S3-1 Fluorescent gel of EcoFiu Mutants. We expressed Fiu alanine mutants into OKN1359, grew them in MOPS medium and labeled them with FM. We characterized the protein expression and labeling reaction by SDS-PAGE. The gel was observed under UV light. FM-labeled OM protein showed the fluorescent band. (A) Ala mutants in binding site 1. (B) Ala mutants in binding site 2. (C) Double mutants. (D) Clone map of EcoFiu

Chapter 4 Fluorescent Sensors of Siderophores Produced by Bacterial Pathogens

Introduction

Siderophores capture trace iron not only from solution but also from host iron binding proteins, forming ferric siderophore complexes. (1-15) Bacteria then internalize the ferric siderophores through outer membrane receptors (16) in the Gram-negative pathogens. (17-22) Since the uptake of ferric siderophores is energized by the inner membrane-anchored protein TonB, the OM receptor family is called TonB-dependent transporter (TBDT). (9,10,12,13,20) They are also referred to as the ligand-gated porins (LGP) (4), as the ligand binding triggers the opening of the closed transmembrane barrels consisting of 22 beta strands. (6,12) Human innate immune system secretes siderocalin (SCN) upon bacterial infection. SCN binds and captures ferric siderophores at a high binding affinity, restricting the TonB-dependent iron acquisition by Gram-negative pathogens, and thus limiting their proliferation in the host. (23,24)

The synthesis and utilization of specific siderophores were found to promote bacterial pathogenesis in the host. (15,18,25,26) The biosynthesis of yersiniabactin (Ybt) by *Y. pestis* promoted the development of pneumonic and bubonic plague. (21,22) The production and utilization of Aerobactin (27) enhanced the virulence of a variety Gram-negative bacterium *like E. coli* CP9, *K. pnemoniae.* (28-33) Additionally,-production of acinetobactin showed a virulence-enhancing effect specifically to *A. baumannii.* (34) Another example, the elaboration of GEnt allowed *K. pneumoniae* and other pathogenic bacteria to evade the innate immune system by escaping sequestration by SCN) (35-43) To understand the complicated dynamics between the elaboration of siderophore and bacterial pathogenesis, we engineered sensors of both apo- and ferric siderophores. LGPs were chemically modified and were expressed in a

transport-deficient *E. coli* system, generating fluorescent decoy sensors (44)With the engineered fluorescent LGPs, we determined their specificities and preferences among a variety of siderophores. We further extended this technique to the detection of siderophore biosynthesis as well as siderophore transport by pathogenic bacteria.

Results

Engineering of Decoy Sensors for Siderophores

We created 18 fluorescent LGP sensors for the detection of various ferric siderophores: catecholate siderophore included enterobactin (Ent), degraded enterobaction (Ent*), glucosylated enterobactin (GEnt), dihydroxybenzoic acid (DHBA), dihydroxybenzoyl serine (DHBS) and two siderophore antibiotics, cefidericol (FDC) (45,46) and MB-1 (47,48); hydroxymate siderophore included ferrichrome (Fc), ferrichrome A (FcA), (27), ferrioxamine B (FxB). Mixed chelation types included-yersiniabactin (Ybt) , pyoverdine (Pvd), acinetobactin (Acn), anguibactin (Agn). The fluorescent LGPs included EcoFepA, EcoFiu, EcoCir, EcoIutA, EcoFhuA, EcoBtuB derived from *E. coli*; KpnIroN, KpnFyuA and three KpnFepA variants (FepA1658, FepA2380, FepA4984) derived from *K. pneumoniae*; AbaPirA, AbaPiuA, AbaFepA and AbaBauA derived from *A. baumannii*; PaeFpvA and PaeFepA derived from *Pseudomonas. aeruginosa*; CcrHutA derived from *Caulobacter crescentus*. We also fluorescently labeled two siderophore binding proteins: siderocalin (HasSCN) from human, and periplasmic binding protein EcoFepB from *E. coli*. My work in this research includes cloning and characterization of EcoFiu, EcoCir, AbaPirA, KpnFyuA and PaeFpvA. These results will be discussed in detail in this chapter.

We PCR-amplified the structural gene of LGPs and cloned them in vector pSHG575, a low-copy plasmid to avoid overexpression of LGP in OM. (49-51) We confirmed the expression of LGPs in OM and sequencing-verified the clones. Next, we modified the receptor by

introducing cysteine residue to the external loop that is exposed to the extracellular environment. After verification by DNA sequencing, we expressed the cysteine mutants in *E. coli* OKN1359 (ΔTonB ΔfepA ΔCir ΔFiu) with a blank OM background. In the absence of TonB, those LGPs can only bind but cannot transport siderophore ligands, making them "decoy" cell sensors. Cells were incubated with fluorescein maleimide (FM) and a designated cysteine residue in the external loops of each LGP was specifically labeled. (52) We then analyzed their fluorescence labeling and quenching during ligand binding. Expression of fluorescent LGPs derived from pathogenic bacteria in nonpathogenic *E. coli* allows high-level FM labeling, due to the lack of capsule or LPS O-antigen. For each LGP, we selected several candidate residues in the external loop for cysteine mutagenesis. Depending on the location, cysteine mutants of some LGP showed different fluorescence labeling and quenching. For each fluorescent LGP, we chose the most accessible and sensitive site for FM-labeling and ligand binding for the affinity determination of relevant ferric siderophores.

Binding Promiscuity of LGPs

With the engineered fluorescent LGPs, we screened and analyzed their specificities for relevant apo- or iron-complexed siderophores. FM-labeled LGPs were titrated with increasing concentrations of siderophore ligand. Ligand binding to corresponding fluorescent LGP induced conformational changes, which quenched the fluorophore attached to designated cysteine residues. As a result, we observed fluorescence quenching upon each binding reaction. We correlated the fluorescence quenching with corresponding ligand concentrations, constructed binding curves and determined the binding affinities. KpnFyuA showed an extremely high binding affinity to FeYbt (KD = 1.3 nM), which allows it to capture FeYbt at nanomolar concentrations. (Table 4-1; Figure 4-5) The high binding affinity may suggest potential

exclusivity of FyuA in binding reactions. But in addition to FeYbt, KpnFyuA also showed considerable binding affinity to apoYbt (KD = 100 nM). (Table 4-1; Figure 4-5) Similar results were also observed in other LGPs: FepA variants (EcoFepA, KpnFepA1658, PaeFepA, KpnFepA4984, AbaFepA, and KpnIroN), EcoFhuA, EcoIutA. Those LGPs bound apo-siderophore ligand with 60 ~ 200 folds lower affinity compared to corresponding ferric siderophore. (Table 4-1)

FeEnt is subjected to spontaneous degradation, producing tri-, di-, and mono catecholates. We purified the degradation product (FeEnt*) from FeEnt solution by Sephadex LH20 chromatography. In addition, FeEnt can be modified by the addition of two glucose groups to form glucosylated FeEnt. We characterized the interactions of these catecholate siderophores with the engineered fluorescent LGPs. Specificities of orthologous LGP pairs showed both difference and correspondence in ligand recognition. EcoFiu and AbaPiuA shared 31% identity in sequence. They both showed overall low binding affinities to siderophore ligands (0.1 ~ 12 μM), but with different preferences (Table 4-1; Figure 4-1):

EcoFiu: FeDHBS > FeGEnt > FeEnt* > FeFDC > FeEnt ≈ FeDHBA > FeMB-1

AbaPiuA: FeEnt* > FeEnt > FeDHBA

AbaPiuA showed no binding affinity to FeGEnt, FeFDC and FeMB-1, while EcoFiu bound all the three ferric siderophores. (Table 4-1)

Another orthologous LGPs pair is EcoCir and AbaPirA with 37% sequence identity. Generally, both EcoCir and AbaPirA showed binding affinities at micromolar range to ferric siderophores with different preferences (Table 4-1; Figure 4-2, 4-3):

EcoCir: FeFDC > FeEnt* ≈ FeDHBS > Fe-MB-1

AbaPirA: FeFDC > FeEnt > FeDHBA > FeEnt* > FeMB-1

EcoCir bound FeFDC at a high affinity (K_D = 63 nM), but did not bind FeEnt, FeGEnt and DHBA. AbaPirA prefers to bind FeFDC, FeEnt and FeDHBA, while showed no specificity to FeGEnt, FeDHBS and FeMB-1. (Table 4-1; Figure 4-2, 4-3) Characterization with fluorescent LGPs revealed complicated recognition spectra of different catecholate receptors. The different preferences and specificities allow Gram-negative bacteria to acquire iron source under different conditions.

Table 4-1 Binding affinities of LGP sensors for apo or ferric siderophores (112)

Sensor		Catecholates[3]								
FLGP or FBP[1]	Residue[2]	FeEnt (Ent)	FeEnt*	FeGEnt	FeCrn	FeDHB	FeDHBS	FeFDC	FeMB-1	FePvd
EcoFiu	A694C	0.55 ± 0.03	0.46 ± 0.04	0.4 ± 0.05	NB	NB	0.1 ± .003	0.4 ± 0.05	4.1 ± 0.5	NB
AbaPiuA	S696C	4.5 ± 0.9	2.8 ± 0.9	NB	NB	12 ± 2	NB	570 ± 350	74 ± 58	NB
EcoFepA	A698C	0.4 ± 0.02 (27 ± 0.2)	38 ± 8	122 ± 37	NB	NB	1.9 ± .3	NB	37 ± 11	NB
KpnFepA1658	A382C	0.6 ± 0.06 (74 ± 19)	23 ± 5	95 ± 12	NB	NB	49 ± 13	0.82 ± 0.4	NB	NB
KpnFepA4984	A390C	14 ± 5 (3.2 0.8)	0.18 ± 0.05	0.87 ± 0.06	NB	1.2 ± 0.4	NB	NB	NB	NB
KpnFepA2380	T255C	13 ± 4	NB	NB	13 ± 3	22 ± 5	NB	27 ± 5	49 ± 13	NB
AbaFepA	S278C	25 ± 6 (1.5 ± 0.4)	12 ± 3	20 ± 4	NB	2.3 ± 0.3	3.2 ± 0.5	0.4 ± 0.1	3.1 ± 0.8	NB
PaeFepA	S271C	10 ± 5 (1.7 ± 0.3)	17 ± 3	0.2 ± .04	NB	2.1 ± 0.2	NB	NB	NB	ND
KpnIroN	T210C	0.4 ± 0.06 (40 ± 15)	18 ± 4	7 ± 0.7	NB	NB	1.2 ± 0.4	0.53 ± 0.2	1.3 ± 0.1	NB
EcoCir	G487C	120 ± 31	7.2 ± 0.3	NB	NB	NB	7.9 ± 0.8	63 ± 4	21 ± 5	NB
AbaPirA	S328C	9.2 ± 1	13 ± 4	NB	NB	9.4 ± 0.9	188 ± 40	6.7 ± 2.4	153 ± 45	NB
PaeFpvA	T660C	8.8 ± 1	5.6 ± 0.9	NB	NB	8 ± 0.6	NB	NB	NB	3.8 ± 0.2
EcoFepB	T297C	41 ± 3 (6 ± 2)	0.14 ± 0.03	13 ± 6.4	10 ± 1.3	5.8 ± 0.9	NB	NB	NB	NB
HsaSCN	Q128C	11 ± 2	10 ± 1	90 ± 25	0.3 ± 0.06	0.3 ± 0.04	NB	NB	NB	NB
Sensor		Hydroxamates				Mixed Chelation				
FLGP or FBP[1]	Residue[2]	Fc (ApoFc)	FcA	FeAbn (Abn)	FxB	FeYbt (Ybt)	FeAgn	FeFDC	FeMB-1	
EcoFhuA	D396C	3.2 ± 0.5 (0.2 ± 0.16)	60 ± 11	NB	0.1 ± 0.02	NB	NB	NB	NB	
EcoIutA	S549C	NB	NB	5.8 ± 0.4 (1.5 ± 0.3)	NB	NB	NB	NB	NB	
KpnFyuA	S631C	NB	NB	NB	277 ± 17	1.3 ± 0.2 (0.1 ± 14)	NB	NB	NB	
AbaBauA	S385C	NB	NB	NB	NB	NB	1.1 ± 0.2	NB	31 ± 6	
HsaSCN	Q128C	0.11 ± 0.05	NB	NB	0.2 ± 0.07	11 ± 1.1	0.16 ± 0.05	NB	NB	

Table 4-1 Binding affinities of LGP sensors for apo or ferric siderophores (112)

The table lists binding affinities of LGPs determined by fluorescence quenching assay. We performed titration on FM-labeled LGPs with ferric siderophores three times and recorded corresponding fluorescence. Normalized fluorescence quenching values were plotted against ligand concentration, and KD values were determined using non-linear fit model (1 binding-site with background) in Grafit 6.012 (Erithacus Ltd, Middlesex , UK)

K_D values in blue, nM; K_D values in black, μM; Underlined K_D values, preferred ligand; NB, no binding; ND, no data

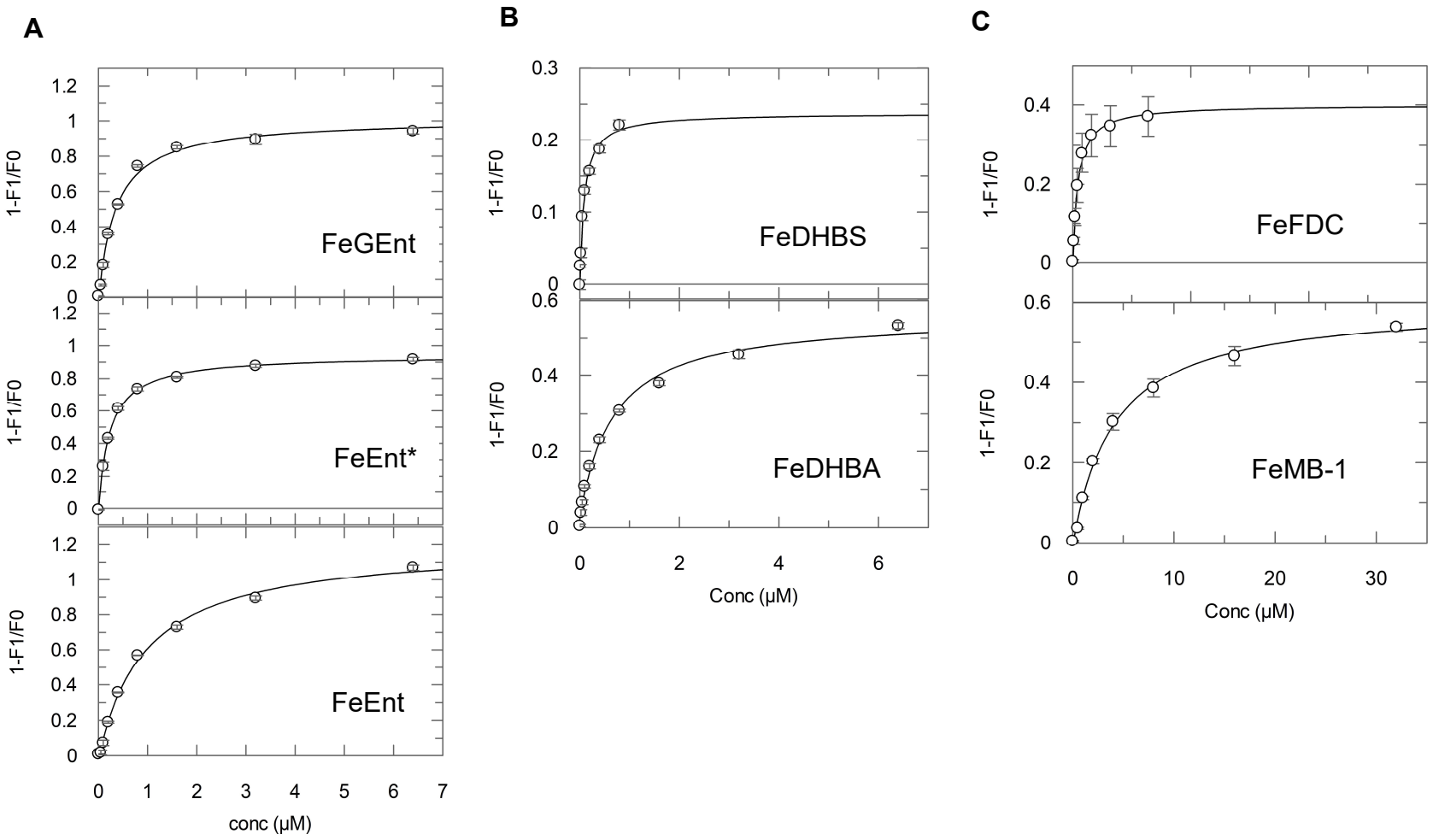
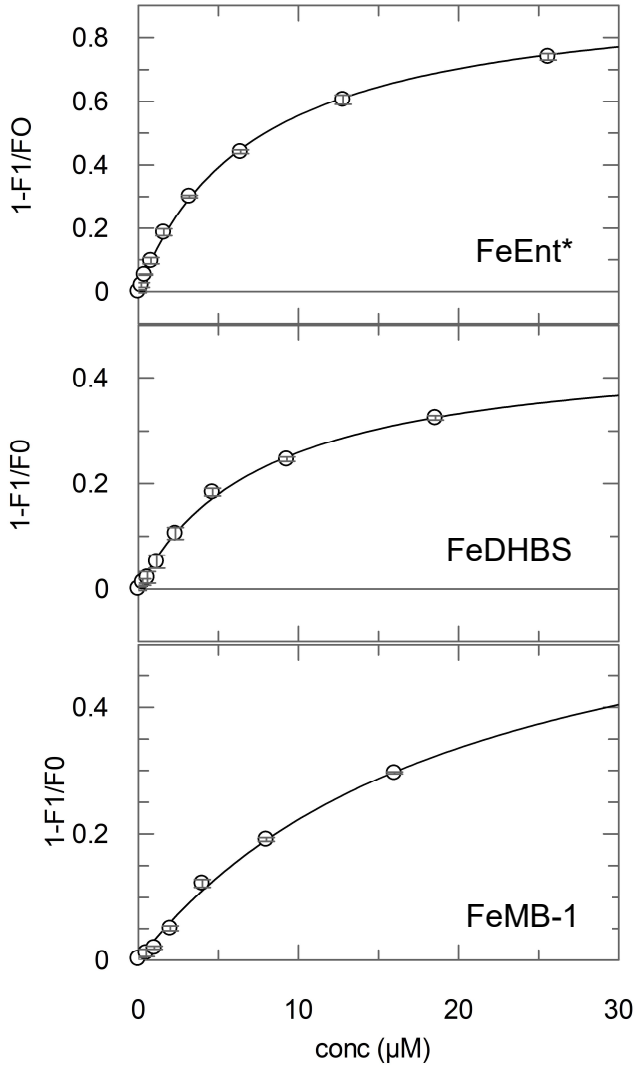

A
B
C
1-F1/F0
FeGEnt
FeEnt*
FeEnt
FeDHBS
FeDHBA
FeFDC
FeMB-1
conc (μM)
Conc (μM)
Conc (μM)

Figure 4-1 Ligand recognition by Fluorescent EcoFiu Sensor.

We cloned *Ecofiu* into pHSG575 vector under the control of fepA promoter, introduced cysteine to the surface loop, labeled the protein with fluorescein maleimide after expressing it in OKN1359 cells and determined the binding affinity of the engineered fluorescent sensor to siderophore ligands: (A) catecholate siderophore FeGEnt, FeEnt* and FeEnt; (B) monomeric catecholate siderophore FeDHBS and FeDHBA; (C) siderophore antibiotics Fe-FDC and FeMB-1. We titrated FM-labeled sensor cells with siderophore ligand and calculated binding affinity by analyzing normalized fluorescence against ligand concentration. Each data point was calculated by three determinations. We plotted the average value of normalized fluorescence against corresponding ligand concentration, created non-linear fit using 1-site binding model (Grafit6.0.12). The determined bind affinities and associated standard errors were listed in Table 4.1


1-F1/FO
0.8
0.6
0.4
0.2
0
FeEnt*
1-F1/F0
0.4
0.2
0
FeDHBS
1-F1/F0
0.4
0.2
0
FeMB-1
0
10
20
30
conc (μM)

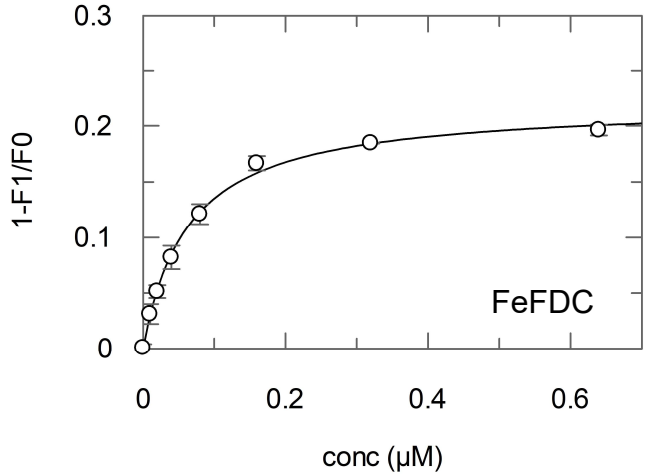
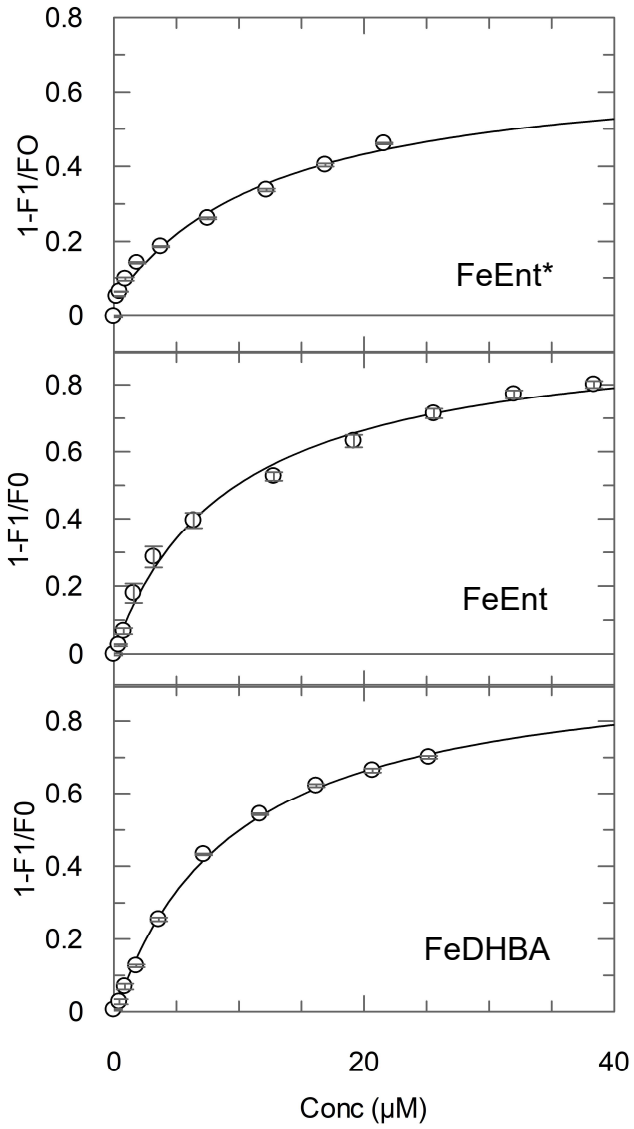

1-F1/F0
0.3
0.2
0.1
0
FeFDC
0
0.2
0.4
0.6
conc (μM)

Figure 4-2 Ligand recognition by Fluorescent EcoCir Sensor.

Ecocir was cloned into pHSG575 vector under the control of fepA promoter. We introduced cysteine to the surface loop of EcoCir, labeled the protein with fluorescein maleimide after expressing it in OKN1359 cells and determined the binding affinity of the engineered fluorescent sensor to siderophore ligands. We titrated FM-labeled sensor cells with siderophore ligand and calculated binding affinity by analyzing normalized fluorescence against ligand concentration. Each data point was calculated by three determinations. We plotted the average value of normalized fluorescence against corresponding ligand concentration, created non-linear fit using 1-site binding model (Grafit6.0.12). The determined bind affinities and associated standard errors were listed in Table 4-1. EcoCir preferred to bind the siderophore antibiotics FeFDC followed by FeEnt*, FeDHBS and FeMB-1. No binding was found for FeEnt, FeDHBA and FeGEnt.


0.8
0.6
0.4
0.2
0
1-F1/FO
FeEnt*
1-F1/F0
FeEnt
FeDHBA
0
20
40
Conc (μM)

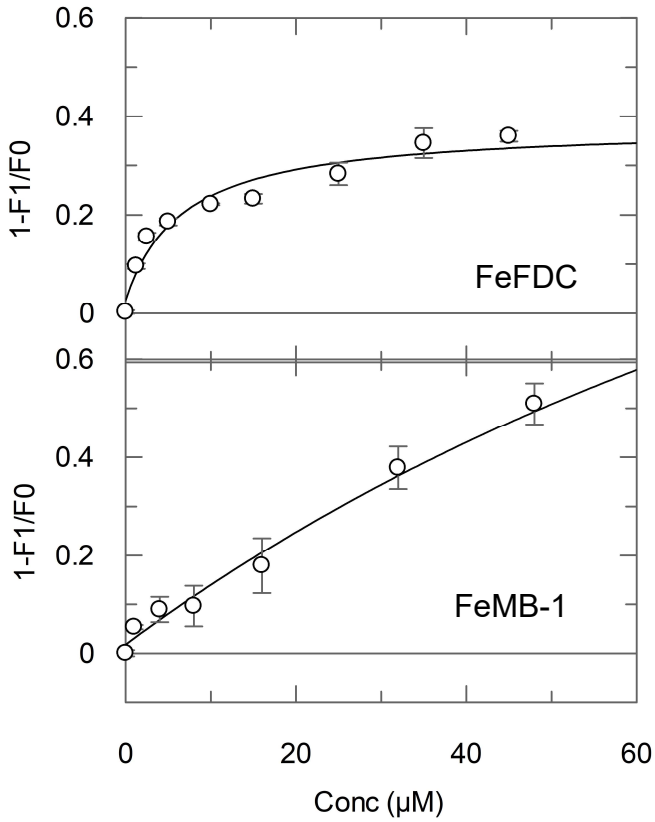
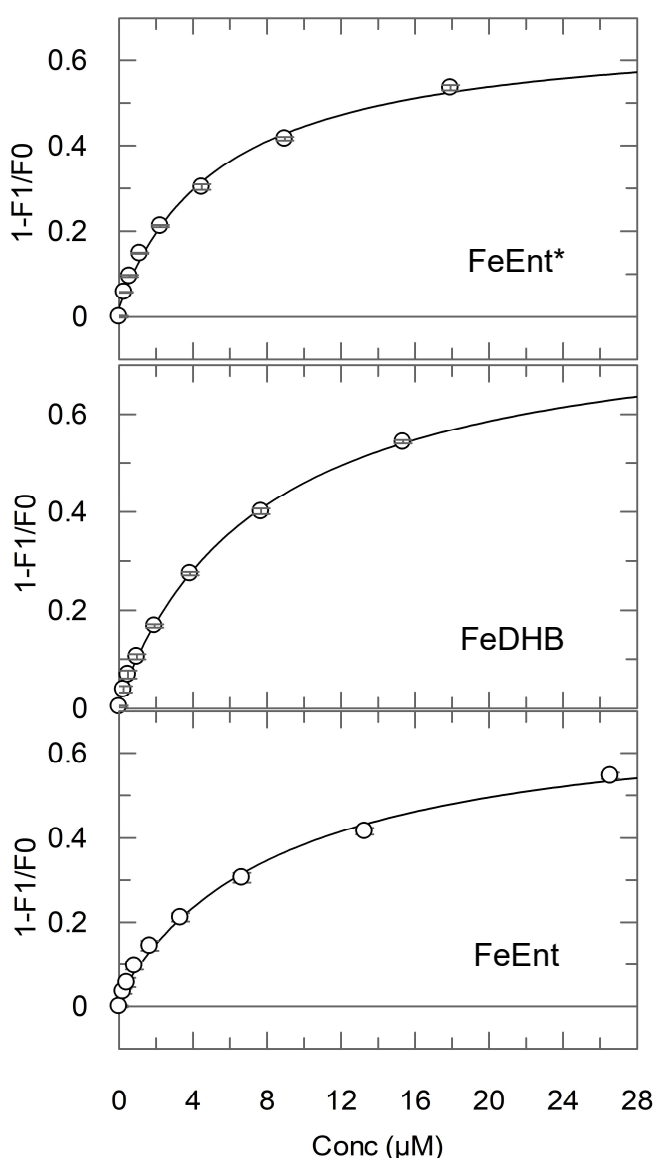

0.6
0.4
0.2
0
1-F1/F0
FeFDC
FeMB-1
0
20
40
60
Conc (μM)

Figure 4-3 Ligand recognition by Fluorescent AbaPirA Sensor.

AbapirA was cloned into pHSG575 vector under the control of fepA promoter. We introduced cysteine to the surface loop of EcoCir, labeled the protein with fluorescein maleimide after expressing it in OKN1359 cells and determined the binding affinity of the engineered fluorescent sensor to siderophore ligands. We titrated FM-labeled sensor cells with siderophore ligand and calculated binding affinity by analyzing normalized fluorescence against ligand concentration. Each data point was calculated by three determinations. We plotted the average value of normalized fluorescence against corresponding ligand concentration, created non-linear fit using 1-site binding model (Grafit6.0.12). The determined bind affinities and associated standard errors were listed in Table 4-1. AbaPirA preferred to bind catecholate siderophore FeEnt*, FeEnt, FeDHBA and siderophore antibiotics FeFDC. No binding was found for FeGEnt, FeDHBS and siderophore antibiotics FeMB-1.

Exclusivity of LGP binding

Unlike catecholate-specific receptor EcoFepA, EcoFiu, EcoCir and AbaPirA that showed broad recognition spectra, KpnFyuA and PaeFpvA were exclusive in the binding reaction with FeYbt and FePvd, respectively. (Table 4-1; Figure 4-4, 4-5) KpnFyuA showed an extremely high binding affinity for FeYbt (KD =1.3 nM), while showed no specificity for other tested catecholate siderophores. (Table 4-1; Figure 4-5) PaeFpvA bound FePvd tightly with a K_D of 3.8 nM, while it only showed weak binding to FeDHBA, FeEnt* and FeEnt. (Table 4-1; Figure 4-4) The exclusivity of these LGP is associated with their biochemical role. Ybt biosynthesis and uptake system are encoded together on a high pathogenicity island. (21,53-57) The singularity of KpnFyuA for FeYbt well complements its production by *Y. pestis. (16,55,56,58)* Other examples of binding exclusivity include EcoIutA for FeAbn, EcoBtuB for vitamin B12, CcrHutA for hemin, and Aba BauA for FeAgn. (Table 4-1)


1-F1/F0
0.6
0.4
0.2
0
FeEnt*
FeDHB
FeEnt
0
4
8
12
16
20
24
28
Conc (μM)

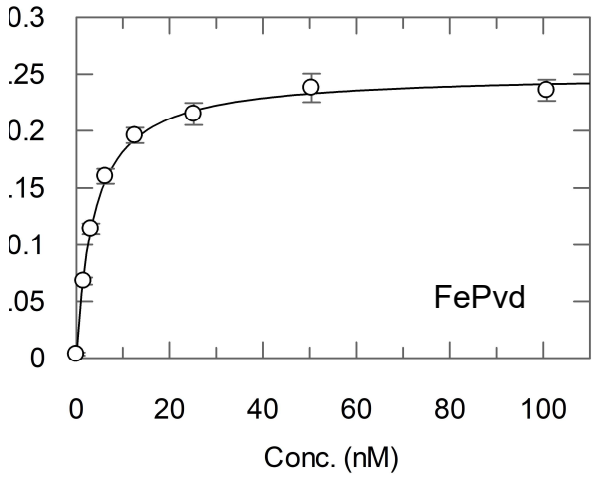

0.3
.25
0.2
.15
0.1
.05
0
FePvd
0
20
40
60
80
100
Conc. (nM)

Figure 4-4 Ligand recognition by Fluorescent PaeFpvA Sensor.

Paefpva was cloned into pHSG575 vector under the control of fepA promoter. We introduced cysteine to the surface loop of EcoCir, labeled the protein with fluorescein maleimide after expressing it in OKN1359 cells and determined the binding affinity of the engineered fluorescent sensor to siderophore ligands. We titrated FM-labeled sensor cells with siderophore ligand and calculated binding affinity by analyzing normalized fluorescence against ligand concentration. Each data point was calculated by three determinations. We plotted the average value of normalized fluorescence against corresponding ligand concentration, created non-linear fit using 1-site binding model (Grafit6.0.12). The determined bind affinities and associated standard errors were listed in Table 4-1. FaeFpvA showed an extremely high affinity to FePvd compared to that of catecholate siderophore FeEnt*, FeEnt, FeDHBA. No binding was found for FeGEnt, FeDHBS and siderophore antibiotics FeFDC and FeMB-1.

.

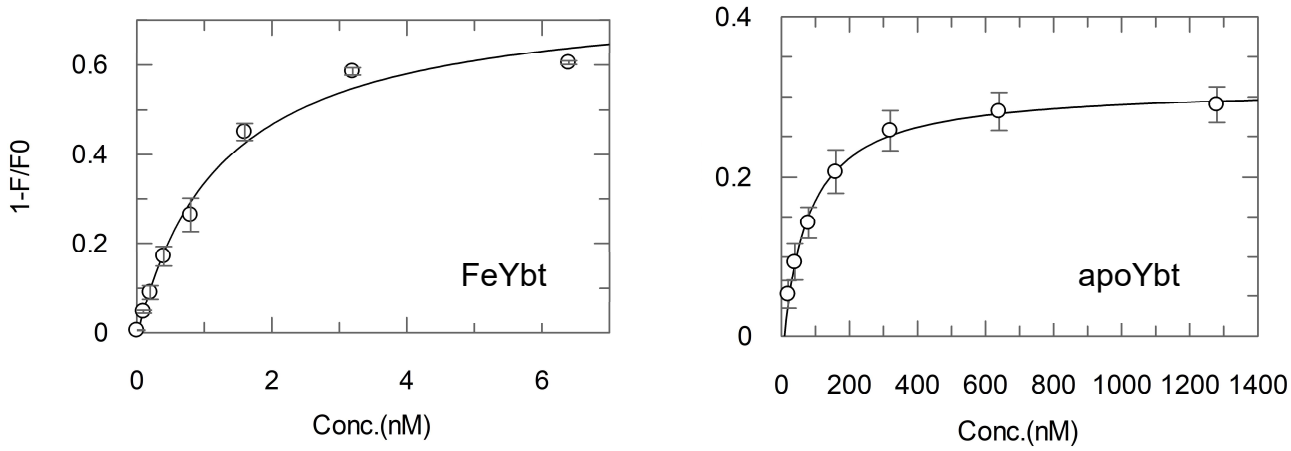


Figure 4-5 Ligand recognition by Fluorescent KpnFyuA Sensor.

KpnfyuA was cloned into pHSG575 vector under the control of fepA promoter. We introduced cysteine to the surface loop of EcoCir, labeled the protein with fluorescein maleimide after expressing it in OKN1359 cells and determined the binding affinity of the engineered fluorescent sensor to siderophore ligands. We titrated FM-labeled sensor cells with siderophore ligand and calculated binding affinity by analyzing normalized fluorescence against ligand concentration. Each data point was calculated by three determinations. We plotted the average value of normalized fluorescence against corresponding ligand concentration, created non-linear fit using 1-site binding model (Grafit6.0.12). The determined bind affinities and associated standard errors were listed in Table 4-1. KpnFyuA showed xclusivity to apo- and FeYbt and FeMB-1. No binding was observed for other tested siderophores.

Measurement of Ferric Siderophores in Samples

Exclusive ligand binding allowed the utilization of decoy fluorescent LGPs sensors to detect and quantify particular siderophore in complex samples. We analyzed this capability of those decoy sensor with supernatant of bacterial cell cultures, including laboratory *E. coli* MG1655 and BN1071, pathogenic *E. coli* CP9, antagonistic *E. coli* Nissle 1917, and two hypervirulent *K. pneumoniae* strains HvKp1 and HvKp2. (Figure 4-6) (33,59-62) Cells were grown in two different iron-deficient media MOPS and M9 to promote siderophore production. (63,64) We collected supernatant by centrifugation and added ferric iron to form the ferric siderophore complexes. The samples were then analyzed using fluorescent decoy sensor KpnFyuA, EcoFepA, KpnIroN and EcoIutA for the detection of FeYbt, FeEnt, FeGEnt and FeAbn, respectively. Detection using LGPs with exclusive specificity (KpnFyuA and EcoIutA) was straightforward: there was no interference from other siderophores due to their singularity for ligand binding. (Table 4-1; Figure 4-6 A)

We found that all the strains grew better in MOPS media (cell density = $5x10^9$/mL) than in M9 media (cell density = $1x\ 10^9$/mL). Correspondingly, most strains grown in MOPS media produced a higher concentration of siderophores than that grown in M9 (about 5- to 10- fold higher). One exception was HvKp2 produced more Ybt in CP9 than in MOPS. CP9 media could favor the production of Ybt in this particular strain. In addition, different tested strains showed different siderophore production under the same growth condition. In the test using Kpn FyuA sensor, we found that *E. coli* MG1655, BN1071, and *K. pneumoniae* HvKpn1 did not produce Ybt, while pathogenic *E. coli* CP9 produced the most Ybt, followed by Nissle and HvKp2. (Figure 4-6 B) The correlations between bacterial virulence and siderophore production are complicated. Tests with other LGPs sensors found that Nissle and ExPEC CP9 produced massive

amounts of GEnt and Ybt, while two hypervirulent K. pneumoniae strains HvKp1 and HvKp2 preferably produced large amounts of Abn. The elaboration of different iron sources by different pathogens suggested a complicated relationship between siderophore biosynthesis and virulence. (Figure 4-6 B)

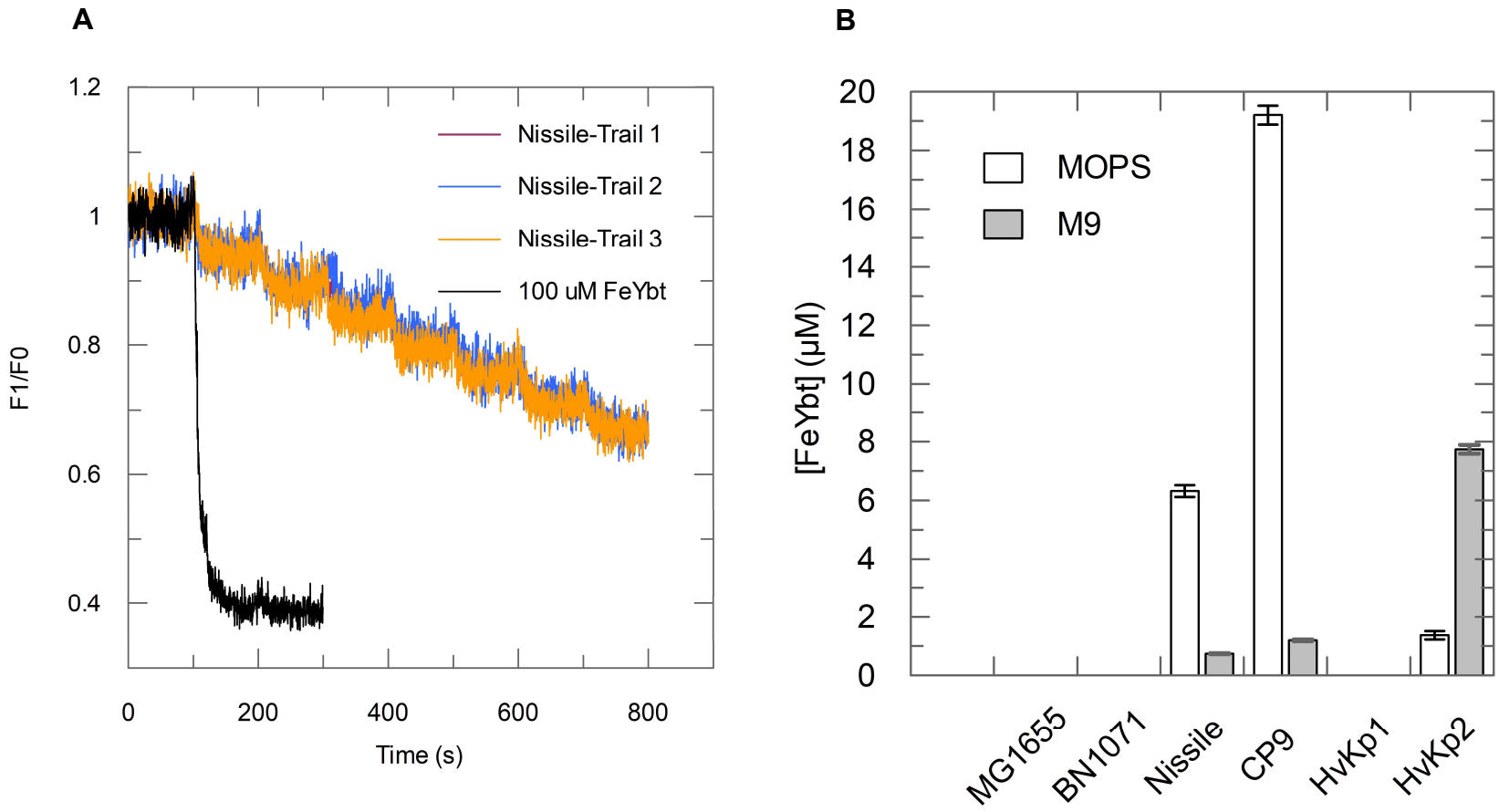

A
1.2
1
0.8
0.6
0.4
F1/F0
0
200
400
600
800
Time (s)
Nissile-Trail 1
Nissile-Trail 2
Nissile-Trail 3
100 uM FeYbt
B
20
18
16
14
12
10
8
6
4
2
0
[FeYbt] (µM)
MOPS
M9
MG1655
BN1071
Nissile
CP9
HvKp1
HvKp2

Figure 4-6 Determination of siderophore in culture supernatants by fluorescent sensor.
We grew bacteria *E. coli* strains B1071, MG1655, Nissle, and CP9 and two K. pneumoniae strains HvKp1 and HvKp2 in MOPS and M9 iron-deficient media, collected supernatant by centrifugation and ferrated the supernatant for siderophore determination assay. We used FM-labeled decoy sensors to detect the presence of particular siderophores in the culture supernatant. A, determination of FeYbt by FyuAS631C-FM sensor. We titrated fluorescent KpnFyuA sensor with diluted supernatant aliquots until the fluorescence reached to 50% quenching and calculated the concentration of FeYbt from the K_D value and the dilution factor. The addition of 100 uM of FeYbt determined the maximal quenching of the sensor. B, Production of siderophores by *K. pneumoniae* and *E. coli* strains. Using FM-labeled decoy sensor, we quantitively characterized the Ybt produced by *E. coli* MG1655, BN1071, Nissile and K. pneumoniae HvKp1 and HvKp2. When cultured in MOPS medium, Nissile and CP9 produced large amount of Ybt, which is 6.3 uM and 19 uM, respectively. When grown in CP9 medium, HvKp2 produced a large amount of Ybt (8 uM). *E. coli* MG1655, BN1071 and *K. pneumoniae* HvKp1 did not produce any Ybt. The concentration of Ybt produced by each test strain and the statistical validation were summarized in Table 4-2.

Measurement of Siderophore Transport

In addition to the detection and quantification of siderophore, we also applied fluorescent decoy sensors to the characterization of siderophore uptake by pathogenic bacteria. (44) TonB-deficient cells expressing LGPs can only bind but cannot transport ferric siderophores. When the siderophore binds to LGP, the attached fluorophore will remain quenched in the absence of TonB-dependent transport. Thus, the fluorescence of FM-labeled decoy sensor is inversely related to siderophore concentration in the sample solution. (44) When incubated along with pathogens that actively transport the corresponding siderophore, the fluorescent decoy sensor is able to detect any changes in siderophore concentration in the solution, and thus the transport of specific siderophore. (Figure 4-7) PaeFpvA tightly bound FePvd (KD = 3.8 nM), making it a sensitive decoy sensor to detect the depletion of FeYbt at nanomolar range by pathogens. For the detection assay, we incubated 2.5 x 10^7 cells/mL of fluorescent PaeFpvA sensor in the cuvette. After recording the initial fluorescence, we added FePvd to ~50 nM, which quenched most of the FM-labeled sensor. We then added the same amount of iron-starved test strains to the cuvette and recorded fluorescence recovery over time. (Figure 4-7)

We used the PaeFpvA decoy sensor to detect FePvd uptake by pathogenic CRE/ESKAPE strains including *E. coli, K. pneumoniae, A. baumannii, P. aeruginosa and E. cloacae*. (Figure 4-7) Among those Gram-negative strains, only *P. aeruginosa* transported FePvd, which was indicated by the fluorescence recovery. (Figure 4-7) But the transport was at a slow rate compared to the transport of FeEnt by EcoFepA. (Figure 4-7) We also used other fluorescent decoy sensors to detect siderophore transport: EcoIutA for FeAbn; EcoBtuB for vitamin B12. All of them quantitatively characterized the transport of corresponding

siderophores by the tested pathogenic strains, which proved the universality of the decoy sensor assay for the detection of ligand uptake.

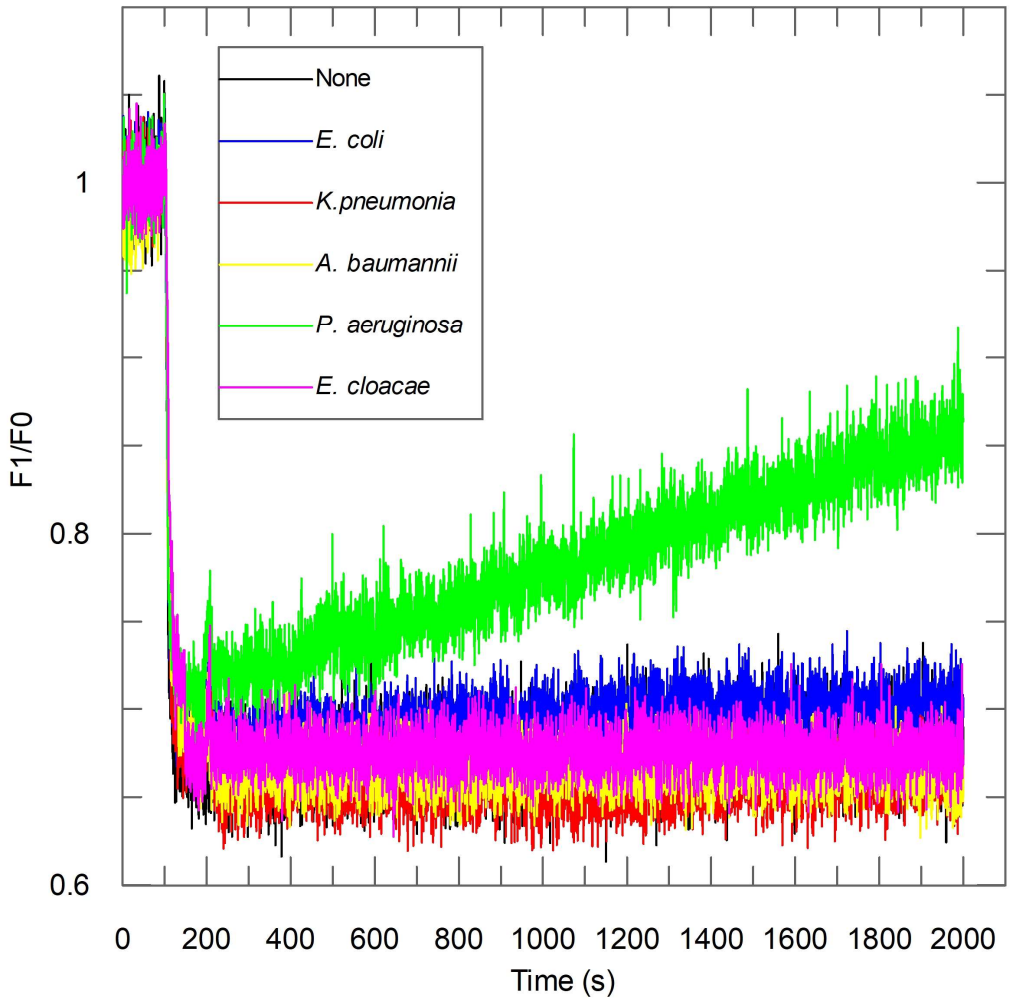


Figure 4-7 Transport Assay by fluorescent decoy sensor.

PaeFpvA decoy sensor was used to characterize the transport of FePvd in five Gram-negative bacteria strains grown in MOPS iron-deficient media: *E. coli* (blue), *K. pneumonia* (red), *A. baumannii* (yellow), *P. aeruginosa* (green) and *E. cloacae* (magenta). We observed an exclusive transport of FePvd by *P. aeruginosa*.

Discussion

Kaback *et al* also made fluorescent derivatives of *E. coli* LacY. (88-93) They found that genetic modification with cysteine did not have strong effect on the functionality of LacY. (65-81) Our previous studies on EcoFepA also confirmed this observation. (6,44,82-91) Besides, site-directed chemical modification to the membrane LGP allows a directed affinity determination by themselves. Using the fluorescent decoy sensors, we revealed complicated ligand preferences of TonB-Dependent LGP. In early studies, EcoFiu and EcoCir were suggested to mediate the uptake of monomeric catecholates like FeDHBA and FeDHBS. (92) Our results suggested a broader ligand spectrum of Fiu with the following binding preference: FeDHBS > FeGEnt > FeEnt* > FeFDC > FeEnt ≈ FeDHBA > FeMB-1. (Table 4-1; Figure 4-1) Its ortholog AbaPiuA shared 31% sequence identity but showed a different ligand preference: AbaPiuA: FeEnt* > FeEnt > FeDHBA. (Table 4-1) The different binding preferences were also observed in another ortholog pair EcoCir and AbaPirA as well as FepA variants. (Table 4-1; Figure 4-2, 4-3) The development of catecholate receptors with different preferences and affinities allows Gram-negative bacteria to acquire different forms of iron source, which makes them adopt and survive in complicated host environments.

Some LGPs were found to recognize and transport siderophore antibiotics FeFDC and FeMB-1 in our test. (45,47,48,93) EcoCir bound FeFDC at the highest affinity (K_D = 63 nM), followed by EcoFiu (K_D = 400 nM) and FepA variants. (Table 4-1) EcoFiu, KpnIroN and AbaFepA showed considerable similarities FeMB-1, with a K_D of 4.1 μM, 1.3 μM, and 3.1 μM, respectively. (Table 4-1) The ligand screening and affinity determination are important for the development of new antibiotics, especially for the ones in the early phase. The uptake and accumulation of siderophore antibiotics is mediated by specific LGPs, which determined the

minimum inhibitory concentration of a chemical compound. It would be problematic without the information of which LGPs participate in the internalization of candidate compound, leading to costly failure during drug development. FDC is the first and only siderophore antibiotics approved by FDA. (94,95) Its clinical efficacy was demonstrated in complicated urinary tract caused by carbapenem-resistant *A. baumannii* and *P. aeruginosa.* (95) But it remained unclear which LGPs were involved in its uptake as well as corresponding binding affinities in these antibiotic-resistant bacterial species. Our studies using the fluorescent decoy sensors revealed the potential LGPs through which the compound was transported.

We further extended the application of fluorescent sensor to the analysis of ligand transport and the detection of clinical samples from humans or other animal hosts. (Figure 4-6, 4-7) Siderophore production has been found to be tightly associated with virulence of pathogenic bacteria. The synthesis and utilization of GEnt, Ybt and Abn by pathogenic strains like *E. coli CP9, K. pneumoniae, A. baumannii and P. aeruginosa* observed in our study appeared to promote their infection and pathogenesis. (28,41,96-101) Besides, a virulence-enhancing effect of the synthesis of a siderophore group has been found specific to *A. baumannii,* including acinetobactin, baumoferrin and fimsbactin. The elaboration of these three siderophore compounds promoted the pathogenesis of *A. baumannii.* (34) Hosts like humans secrete immune protein siderocalin to capture the siderophores like Ent produced by pathogens, and thus to limit their growth and pathogenesis. (23,24,102-104) Some bacteria produced GEnt, the glycosylated form of Ent, to acquire iron from human host. (36,37,41) Due to its low binding affinity to GEnt, siderocalin cannot efficiently removed GEnt from blood serum, allowing the iron acquisition and thus the proliferation of pathogens in hosts. (35,40-43,105-107) Our study using fluorescent HsaSCN sensor reaffirmed its immune function: a broad ligand spectrum of siderophores.

(24,42,108-111) HsaSCN sensor showed a low or no affinity to FeGEnt, FeAbn, FeYbt, FeAbn as well as their corresponding apo forms. These siderophores are elaborated by pathogenic bacteria and are tightly linked to their pathogenesis. The application of fluorescent decoy sensors provided a comprehensive insight into the complicated binding and utilization promiscuity.

Reference

1. Luckey, M., and Nikaido, H. (1980) Specificity of diffusion channels produced by lambda phage receptor protein of Escherichia coli. *Proceedings of the National Academy of Sciences* **77**, 167-171
2. Nikaido, H., and Rosenberg, E. Y. (1983) Porin channels in Escherichia coli: studies with liposomes reconstituted from purified proteins. *Journal of bacteriology* **153**, 241-252
3. Rosenbusch, J. (1990) Structural and functional properties of porin channels in E. coli outer membranes. *Experientia* **46**, 167-173
4. Rutz, J. M., Liu, J., Lyons, J. A., Goranson, J., Armstrong, S. K., McIntosh, M. A., Feix, J. B., and Klebba, P. E. (1992) Formation of a gated channel by a ligand-specific transport protein in the bacterial outer membrane. *Science* **258**, 471-475
5. Nikaido, H. (1994) Porins and specific diffusion channels in bacterial outer membranes. *The Journal of biological chemistry (Print)* **269**, 3905-3908
6. Jiang, X., Payne, M. A., Cao, Z., Foster, S. B., Feix, J. B., Newton, S. M., and Klebba, P. E. (1997) Ligand-specific opening of a gated-porin channel in the outer membrane of living bacteria. *Science* **276**, 1261-1264
7. Saier Jr, M. (2000) Families of proteins forming transmembrane channels. *The Journal of membrane biology* **175**, 165-180
8. Yen, M.-R., Peabody, C. R., Partovi, S. M., Zhai, Y., Tseng, Y.-H., and Saier Jr, M. H. (2002) Protein-translocating outer membrane porins of Gram-negative bacteria. *Biochimica et Biophysica Acta (BBA)-Biomembranes* **1562**, 6-31
9. Pawelek, P. D., Croteau, N., Ng-Thow-Hing, C., Khursigara, C. M., Moiseeva, N., Allaire, M., and Coulton, J. W. (2006) Structure of TonB in complex with FhuA, E. coli outer membrane receptor. *Science* **312**, 1399-1402
10. Shultis, D. D., Purdy, M. D., Banchs, C. N., and Wiener, M. C. (2006) Outer membrane active transport: structure of the BtuB: TonB complex. *Science* **312**, 1396-1399
11. Wish, J. B. (2006) Assessing iron status: beyond serum ferritin and transferrin saturation. *Clinical Journal of the American Society of Nephrology* **1**, S4-S8
12. Newton, S. M., Trinh, V., Pi, H., and Klebba, P. E. (2010) Direct measurements of the outer membrane stage of ferric enterobactin transport: postuptake binding. *Journal of Biological Chemistry* **285**, 17488-17497
13. Jordan, L. D., Zhou, Y., Smallwood, C. R., Lill, Y., Ritchie, K., Yip, W. T., Newton, S. M., and Klebba, P. E. (2013) Energy-dependent motion of TonB in the Gram-negative bacterial inner membrane. *Proceedings of the National Academy of Sciences* **110**, 11553-11558
14. Nagy, T. A., Moreland, S. M., Andrews-Polymenis, H., and Detweiler, C. S. (2013) The ferric enterobactin transporter Fep is required for persistent Salmonella enterica serovar typhimurium infection. *Infection and immunity* **81**, 4063-4070

15. Coffey, R., and Ganz, T. (2017) Iron homeostasis: An anthropocentric perspective. *Journal of Biological Chemistry* **292**, 12727-12734
16. Pollitzer, R. (1954) Plague. *Geneva: WHO*, 409-482
17. BRADBEER, C., JS, K., and Di Masi, D. (1978) Transport of vitamin B12 in Escherichia coli. Corrinoid specificities of the periplasmic B12-binding protein and of energy-dependent B12 transport.
18. Bradbeer, C. (1993) The proton motive force drives the outer membrane transport of cobalamin in Escherichia coli. *Journal of bacteriology* **175**, 3146-3150
19. Gehring, A. M., DeMoll, E., Fetherston, J. D., Mori, I., Mayhew, G. F., Blattner, F. R., Walsh, C. T., and Perry, R. D. (1998) Iron acquisition in plague: modular logic in enzymatic biogenesis of yersiniabactin by Yersinia pestis. *Chemistry & biology* **5**, 573-586
20. Schauer, K., Rodionov, D. A., and de Reuse, H. (2008) New substrates for TonB-dependent transport: do we only see the 'tip of the iceberg'? *Trends in biochemical sciences* **33**, 330-338
21. Fetherston, J. D., Kirillina, O., Bobrov, A. G., Paulley, J. T., and Perry, R. D. (2010) The yersiniabactin transport system is critical for the pathogenesis of bubonic and pneumonic plague. *Infection and immunity* **78**, 2045-2052
22. Perry, R. D., and Fetherston, J. D. (2011) Yersiniabactin iron uptake: mechanisms and role in Yersinia pestis pathogenesis. *Microbes and infection* **13**, 808-817
23. Fluckinger, M., Haas, H., Merschak, P., Glasgow, B. J., and Redl, B. (2004) Human tear lipocalin exhibits antimicrobial activity by scavenging microbial siderophores. *Antimicrobial agents and chemotherapy* **48**, 3367-3372
24. Holmes, M. A., Paulsene, W., Jide, X., Ratledge, C., and Strong, R. K. (2005) Siderocalin (Lcn 2) also binds carboxymycobactins, potentially defending against mycobacterial infections through iron sequestration. *Structure* **13**, 29-41
25. Nazareth, H., Genagon, S. A., and Russo, T. A. (2007) Extraintestinal pathogenic Escherichia coli survives within neutrophils. *Infection and immunity* **75**, 2776-2785
26. Pi, H., Jones, S. A., Mercer, L. E., Meador, J. P., Caughron, J. E., Jordan, L., Newton, S. M., Conway, T., and Klebba, P. E. (2012) Role of catecholate siderophores in gram-negative bacterial colonization of the mouse gut. *PLoS One* **7**, e50020
27. Perry, R. D., Abney, J., Mier, I., Lee, Y., Bearden, S. W., and Fetherston, J. D. (2004) Regulation of the Yersinia pestis Yfe and Ybt iron transport systems. in *The Genus Yersinia*, Springer. pp 275-283
28. Williams, P. H. (1979) Novel iron uptake system specified by ColV plasmids: an important component in the virulence of invasive strains of Escherichia coli. *Infection and Immunity* **26**, 925-932
29. Williams, P., Smith, M. A., Stevenson, P., Griffiths, E., and Tomas, J. M. (1989) Novel aerobactin receptor in Klebsiella pneumoniae. *Microbiology* **135**, 3173-3181
30. McLauchlin, J. (1990) Human listeriosis in Britain, 1967–85, a summary of 722 cases: 1. Listeriosis during pregnancy and in the newborn. *Epidemiology & Infection* **104**, 181-189

31. Brock, J. H., Williams, P. H., Liceaga, J., and Wooldridge, K. G. (1991) Relative availability of transferrin-bound iron and cell-derived iron to aerobactin-producing and enterochelin-producing strains of Escherichia coli and to other microorganisms. *Infection and immunity* **59**, 3185-3190
32. Russo, T. A., Shon, A. S., Beanan, J. M., Olson, R., MacDonald, U., Pomakov, A. O., and Visitacion, M. P. (2011) Hypervirulent K. pneumoniae secretes more and more active iron-acquisition molecules than "classical" K. pneumoniae thereby enhancing its virulence. *PLoS One* **6**, e26734
33. Russo, T. A., Olson, R., MacDonald, U., Beanan, J., and Davidson, B. A. (2015) Aerobactin, but not yersiniabactin, salmochelin, or enterobactin, enables the growth/survival of hypervirulent (hypermucoviscous) Klebsiella pneumoniae ex vivo and in vivo. *Infection and immunity* **83**, 3325-3333
34. Sheldon, J. R., and Skaar, E. P. (2020) Acinetobacter baumannii can use multiple siderophores for iron acquisition, but only acinetobactin is required for virulence. *PLoS pathogens* **16**, e1008995
35. Hantke, K., Nicholson, G., Rabsch, W., and Winkelmann, G. (2003) Salmochelins, siderophores of Salmonella enterica and uropathogenic Escherichia coli strains, are recognized by the outer membrane receptor IroN. *Proceedings of the National Academy of Sciences* **100**, 3677-3682
36. Bister, B., Bischoff, D., Nicholson, G. J., Valdebenito, M., Schneider, K., Winkelmann, G., Hantke, K., and Süssmuth, R. D. (2004) The structure of salmochelins: C-glucosylated enterobactins of Salmonella enterica §. *Biometals* **17**, 471-481
37. Fischbach, M. A., Lin, H., Liu, D. R., and Walsh, C. T. (2006) How pathogenic bacteria evade mammalian sabotage in the battle for iron. *Nature chemical biology* **2**, 132-138
38. Fischbach, M. A., Lin, H., Zhou, L., Yu, Y., Abergel, R. J., Liu, D. R., Raymond, K. N., Wanner, B. L., Strong, R. K., and Walsh, C. T. (2006) The pathogen-associated iroA gene cluster mediates bacterial evasion of lipocalin 2. *Proceedings of the National Academy of Sciences* **103**, 16502-16507
39. Smith, K. D. (2007) Iron metabolism at the host pathogen interface: lipocalin 2 and the pathogen-associated iroA gene cluster. *The international journal of biochemistry & cell biology* **39**, 1776-1780
40. Chan, Y. R., Liu, J. S., Pociask, D. A., Zheng, M., Mietzner, T. A., Berger, T., Mak, T. W., Clifton, M. C., Strong, R. K., and Ray, P. (2009) Lipocalin 2 is required for pulmonary host defense against Klebsiella infection. *The Journal of Immunology* **182**, 4947-4956
41. Bachman, M. A., Lenio, S., Schmidt, L., Oyler, J. E., and Weiser, J. N. (2012) Interaction of lipocalin 2, transferrin, and siderophores determines the replicative niche of Klebsiella pneumoniae during pneumonia. *MBio* **3**, e00224-00211
42. Correnti, C., and Strong, R. K. (2012) Mammalian siderophores, siderophore-binding lipocalins, and the labile iron pool. *Journal of Biological Chemistry* **287**, 13524-13531

43. Sia, A. K., Allred, B. E., and Raymond, K. N. (2013) Siderocalins: Siderophore binding proteins evolved for primary pathogen host defense. *Current opinion in chemical biology* **17**, 150-157
44. Chakravorty, S., Shipelskiy, Y., Kumar, A., Majumdar, A., Yang, T., Nairn, B. L., Newton, S. M., and Klebba, P. E. (2019) Universal fluorescent sensors of high-affinity iron transport, applied to ESKAPE pathogens. *Journal of Biological Chemistry* **294**, 4682-4692
45. Ito, A., Nishikawa, T., Matsumoto, S., Yoshizawa, H., Sato, T., Nakamura, R., Tsuji, M., and Yamano, Y. (2016) Siderophore cephalosporin cefiderocol utilizes ferric iron transporter systems for antibacterial activity against Pseudomonas aeruginosa. *Antimicrobial agents and chemotherapy* **60**, 7396-7401
46. Kohira, N., West, J., Ito, A., Ito-Horiyama, T., Nakamura, R., Sato, T., Rittenhouse, S., Tsuji, M., and Yamano, Y. (2016) In vitro antimicrobial activity of a siderophore cephalosporin, S-649266, against Enterobacteriaceae clinical isolates, including carbapenem-resistant strains. *Antimicrobial agents and chemotherapy* **60**, 729-734
47. Tomaras, A. P., Crandon, J. L., McPherson, C. J., Banevicius, M. A., Finegan, S. M., Irvine, R. L., Brown, M. F., O'Donnell, J. P., and Nicolau, D. P. (2013) Adaptation-based resistance to siderophore-conjugated antibacterial agents by Pseudomonas aeruginosa. *Antimicrobial agents and chemotherapy* **57**, 4197-4207
48. Tomaras, A. P., Crandon, J. L., McPherson, C. J., and Nicolau, D. P. (2015) Potentiation of antibacterial activity of the MB-1 siderophore-monobactam conjugate using an efflux pump inhibitor. *Antimicrobial agents and chemotherapy* **59**, 2439-2442
49. Hashimoto-Gotoh, T., Franklin, F., Nordheim, A., and Timmis, K. (1981) Specific-purpose plasmid cloning vectors I. Low copy number, temperature-sensitive, mobilization-defective pSC101-derived containment vectors. *Gene* **16**, 227-235
50. Takeshita, S., Sato, M., Toba, M., Masahashi, W., and Hashimoto-Gotoh, T. (1987) High-copy-number and low-copy-number plasmid vectors for lacZα-complementation and chloramphenicol-or kanamycin-resistance selection. *Gene* **61**, 63-74
51. Scott, D. C., Cao, Z., Qi, Z., Bauler, M., Igo, J. D., Newton, S. M., and Klebba, P. E. (2001) Exchangeability of N Termini in the Ligand-gated Porins ofEscherichia coli. *Journal of Biological Chemistry* **276**, 13025-13033
52. Smallwood, C. R., Jordan, L., Trinh, V., Schuerch, D. W., Gala, A., Hanson, M., Shipelskiy, Y., Majumdar, A., Newton, S. M., and Klebba, P. E. (2014) Concerted loop motion triggers induced fit of FepA to ferric enterobactin. *Journal of General Physiology* **144**, 71-80
53. Iteman, I., Guiyoule, A., De Almeida, A., Guilvout, I., Baranton, G., and Carniel, E. (1993) Relationship between loss of pigmentation and deletion of the chromosomal iron-regulated irp2 gene in Yersinia pestis: evidence for separate but related events. *Infection and immunity* **61**, 2717-2722
54. Carniel, E., Guilvout, I., and Prentice, M. (1996) Characterization of a large chromosomal" high-pathogenicity island" in biotype 1B Yersinia enterocolitica. *Journal of bacteriology* **178**, 6743-6751

55. Perry, R. D., and Fetherston, J. D. (1997) Yersinia pestis--etiologic agent of plague. *Clinical microbiology reviews* **10**, 35-66
56. Lesic, B., and Carniel, E. (2004) The high pathogenicity island: a broad-host-range pathogenicity island. *Yersinia molecular and cellular biology. Horizon Bioscience, Norfolk, United Kingdom*, 285-306
57. Hinnebusch, B., and Erickson, D. (2008) Yersinia pestis biofilm in the flea vector and its role in the transmission of plague. *Bacterial biofilms*, 229-248
58. Rakin, A., Noelting, C., Schubert, S., and Heesemann, J. (1999) Common and specific characteristics of the high-pathogenicity island of Yersinia enterocolitica. *Infection and immunity* **67**, 5265-5274
59. Blattner, F. R., Plunkett III, G., Bloch, C. A., Perna, N. T., Burland, V., Riley, M., Collado-Vides, J., Glasner, J. D., Rode, C. K., and Mayhew, G. F. (1997) The complete genome sequence of Escherichia coli K-12. *science* **277**, 1453-1462
60. Kokešová, A., Frolova, L., Kverka, M., Sokol, D., Rossmann, P., Bartova, J., and Tlaskalova-Hogenova, H. (2006) Oral administration of probiotic bacteria (E. coli Nissle, E. coli O83, Lactobacillus casei) influences the severity of dextran sodium sulfate-induced colitis in BALB/c mice. *Folia microbiologica* **51**, 478-484
61. Deriu, E., Liu, J. Z., Pezeshki, M., Edwards, R. A., Ochoa, R. J., Contreras, H., Libby, S. J., Fang, F. C., and Raffatellu, M. (2013) Probiotic bacteria reduce salmonella typhimurium intestinal colonization by competing for iron. *Cell host & microbe* **14**, 26-37
62. Pradhan, S., and Weiss, A. A. (2020) Probiotic properties of Escherichia coli Nissle in human intestinal organoids. *Mbio* **11**, e01470-01420
63. Roberts, R. B., Cowie, D. B., Abelson, P. H., Bolton, E. T., and Britten, R. J. (1955) Studies of biosynthesis of Escherichia coli. *Studies of biosynthesis of Escherichia coli.*
64. Neidhardt, F. C., Bloch, P. L., and Smith, D. F. (1974) Culture medium for enterobacteria. *Journal of bacteriology* **119**, 736-747
65. Jung, K., Jung, H., and Kaback, H. R. (1994) Dynamics of lactose permease of Escherichia coli determined by site-directed fluorescence labeling. *Biochemistry* **33**, 3980-3985
66. Frillingos, S., and Kaback, H. R. (1996) Probing the conformation of the lactose permease of Escherichia coli by in situ site-directed sulfhydryl modification. *Biochemistry* **35**, 3950-3956
67. Voss, J., He, M. M., Hubbell, W. L., and Kaback, H. R. (1996) Site-directed spin labeling demonstrates that transmembrane domain XII in the lactose permease of Escherichia coli is an α-helix. *Biochemistry* **35**, 12915-12918
68. Wu, J., Voss, J., Hubbell, W. L., and Kaback, H. R. (1996) Site-directed spin labeling and chemical crosslinking demonstrate that helix V is close to helices VII and VIII in the lactose permease of Escherichia coli. *Proceedings of the National Academy of Sciences* **93**, 10123-10127
69. Frillingos, S., and Kaback, H. R. (1997) The role of helix VIII in the lactose permease of Escherichia coli: II. Site-directed sulfhydryl modification. *Protein Science* **6**, 438-443

70. Voss, J., Hubbell, W. L., Hernandez-Borrell, J., and Kaback, H. R. (1997) Site-directed spin-labeling of transmembrane domain VII and the 4B1 antibody epitope in the lactose permease of Escherichia coli. *Biochemistry* **36**, 15055-15061
71. Venkatesan, P., Hu, Y., and Kaback, H. R. (2000) Site-directed sulfhydryl labeling of the lactose permease of Escherichia coli: helix X. *Biochemistry* **39**, 10656-10661
72. Venkatesan, P., Kwaw, I., Hu, Y., and Kaback, H. R. (2000) Site-directed sulfhydryl labeling of the lactose permease of Escherichia coli: helix VII. *Biochemistry* **39**, 10641-10648
73. Venkatesan, P., Liu, Z., Hu, Y., and Kaback, H. R. (2000) Site-directed sulfhydryl labeling of the lactose permease of Escherichia coli: N-ethylmaleimide-sensitive face of helix II. *Biochemistry* **39**, 10649-10655
74. Kwaw, I., Zen, K.-C., Hu, Y., and Kaback, H. R. (2001) Site-directed sulfhydryl labeling of the lactose permease of Escherichia coli: helices IV and V that contain the major determinants for substrate binding. *Biochemistry* **40**, 10491-10499
75. Zhang, W., Hu, Y., and Kaback, H. R. (2003) Site-directed sulfhydryl labeling of helix IX in the lactose permease of Escherichia coli. *Biochemistry* **42**, 4904-4908
76. Ermolova, N., Madhvani, R. V., and Kaback, H. R. (2006) Site-directed alkylation of cysteine replacements in the lactose permease of Escherichia coli: helices I, III, VI, and XI. *Biochemistry* **45**, 4182-4189
77. Guan, L., and Ronald Kaback, H. (2007) Site-directed alkylation of cysteine to test solvent accessibility of membrane proteins. *Nature protocols* **2**, 2012-2017
78. Kaback, H. R., Dunten, R., Frillingos, S., Venkatesan, P., Kwaw, I., Zhang, W., and Ermolova, N. (2007) Site-directed alkylation and the alternating access model for LacY. *Proceedings of the National Academy of Sciences* **104**, 491-494
79. Majumdar, D. S., Smirnova, I., Kasho, V., Nir, E., Kong, X., Weiss, S., and Kaback, H. R. (2007) Single-molecule FRET reveals sugar-induced conformational dynamics in LacY. *Proceedings of the National Academy of Sciences* **104**, 12640-12645
80. Nie, Y., Ermolova, N., and Kaback, H. R. (2007) Site-directed alkylation of LacY: effect of the proton electrochemical gradient. *Journal of molecular biology* **374**, 356-364
81. Jiang, X., Nie, Y., and Kaback, H. R. (2011) Site-directed alkylation studies with LacY provide evidence for the alternating access model of transport. *Biochemistry* **50**, 1634-1640
82. Liu, J., Rutz, J. M., Klebba, P. E., and Feix, J. B. (1994) A site-directed spin-labeling study of ligand-induced conformational change in the ferric enterobactin receptor, FepA. *Biochemistry* **33**, 13274-13283
83. Klug, C. S., Su, W., Liu, J., Klebba, P. E., and Feix, J. B. (1995) Denaturant unfolding of the ferric enterobactin receptor and ligand-induced stabilization studied by site-directed spin labeling. *Biochemistry* **34**, 14230-14236
84. Payne, M. A., Igo, J. D., Cao, Z., Foster, S. B., Newton, S. M., and Klebba, P. E. (1997) Biphasic binding kinetics between FepA and its ligands. *Journal of Biological Chemistry* **272**, 21950-21955

85. Cao, Z., Qi, Z., Sprencel, C., Newton, S. M., and Klebba, P. E. (2000) Aromatic components of two ferric enterobactin binding sites in Escherichia coli FepA. *Molecular microbiology* **37**, 1306-1317
86. Cao, Z., Warfel, P., Newton, S. M., and Klebba, P. E. (2003) Spectroscopic observations of ferric enterobactin transport. *Journal of Biological Chemistry* **278**, 1022-1028
87. Annamalai, R., Jin, B., Cao, Z., Newton, S. M., and Klebba, P. E. (2004) Recognition of ferric catecholates by FepA. *Journal of bacteriology* **186**, 3578-3589
88. Ma, L., Kaserer, W., Annamalai, R., Scott, D. C., Jin, B., Jiang, X., Xiao, Q., Maymani, H., Massis, L. M., and Ferreira, L. C. (2007) Evidence of ball-and-chain transport of ferric enterobactin through FepA. *Journal of Biological Chemistry* **282**, 397-406
89. Hanson, M., Jordan, L. D., Shipelskiy, Y., Newton, S. M., and Klebba, P. E. (2016) High-throughput screening assay for inhibitors of TonB-dependent iron transport. *Journal of Biomolecular Screening* **21**, 316-322
90. Nairn, B. L., Eliasson, O. S., Hyder, D. R., Long, N. J., Majumdar, A., Chakravorty, S., McDonald, P., Roy, A., Newton, S. M., and Klebba, P. E. (2017) Fluorescence high-throughput screening for inhibitors of TonB action. *Journal of bacteriology* **199**, e00889-00816
91. Majumdar, A., Trinh, V., Moore, K. J., Smallwood, C. R., Kumar, A., Yang, T., Scott, D. C., Long, N. J., Newton, S. M., and Klebba, P. E. (2020) Conformational rearrangements in the N-domain of Escherichia coli FepA during ferric enterobactin transport. *Journal of Biological Chemistry* **295**, 4974-4984
92. Nikaido, H., and Rosenberg, E. Y. (1990) Cir and Fiu proteins in the outer membrane of Escherichia coli catalyze transport of monomeric catechols: study with beta-lactam antibiotics containing catechol and analogous groups. *Journal of bacteriology* **172**, 1361-1367
93. Wu, J. Y., Srinivas, P., and Pogue, J. M. (2020) Cefiderocol: a novel agent for the management of multidrug-resistant Gram-negative organisms. *Infectious diseases and therapy* **9**, 17-40
94. Wright, H., Bonomo, R. A., and Paterson, D. L. (2017) New agents for the treatment of infections with Gram-negative bacteria: restoring the miracle or false dawn? *Clinical Microbiology and Infection* **23**, 704-712
95. Mabayoje, D. A., NicFhogartaigh, C., Cherian, B. P., Tan, M. G. M., and Wareham, D. W. (2021) Compassionate use of cefiderocol for carbapenem-resistant Acinetobacter baumannii prosthetic joint infection. *JAC-antimicrobial resistance* **3**, i21-i24
96. Montgomerie, J., Bindereif, A., Neilands, J., Kalmanson, G., and Guze, L. (1984) Association of hydroxamate siderophore (aerobactin) with Escherichia coli isolated from patients with bacteremia. *Infection and Immunity* **46**, 835-838
97. Faundez, G., Figueroa, G., Troncoso, M., and Cabello, F. (1988) Characterization of enteroinvasive Escherichia coli strains isolated from children with diarrhea in Chile. *Journal of clinical microbiology* **26**, 928-932

98. Der Vartanian, M., Jaffeux, B., Contrepois, M., Chavarot, M., Girardeau, J., Bertin, Y., and Martin, C. (1992) Role of aerobactin in systemic spread of an opportunistic strain of Escherichia coli from the intestinal tract of gnotobiotic lambs. *Infection and immunity* **60**, 2800-2807
99. Torres, A. G., Redford, P., Welch, R. A., and Payne, S. M. (2001) TonB-dependent systems of uropathogenic Escherichia coli: aerobactin and heme transport and TonB are required for virulence in the mouse. *Infection and immunity* **69**, 6179-6185
100. Garcia, E. C., Brumbaugh, A. R., and Mobley, H. L. (2011) Redundancy and specificity of Escherichia coli iron acquisition systems during urinary tract infection. *Infection and immunity* **79**, 1225-1235
101. Holden, V. I., Breen, P., Houle, S., Dozois, C. M., and Bachman, M. A. (2016) Klebsiella pneumoniae siderophores induce inflammation, bacterial dissemination, and HIF-1α stabilization during pneumonia. *MBio* **7**, e01397-01316
102. Goetz, D. H., Holmes, M. A., Borregaard, N., Bluhm, M. E., Raymond, K. N., and Strong, R. K. (2002) The neutrophil lipocalin NGAL is a bacteriostatic agent that interferes with siderophore-mediated iron acquisition. *Molecular cell* **10**, 1033-1043
103. Flo, T. H., Smith, K. D., Sato, S., Rodriguez, D. J., Holmes, M. A., Strong, R. K., Akira, S., and Aderem, A. (2004) Lipocalin 2 mediates an innate immune response to bacterial infection by sequestrating iron. *Nature* **432**, 917-921
104. Clifton, M. C., Corrent, C., and Strong, R. K. (2009) Siderocalins: siderophore-binding proteins of the innate immune system. *Biometals* **22**, 557-564
105. Williams, P., Rabsch, W., Methner, U., Voigt, W., Tschäpe, H., and Reissbrodt, R. (2006) Catecholate receptor proteins in Salmonella enterica: role in virulence and implications for vaccine development. *Vaccine* **24**, 3840-3844
106. Caza, M., Lépine, F., Milot, S., and Dozois, C. M. (2008) Specific roles of the iroBCDEN genes in virulence of an avian pathogenic Escherichia coli O78 strain and in production of salmochelins. *Infection and immunity* **76**, 3539-3549
107. Lee, I. R., Molton, J. S., Wyres, K. L., Gorrie, C., Wong, J., Hoh, C. H., Teo, J., Kalimuddin, S., Lye, D. C., and Archuleta, S. (2016) Differential host susceptibility and bacterial virulence factors driving Klebsiella liver abscess in an ethnically diverse population. *Scientific reports* **6**, 1-12
108. Yang, J., Goetz, D., Li, J.-Y., Wang, W., Mori, K., Setlik, D., Du, T., Erdjument-Bromage, H., Tempst, P., and Strong, R. (2002) An iron delivery pathway mediated by a lipocalin. *Molecular cell* **10**, 1045-1056
109. Abergel, R. J., Moore, E. G., Strong, R. K., and Raymond, K. N. (2006) Microbial evasion of the immune system: structural modifications of enterobactin impair siderocalin recognition. *Journal of the American Chemical Society* **128**, 10998-10999
110. Hoette, T. M., Abergel, R. J., Xu, J., Strong, R. K., and Raymond, K. N. (2008) The role of electrostatics in siderophore recognition by the immunoprotein siderocalin 1. *Journal of the American Chemical Society* **130**, 17584-17592

111. Allred, B. E., Correnti, C., Clifton, M. C., Strong, R. K., and Raymond, K. N. (2013) Siderocalin outwits the coordination chemistry of vibriobactin, a siderophore of Vibrio cholerae. *ACS chemical biology* **8**, 1882-1887
112. Kumar, A., Yang, T., Chakravorty, S., Majumdar, A., Nairn, B. L., Six, D. A., Dos Santos, N. M., Price, S. L., Lawrenz, M. B., and Actis, L. A. (2022) Fluorescent sensors of siderophores produced by bacterial pathogens. *Journal of Biological Chemistry* **298**

Supplementary Materials

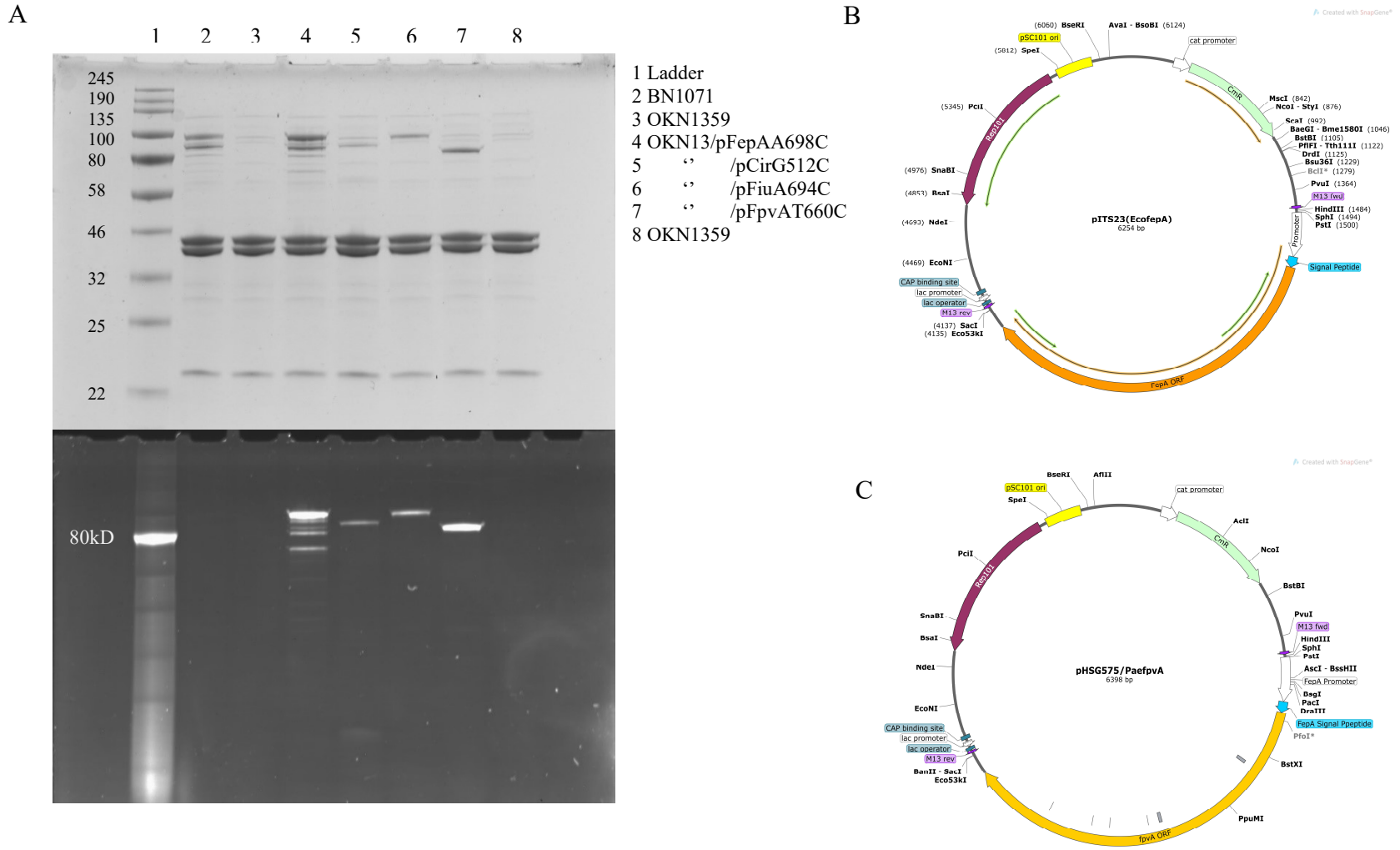


Figure S4-1 SDS-PAGE and Fluorescent gel of fluorescent sensors. (A) We isolated the OM fraction from the FM-labeled sensor cells and characterized their protein expression and labeling reaction by SDS-PAGE. The gel was observed under UV light to visualize the FM labeled proteins and was stained by SDS staining solution to visualize the protein expressions. Clone map of (B) EcoFepA and (C) PaeFpvA

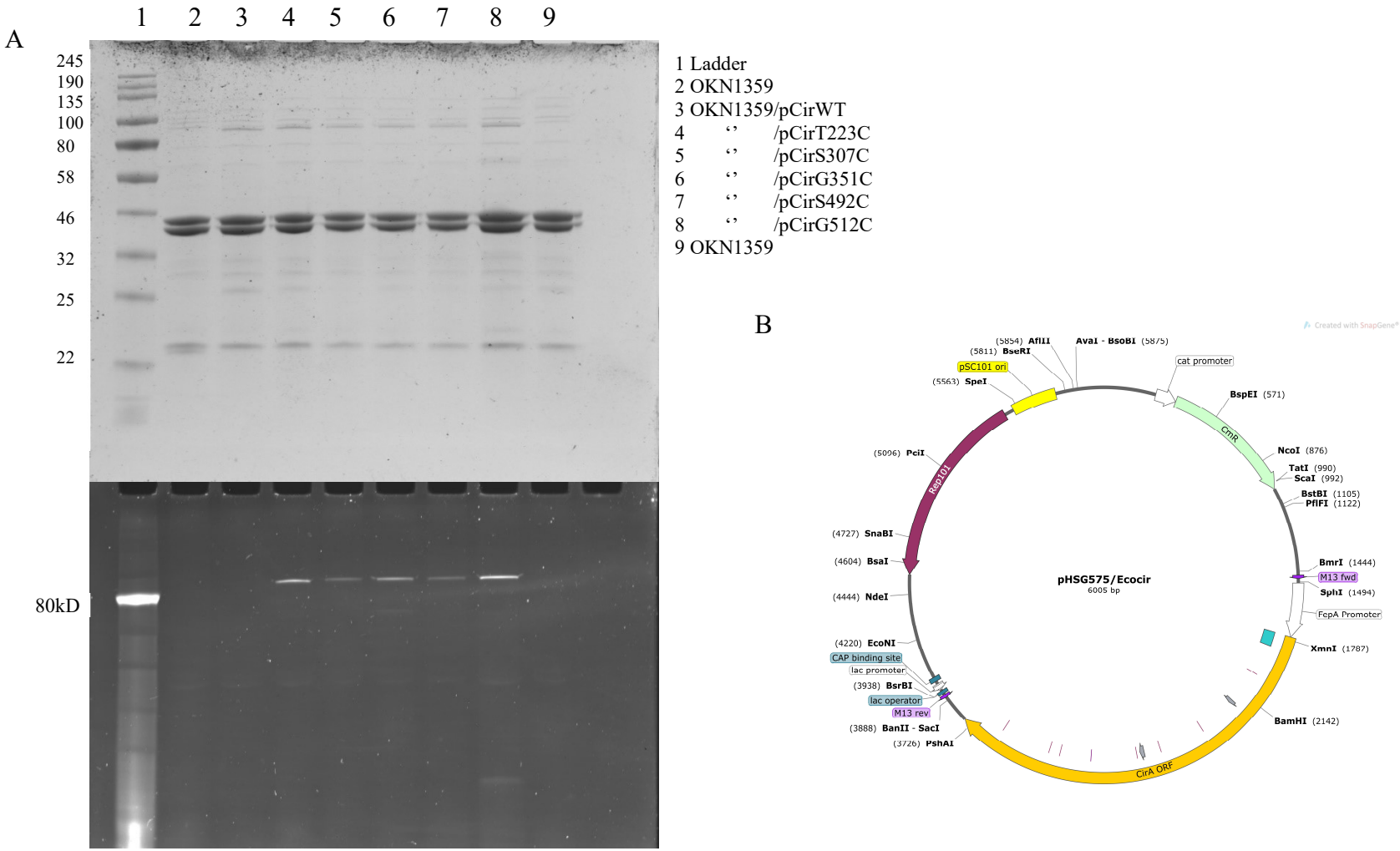
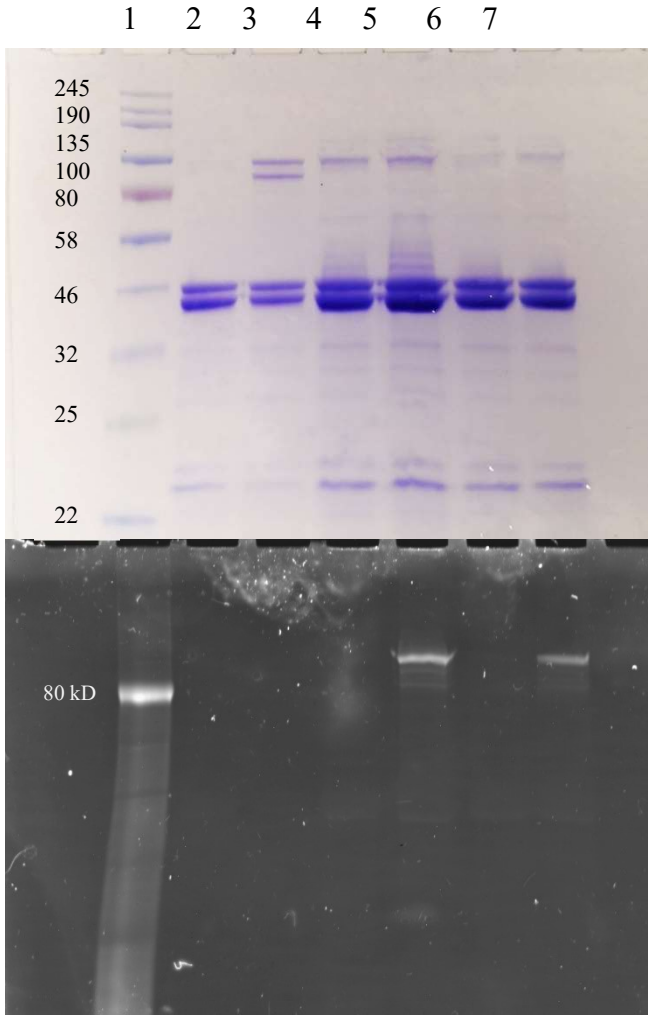


Figure S4-2 SDS-PAGE and Fluorescent gel of EcoCir sensors. (A) We engineered EcoCir cysteine mutants, transformed them into OKN1359, grew them in MOPS media and labeled them with FM. We isolated the OM fractions and ran SDS polyacrylamide gel to analyze their expressions and labeling reactions. The gel was observed under UV light to visualize the FM labeled proteins and was stained by SDS staining solution to visualize the protein expression. (B) Clone map of EcoCir.

A



1 Ladder
2 OKN1359
3 BN1071
4 ‘’ / pPirAWT
5 ‘’ / pPirAS328C
6 ‘’ / pPirAT556C
7 ‘’ / pPirAS660C

B

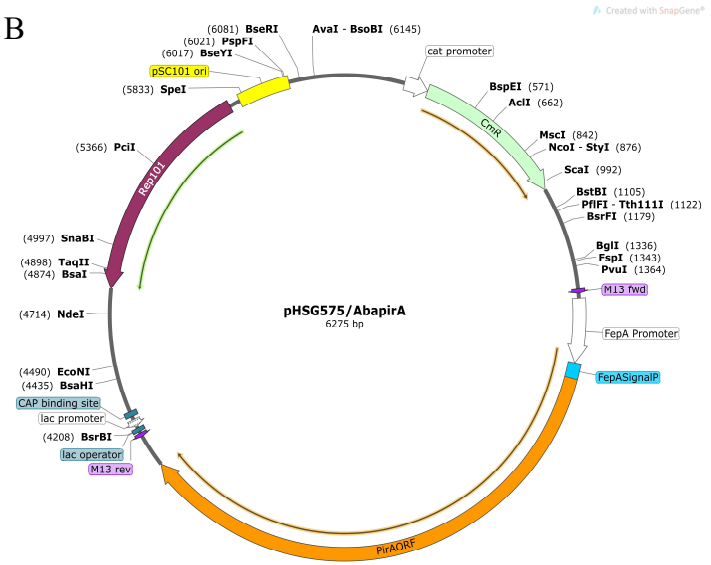


Figure S4-3 SDS-PAGE and Fluorescent gel of AbaPirA sensors. (A) We engineered AbaPirA cysteine mutants, transformed them into OKN1359, grew them in MOPS media and labeled them with FM. We isolated the OM fractions and ran SDS polyacrylamide gel to analyze their expressions and labeling reactions. The gel was observed under UV light to visualize the FM labeled proteins and was stained by SDS staining solution to visualize the protein expression**.** (B) Clone map of AbaPirA.

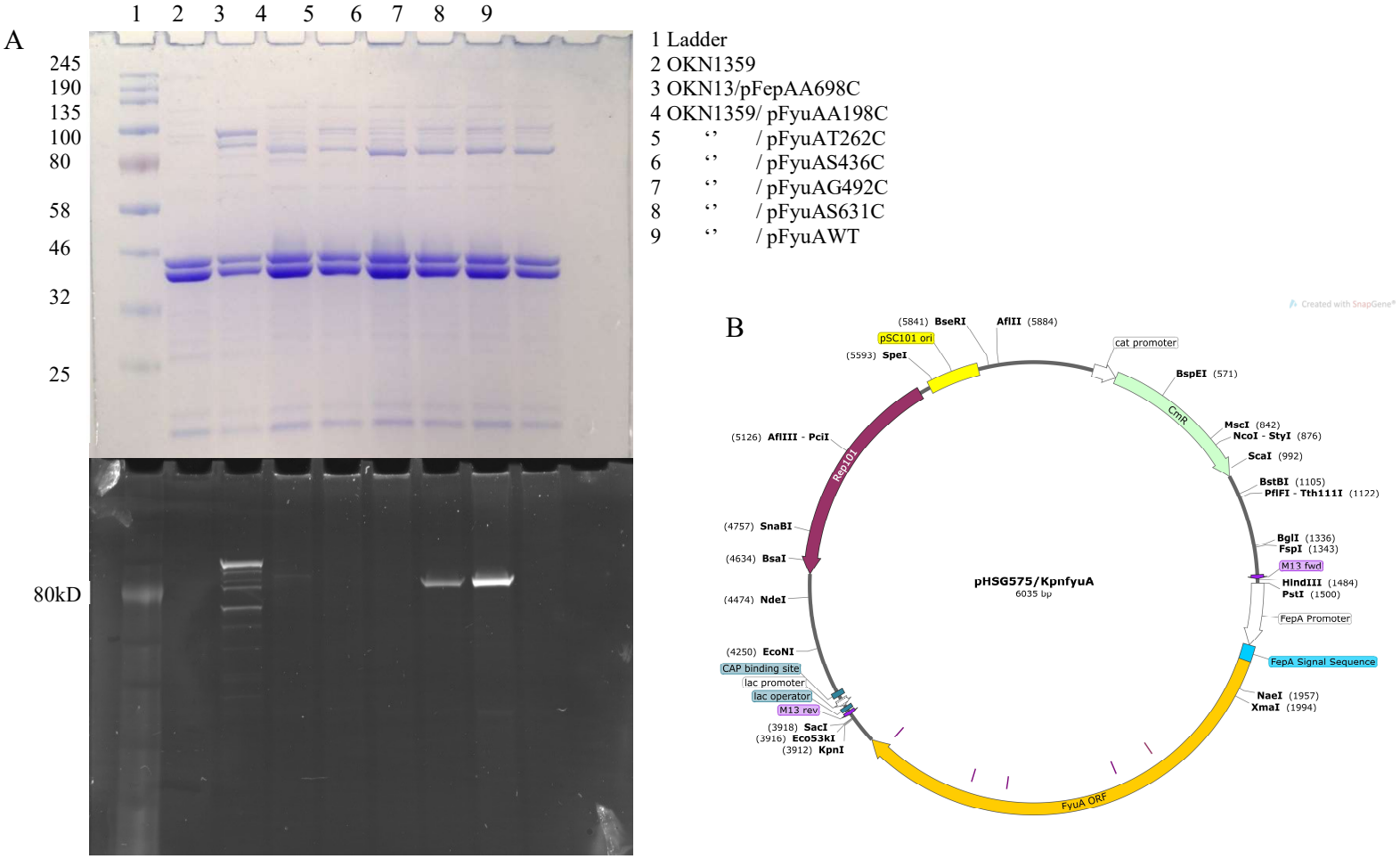


Figure S4-4 SDS-PAGE and Fluorescent gel of KpnFyuA sensors. (A) We engineered KpnFyuA cysteine mutants, transformed them into OKN1359, grew them in MOPS media and labeled them with FM. We isolated the OM fractions and ran SDS polyacrylamide gel to analyze their expressions and labeling reactions. The gel was observed under UV light to visualize the FM labeled proteins and was stained by SDS staining solution to visualize the protein expression**.** (B) Clone map of KpnFyuA.

Chapter 5 Other Studies

Universal fluorescent sensors of high-affinity iron transport, applied to ESKAPE pathogens (1) (see Appendix)

In this project, we created fluorescent decoy sensors for the determination of ligand binding to the outer membrane (OM) receptors in ESKAPE pathogens. We introduced cysteine residues to the external loops of OM receptors, expressed them in a transport-deficient *E. coli* system and labeled them with fluoresceine maleimide. Ligand binding induces conformational changes that quench attached fluorophores in the surface loops and the resulting fluorescence quenching reflects ligand binding at different concentrations. Due to the lack of siderophore transport in a TonB-deficient host cell background, those fluorescent sensors are sensitive to any changes in ligand concentration, which is inversely proportional to the fluorescence quenching. Thus, we utilized those fluorescent decoy sensors to detect the siderophore uptake by bacterial pathogens.

My work in this project included the production and purification of FeGEnt, the glucosylated form of FeEnt, for binding and transport assays using fluorescent decoy sensors. Pathogenic *E. coli* CP9 was known to produce a large amount of FeGEnt, so we purified FeGEnt from its culture supernatant following the procedure described in Hantke *et al* 2003. (10) We grew cells in LB medium to stationary phase, and sub-cultured them into TY medium at 1%. After 30 hours incubation, cells were sedimented and removed by centrifugation. We next added $FeSO_4$ to form ferric siderophore complexes. Supernatant was passed through Sephadex DE52

cellulose chromatography, allowing the negatively charged ferric siderophore to bind. After washing the column with Tris-HCl pH7.0, we eluted ferric-siderophores with a gradient of 2 M ammonium chloride and found three elution peaks (Figure 5-1). We concentrated each elution peak by evaporation and further purified them by Sephadex G-10 chromatography for de-salting. The concentrated fractions were then analyzed by UV-Vis spectrometry and mass spectrometry and peak 1 was identified as FeGEnt. (Figure 3-1 C)

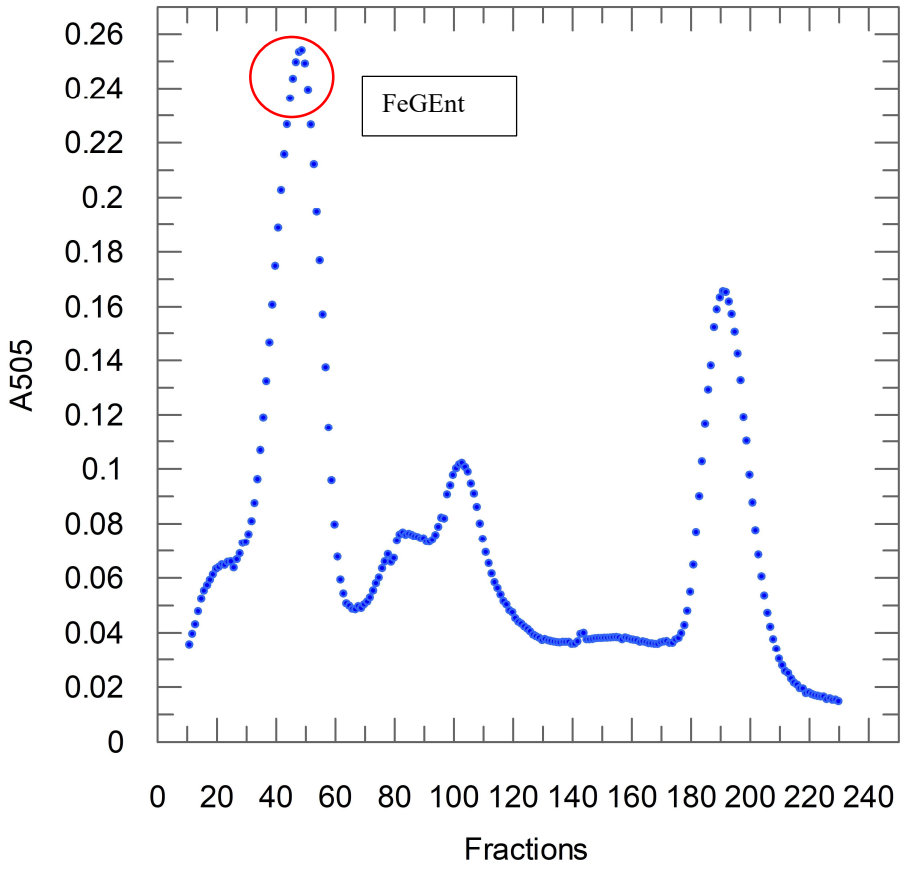


Figure 5-1 Elution profile of ferric siderophores by Sephadex DE52 anion chromatography.

We passed the ferrated culture supernatant through the packed column, washed it with TrisCl pH7.0, and eluted the bound ferric siderophores with a gradient of 2 M ammonium chloride. We read the absorbance of each fraction at 505 nm and identified three elution peaks. Fractions 30 – 60 contained FeGEnt, fractions 80-110 contained FeEnt*, and fractions 180-210 contained FeEnt.

Conformational rearrangements in the N-domain of *Escherichia coli* FepA during ferric enterobactin transport (2) (see Appendix)

FepA transports FeEnt across OM in a TonB-dependent manner, which includes a conformational rearrangement at its N-terminal domain. To understand the conformational changes in the N-domain, we introduced cysteine pairs in different regions of FepA, which may form disulfide bonds that restrict the conformational rearrangement. We created FepA mutants carrying intra-N cysteine pairs that formed disulfide bonds between adjacent beta-strands of N-domain, or inter-N-C cysteine pairs that bridged N-domain and C-domain at their external and exterior surface, respectively. We then characterized the effect of these cysteine mutations on ligand binding and transport using siderophore nutrition tests, fluorescence decoy sensor assays and [^{59}Fe] accumulation assays. Our results showed that intra-N cysteines pairs significantly affected siderophore transport, due to the formation of disulfide bonds that restricted conformational change within the N-domain. Most inter-N-C cysteine pairs – limiting movement between N- and C- domains - did not affect siderophore transport. Our experiments suggested an important role of N-domain conformational rearrangement on siderophore uptake and supported the hypothesis that N-domain remained within the transmembrane beta-barrel during the siderophore transport, rather than moved out of the transmembrane channel.

My work in this project included the engineering of a FepA mutant and the characterization of associated siderophore transport. The locations of cysteine pairs were chosen based on their proximity to each other on the crystal structure of FepA. I engineered a FepA mutant carrying an inter-N-C cysteine pair 137-465 by site-directed mutagenesis. After verifying

the mutations by DNA sequencing and confirming the expression by SDS-PAGE, we analyzed its FeEnt uptake by siderophore nutrition test in the presence or absence of βME. βME prevents the formation of disulfide between adjacent cysteine pairs. FepA mutant 137-465 showed similar growth halo to the WT in both reducing and nonreducing conditions, indicating that conformation change at this region did not affected transport. (Figure 5-2) Most other inter-N-C cysteine pairs did not have impact on FeEnt transport, while intra-N cysteine pairs showed inhibitory effects. FepA mutants carrying those intra-N cysteine pairs showed larger but fainter growth halos, which reflected low transport rates. (3,4) Radioisotopic accumulation assay and fluorescence binding assay consistently confirmed this observation.

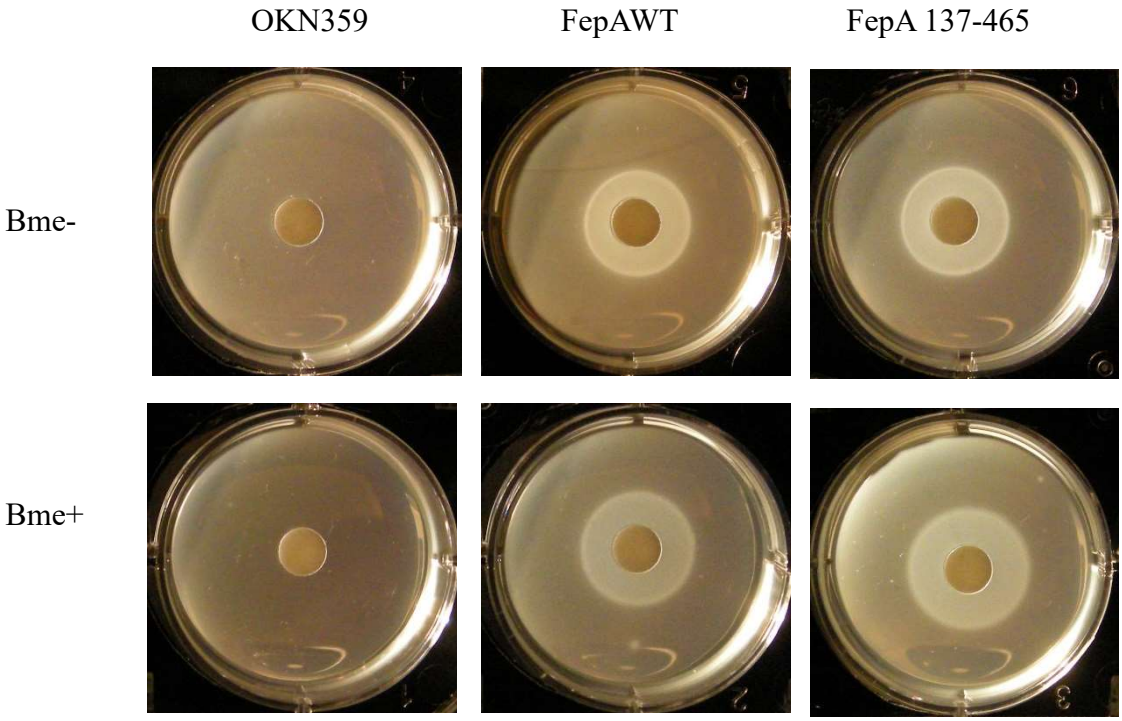


Figure 5-2 Siderophore nutrition test in the presence or absence of βME.

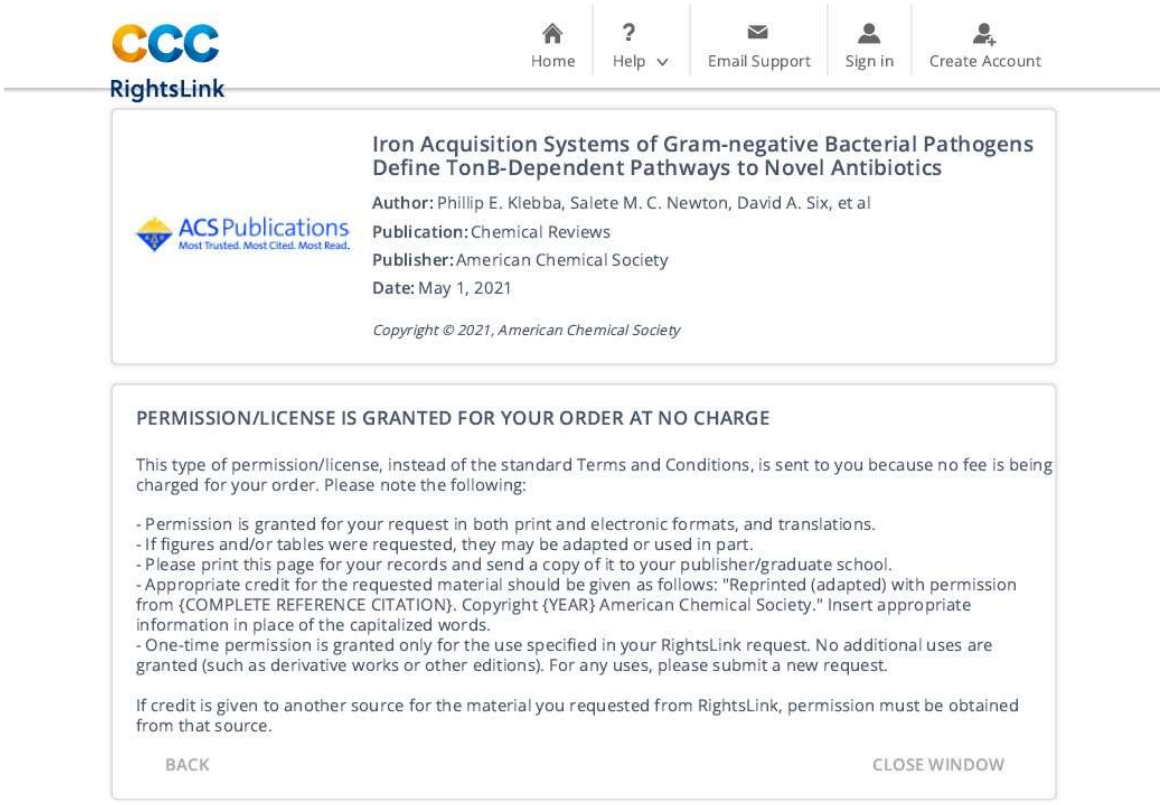
We analyzed the transport of FeEnt by WT FepA and FepA mutant carrying cysteine pair 137-465, with OKN359 as the negative control. 3 mM βME was added to create the reducing condition

Reference

1. Chakravorty, S., Shipelskiy, Y., Kumar, A., Majumdar, A., Yang, T., Nairn, B. L., Newton, S. M., and Klebba, P. E. (2019) Universal fluorescent sensors of high-affinity iron transport, applied to ESKAPE pathogens. *Journal of Biological Chemistry* 294, 4682-4692
2. Majumdar, A., Trinh, V., Moore, K. J., Smallwood, C. R., Kumar, A., Yang, T., Scott, D. C., Long, N. J., Newton, S. M., and Klebba, P. E. (2020) Conformational rearrangements in the N-domain of Escherichia coli FepA during ferric enterobactin transport. *Journal of Biological Chemistry* 295, 4974-4984
3. Cao, Z., Qi, Z., Sprencel, C., Newton, S. M., and Klebba, P. E. (2000) Aromatic components of two ferric enterobactin binding sites in Escherichia coli FepA. *Molecular microbiology* 37, 1306-1317
4. Annamalai, R., Jin, B., Cao, Z., Newton, S. M., and Klebba, P. E. (2004) Recognition of ferric catecholates by FepA. *Journal of bacteriology* 186, 3578-3589

Appendix A – Copyright Permissions

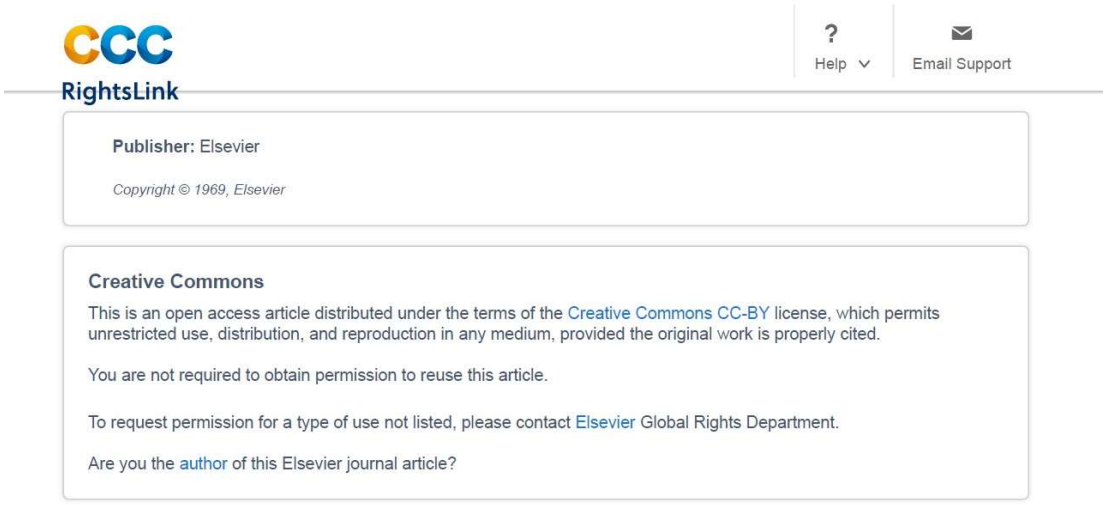
Chapter 1 Published figure and table



Chapter 4 Published figures and tables



Appendix B – Published Studies



JBC ARTICLE

Universal fluorescent sensors of high-affinity iron transport, applied to ESKAPE pathogens

Received for publication, December 3, 2018, and in revised form, January 18, 2019 Published, Papers in Press, January 24, 2019, DOI 10.1074/jbc.RA118.006921

Somnath Chakravorty[‡1,2], Yan Shipelskiy[‡1,3], Ashish Kumar[‡], Aritri Majumdar[‡], Taihao Yang[‡], Brittany L. Nairn[§], Salete M. Newton[‡], and Phillip E. Klebba[‡4]

From the [‡]Department of Biochemistry and Molecular Biophysics, Kansas State University, Manhattan, Kansas 66506 and the [§]Department of Biological Sciences, Bethel University, St. Paul, Minnesota 55112

Edited by Chris Whitfield

Sensitive assays of biochemical specificity, affinity, and capac- ity are valuable both for basic research and drug discovery. We created fluorescent sensors that monitor high-affinity binding reactions and used them to study iron acquisition by ESKAPE bacteria, which are frequently responsible for antibiotic-resist- ant infections. By introducing site-directed Cys residues in bac- terial iron transporters and modifying them with maleimide fluorophores, we generated living cells or purified proteins that bind but do not transport target compounds. These constructs sensitively detected ligand concentrations in solution, enabling accurate, real-time spectroscopic analysis of membrane trans- port by other cells. We assessed the efficacy of these "fluorescent decoy" (FD) sensors by characterizing active iron transport in the ESKAPE bacteria. The FD sensors monitored uptake of both ferric siderophores and hemin by the pathogens. An FD sensor for a particular ligand was universally effective in observing the uptake of that compound by all organisms we tested. We adapted the FD sensors to microtiter format, where they allow high-throughput screens for chemicals that block iron uptake, without genetic manipulations of the virulent target organisms. Hence, screening assays with FD sensors facilitate studies of mechanistic biochemistry, as well as discovery of chemicals that inhibit prokaryotic membrane transport. With appropriate design, FD sensors are potentially applicable to any pro- or eukaryotic high-affinity ligand transport process.

Sensitive assays of biochemical specificity, affinity, and capacity are valuable in many experimental settings, including biochemical measurements of living cells, and the discovery of new therapeutic compounds. At present, a need exists for new antibiotics against multidrug-resistant bacteria because without them treatment options for many infections will dwindle (1). Gram-negative strains cause about two-thirds of the mortality from bacteria in United States hospitals, and up to 20% of these strains are resistant to all antibiotics (2). The World Health Organization identified the Gram-negative ESKAPE[5] pathogens *Klebsiella pneumoniae*, *Acinetobacter baumannii*, *Pseudomonas aeruginosa*, and *Enterobacter* spp. as well as carbapenem-resistant strains of *K. pneumoniae* and *Escherichia coli* as critical targets for drug discovery (3). Compounds that inhibited bacterial cell envelope processes were once the most potent antibiotics, but now their efficacy has diminished as a result of bacterial adaptation (4). Gram-negative bacterial antibiotic resistance largely originates from cell envelope physiology: the outer membrane (OM) excludes large or hydrophobic compounds (5), periplasmic enzymes degrade or inactivate chemicals that breach the OM barrier, and inner membrane (IM) pumps expel hydrophobic molecules, including antibiotics (6). Similar processes in Gram-positive bacteria heighten the need for new treatments of bacterial infections.

Nevertheless, bacterial pathogens face nutritional obstacles in human and animal hosts that we may exploit against them. Iron, for example, is a cofactor in many biochemical pathways, including catabolism, DNA synthesis, and bioenergetics (7). Iron deprivation retards bacterial growth, whereas iron availability promotes it (8). Animals sequester iron in transferrin, lactoferrin, and ferritin to minimize bacterial infections (9). However, microbial siderophores (10–12) capture the metal from host proteins (13), and ferric siderophores then enter bac- terial cells through high-affinity acquisition systems (14). The balance of these competing processes influences the outcome of infection, so bacterial iron uptake systems are potential tar- gets for antibiotics.

Toward that end, we studied the ferric enterobactin (FeEnt) uptake system (14) of Gram-negative bacteria. FeEnt enters

This work was supported by NIAID, National Institutes of Health Award R21AI115187 (to P. E. K. and S. M. N.) and a Kansas IDeA Network of Biomedical Research Excellence (K-INBRE; National Institute of General Medical Sciences of the National Institutes of Health Grant P20GM103418) postdoctoral research award (to S. C.). The authors declare that they have no conflicts of interest with the contents of this article. The content is solely the responsibility of the authors and does not necessarily represent the official views of the National Institutes of Health.
This article contains Figs. S1–S4 and Table S1.

[1] Both authors made equal contributions to this work.
[2] Present address: Jacobs School of Medicine and Biomedical Sciences, Buffalo, NY 14203.
[3] Present address: Battelle Memorial Institute, Pueblo Chemical Depot (PCAPP), Pueblo, CO 81006.
[4] To whom correspondence should be addressed: Dept. of Biochemistry and Molecular Biophysics, 141 Chalmers Hall, Kansas State University, Manhattan, KS 66506. Tel.: 785-532-6268; E-mail: peklebba@ksu.edu.

[5] The abbreviations used are: ESKAPE, *E. faecalis*, *S. aureus*, *K. pneumoniae*, *A. baumannii*, *P. aeruginosa*, *Enterobacter* spp.; FD, fluorescent decoy; OM, outer membrane; IM, Inner membrane; FeEnt, ferric enterobactin; TBDT, TonB-dependent transporter; FM, fluorescein maleimide; Hn, hemin; FeGEnt, glucosylated form of FeEnt; Fc, ferrichrome; CPM, 7-diethylamino-3-(4 -maleimidylphenyl)-4-methyl coumarin; HTS, high-throughput screening; FLHTS, fluorescence high-throughput screening; Eco, *E. coli*; Lmo, *L. monocytogenes*; Kpn, *K. pneumoniae*; Aba, *A. baumannii*; CCCP, carbonyl cyanide *p*-chlorophenylhydrazone; NEAT, NEAr Transporter.

This is an Open Access article under the CC BY license.

© 2019 Chakravorty et al. Published under exclusive license by The American Society for Biochemistry and Molecular Biology, Inc.

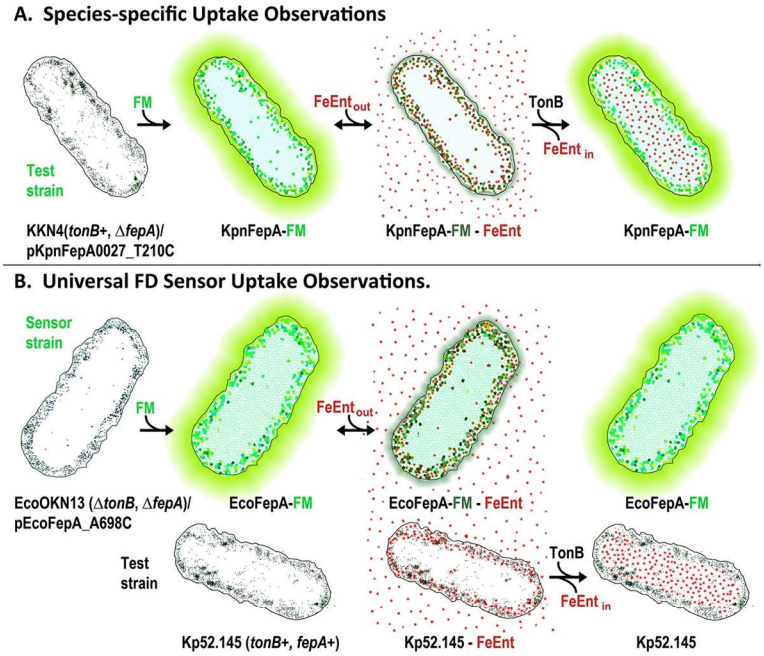


Figure 1. Fluorescence observations of membrane transport. *A*, species-specific assay design. The target organism (*e.g. K. pneumoniae*) contains a Cys substitution for a surface-exposed residue in a TonB-dependent transporter (KpnFepA_T210C) labeled with FM. Fluorescence emissions depict FeEnt binding and TonB-dependent FeEnt transport in *K. pneumoniae*. *B*, universal FD sensor assay design. The fluorescence of a TonB-deficient *E. coli* "sensor" strain OKN13 (11*tonB*, 11*fepA*)/pEcoFepA_A698C-FM reflects TonB-dependent FeEnt transport by a second test strain (*e.g. K. pneumoniae* strain Kp52.145) in the same solution.

through the OM protein FepA, which selectively binds and transports it. The uptake reaction requires the additional cell envelope protein TonB (15), so FepA and other OM proteins in this superfamily are called "TonB-dependent transporters" (TBDTs) (16). TonB action, which is proposed to transmit the potential energy of the electrochemical proton gradient across the IM to TBDT in the OM (17), underlies the active intake of bound iron complexes (18). TonB is ubiquitous in Gram-negative bacteria and a determinant of their pathogenesis (12, 14, 19). Iron acquisition through TBDT contributes to the invasiveness of the Gram-negative ESKAPE pathogens (20), the determination of their ultimate localization in human and animal tissues (21, 22), and the overall outcome of their infections (9, 12, 14).

We previously designed fluorescence methods that monitored high-affinity ligand binding and uptake (23, 24). By genet- ically engineering FepA and then labeling it with fluorescein maleimide (FM; Fig. S1), we created a sensor that reflected [FeEnt] in the environment. When FeEnt bound to FepA-FM, it quenched its fluorescence. Quenching originated from bind- ing-induced conformational motion in the external loops of FepA, which subjected attached fluorophores to collisions with other residue side chains or elements of protein structure or increased interactions with the aqueous environment (23, 24). When cellular uptake depleted FeEnt from solution, fluores- cence rebounded. Consequently, FepA-FM tracked the binding and transport of FeEnt by living bacteria.

In this study, we created both species-specific and generic fluorescence spectroscopic assays (Figs. 1 and S1) that measure ligand uptake. Fluorescently labeled, binding-competent, but transport-defective cells and fluorescently labeled purified pro- teins were key innovations in these experiments. Such geneti- cally engineered cells or proteins comprise "fluorescent decoy" (FD) sensors, which report ligand concentrations in solution and monitor transport of the same ligand by other cells. We illustrate these applications by observations of iron transport activity through Gram-negative bacterial TBDTs and Gram- positive bacterial NEAT domain–dependent hemin (Hn) uptake systems. Both high-affinity pathways function at nano- molar concentrations, and both contribute to bacterial coloni- zation of eukaryotic hosts (10, 12). We adapted these fluores- cence tests to a microtiter high-throughput screening format to enable discovery of inhibitors that retard iron acquisition and thereby prevent bacterial growth and pathogenesis.

Results

Universal fluorescence sensor of FeEnt acquisition

We originally devised species- or transporter-specific fluorescence assays of FeEnt uptake for FepA of *E. coli* (23) and *A. baumannii* (25); the same approach was effective for FepA of *K. pneumoniae* (Fig. 2). We cloned and genetically engineered *KpnfepA* of strain Kp52.145 to enable site-directed fluoresceination in its native cellular (*i.e. K. pneumoniae*) environment and in *E. coli*. These studies compared the acquisition of FeEnt

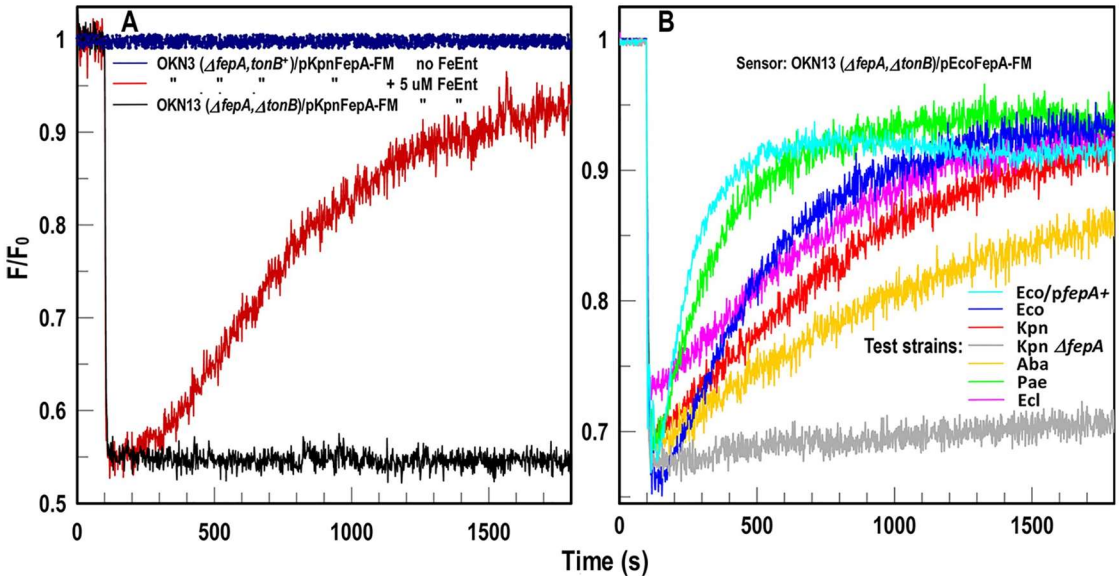


Figure 2. FD sensor analysis of FeEnt acquisition by ESKAPE pathogens. *A*, species-specific fluorescence assay of FeEnt uptake. KpnFepA-FM. *E. coli* OKN3 (11*fepA*) expressing KpnFepA-FM was exposed to FeEnt in PBS + 0.2% glucose. The tracings show emissions of living cells in the absence (*dark blue*) or presence (*dark red* or *black*) of FeEnt. In *tonB*$^+$ cells (*dark red*), FeEnt binding to KpnFepA-FM (at 100 s) quenched emissions, but subsequent uptake depleted FeEnt from solution, restoring fluorescence. In TonB-deficient *E. coli* OKN13 (11*fepA*, 11*tonB*)/pKpnFepA-FM; *black*), which cannot transport FeEnt, quenching occurred but not recovery. *B*, Universal fluorescence assay of FeEnt uptake using sensor strain OKN13/pEcoFepA-FM. FeEnt binding at 100 s quenched the fluorescence of the FD sensor strain *E. coli* OKN13/pEcoFepA-FM. It cannot transport FeEnt, so subsequent recovery did not occur. However, the fluorescence of the *E. coli* strain reflected FeEnt uptake by other bacteria in the same solution: as they decreased [FeEnt] by cellular transport, the intensity of OKN13/pEcoFepA-FM returned to initial levels (as described in Fig. 1*B*). The assay monitored FeEnt uptake by *E. coli* expressing chromosomal (*Eco*; *cyan*) or plasmid-mediated (*Eco/pfepA*$^+$; *blue*) FepA, and ESKAPE species *K. pneumoniae* (*Kpn*; *red*), *A. baumannii* (*Aba*; *gold*), *P. aeruginosa* (*Pae*; *green*), and *E. cloacae* (*Ecl*; *magenta*). FepA-deficient *K. pneumoniae* (KKN4; *black*) does not transport FeEnt and did not recover. Hence, OKN13/pEcoFepA-FM was a universal sensor of [FeEnt] that monitored FeEnt acquisition by all the bacteria. The panels show the results of single representative experiments that were performed in triplicate, from which we calculated and plotted the mean values. Standard deviations of the mean measurements (data not shown) were 1.7–2.7%.

by FepA orthologs in different bacteria. As for FepA of *E. coli* (23) and *A. baumannii* (25), FM exclusively labeled KpnFepA in living cells (Figs. S1 and S2; see Table S1 for strains, plasmids, and abbreviations), and the fluoresceinated OM protein detected and quantified its ligand, FeEnt. Binding of FeEnt to KpnFepA-FM quenched its fluorescence, but as the transporter's activity depleted FeEnt from solution, fluorescence intensity rebounded (Fig. 2*A*). Thus, by the species-specific approach, EcoFepA-FM (23), AbaFepA-FM (25), and KpnFepA-FM (Fig. 2*A*) all detected FeEnt binding and reflected its transport. Each of these transporters requires TonB action for FeEnt uptake: its absence or inhibition prevented fluorescence recovery. By engineering the individual transporters of specific bacteria, we observed, monitored, and characterized their TonB-dependent iron uptake processes.

The species-specific method was sensitive and accurate, but genetic and biochemical manipulations of ESKAPE organisms and other pathogens are technically challenging and potentially hazardous. We discovered a modification that extends the scope of the assay to allow observations of FeEnt uptake by other organisms, including clinical isolates, without genetically engineering them. TonB-deficient Gram-negative cells adsorb ferric siderophores and other metal complexes (*e.g.* vitamin B_{12} (15, 16)) but cannot transport them. Thus, FeEnt bound to *E. coli* OKN13 (11*tonB*, 11*fepA*)/pEcoFepA-FM, quenching its fluores- cence, but the strain's TonB deficiency prevented FeEnt internalization (Figs. 1*B* and 2*B*). The placement of EcoFepA-FM in OKN13 transformed the cell into an FD sensor, whose emissions inversely related to [FeEnt]. The transport-defective, physiologi- cally inert, fluorescent 11*tonB* bacteria detected the presence and concentration of FeEnt. When this strain cohabited an environ- ment with other bacteria, it reflected their uptake of FeEnt. Solu- tion levels that saturated EcoFepA-FM (K_d = 0.2 nM (24, 26)) quenched its fluorescence, but if the ambient [FeEnt] decreased from its uptake by other cells, then fluorescence rebounded. The upshot is that the 11*tonB* FD sensor cells monitored FeEnt trans- port by wild isolates of *K. pneumoniae*, *A. baumannii*, *P. aerugi- nosa*, and *Enterobacter cloacae* (Figs. 1*B* and 2*B*). The FD sensor observed FeEnt uptake by all the organisms we tested, reflecting TonB action in the pathogens.

Affinity determinations by spectroscopic analyses

The analytical capabilities of the fluorescence spectroscopic determinations stood out when we compared the recognition of FeEnt and its glucosylated form, FeGEnt (also known as ferric salmochelin (27)), by EcoFepA and KpnFepA. The ability of Gram-negative pathogens, including *K. pneumoniae*, to glucosylate enterobactin and transport FeGEnt enhances their invasiveness (21), in part because glucosylation impairs recognition of the iron complex by lipocalins (28, 29). Additionally, whereas
E. coli K12 contains a single chromosomal *fepA* locus that encodes its FeEnt transporter, pathogenic *K. pneumoniae* con-

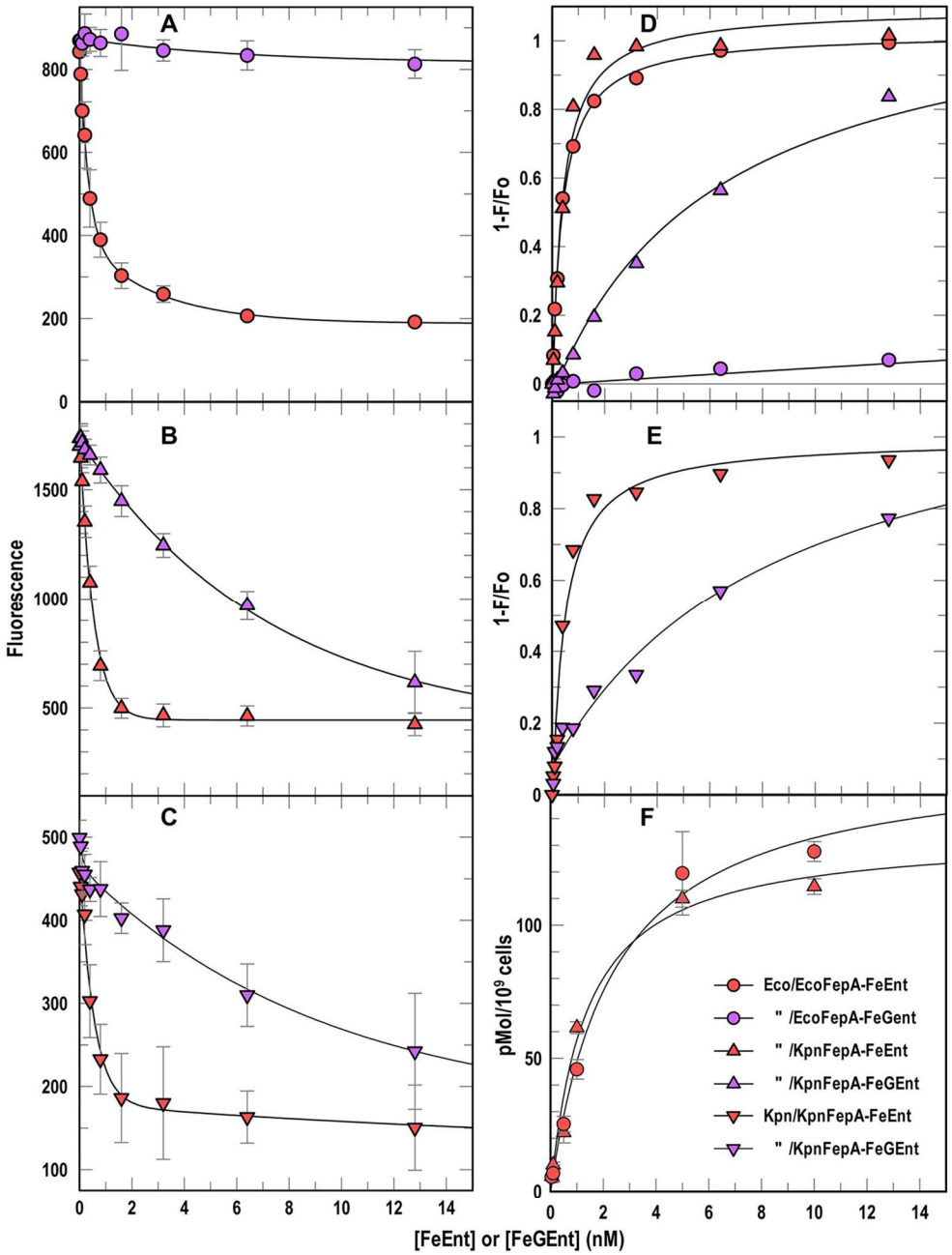


Figure 3. Binding affinities from spectroscopic assays. *A–E*, we added FeEnt (*red symbols*) or FeGEnt (*purple symbols*) to *E. coli* OKN13/pEcoFepA-FM (*A* and *D*, *circles*) or OKN13/pKpnFepA-FM (*B* and *D*, triangles) or *K. pneumoniae* KKN4/pKpnFepA-FM (*C* and *E*, *inverted triangles*). *A–C*, quenching data from this species-specific test quantified binding of the iron complexes. Nonlinear fits of $1 - F/F_0$ (*D* and *E*) using the one-site (with background) equation of Grafit 6.02 revealed the affinities (K_d) of the binding reactions (Table 1). *F*, [^{59}Fe]Ent binding measurements. We added varying concentrations of [^{59}Fe]Ent to OKN3/pEcoFepA (*circles*) or OKN3/pKpnFepA (*triangles*), measured adsorption of the ferric siderophore by filter-binding assays (26), and obtained nonlinear fits to the one-site (with background) equation of Grafit 6.02, which gave the affinities (K_d) of the binding reactions (Table 1). In each panel the error bars represent S.D. of triplicate measurements at each concentration tested.

tain at least three *fepA* orthologs (chromosomal loci *1658* and *4984* and plasmid PII locus *0027*). IroN of *Salmonella enterica* serovar Typhimurium has a role in FeGEnt uptake (27); its closest ortholog in *K. pneumoniae* is plasmid-mediated *fepA0027*. After bioinformatics analyses and structural modeling of KpnFepA0027, we cloned its structural gene and engineered the Cys

Table 1
Affinities of EcoFepA and KpnFepA0027 for ferric catecholates

	K_d (S.E.)[1]			
Strain/Species[2]	FeEnt[3]	FeGEnt[3]	Strain/Species[2]	[^{59}Fe]Ent[4]
OKN13/pEcoFepA-FM	0.39 (0.03)	279 (278)	OKN3/pEcoFepA	2.35 (0.68)
OKN13/pKpnFepA-FM	0.38 (0.07)	6.26 (0.54)	OKN3/pKpnFepA	1.34 (0.03)
KKN4/pKpnFepA-FM	0.45 (0.12)	8.57 (2.15)		

[1] K_d values were calculated by the one-site (with background) equation of Grafit 6.02.
[2] Bacteria were grown in iron-deficient minimal MOPS medium to 5 X 10^8 cells/ml. For fluorescence studies, they were modified with FM and washed with and resuspended in PBS.
[3] Binding determinations were conducted in a 10 ml volume in an Olis Clarity spectrofluorometer by adding varying concentrations of purified FeEnt or FeGEnt to bacteria at 1.25 X 10^7 cells/ml and observing quenching. The excitation/emission maxima were 488/520 nm.
[4] [^{59}Fe]Ent binding determinations were conducted in 10 ml of ice-cold PBS (26), with cells chilled on ice.

substitution T210C (Fig. S1), which is nominally equivalent to T216C in EcoFepA (24). To define its recognition specificity, we expressed and FM-labeled KpnFepA0027_T210C (KpnFepA-FM) in *E. coli* OKN13 (11*tonB*, 11*fepA*) and in *K. pneumoniae* KKN4 (11*entB*, 11*fepA0027*, 11*fepA1658*, 11*fepA4984*) relative to EcoFepA-FM in OKN13. The comparison of FeEnt and FeGEnt adsorption to KpnFepA-FM and EcoFepA-FM in different bacteria revealed several things. First, KpnFepA was fluoresceinated to 3-fold higher levels in *E. coli* (Fig. 3*B*) than in its native *K. pneumoniae* (Fig. 3*C*). The better labeling of KpnFepA in the *E. coli* sensor strain made it more responsive to quenching, resulting in more accurate measurements (smaller variations in the mean extent of quenching). Second, both KpnFepA-FM and EcoFepA-FM preferred FeEnt (K_d = 0.38 nM) over FeGEnt (K_d = 6–280 nM; Fig. 3 and Table 1). These data recapitulate previously published affinities and specificities of EcoFepA for FeEnt (26, 30). FeGEnt adsorbed to KpnFepA with 20-fold lower affinity (K_d = 6.3 nM) than FeEnt, and FeGEnt barely bound to EcoFepA at all (Fig. 3*A*), so weakly that it was problematical to make an accurate measurement (Table 1). Despite its 3-fold lower specific fluoresceination in *K. pneumoniae*, KpnFepA-FM showed the same preferences and affinities in that environment (Fig. 3, *B* and *C*). Lastly, we compared the spectroscopic tests with conventional radioisotopic binding measurements. The latter approach with [^{59}Fe]Ent yielded comparable affinities of EcoFepA and KpnFepA for FeEnt (Fig. 3*E* and Table 1), but the former fluorescence methods were more sensitive, with equivalent or better reproducibility and more accurate statistical fits (Table 1). Overall, the experi- ment showed that individual, fluorescently labeled transport- ers (*i.e.* the species-specific approach) accurately depicted the concentration dependence of ligand binding, with best sensitiv- ity in the *E. coli* cell envelope and less but acceptable accuracy in
the more complex cell envelopes of the infectious bacteria.

Transport rates from spectroscopic analyses

The rate of fluorescence recovery in the spectroscopic system correlates to the rate of ligand depletion by bacterial transport (23), and comparisons of test strains in universal FD uptake assays reiterated this point. The various ESKAPE bacteria conferred fluorescence recovery at different rates (Fig. 2*B*). Because we tested the individual bacteria at equal cell concentrations, their rates were directly comparable with one another. However, absolute calculations of rate parameters (*i.e.* V_{max} and k_{cat}) from FD recovery time courses are complicated by other factors besides the kinetic attributes of the transporters, including their expression levels and, in this system, the expres- sion of TonB. Consequently, FD assays are best suited to com- parative rate measurements among the test strains, from either the slope of the recovery curve or the duration of quenching after initiation of uptake (Fig. 4). In the former case, when uptake of FeEnt reverts fluorescence to a level of 50%, the EcoFepA-FM sensor is half-saturated, so [FeEnt] = K_d (0.38 nM). The slope of the time course at this point reveals the uptake rate of the test strain at [FeEnt] = 0.38 nM. In the latter case, the test strain's transport rate determines the elapsed time from addition of FeEnt to half-maximal quenching (*i.e.* half-satura- tion). For example, at 10^7 cells/ml, *K. pneumoniae* Kp52.145 required 520 s to deplete 5 nM FeEnt to 0.38 nM (*i.e.* half-satu- ration), which translates into a mean uptake rate over the first 520 s of 53 pmol/10^9 cells/min. The hypothetical mean uptake rate over this range of saturation ($14.3K_m$ ≈ K_m) is ~ 0.8 V_{max}, suggesting that for *K. pneumoniae* Kp52.145, V_{max} = 53 pmol/10^9 cells/min 0.8 = 66 pmol/10^9 cells/min. This value approximates V_{max} for chromosomally expressed FepA in *E. coli* (50–100 pmol/min/10^9 cells (31)). We conducted this prototypic assay with *K. pneumoniae* in the presence of an *E. coli* EcoFepA-FM FD sensor, but the test similarly functioned for all of the Gram-negative bacteria (Fig. 2). FD assays are conceptually universal in that an appropriately configured sensor will function in many biological systems, with few excep-

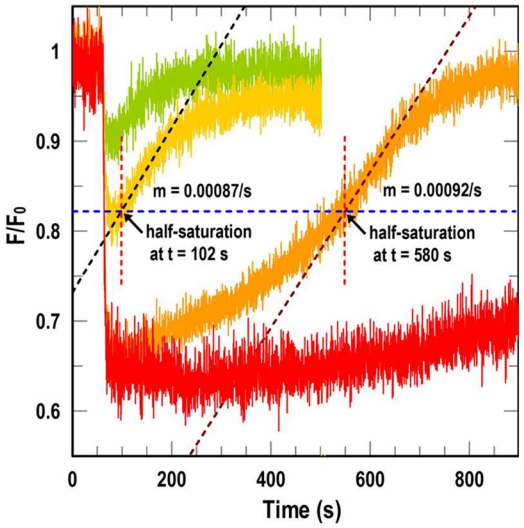


Figure 4. Uptake rates from FD assays. At t = 60 s we added varying concentrations of FeEnt ((0.5 (*green*),1 (*yellow*),5 (*orange*), and 10 nM (*red*)) to sensor strain OKN13/pEcoFepA-FM in the presence of test strain *K. pneumoniae* isolate Kp52.145. 10 nM FeEnt gave maximal quenching. For 1 and 5 nM FeEnt, at half-saturation (*blue dashed line*) we determined the slope of the time course (*black dashed line*) and the elapsed time (*dashed red line*). Either parameter estimated the transport rate of the test strain (see text).

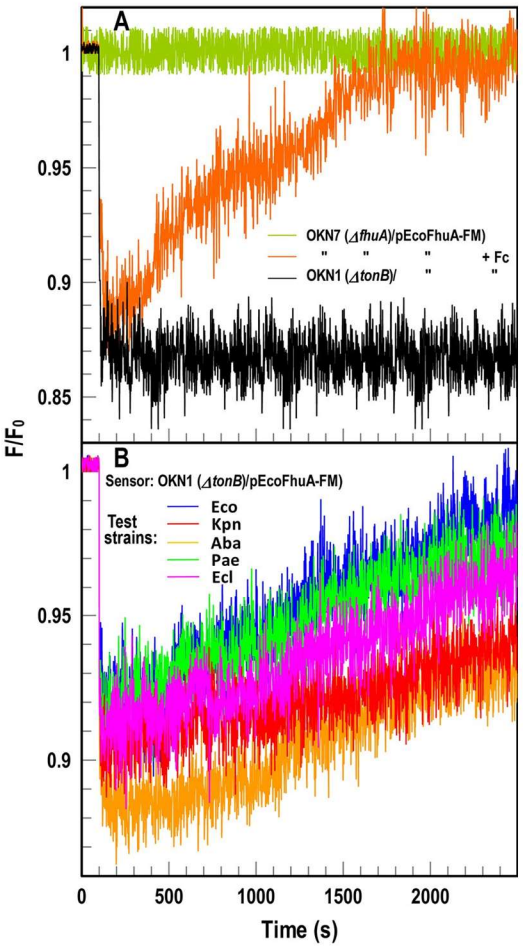


Figure 5. FD sensor analysis of Fc acquisition by ESKAPE pathogens. *A*, species-specific fluorescence assay of Fc uptake. OKN7 (Δ*fhuA*)/pEcoFhuA-FM reflects Fc binding and transport (*orange*). In OKN1 (Δ*tonB*; *black*) the same construct became an inert sensor of [Fc]: binding of Fc quenched fluorescence, and the absence of transport prevented recovery to initial levels. *B*, universal assay of Fc uptake. We incubated the sensor strain with 1.5 X 10^7 cells of Gram-negative ESKAPE pathogens. Colored tracings denote the same strains as in Fig. 2. In each case, the pathogens acquired Fc, causing fluorescence recovery of the sensor strain. Uptake of Fc occurred at a slower rate than FeEnt (30), resulting in slower fluorescence recovery. The panels show the results of single representative experiments that we performed in triplicate, from which we calculated and plotted the mean values. Standard deviations of the mean measurements (data not shown) were 2.5–4%.

tions (see "Discussion"), to monitor changes in the concentration of its target ligand.

Universal FD sensor of ferrichrome (Fc) acquisition

The FD sensor approach was relevant to the uptake of other iron complexes by *E. coli* and other bacteria. We engineered mutation D396C in EcoFhuA, the OM Fc transporter (32), and modified it with FM (Fig. S1*B*). EcoFhuA-FM measured Fc uptake in *tonB*$^+$ *E. coli* (Fig. 5*A*), but in the TonB-deficient strain OKN1, EcoFhuA-FM was an FD sensor that detected Fc uptake by any of the carbapenem-resistant/ESKAPE bacteria (Fig. 5*B*). As seen for FeEnt–EcoFepA-FM, binding of Fc to EcoFhuA-FM quenched its emissions, and depletion of Fc from solution by microbial transport restored fluorescence intensity. This additional test of a second TonB-dependent transport reaction by the ESKAPE species, without the need to genetically modify them, showed the breadth of the FD concept: an appro- priately labeled TBDT in a Δ*tonB* host became a transport- deficient FD sensor cell that reflected the concentration of its ligand in solution. This approach potentially encompasses the diverse repertoire of microbial ferric siderophores (33) and their membrane protein receptors. It is also adaptable to other metal complexes that microbes utilize and nonmetal, high-af- finity ligand–receptor pairs.

Universal FD sensor of heme uptake

Using a slightly modified method, the FD sensor technology described a third relevant microbial transport system: Hn uptake by Gram-positive bacteria. *Listeria monocytogenes*, *Staphylococ- cus aureus*, *Streptococcus pyogenes*, *Bacillus anthracis*, and other Gram-positive bacteria produce NEAT domain–containing Hn- binding proteins, which either anchor to peptidoglycan by the actions of sortases A (34) and B (35) or pass to the external envi- ronment where they act as hemophores (36). Some Gram-nega- tive species like *Serratia marcescens* also secrete hemophores (*e.g.* HasA (37)), and others (*e.g. Vibrio cholerae* (38)) directly transport the iron porphyrin. We engineered the listerial NEAT-domain protein Hbp2 to create an FD sensor of Hn binding and uptake (Figs. S1*C* and S3). Introduction of Cys in NEAT1 of LmoHbp2 allowed its modification by extrinsic fluorophores, transforming the purified binding protein into a sensitive sensor whose emissions inversely related to [Hn]. LmoHbp2_S154C-CPM (LmoHbp2-CPM) detected Hn in solution (Fig. 6*A*) with an affinity (K_d = 12 ± 3.1 nM) that was consistent with isocalorimetric (K_d = 25–48 nM (39)) and radioisotopic (K_d = 12 nm (36)) data. The sensor also revealed the ability of other bacteria to transport Hn (Fig. 6*B*) at different rates. Overall, the bacterial cells OKN13/pEcoFepA-FM and OKN1/pEcoFhuA-FM and the purified protein LmoHbp2-CPM functioned as universal sensors of extracellular iron in different forms: FeEnt, Fc, and hemin, respectively.

Adaptation of FD sensors to fluorescence high-throughput screening (FLHTS)

Compounds that block iron acquisition by inhibiting TonB action in Gram-negative bacteria or by reducing Hn uptake into Gram-positive cells may combat bacterial proliferation in human and animal hosts. We previously used the species-specific spectroscopic test in microtiter format to screen chemical libraries for inhibitors of *E. coli* TonB. Consequently, we transposed the FD sensor assays to microtiter format for FLHTS. However, despite the fact that all the Gram-negative ESKAPE bacteria utilized FeEnt (Fig. 2), the adaptation of this method to screen against them faced obstacles. First, bacterial pathogens often manifest reduced cell envelope permeability that lowers antibiotic susceptibility. Compounds that penetrate *E. coli* may not enter ESKAPE organisms. Second, protein orthologs in dif- ferent bacteria typically manifest cross-species sequence diver- gence, so compounds that inhibit EcoTonB may not similarly impair TonB in Gram-negative ESKAPE bacteria. For these rea-

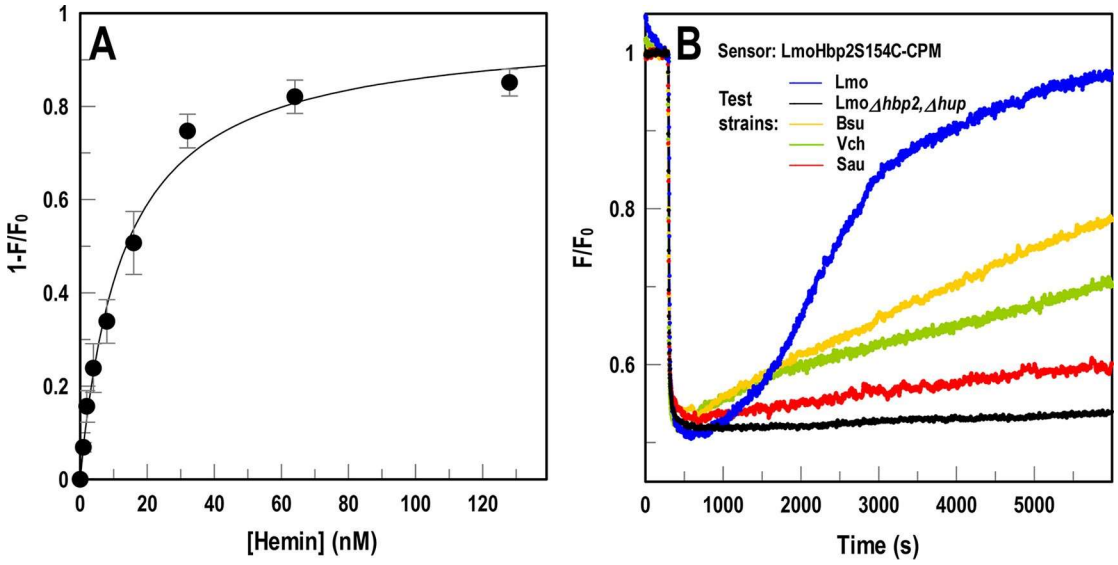


Figure 6. FD sensor assay of hemin uptake. We substituted Cys for residue Ser-154 in NEAT1 of LmoHbp2, expressed and purified the binding protein, and covalently modified it with CPM. *A*, concentration dependence of hemin binding to LmoHbp2-CPM. Using purified LmoHbp2-CPM, plots of $1 - F/F_0$ *versus* [hemin], analyzed by nonlinear fit to the one-site (with background) equation of Grafit 6.02, produced a saturation curve with $K_d = 12 \pm 3.1$ nM. The *error bars* represent S.D. of triplicate measurements at each concentration tested. *B*, Hbp2-CPM detects and quantifies bacterial hemin transport. When we mixed Hbp2-CPM with heterologous bacteria in solution, the assay reflected their hemin uptake. Addition of hemin at 300 s quenched LmoHbp2-CPM emissions, but fluorescence rebounded as bacteria (*L. monocytogenes* (*Lmo*; *blue*), *Bacillus subtilis* (*Bsu*; *gold*), *S. aureus* (*Sau*; *red*), and *V. cholerae* (*Vch*; *green*)) transported the porphyrin and depleted it from solution. Conversely, hemin transport– deficient cells (EGDe 11*hbp2*, 11*hup*; *black*) did not elicit fluorescence recovery. The panel shows the results of a single representative experiment that was performed in triplicate, from which we calculated and plotted the mean values. Standard deviations of the mean measurements (data not shown) were 2–2.9%.

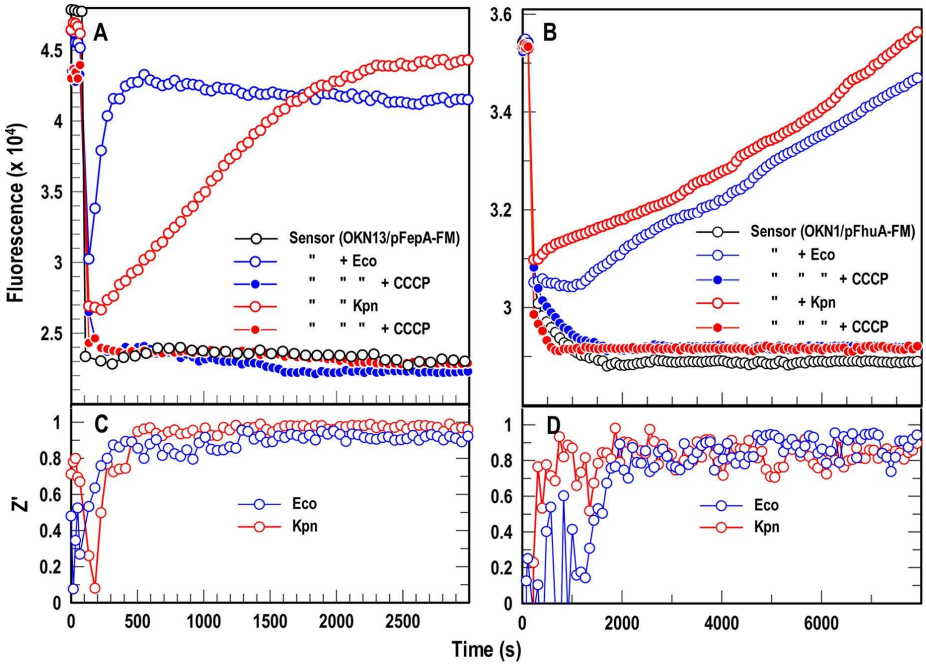


Figure 7. *A* and *B*, FD HTS assay for Gram-negative bacterial TonB-dependent FeEnt (*A*) and Fc (*B*) transport. We used a 11*tonB* host harboring either pEcoFepA-FM (*A*) or pEcoFhuA-FM (*B*), suspended in microtiter plates, to create universal FD sensors of FeEnt or Fc uptake, respectively. The inert sensors effectively monitored active iron transport in 96-well microtiter plates by both *E. coli* (*blue*) and *K. pneumoniae* (*red*). The proton ionophore CCCP (23) abrogated iron uptake, so fluorescence did not recover in the presence of these compounds. *C* and *D*, statistical comparisons of these positive and negative controls yielded Z' factors approaching 1.0 within 10 min in the case of FeEnt (*C*) and 35 min in the case of Fc (*D*). The panels show the results of single representative experiments that were performed in triplicate, from which we calculated and plotted the mean values. Standard deviations of the mean measurements (data not shown) were 1.9–4.1%.

sons it is preferable to directly screen chemical libraries against the target ESKAPE pathogens. The species-specific approach is adaptable to ESKAPE bacteria for FLHTS (as seen for *A. bau- mannii* (25)) and *K. pneumoniae* (Fig. 2), but more extensive lipopolysaccharides and capsular polysaccharides in clinical isolates reduce the efficiency of modifying their OM proteins with fluorophores (*e.g.* Kp52.145 in Fig. 3). FD sensor assays with fluorescent cells or proteins circumvent this problem because they allow FLHTS against the pathogens (with ade- quate Z' of 0.8 –1.0; Fig. 7) without the need to fluorescently modify them. The *E. coli* FD sensor cells in microtiter wells followed the TonB-dependent uptake of both FeEnt and Fc by *K. pneumoniae.* The sensors minimized the experimental manipulations of the pathogen while allowing spectroscopic observations of its physiology that were sensitive to varying concentrations of both the ligands and the bacterial cells (Fig. S4).

Discussion

We considered several attributes of the FD constructs in making the designation "universal." (i) Sensors for FeEnt, Fc, or heme had the ability to detect and quantify the uptake of their target ligand by any Gram-positive or -negative bacterium we tested. This unrestricted scope alone strongly supported the term universal, but FD sensors had additional universalities. (ii) The technical concept was applicable to virtually any high-af- finity ligand whether ferric siderophores, other metal complexes, or other molecules. (iii) FD sensors were straightforward to create from any cloned, high-affinity binding protein as we showed for EcoFepA, KpnFepA, EcoFhuA, and LmoHbp2. These fluorescently labeled, Cys-mutant proteins detected and discriminated FeEnt, FeGEnt, Fc, and hemin. Hence, it is conceivable to create sensors for any iron complex of interest or other high-affinity ligand. (iv) The site-directed Cys-fluorophore labeling approach succeeded with any maleimide fluorophore we tried: FM, 7-diethylamino-3-(4'-maleimidylphenyl)-4-methyl coumarin (CPM), and in previous work Alexa Fluors 546, 555, 647 and 680, which differ in mass, structure, and spec- tral properties. (v) Because the sensors are expressed from plas- mids, the engineered BSL-1 sensor strains that host them may be centrally stored and distributed to any interested researcher.
(vi) FD sensors may achieve many biochemical and microbiologi- cal purposes: determination of the presence and concentrations of siderophores in natural and host environments; identification of the siderophores elaborated or the ferric siderophores transported by an organism; surveys of microbiological families, genera, or spe- cies to determine which members use a certain metal complex; and measurements of the specificities, affinities, and kinetic attri- butes of a transport system for a single ligand or a family of ligands. All these applications have the inherent analytical power to discriminate ligands in the nanomolar concentration range.

A technology that quantitatively monitors (i) *any* microorganism for uptake of (ii) *any* specific ligand using (iii) *any* cloned, high-affinity binding protein modified by (iv) *any* maleimide fluorophore with (v) central distribution to *any* investigator for applications that span (vi) a variety of microbiological and biochemical purposes has a claim to the term universal. Exceptions or clarifications may arise to this designa- tion, but these may be recognized and stipulated.

The general applicability and technical attributes of FD sensors will aid antibiotic discovery. An HTS plan must include secondary screens and controls to exclude false positives. Fluorescence assays, for example, are susceptible to quenching artifacts that mimic inhibition. FLHTS against TonB (25) was complicated by the involved secondary screening needed to eliminate nonspecific quenchers and other irrelevant compounds. However, FD technology enables new fluorescence tests, in microtiter format, that measure the uptake of relevant compounds or identify artifacts. The FD sensor of Fc uptake is one such assay, which may validate or refute the TonB specificity of primary hits from FeEnt uptake screens. FD sensors of other relevant ligands (vitamin B_{12} and ferric aerobactin) are within reach, and each additional test of TonB-dependent transport focuses the experiments on the most valid candidates. FD sensors in FLHTS format permit more rapid screening, allowing expansion of screening programs to larger chemical libraries.

We found that FM modified KpnFepA to higher levels in *E. coli* than in a clinical isolate of *K. pneumoniae*, which was a technical advantage. This higher intensity, which likely derived from better fluoresceination in the unencapsulated, rough laboratory strain, led to better sensitivity to quenching during ligand binding. Consequently, the FD sensor yielded more accurate measurements in *E. coli* than in *K. pneumoniae*.

From this work and our experience with binding determinations (24, 26, 30), fluorescence studies are faster, simpler, more sensitive, more reproducible, and less hazardous than radioiso- topic experiments. Optimum measurements of [^{59}Fe]Ent– FepA affinity require a large assay volume (~25 ml), to avoid substrate depletion at low concentrations, and [^{59}Fe] with high specific radioactivity. The short half-life of the isotope (44.6 days) results in rapid loss of sensitivity. Fluorescence binding assays are not confounded by such problems because of the high intensity and environmental sensitivity of selected fluoro- phores (*e.g.* FM). Our fluorescent sensors reported higher affin-
ities (K_d = 0.4 nM; Table 1) than the [^{59}Fe]Ent–EcoFepA binding studies (K_d = 1–2 nM). The spectroscopic tests were also most consistent with previous determinations (K_d = 0.2– 0.5 nM (26, 30)).

FD sensor assays are not undermined by adventitious iron or by siderophores secreted by test bacteria. We supplied chelated iron, as FeEnt, Fc, or Hn, for transport by the target cells. Nei- ther extraneous Fe^{2+} nor Fe^{3+} interfere because FepA, FhuA, and Hbp2 have no affinity for unchelated iron. FD sensor cells carry mutations that block siderophore production. Aposidero- phores from the test cells (*e.g.* enterobactin, aerobactin, acin- etobactin, etc.) may bind adventitious iron in the assay buffers, but we curtail this problem by washing cells before analysis to remove any associated siderophores. The relatively short FD assay duration (<30 min) minimizes siderophore production by the test bacteria, which generally requires extended growth in iron-deficient media for secretion of substantial amounts. The FD assay buffer (PBS + 0.2% glucose) contains little adventitious iron and no metabolites, so it constrains biosynthesis by the test bacteria.

It is worthwhile to stipulate the limitations of the fluorescence approaches in determination of membrane transport parameters. Light absorption/scatter by the bacterial cells, which obscures emitted light from fluorophores, is an obstacle to accurate measurements. Dilute bacterial suspensions (*i.e.* low turbidity) produce the best data. The assay requires high-level, specific labeling of the cells or binding protein, resulting in bright emission from dilute cells (*i.e.* ~10^7/ml) or protein. FD sensor assays do not directly yield cellular binding capacities or absolute transport rates (*e.g.* V_{max} and k_{cat}), both of which are available from radioisotopic studies (24, 26, 30). The FD sensor approach may fail for certain transport processes. The Tbp-mediated iron uptake systems of pathogenic *Neisseria*, which do not deplete their external transferrin ligand (40), illustrate this point. Although a neisserial TbpB-FM sensor that discriminates between holo- and apotransferrin (*e.g.*) is feasible, this objective requires further research and development.

The overall advantages of the FD sensor technology include high sensitivity, the technical sophistication of fluorescence instrumentation, and facile miniaturization/automation. In the ab- sence of excessive turbidity, the strategic selection of maleimide fluorophores confers the potential to quantify ligands in numerous environments, including solutions of blood, serum, and eukaryotic cells. Appropriate adaptations may enable observations of bacte- rial IM or mammalian plasma membrane uptake reactions. If applied to eukaryotic phenomena like cancer, neurobiology, or metabolism, FD sensors will measure molecular concentrations, facilitate *in vivo* thermodynamic or kinetic characterizations of biochemical reactions, and empower identification of clinically relevant therapeutic agents.

Experimental procedures

Bacteria, plasmids, genetic engineering, and cell growth

E. coli strains were descended from BN1071 (*entA* (8)): OKN1 (1 1*tonB*), OKN3 (1 1*fepA*), OKN7 (1 1*fhuA*), and OKN13 (1 1*tonB*, 1 1*fepA*) (41). ESKAPE strains included *K. pneumoniae* Kp52.145 (42) (courtesy of Regis Tournebiz, Institut Pasteur), *A. baumannii* ATCC 17978, *P. aeruginosa* PA01 (courtesy of Stephen Lory, Harvard University), and *E. cloacae* (43). *K. pneumoniae* KKN4 originated from Kp52.145 by sequential site-directed deletions of *entB* and three annotated *kpnfepA* structural genes, chromosomal loci *1658* and *4984* and plasmid (pII) locus *0027*. The resultant mutant strain did not synthesize or secrete enterobactin or transport ferric catecholate iron complexes. However, it was an effective host for plasmids carrying *fepA* alleles.

Cys-mutant proteins

To generate Cys substitution mutants of FepA and FhuA we used QuikChange mutagenesis (Agilent) of the WT genes on pITS23 (41) and pITS11 (30), respectively. Both plasmids were derived from the low-copy plasmid pHSG575 (44). pEcoFepA_A698C is a pITS23 derivative with the engineered substitution A698C, pITS11 hosts WT *ecofhuA* (30), and pEcoFhuA_D396C is a pITS11 derivative with the engineered mutation D396C (this study). pKpnFepA_T210C is a pHSG575 derivative that encodes KpnFepA (allele *0027*) under the control of its native promoter, with the engineered substitution T210C (this study). For structural predictions of KpnFepA, which has 82% identity to EcoFepA, we relied on the guideline that >25% sequence identity strongly predicts an overall identical protein fold (45, 46). To determine labeling targets in KpnFepA, we performed a ClustalW alignment against EcoFepA (Protein Data Bank (PDB) code 1FEP (47)) and used the Modeller function of UCSF Chimera to predict its tertiary structure, including surface loops. Cells expressing T210C, located in L2, were quantitatively modified by FM (Fig. S2).

To generate Cys mutants in LmoHbp2, we cloned the *hbp2* structural gene (*lmo2185*) in pAT28 (48), introduced Cys substitutions at positions of interest by QuikChange mutagenesis, and verified the mutations by DNA sequencing. We transformed the pAT28 derivative pLmoHbp2_S154C into *L. monocytogenes* EGDe1 1*hbp2* (36), grew the strain to late exponential phase in iron-deficient MOPS-L (36) media, and purified the secreted Cys-mutant protein from iron-deficient bacterial cul- tures (49). After removing the cells by centrifugation, we pre- cipitated secreted Hbp2_S154C from the supernatant with 0.6 M neutralized TCA, collected the precipitate at 10,000 X *g* for 30 min, washed the precipitated protein with 70% acetone, and then washed it with and resuspended it in 50 mM $NaHPO_4$, pH 6.7.

Fluorescence modifications of Cys-mutant proteins

We inoculated OKN3, OKN11, OKN13, and KKN4, harboring plasmids and expressing Cys-mutant FepA proteins, from frozen stocks into LB broth, grew them overnight, and subcul- tured them at 1% into iron-deficient MOPS minimal medium with shaking (200 rpm) at 37 °C for 6–7 h until late exponential phase. We labeled Cys-mutant FepA proteins in these strains with 5 μM FM in 50 mM $NaHPO_4$, pH 6.7, for 15 min at 37 °C. We labeled LmoHbp2_S154C with 5 μM CPM in 50 mM $NaHPO_4$, pH 6.7, for 30 min at 37 °C; precipitated the reaction mixture with 70% acetone; and collected LmoHbp2-CPM by centrifugation at 10,000 X *g* for 20 min. We chromatographi- cally purified LmoHbp2-CPM over Sephacryl S-300HR in PBS (Fig. S3) and consolidated fractions 42–47 for spectroscopic studies. In all experiments with Hbp2 and Hn, we took precau- tions to maximize the solubility of the porphyrin (36, 39) by using fresh solutions of Hn formulated in DMSO and dispensed to physiological concentrations in alkaline buffers.

Fluorescence spectroscopy

We observed fluorophore-labeled cells in an SLM-Aminco 8100 fluorescence spectrometer, upgraded with an Olis operat- ing system and software (Olis SpectralWorks, Olis Inc., Bogart, GA), to control its shutters, polarizers, and data collection. We also utilized an Olis Clarity fluorescence spectrometer for fluo- rescence assays of ferric catecholate binding. For species-spe- cific ferric siderophore transport assays of Gram-negative bac- teria we added an iron complex to 2 X 10^7 labeled cells in a quartz cuvette (final volume, 2 ml) with stirring at 37 °C and monitored the time course of fluorescence emissions at 520 nm. For FD assays, we incubated 10^7 sensor cells and 1.5 X 10^7 cells of the test organism (*E. coli* MG1655, *K. pneumoniae* Kp52.145 or KKN4, *A. baumannii* 17978, *P. aerugi- nosa* PA01, or *E. cloacae*) together in 2 ml of PBS + 0.4%

glucose at 37 °C in a quartz cuvette. After addition of the ferric siderophore, we monitored the time course of fluorescence emissions at 520 nm for 15–30 min with stirring. FD assays in microtiter plates (23) contained 4 X 10^6 FD sensor cells and 3 X 10^6 cells of test organisms (*E. coli* MG1655 or *K. pneumoniae* Kp52.145) in 200 μl of PBS + 0.4% glucose at 37 °C. We monitored quenching and recovery of fluorescence by ferric siderophores added to a final concentration of 5 nM in the presence or absence of CCCP.

For fluorescence spectroscopic determinations of Gram-positive bacterial heme acquisition we used the FD sensor LmoHbp2_S154C-CPM. We determined its affinity for Hn by titrations of 30 nM LmoHbp2_S154C-CPM with 1–255 nM hemin while monitoring fluorescence in an SLM-Olis fluorimeter at excitation/emission wavelengths of 390/480 nm and plotted the ensuing fluorescence quenching with Grafit 6.012 (Erithacus Ltd., Middlesex, UK). For measurements of Hn uptake by heterologous bacteria we suspended the LmoHbp2_S154C- CPM sensor protein at 30 nM in PBS + 0.2% glucose in a 2-ml cuvette, added Hn to 15 nM after 300 s, and then added iron- starved bacterial cells at 600 s to a final concentration of 5 X 10^7/ ml, and monitored fluorescence for 2 h.

When collecting fluorescence spectroscopic data of bacterial transport processes, we performed each experiment at least three times and repeated each individual time course or condition within an experiment in triplicate. We calculated the mean values and standard deviations of the triplicate measurements and plotted the resulting data with Grafit 6.02.

Author contributions—S. C., Y. S., A. K., S. M. N., and P. E. K. data curation; S. C., Y. S., and P. E. K. formal analysis; S. C., Y. S., A. K., S. M. N., and P. E. K. validation; S. C., Y. S., A. K., A. M., T. Y., B. N., S. M. N., and P. E. K. investigation; S. C., Y. S., A. K., A. M., T. Y., S. M. N., and P. E. K. methodology; Y. S., S. M. N., and P. E. K. conceptualization; T. Y. and P. E. K. resources; S. M. N. and P. E. K. supervision; S. M. N. and P. E. K. funding acquisition; S. M. N. and P. E. K. project administration; S. M. N. and P. E. K. writing-review and editing; P. E. K. visualization; P. E. K. writing-original draft.

Acknowledgments—We thank Stephen Lory, Regis Tournebiz, and Luis Actis for providing bacterial strains and Jesse Aaron and Teng Leong Chew at the Advanced Imaging Center of Howard Hughes Medical Institute Janelia Farms for assistance with microscopic imaging of bacteria.

References

1. Khan, S. N., and Khan, A. U. (2016) Breaking the spell: combating multidrug resistant 'superbugs'. *Front. Microbiol.* **7,** 174 CrossRef Medline
2. Elemam, A., Rahimian, J., and Mandell, W. (2009) Infection with panresistant *Klebsiella pneumoniae*: a report of 2 cases and a brief review of the literature. *Clin. Infect. Dis.* **49,** 271–274 CrossRef Medline
3. Tacconelli, E., and Magrini, N. (2017) *Global Priority List of Antibiotic-resistant Bacteria to Guide Research, Discovery, and Development of New Antibiotics*, World Health Organization, Geneva
4. Fisher, J. F., and Mobashery, S. (2016) -Lactam resistance mechanisms: Gram-positive bacteria and *Mycobacterium tuberculosis*. *Cold Spring Harb. Perspect. Med.* **6,** a025221 CrossRef Medline
5. Nikaido, H. (2003) Molecular basis of bacterial outer membrane permea- bility revisited. *Microbiol. Mol. Biol. Rev.* **67,** 593– 656 CrossRef Medline
6. Yu, E. W., McDermott, G., Zgurskaya, H. I., Nikaido, H., and Koshland, D. E., Jr. (2003) Structural basis of multiple drug-binding capacity of the AcrB multidrug efflux pump. *Science* **300,** 976 –980 CrossRef Medline
7. Rouault, T. A., and Maio, N. (2017) Biogenesis and functions of mammalian iron-sulfur proteins in the regulation of iron homeostasis and pivotal metabolic pathways. *J. Biol. Chem.* **292,** 12744–12753 CrossRef Medline
8. Klebba, P. E., McIntosh, M. A., and Neilands, J. B. (1982) Kinetics of biosynthesis of iron-regulated membrane proteins in *Escherichia coli*. *J. Bac- teriol.* **149,** 880 – 888 Medline
9. Parrow, N. L., Fleming, R. E., and Minnick, M. F. (2013) Sequestration and scavenging of iron in infection. *Infect. Immun.* **81,** 3503–3514 CrossRef Medline
10. Hammer, N. D., and Skaar, E. P. (2011) Molecular mechanisms of *Staphylococcus aureus* iron acquisition. *Annu. Rev. Microbiol.* **65,** 129 –147 CrossRef Medline
11. Neilands, J. B. (1952) A crystalline organo-iron pigment from a rust fungus (*Ustilago sphaerogena*). *J. Am. Chem. Soc.* **74,** 4846 – 4847 CrossRef
12. Tsolis, R. M., Ba¨umler, A. J., Heffron, F., and Stojiljkovic, I. (1996) Contribution of TonB- and Feo-mediated iron uptake to growth of *Salmonella typhimurium* in the mouse. *Infect. Immun.* **64,** 4549 – 4556 Medline
13. Konopka, K., Bindereif, A., and Neilands, J. B. (1982) Aerobactin-mediated utilization of transferrin iron. *Biochemistry* **21,** 6503– 6508 CrossRef Medline
14. Nagy, T. A., Moreland, S. M., Andrews-Polymenis, H., and Detweiler, C. S. (2013) The ferric enterobactin transporter Fep is required for persistent *Salmonella enterica* serovar Typhimurium infection. *Infect. Immun.* **81,** 4063– 4070 CrossRef Medline
15. Noinaj, N., Guillier, M., Barnard, T. J., and Buchanan, S. K. (2010) TonB-dependent transporters: regulation, structure, and function. *Annu. Rev. Microbiol.* **64,** 43– 60 CrossRef Medline
16. Schauer, K., Rodionov, D. A., and de Reuse, H. (2008) New substrates for TonB-dependent transport: do we only see the 'tip of the iceberg'? *Trends Biochem. Sci.* **33,** 330 –338 CrossRef Medline
17. Jordan, L. D., Zhou, Y., Smallwood, C. R., Lill, Y., Ritchie, K., Yip, W. T., Newton, S. M., and Klebba, P. E. (2013) Energy-dependent motion of TonB in the Gram-negative bacterial inner membrane. *Proc. Natl. Acad. Sci. U.S.A.* **110,** 11553–11558 CrossRef Medline
18. Klebba, P. E. (2016) ROSET model of TonB action in Gram-negative bacterial iron acquisition. *J. Bacteriol.* **198,** 1013–1021 CrossRef Medline
19. Pi, H., Jones, S. A., Mercer, L. E., Meador, J. P., Caughron, J. E., Jordan, L., Newton, S. M., Conway, T., and Klebba, P. E. (2012) Role of catecholate siderophores in Gram-negative bacterial colonization of the mouse gut. *PLoS One* **7,** e50020 CrossRef Medline
20. Williams, P. H. (1979) Novel iron uptake system specified by ColV plasmids: an important component in the virulence of invasive strains of *Esch- erichia coli*. *Infect. Immun.* **26,** 925–932 Medline
21. Bachman, M. A., Lenio, S., Schmidt, L., Oyler, J. E., and Weiser, J. N. (2012) Interaction of lipocalin 2, transferrin, and siderophores determines the replicative niche of *Klebsiella pneumoniae* during pneumonia. *MBio* **3,** e00224-11 CrossRef Medline
22. Russo, T. A., Shon, A. S., Beanan, J. M., Olson, R., MacDonald, U., Pomakov, A. O., and Visitacion, M. P. (2011) Hypervirulent *K. pneumoniae* secretes more and more active iron-acquisition molecules than "classical"
K. pneumoniae thereby enhancing its virulence. *PLoS One* **6,** e26734 CrossRef Medline
23. Hanson, M., Jordan, L. D., Shipelskiy, Y., Newton, S. M., and Klebba, P. E. (2016) High-throughput screening assay for inhibitors of TonB-dependent iron transport. *J. Biomol. Screen.* **21,** 316 –322 CrossRef Medline
24. Smallwood, C. R., Jordan, L., Trinh, V., Schuerch, D. W., Gala, A., Hanson, M., Hanson, M., Shipelskiy, Y., Majumdar, A., Newton, S. M., and Klebba, P. E. (2014) Concerted loop motion triggers induced fit of FepA to ferric enterobactin. *J. Gen. Physiol.* **144,** 71– 80 CrossRef Medline
25. Nairn, B. L., Eliasson, O. S., Hyder, D. R., Long, N. J., Majumdar, A., Chakravorty, S., McDonald, P., Roy, A., Newton, S. M., and Klebba, P. E. (2017) Fluorescence high-throughput screening for inhibitors of TonB action. *J. Bacteriol.* **199,** e00889-16 CrossRef Medline

1. Newton, S. M., Trinh, V., Pi, H., and Klebba, P. E. (2010) Direct measurements of the outer membrane stage of ferric enterobactin transport: postuptake binding. *J. Biol. Chem.* **285,** 17488 –17497 CrossRef Medline
2. Williams, P. H., Rabsch, W., Methner, U., Voigt, W., Tscha¨pe, H., and Reissbrodt, R. (2006) Catecholate receptor proteins in *Salmonella enterica*: role in virulence and implications for vaccine development. *Vac- cine* **24,** 3840 –3844 CrossRef Medline
3. Smith, K. D. (2007) Iron metabolism at the host pathogen interface: lipocalin 2 and the pathogen-associated *iroA* gene cluster. *Int. J. Biochem. Cell Biol.* **39,** 1776 –1780 CrossRef Medline
4. Valdebenito, M., Mu¨ller, S. I., and Hantke, K. (2007) Special conditions allow binding of the siderophore salmochelin to siderocalin (NGAL-lipocalin). *FEMS Microbiol. Lett.* **277,** 182–187 CrossRef Medline
5. Scott, D. C., Cao, Z., Qi, Z., Bauler, M., Igo, J. D., Newton, S. M., and Klebba, P. E. (2001) Exchangeability of N termini in the ligand-gated porins of *Escherichia coli*. *J. Biol. Chem.* **276,** 13025–13033 CrossRef Medline
6. Thulasiraman, P., Newton, S. M., Xu, J., Raymond, K. N., Mai, C., Hall, A., Montague, M. A., and Klebba, P. E. (1998) Selectivity of ferric enterobactin binding and cooperativity of transport in Gram-negative bacteria. *J. Bac- teriol.* **180,** 6689 – 6696 Medline
7. Pawelek, P. D., Croteau, N., Ng-Thow-Hing, C., Khursigara, C. M., Moiseeva, N., Allaire, M., and Coulton, J. W. (2006) Structure of TonB in complex with FhuA, *E. coli* outer membrane receptor. *Science* **312,** 1399 –1402 CrossRef Medline
8. Hider, R. C., and Kong, X. (2010) Chemistry and biology of siderophores. *Nat. Prod. Rep.* **27,** 637– 657 CrossRef Medline
9. Mazmanian, S. K., Liu, G., Ton-That, H., and Schneewind, O. (1999) *Staphylococcus aureus* sortase, an enzyme that anchors surface proteins to the cell wall. *Science* **285,** 760 –763 CrossRef Medline
10. Bierne, H., Garandeau, C., Pucciarelli, M. G., Sabet, C., Newton, S., Garcia-del Portillo, F., Cossart, P., and Charbit, A. (2004) Sortase B, a new class of sortase in *Listeria monocytogenes*. *J. Bacteriol.* **186,** 1972–1982 CrossRef Medline
11. Xiao, Q., Jiang, X., Moore, K. J., Shao, Y., Pi, H., Dubail, I., Charbit, A., Newton, S. M., and Klebba, P. E. (2011) Sortase independent and depen- dent systems for acquisition of haem and haemoglobin in *Listeria mono- cytogenes*. *Mol. Microbiol.* **80,** 1581–1597 CrossRef Medline
12. Le´toffe´, S., Deniau, C., Wolff, N., Dassa, E., Delepelaire, P., Lecroisey, A., and Wandersman, C. (2001) Haemophore-mediated bacterial haem transport: evidence for a common or overlapping site for haem-free and haem-loaded haemophore on its specific outer membrane receptor. *Mol. Microbiol.* **41,** 439 – 450 CrossRef Medline
13. Henderson, D. P., and Payne, S. M. (1993) Cloning and characterization of the *Vibrio cholerae* genes encoding the utilization of iron from haemin and haemoglobin. *Mol. Microbiol.* **7,** 461– 469 CrossRef Medline
14. Malmirchegini, G. R., Sjodt, M., Shnitkind, S., Sawaya, M. R., Rosinski, J., Newton, S. M., Klebba, P. E., and Clubb, R. T. (2014) Novel mechanism of hemin capture by Hbp2, the hemoglobin-binding hemophore from *Liste- ria monocytogenes*. *J. Biol. Chem.* **289,** 34886 –34899 CrossRef Medline
15. Ostberg, K. L., DeRocco, A. J., Mistry, S. D., Dickinson, M. K., and Cornelissen, C. N. (2013) Conserved regions of gonococcal TbpB are critical for surface exposure and transferrin iron utilization. *Infect. Immun.* **81,** 3442–3450 CrossRef Medline
16. Ma, L., Kaserer, W., Annamalai, R., Scott, D. C., Jin, B., Jiang, X., Xiao, Q., Maymani, H., Massis, L. M., Ferreira, L. C., Newton, S. M., and Klebba, P. E. (2007) Evidence of ball-and-chain transport of ferric enterobactin through FepA. *J. Biol. Chem.* **282,** 397– 406 CrossRef Medline
17. Lery, L. M., Frangeul, L., Tomas, A., Passet, V., Almeida, A. S., Bialek-Davenet, S., Barbe, V., Bengoechea, J. A., Sansonetti, P., Brisse, S., and Tournebize, R. (2014) Comparative analysis of *Klebsiella pneumoniae* ge- nomes identifies a phospholipase D family protein as a novel virulence factor. *BMC Biol.* **12,** 41 CrossRef Medline
18. Rutz, J. M., Abdullah, T., Singh, S. P., Kalve, V. I., and Klebba, P. E. (1991) Evolution of the ferric enterobactin receptor in Gram-negative bacteria. *J. Bacteriol.* **173,** 5964 –5974 CrossRef Medline
19. Hashimoto-Gotoh, T., Kume, A., Masahashi, W., Takeshita, S., and Fukuda, A. (1986) Improved vector, pHSG664, for direct streptomycin-resistance selection: cDNA cloning with G:C-tailing procedure and subcloning of double-digest DNA fragments. *Gene* **41,** 125–128 CrossRef Medline
20. Ginalski, K. (2006) Comparative modeling for protein structure prediction. *Curr. Opin. Struct. Biol.* **16,** 172–177 CrossRef Medline
21. Stokes-Rees, I., and Sliz, P. (2010) Protein structure determination by ex- haustive search of Protein Data Bank derived databases. *Proc. Natl. Acad. Sci. U.S.A.* **107,** 21476 –21481 CrossRef Medline
22. Buchanan, S. K., Smith, B. S., Venkatramani, L., Xia, D., Esser, L., Palnitkar, M., Chakraborty, R., van der Helm, D., and Deisenhofer, J. (1999) Crystal structure of the outer membrane active transporter FepA from *Escherichia coli*. *Nat. Struct. Biol.* **6,** 56–63 CrossRef Medline
23. Trieu-Cuot, P., Carlier, C., Poyart-Salmeron, C., and Courvalin, P. (1990) A pair of mobilizable shuttle vectors conferring resistance to spectinomy- cin for molecular cloning in *Escherichia coli* and in Gram-positive bacte- ria. *Nucleic Acids Res.* **18,** 4296 CrossRef Medline
24. Newton, S. M., Klebba, P. E., Raynaud, C., Shao, Y., Jiang, X., Dubail, I., Archer, C., Frehel, C., and Charbit, A. (2005) The svpA-srtB locus of *Listeria monocytogenes*: Fur-mediated iron regulation and effect on viru- lence. *Mol. Microbiol.* **55,** 927–940 CrossRef Medline

JBC ARTICLE

Conformational rearrangements in the N-domain of *Escherichia coli* FepA during ferric enterobactin transport

Received for publication, November 26, 2019, and in revised form, February 14, 2020 Published, Papers in Press, February 25, 2020, DOI 10.1074/jbc.RA119.011850

Aritri Majumdar‡, Vy Trinh§, Kyle J. Moore¶, Chuck R. Smallwood‖, Ashish Kumar‡, Taihao Yang‡, Daniel C. Scott**, Noah J. Long‡, Salete M. Newton‡, and Phillip E. Klebba‡1

*From the ‡Department of Biochemistry and Molecular Biophysics, Kansas State University, Manhattan, Kansas 66506, the §Department of Chemistry and Biochemistry, University of Oklahoma, Norman, Oklahoma 73019, the ¶Department of Chemistry, Physics and Engineering, Cameron University, Lawton, Oklahoma 73505, the ‖Sandia National Laboratories, Albuquerque, New Mexico 87185, and the **Howard Hughes Medical Institute, St. Jude Children's Research Hospital, Memphis, Tennessee 38105*

Edited by Chris Whitfield

The *Escherichia coli* outer membrane receptor FepA transports ferric enterobactin (FeEnt) by an energy- and TonB-dependent, but otherwise a mechanistically undetermined process involving its internal 150-residue N-terminal globular domain (N-domain). We genetically introduced pairs of Cys residues in different regions of the FepA tertiary structure, with the poten- tial to form disulfide bonds. These included Cys pairs on adja- cent β-strands of the N-domain (intra-N) and Cys pairs that bridged the external surface of the N-domain to the interior of the C-terminal transmembrane β-barrel (inter-N–C). We char- acterized FeEnt uptake by these mutants with siderophore nutrition tests, [^{59}Fe]Ent binding and uptake experiments, and fluorescence decoy sensor assays. The three methods consistent- ly showed that the intra-N disulfide bonds, which restrict con- formational motion within the N-domain, prevented FeEnt uptake, whereas most inter-N–C disulfide bonds did not pre- vent FeEnt uptake. These outcomes indicate that conforma- tional rearrangements must occur in the N terminus of FepA during FeEnt transport. They also argue against disengagement of the N-domain out of the channel as a rigid body and suggest instead that it remains within the transmembrane pore as FeEnt enters the periplasm.

The crystal structures of some Gram-negative bacterial outer membrane (OM)[2] proteins clarified or rationalized their functionalities. For instance, the crystal structures of general porins (1, 2) showed open trans-OM channels, with a 10 Å constriction zone that explained the size-exclusion properties of the pore. These data revealed why OmpF and its relatives exclude large molecules but allow passage of small (< ~600 Da) hydrophilic solutes, as was previously defined (3, 4). Similarly, the structure of the maltoporin, LamB (5), revealed a narrower (~6 Å diam- eter) open pore decorated on the exterior and within the pore constriction zone by aromatic residues, that explained its selec- tivity for maltodextrins (6, 7). The situation was different for OM siderophore receptors like FepA and its relatives. Aside from revealing 22 stranded (3-barrels topped with large loops that form a cell-surface vestibule for ligand binding, their crys- tal structures (8–12) did not explain their transport mecha- nisms and posed the quandary of transmembrane channels obstructed by ~20-kDa globular domains. Instead of revealing an obvious path for ligand uptake, the structures implied that conformational changes must occur to allow internalization of bound ligands. The energy and TonB dependence (13) of OM iron transport rationalized these predicted protein dynamics. Despite this insight, the structural changes that facilitate ligand uptake through TonB-dependent transporters (14) are not yet understood. Such OM proteins are not typical transporters, a term that usually refers to ATP- or protonmotive force-driven inner membrane permeases (15). Another designation for OM siderophore receptors in this superfamily (16, 17) is ligand-gated porin (LGP) (18), which alludes to the fact that ligand binding initiates their uptake reaction and calls to mind their transmembrane porin (3-barrels. However, LGPs are not diffusive porins. Unlike OmpF (3, 19) or LamB (20), LGPs like FepA (8) do not contain open transmembrane pores. Rather, energy-dependent uptake through their closed channels (a globular N terminus situated within a C-terminal (3-barrel) is regulated by TonB action (13). This report focuses on conformational rear- rangements within LGP that allow internalization of bound ligands.

Many different LGPs across many families of Gram-negative bacteria transport ferric siderophores, heme, other metal complexes (21) and other small molecules (*e.g.* sugars in *Caulobacter crescentus* (22–24)). Iron acquisition systems are virulence determinants (25) of bacterial pathogens that secrete siderophores to scavenge iron or hemophores to strip heme from host-binding proteins (26). Hence, explication of the molecular mechanism of OM iron uptake may lead to new approaches or new compounds against bacterial pathogens (27). LGPs bind ligands in their surface vestibules by induced fit (28, 29), creating sub-nanomolar affinities at binding equilibrium (28, 30–33)

This work was supported by National Science Foundation Grant MCB09522999 and National Institutes of Health Grants GM53836 and AI115187. The authors declare that they have no conflicts of interest with the contents of this article. The content is solely the responsibility of the authors and does not necessarily represent the official views of the National Institutes of Health.

This work is dedicated to the memories of Dr. Aritri Majumdar and Distinguished Professor H. Ronald Kaback.

This article contains Figs. S1 and S2.

[1] To whom correspondence should be addressed: Dept. of Biochemistry and Molecular Biophysics, 141 Chalmers Hall, Kansas State University, Manhattan, KS 66506. Tel.: 785-532-6268; E-mail: peklebba@ksu.edu.

[2] The abbreviations used are: OM, outer membrane; (3ME, (3-mercaptoethanol; FeEnt, ferric enterobactin; Ent, enterobactin; FD, fluorescent decoy; LGP, ligand-gated porin; FM, fluorescein maleimide; NC, nitrocellulose.

This is an Open Access article under the CC BY license.

ASBMB

Published in the U.S.A.

and triggering internal protein dynamics that result in signal transduction to TonB in the bacterial periplasm (11, 12, 34, 35). Previous studies concluded that the 150-residue N-terminal globular domain (N-domain) likely exits the C-domain channel into the periplasm during ligand uptake (29, 36, 37). However, these results did not address how the N-domain moves or changes in structure to promote passage of metal complexes or other molecules (38, 39) through the transmembrane pore. The N-domain contains a four-stranded (3-sheet, short turns of a-helix, and loops that project into the surface vestibule (Fig. 1*A*). Hypothetically, the N termini of LGP may allow metal transport by rearranging within the (3-barrel to create a pore or by dislodging from the (3-barrel, either as a folded domain or by unfolding. During FeEnt uptake through *Escherichia coli* FepA, substitution G54C, on the surface of the N-domain globule, became accessible to alkylation by extrinsic fluorescein maleimide (FM) (37)). This TonB-dependent fluoresceination of G54C did not occur in the absence of FeEnt transport, and the labeling originated from the presence of FM in the periplasm. We concluded from these data that during iron transport the actions of TonBExbBD promoted full or partial exit of the N-domain out of the (3-barrel into the periplasmic space.

Herein, we genetically engineered Cys substitutions in *fepA*, encoding pairs of sulfhydryls in presumably close enough prox- imity to form disulfide bonds, either exclusively within the N-domain (intra-N) of FepA or between its N- and C-domains (inter-N–C) (Fig. 1). If N-domain unfolding or rearrangement occurs during ligand uptake, then we expected intra-N Cys pairs to impair or abrogate FeEnt transport. Conversely, if the N-domain exits the barrel as a folded unit, then disulfide bonds within it may not prevent ligand uptake, but inter-N–C disul- fides that hold the N-domain within the (3-barrel will inhibit FeEnt uptake. The experiments found that intra-N disulfide bonds prevented FeEnt transport, but the majority of inter- N–C disulfides did not impair iron uptake. These findings indi- cate that the N terminus of FepA must rearrange during FeEnt uptake, does not exit the channel as a rigid body, and may instead remain within the pore as it allows or promotes passage of FeEnt into the periplasm.

Results

Formation of disulfide bonds in site-directed Cys pair substitution mutants

We analyzed six pairs of Cys substitutions in adjacent (3-strands or other parts of the N-domain and nine Cys pairs in regions that potentially bridged the N-domain and (3-barrel (Fig. 1) of otherwise WT *fepA* (all carried on pITS23 (40)). For both types of Cys-pair mutants, disulfide bond formation may retard or abrogate FeEnt transport by interfering with conformational dynamics or motions that involve the N-domain of FepA. We selected the locations for the Cys mutations based on their expected proximity to each other in the FepA tertiary structure (Fig. 1). Analysis of the mutant proteins in nonreducing SDS-PAGE (*i.e.* in the absence of (3-mercaptoethanol ((3ME)), visualized by anti-FepA immunoblots developed with ^{125}I-protein A, allowed quantification of their expression and often showed the extent of disulfide bond formation. However, SDS-PAGE/immunoblot analyses did not always reveal the presence of disulfides in FepA. Some Cys pairs (33–120, 42–162, 56 –73, and 149 –180; Fig. 2*A*) showed no evidence of disulfide bond formation in the gels or immunoblots; *i.e.* the electrophoretic mobility of those double-Cys derivatives exactly matched that of WT FepA, despite the fact that other experiments showed that they were disulfide-bonded. For many Cys pairs, however, we saw anti-FepA–reactive band(s) with different electrophoretic mobilities than WT FepA (14 – 300, 27–126, 51– 608, 54 –585, 77–511, 84 –142, 125–141, 128,463,138 – 427, and 138 – 445; Fig. 2*A*), verifying the presence of disulfide bonds. Nevertheless, disulfide formation appeared incomplete for all but one of these double-Cys constructs: only mutant I14C-G300C produced a homogeneous band with different mobility than that of FepA (Fig. 2*A*).

The partial disulfide bonding suggested that a fraction of the engineered Cys side chains remained native and unoxidized. To estimate the amount of unreacted Cys sulfhydryls in the mutant proteins, we exposed SDS-denatured cell-envelope fractions from the Cys-pair mutants to FM (5 μM; 5 min), before and after reduction by 10 mM (3ME. Cys side chains in stable disulfide bonds do not react with the extrinsic fluorophore (*e.g.* Cys-487–Cys-494 in WT FepA (41); Fig. S1*A*). Fluorescent images of the gels (Fig. S1, *A* and *B*), standardized by expression levels gleaned from the immunoblots (Fig. S1, *C* and *D*) and quantified by image analysis (Fig. S1*E*), indicated different extents of disulfide formation among the mutants. Prior to reduction, the six intra-N Cys-pair proteins showed variable reactivity with FM (Fig. S1, *A* and *E*), showing different extents of disulfide bond formation. Some (27–126 and 125–141) were only slightly modified by FM, suggesting that they were predominantly disulfide-bonded. Others (14 –300, 33–120, 56 –73, and 84 –142) were more reactive and less disulfide-bonded. 44 – 111 was the most reactive and the least disulfide-bonded. Unlike other intra-N Cys pairs, it was quantitatively modified by FM before exposure to (3ME, implying that it did not significantly form a disulfide bond *in vivo*. 14 –300, which appeared fully disulfide-bonded in SDS-PAGE/immunoblots (Fig. 2*A*), was still partially labeled by FM. After reduction by (3ME, all the intra-N Cys-pair proteins were better labeled by FM. WT FepA (two Cys) behaved as anticipated: without reduction it was not labeled; after reduction it was labeled to approximately half the level of 44 –111 (four Cys). Overall, from observations of the different electrophoretic mobilities of the Cys-pair mutant pro- teins, and the reactivity of their sulfhydryls to FM, we obtained evidence of their disulfide-bond formation *in vivo*. The experi- ments revealed that some disulfide bonds (*e.g.* 33–120 and 56 –73) did not alter FepA's mobility in SDS-PAGE, that each mutant protein was unique, and that whether particular Cys pairs formed bonds was unpredictable *a priori*. For example, from its position in the crystal structure of FepA, we expected 44 –111 to form a disulfide bond, but apparently it did not.

As seen for intra-N Cys pairs, gels and immunoblots of inter-N–C Cys pairs showed partial disulfide-bond formation. Although the 14 –300 disulfide appeared complete, a fraction of these mutant proteins was still modified by FM (Fig. S1, *A* and *E*), indicating the presence of free sulfhydryls. Partial disulfide

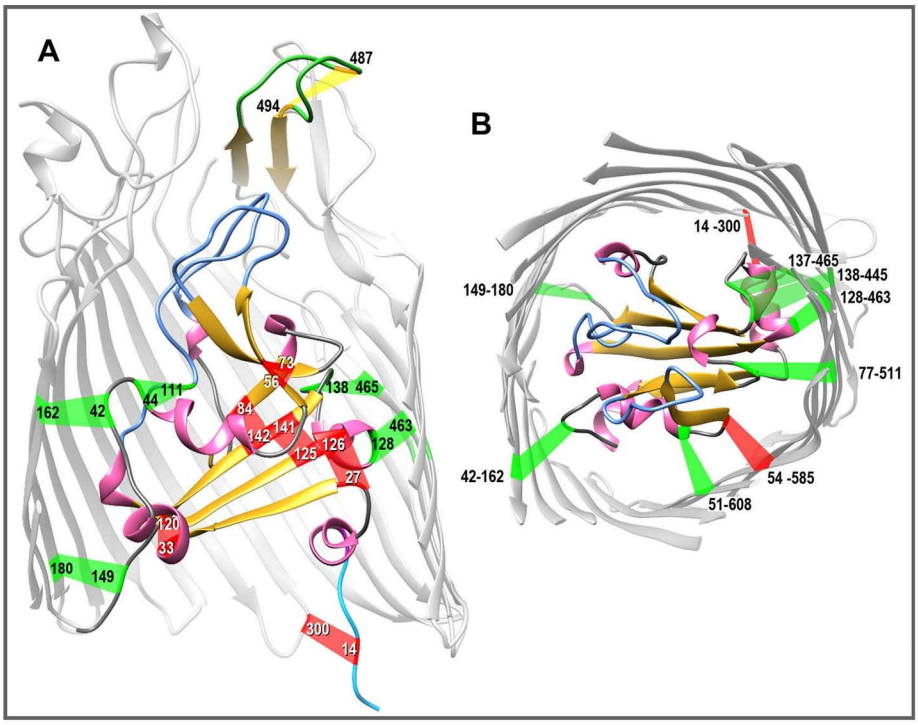


Figure 1. Native and engineered Cys pairs in FepA. From the crystal structure of FepA (1FEP (8)), we modeled the polypeptide (using the Modeller function of CHIMERA) to contain 15 novel Cys pairs, in addition to the native Cys-487–Cys-494 disulfide in L7 of FepA that is resistant to modification unless reduced (46). *A*, side view of Cys pairs. The structure of FepA encompasses a 150-residue globular N-domain within a 574-residue C-terminal (3-barrel (only partially rendered to allow a better view of the N-domain). With few exceptions, FepA orthologs contain a natural Cys pair (residues 487–494 in *E. coli* FepA) in L7 (*yellow*). The flexibility of L7 prevented its delineation in 1FEP (8), but Modeller predicted its disposition. We engineered six individual Cys pairs within the internal globular domain: 27–126, 33–120, 44–111, 56–73, 84–142, and 125–141. We also constructed nine Cys pairs that conjoin the surface of the N-domain and the interior of the (3-barrel: 14–300 (37), 42–162, 51–608, 54–585, 77–511, 128–463, 137–465, 138–445, and 149–180. *B*, top view of Cys pairs. We hid the surface loops in the model shown in *A* and rotated it 90° on the *x* axis to reveal the interior of the channel. In both panels, a-helices are *pink*; (3-strands are *gold*; N-domain loops are *blue*; and putative disulfide bonds formed by the Cys pairs are colored *red* if they inhibited FeEnt uptake or *green* if they did not inhibit FeEnt uptake, as described in the text. The images were rendered from PDB code 1FEP (8) by CHIMERA (UCSF).

formation also occurred between sites 51–608, 54–585, 77–511, 128–463, and 137–465 (Fig. 2*A*). We did not observe any immunoreactive bands with altered mobility for Cys pairs 42–162 and 149–180.

Effect of engineered Cys pairs on FeEnt utilization in nutrition tests

FeEnt nutrition tests (42) in the absence or presence of (3ME showed that the intra-N bonds impaired FepA-mediated transport (Fig. 2*D*, Fig. S2, and Table 1). In every case that we observed disulfide formation by intra-N Cys pairs, we also observed inhibition of FeEnt uptake through FepA. In the absence of any reducing agent, Cys pairs 27–126, 33–120, 56–73, 84–142, and 125–141 produced 2–3-fold larger and often fainter halos than that of WT FepA (Fig. 2 and Fig. S2). These differences reflected a lower FeEnt uptake rate (43, 44) that was overcome by the inclusion of 1 mM (3ME in the test plate. None of the individual Cys substitutions comprising the Cys pairs that we tested impaired FeEnt utilization (Fig. S2). The inhibitory Cys pairs all linked adjacent (3-strands in the N-domain, suggesting that these structural elements must remain unfettered during FeEnt transit through FepA. The 44–111 pair, which was projected to link short helices in the N-domain (but showed no evidence of disulfide formation), did not inhibit FeEnt acquisition. In summary, each of the engineered Cys pairs in the N-domain that demonstrably formed a disulfide bond blocked FeEnt uptake through FepA.

Among Cys pairs that bridged the N-and C-domains of FepA, we previously engineered and characterized 14–300 (37). Residue I14C is situated in the TonB-box region of the N-domain; G300C is located on the periplasmic rim of the (3-barrel in (3-strand 7. Disulfide formation by 14–300 therefore precludes movement of the N-domain from the (3-barrel, and accordingly, the 14–300 pair severely reduced FeEnt uptake in nutrition tests (Fig. 2, Fig. S2, and Table 1 (37)). Other inter-N–C Cys pairs produced less definitive effects. Six of them (42–162, 51–608, 128–463, 137–465, 138–445, and 149–180) showed normal halos of growth, even in the absence of (3ME. Among these, 51–608, 128–463, 137–465, and 138–445 formed disulfide bonds that altered FepA's mobility in the gels/blots (Fig. 2*A*). These data indicated that tethering the N-domain to the (3-barrel at these points did not prohibit FeEnt uptake. 42–162 and 149–180 showed no aberrant bands nor any inhibition of FeEnt uptake. The remaining inter-N–C Cys

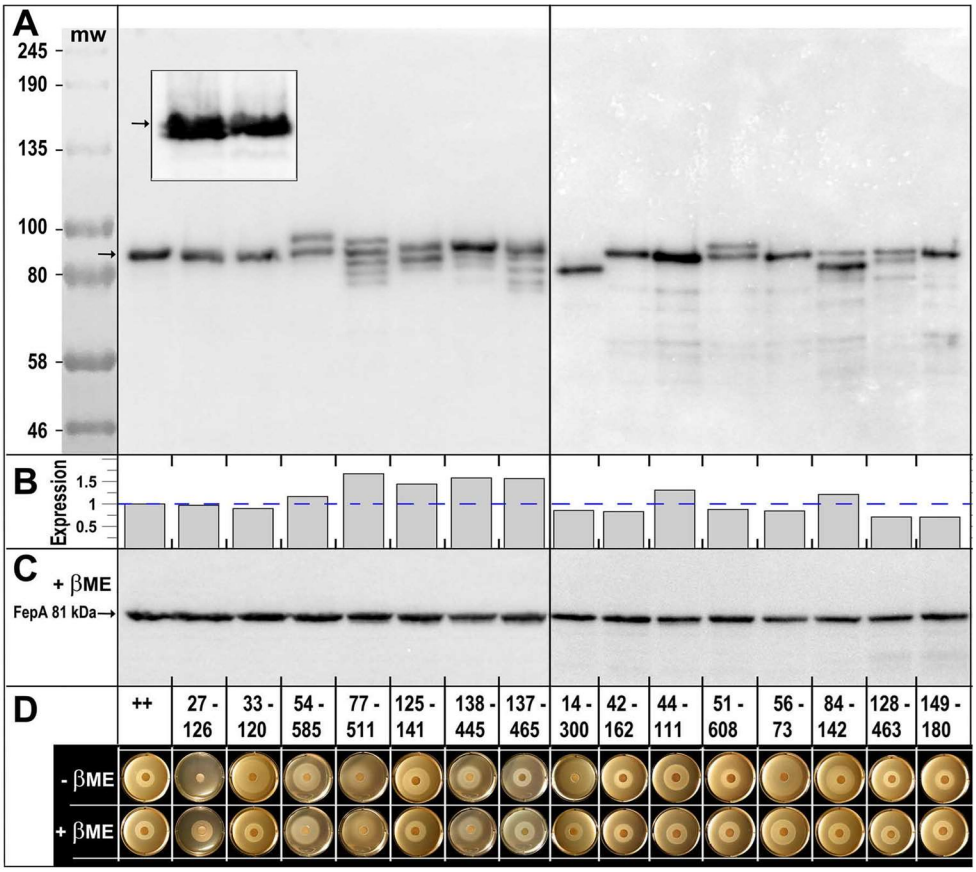


Figure 2. *A*, SDS-PAGE/western immunoblot analysis of disulfide formation by engineered Cys pairs. After growth of *E. coli* OKN3 harboring *fepA* mutants on the low-copy plasmid pHSG575 (75), in iron-deficient MOPS minimal media, we prepared cell-envelope fragments from *E. coli* OKN3 expressing WT FepA and each of the 15 Cys-pair mutants. We subjected the samples to SDS-PAGE (in the absence of any reducing agent), transferred the proteins to nitrocellulose, and performed western immunoblots with anti-FepA MAbs 41 and 45 (43), developed with ^{125}I-protein A (33). Five of the mutant proteins (33–120, 42–162, 44–111, 56–73, and 149–180) had the same electrophoretic mobility as native FepA: a single band at 81.5 kDa (76). Conversely, 10 of the mutant proteins showed single (14–300) or multiple (27–126, 54–585, 77–511, 125–141, 51–608, 84–142, 128–463, 137–465, and 138–445) immunoreactive bands with altered mobility, suggesting that they were fully or partially disulfide-bonded. The illustration derives from two separate immunoblots, separated by a *vertical line*. The gels also contained pre-stained molecular weight markers (New England Biolabs, catalog no. P77195) that we photographed on the nitrocellulose and added to the immunoblot images. The *inset* shows a magnified view, from another blot, of mutants 27–126 and 33–120. The former Cys pair forms two immunoreactive bands of nearly indistinguishable electrophoretic mobility, indicating that this Cys pair does form a disulfide bond. 33–120, conversely, migrates as a single band. *B*, quantification of FepA expression. The *arrows* in *A*, *C*, and the *inset* define the position of WT FepA that migrates at ~81 kDa (76). The immunoblot in *A* was developed with ^{125}I-protein A and scanned on a Typhoon Biomolecular imager, which allowed quantification of the immunoreactive material in each lane, using ImageJ (73). We normalized the expression values to the level of WT FepA (*dashed blue line*): Cys-pair mutant expression ranged from 0.71 to 1.67 of WT FepA expression; the mean expression among 15 mutants was 0.95 of WT FepA. *C*, we subjected the same samples as in *A* to reduction by 3 mM (3ME, resolved them on a duplicate SDS-polyacrylamide gel, transferred the proteins to NC, and immunoblotted as described in *A*. This immunoblot, as well as that of *A*, contains WT FepA, that provides an internal molecular mass marker at 81.5 kDa. *D*, FeEnt nutrition tests in the absence and presence of (3ME. We evaluated the ability of the WT FepA (++) and its Cys-pair mutants to acquire FeEnt in nonreducing or reducing conditions.

pairs, 54–585 and 77–511, produced slightly aberrant halos in the absence of (3ME that did not revert to normal in the presence of (3ME. The inability of the reducing agent to relieve inhibition complicated the interpretation of these Cys-pair mutants in the nutrition tests.

Effect of J3*ME on binding of [^{59}Fe]Ent by FepA*

Native *E. coli* FepA contains a single disulfide bond in L7 (Cys-487–Cys-494), which is needed for efficient transport of FeEnt (41, 43, 44). Because our experiments involved the reduction of engineered disulfide bonds in FepA, we determined the effect of varying concentrations of (3ME on [^{59}Fe]Ent binding by OKN3 (6.*fepA*)/pITS23 (*fepA*$^+$). The results (Fig. 3*A*) showed little impact of the reductant at concentrations <1 mM, but a 20% reduction in [^{59}Fe]Ent binding capacity at 5 mM (3ME.

Effect of engineered disulfide bonds on [^{59}Fe]Ent transport

As in nutrition tests, all the engineered intra-N Cys pairs except 44–111 decreased the [^{59}Fe]Ent uptake rate (V_{max}) (Fig. 3*C*). They inhibited [^{59}Fe]Ent uptake to a level that was 25–30% of WT FepA, and (3ME reversed their effects, reiterating that

Table 1

Attributes of Cys-pair mutants of FepA

Cys pair[a]	Location[b]	Expr[c], -J3ME	S-S[d], -J3ME	Siderophore nutrition[e] -J3ME	Siderophore nutrition[e] +J3ME	[59Fe]Ent uptake[f] -J3ME	[59Fe]Ent uptake[f] +J3ME	FD sensor uptake[g] -J3ME	FD sensor uptake[g] +J3ME
None (++)	NA[h]	1.0		15	15	1.0	1.03	+++	++++
Intra-N-domain Cys pairs									
G27C:R126C	N(31–N(35	0.97	+	21	18	0.23	1.08		++
A33C:E120C	Na2–N(35	0.90	+	28*	15	0.31	1.24		+++
D44C:T111C	Na3–NL2	1.31	-	20	16	1.05	1.26	+++	+++
N56C:D73C	N(32–N(33	0.85	+	33*	20	0.19	0.99		+++
I84C:V142C	N(34–N(36	1.2	+	24	17	0.13	0.95		++
L125C:V141C	N(35–N(36	1.44	+	23	16	0.12	0.88		++
Inter-N-domain–C-domain Cys pairs									
I14C:G300C	TonB-box–(37	0.86	+	17*	15	0.03	1.03		
A42C:N162C	Na3–(31	0.83		15	15	ND[i]	ND	+++	ND
T51C:N608C	N(32–(318	0.88	+	15	16	0.57	0.74	+++	ND
G54C:T585C	N(32–(317	1.17	+	22	23	0.37	0.31		
M77C:E511C	N(33–(314	1.67	+	21*	18*	0.57	0.48	+++	ND
R138C:A426C	N(35–(313	0.71	+	13	14	ND	ND	+++	ND
A137C:A426C	N(36–(313	1.37	+	24	15	ND	ND	+++	ND
A138C:A426C	N(36–(312	1.38	+	19	20	ND	ND	+++	ND
G149C:T180C	N(36–(35	0.71	+	13	15	ND	ND	+++	ND

[a] Cys-pair mutants were engineered in wildtype FepA and carried on the pHSG575 (66) derivative pITS23 (39). Mutants identified in bold type showed severely impaired FeEnt uptake, unless exposed to (3ME.

[b] We designed Cys pairs using the Modeller algorithm (CHIMERA (UCSF) and PDB file 1FEP (34).

[c] Using anti-FepA immunoblots, we quantified the immunoreactive bands of each Cys pair mutant in Fig. 2*A* relative to the amount of wildtype FepA. Mean expression among 15 mutants was 0.96 of wildtype; the range of expression values was 0.71–1.67 of wildtype expression.

[d] Evidence of disulfide formation, from observation of altered mobility in anti-FepA immunoblots of SDS-polyacrylamide gels of OM fractions, or reversible (*i.e.* relieved by (3ME) inhibition of FeEnt uptake.

[e] The tabulated values are the diameters of the growth halo (41, 42) around a paper disk containing 50 μM FeEnt, after incubation at 37 °C overnight. Results marked with an asterisk (*) denote samples with a faint halo.

[f] V_{max} values of [59Fe]Ent uptake from V_{max} screening experiments were calculated relative to the rate of wildtype FepA (96 pmol/10^9 cells/min; Fig. 3, *C* and *D*).

[g] FeEnt uptake was measured as the rate of fluorescence recovery in FD sensor experiments, relative to wildtype FepA.

[h] NA means not applicable.

[i] ND means no data.

disulfides within the N-domain interfere with [59Fe]Ent transport. [59Fe]Ent binding capacity was also lower in several of the Cys-pair mutants (Fig. 3*B*); for the most part, the addition of (3ME did not reverse this decrease (the exception was 84 –142). In some cases, a lower [59Fe]Ent-binding capacity contrasted with a relatively normal [59Fe]Ent uptake rate (56 –73 and 125– 141, plus (3ME). But LGP turnover numbers are low (5.5/min (47)), so the extent of FepA saturation may not limit the uptake rate.

The impact of inter-N–C Cys pairs on [59Fe]Ent uptake was more complicated. 14 –300 nearly abolished [59Fe]Ent uptake (29), but none of the others we assayed comparably inhibited acquisition of [59Fe]Ent (Table 1). 54 –585 decreased the FeEnt uptake rate by 65%, but other inter-N–C Cys pairs that we tested showed much less effect, in the range of 10 – 45%.

Fluorescent measurements of FeEnt uptake by Cys-pair mutants

Electrophoretic analyses did not always reveal disulfide bonds between Cys pairs, and most of the disulfides that we observed in SDS-PAGE/immunoblots were only partially formed. Consequently, the partial reductions in FeEnt uptake that we saw in nutrition tests and radioisotopic assays were difficult to interpret. We employed a fluorescent decoy (FD) sensor (30) to monitor TonB-dependent FeEnt uptake through FepA, as a better measure of whether the FeEnt uptake portal was open or held shut by engineered disulfide bonds. In a 6.*tonB* host (OKN13 (37)), FepA-FM (29) binds but cannot transport FeEnt. As a result, it becomes an FD sensor (30): the extent of its quenching reflects [FeEnt] and therefore the uptake of FeEnt (*i.e.* its depletion) by other cells in the same solution. Incubation of FD sensor cells with the Cys-pair mutant cells allowed observations of the latter's ability to transport FeEnt, which appears as a reversal of FeEnt-mediated quenching (*i.e.* fluorescence recovery; Fig. 4). These data provided a quantitative time course of FepA's transport functionality.

The FD sensor provided more definitive data on the ability of the intra-N mutants of FepA to acquire FeEnt. Whereas transport of FeEnt by WT FepA quickly reverted the FeEnt-mediated quenching of the sensor, five of the six intra-N-domain Cys-pair mutants of FepA (27–126, 33–120, 56 –73, 84 –142, and 125–141) did not promote fluorescence recovery until we reduced their disulfides by adding (3ME to the cuvette. The only exception was 44 –111, which supported fluorescence recovery like WT FepA, albeit at a slower rate. Given the uncertain status of the 44 –111 disulfide bond, the fluorescence data either con- firmed that it did not form or that its presence did not corrupt the FeEnt transport process. Overall, the results of the intra-N Cys pairs were consistent: disulfide formation in the N-domain prevented FeEnt transport, and reduction of those bonds restored the FeEnt uptake process.

Regarding inter-N–C Cys pairs, the FD sensor reiterated that the majority did not impair FeEnt uptake, despite that we observed disulfide bond formation by five of them. Cys-pair 77–511, which produced an inconclusive nutrition test with FeEnt, showed definitive transport in the FD sensor assay (Fig. 4 and Table 1). Overall, among the nine inter-N–C Cys pairs that we tested, besides 14 –300, which falls into its own category, only 54 –585 inhibited FeEnt transport in FD sensor assays. As

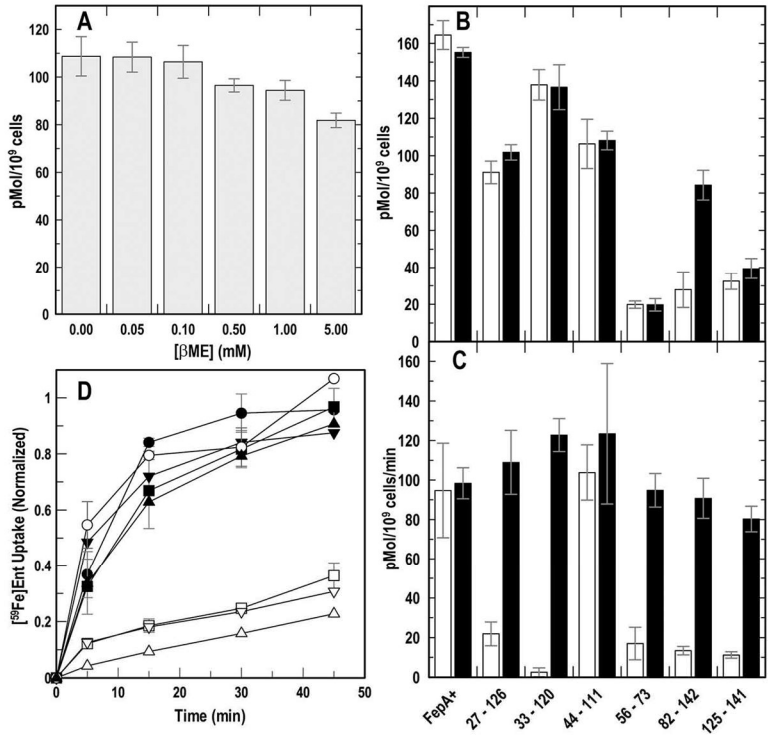


Figure 3. [^{59}Fe]Ent binding and transport by intra-N Cys-pair mutants of FepA. After growth in iron-deficient MOPS medium, we tested *E. coli* expressing WT FepA or its Cys-pair mutants for binding and transport of [^{59}Fe]Ent (74). *A*, effect of (3ME on [^{59}Fe]Ent binding to WT FepA. The FeEnt binding capacity of OKN3 (Δ*fepA*)/pITS23 (*fepA*$^{+}$) slightly decreased (up to 20%) in the presence of 5 mM (3ME. *B*, [^{59}Fe]Ent binding to Cys-pair mutants: binding capacities in the presence of saturating (10 nM) [^{59}Fe]Ent, in the absence or presence of 5 mM (3ME. *C*, [^{59}Fe]Ent uptake by Cys-pair mutants: V_{max} in the presence of saturating (10 nM) [^{59}Fe]Ent, in the absence or presence of 5 mM (3ME. *D*, accumulation of [^{59}Fe]Ent: rates of [^{59}Fe]Ent uptake in the absence (*open symbols*) and presence (*filled symbols*) of 5 mM (3ME by WT FepA (●), 27–126 (□), 33–120 (▼), and 125–141 (▲). (3ME restored WT FeEnt uptake to all the intra-N Cys-pair mutants.

in nutrition tests, (3ME did not relieve the inhibition of 54 –585, confounding its interpretation.

In summary, we observed evidence of disulfide bond formation in 12 of the 15 Cys-pair mutants (Table 1). 10 FepA variants showed a band of altered electrophoretic mobility (Fig. 2*A*). Among the intra-N Cys pairs, 33–120, 44 –111, and 56 –73 showed no electrophoretic evidence of disulfide bond formation, but 33–120 and 56 –73 reversibly (*i.e.* relieved by (3ME) inhibited FeEnt utilization, indicating that they did bond. The observation of disulfide bond formation by intra-N Cys pairs always correlated with impaired FeEnt uptake (Table 1). Among inter-N–C Cys pairs, we saw anti-FepA–reactive bands with altered migration in all mutants except 42–162 and 149 –180 (Fig. 2*A* and Table 1). In five of seven of these instances disulfide bond formation did not inhibit FeEnt uptake (Table 1). The exceptions (14 –300 and 54 –585) each had individual considerations that rationalized their behavior (discussed below).

Discussion

Delineation of the FepA transport mechanism requires insight into the actions of its N-domain during FeEnt internalization. In three disparate assays, the phenotypes of the Cys-pair mutants under investigation led to the same conclusion: intra-N disulfide bonds generally prevented FeEnt transport, whereas inter-N–C disulfide bonds generally did not prevent FeEnt transport (Fig. 1). These data imply several conclusions. (i) The internal (3-structure of the N-domain must rearrange during FeEnt uptake, because bonds that block such a transition also block transport. Disulfide bonds in the N-domain will restrict its potential motion, constraining conformational changes that are apparently required to achieve FeEnt import.
(ii) The N-domain does not move out of the transmembrane pore as a folded rigid body (37), because bonds that hold it within the channel do not block FeEnt uptake. (iii) Numerous disulfide bonds that restrained the N-domain within the (3-barrel did not prevent ligand uptake. These data suggest that most of the N terminus remains within the channel, which infers the formation of a transient pore (37) through which FeEnt passes into the periplasm.

It was a challenge to determine the extent of engineered disulfide bond formation *in vivo*. The Cys pairs produced a gamut of possible outcomes. Some formed disulfides that altered the R_f of FepA, whereas others did not change R_f, either because they did not form or because the disulfide did not alter migration in the gels. Even a single amino acid substitution may dramatically change the electrophoretic mobility of a protein (45), but the effects of engineered disulfides on the electrophoretic behavior of FepA were unpredictable: some created a

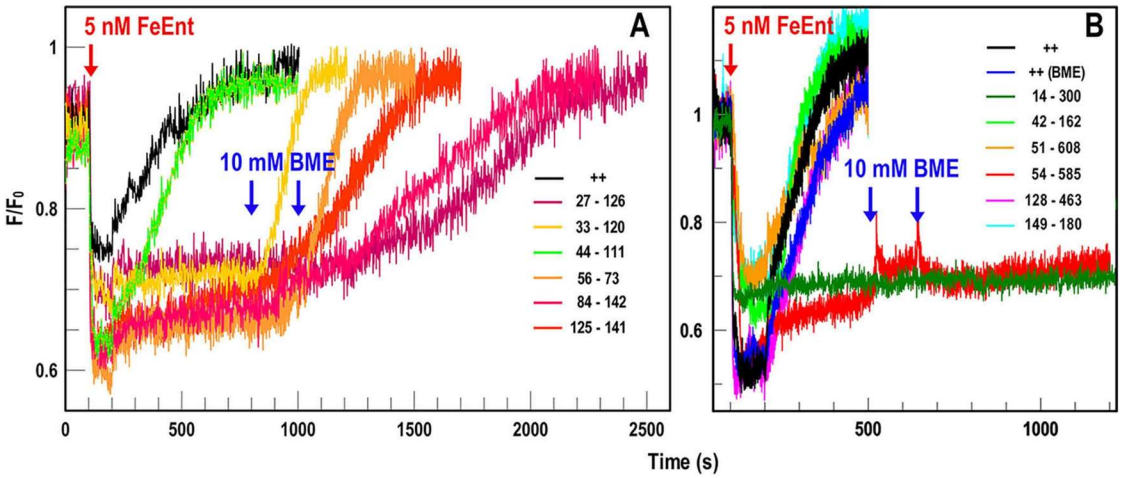


Figure 4. FD sensor measurements of FeEnt uptake by Cys-pair mutants of FepA. OKN3 expressing FepA with individual Cys pairs was incubated with the FD sensor OKN13 (Δ*tonB* and Δ*fepA*)/pFepA-FM and observed in response to the addition of FeEnt (5 nM) at 37 °C. *A*, intra-N mutants. After quenching by addition of FeEnt at 100 s, WT FepA (++) and 44–111 conferred complete recovery (*i.e.* FeEnt uptake) within 500 s. Addition of 10 mM (3ME at 800 s enabled recovery by 33–120, but all the remaining Cys pairs required a second aliquot of 10 mM (3ME to confer recovery. *B*, inter-N and -C mutants. None of the Cys pairs prevented fluorescence recovery except 14–300 and 54–585, which were not affected by up to 20 mM (3ME.

compact isoform of the denatured protein that moved faster, whereas others stabilized a larger isoform that moved slower. Anti-FepA immunoblots of 33–120 and 56–73 did not reveal any additional bands, despite the fact that both Cys pairs impaired FeEnt uptake and reverted to normal transport when reduced by (3ME. Hence, disulfides formed in both 33–120 and 56–73, but the immunoblots did not reveal them. Furthermore, when we observed a Cys pair mutant band with different R_f values, usually only ~50% of the protein was in the altered state. The engineered Cys-pair sulfhydryls were hypothetically close enough (<2.5 Å between sulfur atoms (8)) to form disulfides, but without the crystallographic data on each mutant protein their impact on local folding and side-chain projection was unknown. Furthermore, for numerous engineered Cys pairs the DsbAB system (46–50) did not efficiently oxidize disulfide bond formation, as evidenced by the susceptibility of the com- ponent sulfhydryls to alkylation by FM. Finally, we saw multiple immunoreactive electrophoretic forms of some FepA Cys-pair mutants. Besides fully synthesized, secreted, and folded OM proteins, immunoblots may reveal nascent or incomplete mutant proteins, in a pre-or post-disulfide–bonded state, which may explain some of the multiple bands. Overall, the electrophoretic studies of Cys-pair mutants were informative, but insufficient to quantify the extent of disulfide formation or to explain the nature of each immunoreactive band.

The intrinsic disulfide in FepA L7 (C487–C494) was another complication, which raised the possibility of aberrant disulfides with engineered Cys sulfhydryls. However, C487–C494 is a sta- ble bond; without reduction, residues C487 and C494 are unre- active with methane thiosulfonate or maleimide probes (Fig. S2*A*) (29, 39, 41, 51). Furthermore, the L7 disulfide is essential to transport activity: substitutions C487S, C494S, and their combined double-mutant all abrogate FeEnt uptake (data not shown). Consequently, if engineered Cys residues erroneously bond with either native Cys, blocking formation of C487–C494, then FeEnt uptake will diminish. We did not observe that result with the single mutants we generated herein (Fig. S2), nor with >25 other individual Cys substitutions in FepA, at diverse loca- tions in its primary structure (29, 30, 37, 51). So, it is unlikely that the Cys-pair sulfhydryls we engineered formed incorrect disulfides with C487 and C494. The native cysteines are sepa- rated by only six residues in L7 and probably immediately bond as that region of the polypeptide exits the ribosome and folds. FD sensor assays provided unique, real-time insight into the transport behavior of the FepA mutants. Nutrition tests and [^{59}Fe]Ent uptake assays were useful but sometimes hard to interpret, whereas FD assays were unambiguous about the impact of each Cys pair on FeEnt transport. The sensor cell OKN13/pFepA-FM depicted uptake of FeEnt by the FepA Cys- pair mutants *in vivo*. It showed that except for 44–111 (which did not form a disulfide bond), all intra-N Cys pairs blocked FeEnt uptake until exposed to 10 mM (3ME. Conversely, with the exception of 14–300 and 54–585, none of the other seven inter-N–C Cys pairs inhibited FeEnt uptake. Cys pair 14–300 is unique among all the mutants, because its immobilization of the TonB-box both holds the N-domain within the (3-barrel and interferes with signal transduction to TonB. 54–585 blocked FeEnt uptake, but its inhibition was not reversed by (3ME, suggesting that its negative phenotype was unrelated to disulfide formation. Despite these two exceptions, the more definitive FD sensors corroborated and clarified the sidero-phore nutrition and [^{59}Fe]Ent accumulation results.

The crystal structures of ligand-free and ligand-bound trans-porters (9–12, 28, 32) revealed that when LGP adsorbs metal complexes by induced fit (29), subtle changes propagate through their N termini that alter the disposition of residues in the periplasm, promoting interactions with the TonB C termi-nus (34, 35). These dynamics raise the possibility that intra-N disulfides interfere with FeEnt uptake because they corrupt sig- nal transduction to TonBExbBD. However, inspection of the

ligand-free and ligand-bound forms of FhuA, FecA, and BtuB show little or no deviation in the regions of the N-domain that contain the Cys pairs we engineered in FepA. We cannot exclude the notion that intra-N Cys pairs interfere with signal transduction to TonBExbBD, but this explanation seems unlikely.

Despite the importance of TonB-dependent iron acquisition to Gram ( ) bacterial pathogenesis (52–61) and the solution of many LGP crystal structures (FepA (8), Cir (8), FhuA (11, 12), FecA (11, 12), FoxA (32), BtuB (9), FptA (62), FpvA (63), PfeA (28), and FyuA (64)), it is unknown how metal complexes move through their channels or how the actions of TonB facilitate uptake. Biochemical data on FepA (65) and crystallographic studies of other LGPs (28, 32) indicated a two-site model during FeEnt adsorption. Other approaches, including site-directed alkylation of FepA during FeEnt transport (37) and molecular dynamics simulations of the interaction between TonB and BtuB (36), suggested that the N-domain globules of LGP exit their transmembrane (3-barrels, either stably folded or by unfolding into the periplasm. Our results argue against both these mechanisms. First, seven of nine inter-N–C Cys pairs that we tested did not inhibit FeEnt uptake, refuting the notion that the N-domain exits the (3-barrel as an intact globule. Second, tethering Cys residues at 51, 77, 128, 137, or 138 to the (3-barrel (verified by immunoblot) did not prevent transport, which sup- ports the alternative idea that the N-domain remains within the pore as FeEnt enters. It is now apparent that conformational motion *within* the N-domain is indispensable to the uptake reaction, because five of six the intra-N domain Cys pairs we created prevented FeEnt internalization, unless exposed to (3ME.

Experimental procedures

Bacterial strains, plasmids, and culture conditions

Plasmid pITS23 (39, 40) is a derivative of pHSG575 (66) that carries *fepA*$^+$ under the control of its natural Fur-regulated promoter. We engineered Cys-pair alleles of *fepA* in this vector. Derivatives of BN1071 (67) with precise deletions (OKN1, Δ*tonB*; OKN3, Δ*fepA*; and OKN13, Δ*tonB*, Δ*fepA* (37)), harboring variants of pITS23 that encode WT or mutant alleles, were grown at 37 °C with shaking to stationary phase in Luria-Bertani (LB) broth. We added streptomycin (100 μg/ml) to the growth media and chloramphenicol (20 μg/ml) to select for the plasmids when appropriate. We de-repressed the FeEnt transport system by subculturing bacteria from stationary phase LB cultures at 1% into iron-deficient MOPS minimal medium (68) and shaking at 200 rpm for 5.5–6 h at 37 °C, until cell density reached an absorbance at 600 nm of 0.8–0.9.

Site-directed mutagenesis of E. coli fepA

We used QuikChange (Stratagene) for single- and double-Cys substitutions in FepA, using complementary oligonucleotides flanking the mutation, followed by digestion of the WT vector by DpnI. We confirmed the mutations by sequencing (Genesys, Daly City, CA) of purified plasmids.

Intra-N Cys pairs—We constructed six Cys pairs (G27C-R126C, A33C-E120C, D44C-T111C, N56C-D73C, I84C-V142C, and L125C-V141C) in different regions of the N-domain of FepA. Each pair may form a disulfide bond within the globular domain, which prevents separation of its constituent (3-strands (Fig. 1 and Table 1).

Inter-N–C Cys pairs—We analyzed another group of nine Cys pairs (I14C-G300C, A42C-N162C, T51C-N608C, G54C- T585C, M77C-E511C, P128C-A463C, A137C-A465C, A138C-A445C, and G149C-T180C) in which one sulfhydryl was on the surface of the N-domain and a second was on the internal wall of the FepA (3-barrel (Fig. 1 and Table 1).

Siderophores

We purified enterobactin from *E. coli* and formed the iron(III) complex with ^{56}Fe or ^{59}Fe (33) and chromatographically-purified FeEnt over Sephadex LH20 (42). We stored the [^{56}Fe]Ent and [^{59}Fe]Ent complexes on ice and re-purified them over LH20 to remove oxidized and degraded compounds when $A_{393\ nm}/A_{495\ nm}$ exceeded 0.7.

Siderophore nutrition tests

To qualitatively evaluate the FeEnt uptake abilities encoded by the mutant *fepA* alleles, we performed siderophore nutrition tests (42, 44). We expressed the results as the diameter of bac- terial growth around the paper disk, and we compared mutant halos to the growth halo conferred by a strain harboring pITS23 (*fepA*$^+$). To test the effect of disulfide bond reduction on FeEnt transport by the FepA mutants, we added 1 mM (3ME to the molten agar.

Preparation of cell-envelope fractions

After growth in LB broth overnight, we sub-cultured FepA Cys-pair mutant derivatives of OKN3/pITS23 at (1%) into 20 ml of iron-deficient MOPS media, and we incubated the cultures with shaking for 5.5–6 h at 37 °C, to an $A_{600\ nm}$ = 1–1.2 (5–6 × 10^8 cells/ml). We collected the cells by centrifugation at 7500 × *g*, resuspended the pellets in 2 ml of PBS containing trace amounts of DNase and RNase, and passed the cell suspensions (three times) through a French pressure cell at 14,000 p.s.i. (69). After spinning the lysates at 3000 × *g* for 10 min to remove unbroken cells and debris, we transferred the supernatants to microcentrifuge tubes and pelleted the cell envelopes by centrifugation at 13,000 × *g* for 45 min. We resuspended the cell envelopes in 400 μl of 50 mM $NaHPO_4$, pH 6.7, containing 1% SDS, added 3% (3ME to one-half of the sample (reduced), left the remainder unaltered (nonreduced), and denatured the pro- teins in both samples by boiling for 5 min.

Electrophoresis and western immunoblots

We electrophoretically and immunochemically analyzed cell-envelope fractions of the mutants. For SDS-PAGE (70, 71), we suspended 30 μg of cell-envelope protein (measured by UV absorbance) in sample buffer (containing 1% SDS), with or without 3% (3ME, boiled the sample for 5 min, and resolved the samples by SDS-PAGE at 30 mA. To enhance the separation of proteins in the 80-kDa range, we continued electrophoresis at 30 mA for an additional 45 min after the tracking dye left the gels. To visualize FepA in western immunoblots, we electrophoretically transferred the proteins from the SDS-polyacrylamide gels to nitrocellulose (NC) paper, blocked the paper with

1% gelatin in 50 mM Tris chloride, pH 7.4, 0.9% NaCl (TBSG), and incubated with a mixture of anti-FepA mouse monoclonal antibodies (mAbs) 41 and 45 (72), both of which have Ig2b heavy chains, in the same buffer. After incubation with the antisera for 1 h at room temperature, we washed the NC five times with 0.5% Tween 20 in TBS, incubated it with ^{125}I-protein A in TBSG for 1 h at room temperature, washed with three rinses of tap water, dried the paper, and visualized the adsorbed ^{125}I-protein A on a Typhoon 8600 Biomolecular Scanner (GE/Amersham Biosciences).

Labeling reactions with FM

We estimated the extent of disulfide formation in Cys-pair mutants of FepA by modifying them with FM. We precipitated 100 μl of the denatured, reduced, and nonreduced cell-envelope samples described above with 7 volumes of ice-cold acetone, and after incubation at −20 °C for 2 h, we pelleted the proteins by centrifugation at 13,000 × *g* for 5 min and washed the pellets twice with ice-cold 70% acetone. We resuspended the reduced and nonreduced cell-envelope proteins in 50 mM $NaHPO_4$, pH 6.7, containing 1% SDS, added FM to 5 μM, incubated for 15 min at 37 °C (29), and stopped the labeling reactions by precipitation with ice-cold acetone as described above. We washed the samples with ice-cold 70% acetone, solubilized them with SDS-PAGE sample buffer, and subjected them to SDS-PAGE/Western immunoblot.

Image analysis

We analyzed images from SDS-polyacrylamide gels of fluoresceinated proteins and from phosphorimagery of ^{125}I-protein A immunoblots, collected on a Typhoon Biomolecular scanner (GE Healthcare) using ImageJ (73).

Effect of J3*ME on FeEnt binding by FepA*

Because in several experiments we used (3ME to reduce disul- fide bonds within FepA, we tested its effects on the adsorption of [^{59}Fe]Ent by OKN3/pITS23 (*fepA*$^+$). We grew the bacteria in LB overnight, subcultured at 1% in iron-deficient MOPS mini- mal medium, shook the cultures for 5 h at 37 °C, added (3ME at increasing concentrations to 5 mM, and shook the cultures for additional 30 min at 37 °C. We created a duplicate control cul- ture that we subjected to the same conditions, but without any (3ME. To determine the [^{59}Fe]Ent-binding capacities, we added the ferric siderophore at 10 nM, filtered the cells after 1 min, washed the filters with 10 ml of 0.9% LiCl, and determined the amount of adsorbed radioactivity in a Packard gamma counter. The parent host strain (OKN3, Δ*fepA*) does not adsorb [59Fe]Ent. We employed it in these binding studies as a nega- tive (background) control.

Ferric enterobactin accumulation

We subcultured overnight LB cultures at 1% in iron-deficient MOPS medium with appropriate antibiotics and continued growth at 37 °C with shaking for 5.5 h. In some cases, the bacteria were exposed to 5 mM (3ME in the final 30 min of growth. We next added [^{59}Fe]Ent to 3-ml aliquots of the cells at 37 °C (in the original culture medium) to a final concentration of 10 μM, removed 100-μl aliquots at 5, 10, 15, 30, and 45 min, filtered them, and washed them with 10 ml of 0.9% LiCl, and we determined the amounts of [^{59}Fe] on the filters in a Packard gamma counter. For each accumulation experiment, we collected triplicate samples at each time point and averaged the data. At a density of ~5 × 10^8 cells/ml, the added [^{59}Fe]Ent was sufficient to remain in excess for more than 2 h of transport at V_{max} (74).

Fluorescence assays of FeEnt transport

We employed FD sensors (30) to monitor TonB-dependent FeEnt uptake through FepA, as a measure of whether the FeEnt uptake portal was open or held shut by engineered disulfide bonds. In this approach, we used the transport-defective host strain OKN13 (Δ*tonB* and Δ*fepA*) harboring a plasmid (pITS23) encoding *fepA* with a single amino acid substitution (A698C), which was modifiable by FM (FepA_A698C-FM; henceforth called FepA-FM). OKN13/pFepA-FM bound FeEnt, which quenched its fluorescence (29), but its TonB deficiency prevented it from transporting the bound iron complex. The absence of TonB transformed the fluoresceinated bacteria into spectroscopic sensors of [FeEnt] (30); if transport-competent cells cohabited the same environment, then the emissions of OKN13/pFepA-FM reflected their FeEnt uptake activity. Hence, in fluorescence spectroscopic uptake studies, OKN13/pFepA-FM was a decoy sensor that monitored FeEnt uptake by the FepA Cys-pair mutants in a host strain OKN3 (Δ*fepA*). These data provided a quantitative time course of FepA's transport functionality.

For each assay, we used 50 μl of OKN13/pFepA-FM (44) at 5 × 10^8 cells/ml. We analyzed the aliquot in 2 ml of PBS + 0.4% glucose at 37 °C, and we recorded its fluorescence intensity for 100 s, before adding FeEnt to the cuvette at a final concentration of 5 nM. We incubated the sample for 100 s, during which time fluorescence was quenched (~60% quenching for FepA labeled at position A698C), and we then added 50 μl of the test strain (~5 × 10^6 cells) at 200 s while monitoring fluorescence. If no increase in fluorescence occurred (indicating lack of uptake) by 800 s, we added (3ME to a final concentration of 10 mM. For some strains, we added a second aliquot of (3ME at 1000 s that raised the final concentration to 20 mM.

Author contributions—A. M., V. T., K. J. M., C. R. S., D. C. S., S. M. N., and P. E. K. conceptualization; A. M. and P. E. K. resources; A. M., V. T., S. M. N., and P. E. K. data curation; A. M., V. T., S. M. N., and P. E. K. formal analysis; A. M., S. M. N., and P. E. K. supervision; A. M. and P. E. K. funding acquisition; A. M. and P. E. K. validation; A. M., V. T., K. J. M., C. R. S., A. K., T. Y., D. C. S., N. J. L., S. M. N., and P. E. K. investigation; A. M., V. T., K. J. M., C. R. S., D. C. S., N. J. L., S. M. N., and P. E. K. methodology; A. M. and P. E. K. writing-original draft; A. M., S. M. N., and P. E. K. project administration; A. M. and P. E. K. writing-review and editing.

Acknowledgment—We thank Ron Kaback for helpful discussions about the experiments.

References

1. Cowan, S. W., Schirmer, T., Rummel, G., Steiert, M., Ghosh, R., Pauptit, R. A., Jansonius, J. N., and Rosenbusch, J. P. (1992) Crystal structures explain functional properties of two *E. coli* porins. *Nature* **358,** 727–733 CrossRef Medline

1. Weiss, M. S., Wacker, T., Weckesser, J., Welte, W., and Schulz, G. E. (1990) The three-dimensional structure of porin from *Rhodobacter cap- sulatus* at 3 Å resolution. *FEBS Lett.* **267,** 268 –272 CrossRef Medline
2. Nikaido, H., and Rosenberg, E. Y. (1981) Effect on solute size on diffusion rates through the transmembrane pores of the outer membrane of *Esch- erichia coli*. *J. Gen. Physiol.* **77,** 121–135 CrossRef Medline
3. Nikaido, H., and Vaara, M. (1985) Molecular basis of bacterial outer membrane permeability. *Microbiol. Rev.* **49,** 1–32 CrossRef Medline
4. Schirmer, T., Keller, T. A., Wang, Y. F., and Rosenbusch, J. P. (1995) Structural basis for sugar translocation through maltoporin channels at

   3.1 A resolution (see comments). *Science* **267,** 512–514 CrossRef Medline
5. Klebba, P. E., Hofnung, M., and Charbit, A. (1994) A model of maltodextrin transport through the sugar-specific porin, LamB, based on deletion analysis. *EMBO J.* **13,** 4670 – 4675 CrossRef Medline
6. Luckey, M., and Nikaido, H. (1980) Diffusion of solutes through channels produced by phage '1 receptor protein of *Escherichia coli*: inhibition by higher oligosaccharides of maltose series. *Biochem. Biophys. Res. Com- mun.* **93,** 166 –171 CrossRef Medline
7. Buchanan, S. K., Smith, B. S., Venkatramani, L., Xia, D., Esser, L., Palnitkar, M., Chakraborty, R., van der Helm, D., and Deisenhofer, J. (1999) Crystal structure of the outer membrane active transporter FepA from *Escherichia coli* (see comments). *Nat. Struct. Biol.* **6,** 56–63 CrossRef Medline
8. Chimento, D. P., Mohanty, A. K., Kadner, R. J., and Wiener, M. C. (2003) Substrate-induced transmembrane signaling in the cobalamin transporter BtuB. *Nat. Struct. Biol.* **10,** 394 – 401 CrossRef Medline
9. Ferguson, A. D., Chakraborty, R., Smith, B. S., Esser, L., van der Helm, D., and Deisenhofer, J. (2002) Structural basis of gating by the outer membrane transporter FecA. *Science* **295,** 1715–1719 CrossRef Medline
10. Ferguson, A. D., Hofmann, E., Coulton, J. W., Diederichs, K., and Welte, W. (1998) Siderophore-mediated iron transport: crystal structure of FhuA with bound lipopolysaccharide (see comments). *Science* **282,** 2215–2220 CrossRef Medline
11. Locher, K. P., Rees, B., Koebnik, R., Mitschler, A., Moulinier, L., Rosenbusch, J. P., and Moras, D. (1998) Transmembrane signaling across the ligand-gated FhuA receptor: crystal structures of free and ferrichrome- bound states reveal allosteric changes. *Cell* **95,** 771–778 CrossRef Medline
12. Jordan, L. D., Zhou, Y., Smallwood, C. R., Lill, Y., Ritchie, K., Yip, W. T., Newton, S. M., and Klebba, P. E. (2013) Energy-dependent motion of TonB in the Gram-negative bacterial inner membrane. *Proc. Natl. Acad. Sci. U.S.A.* **110,** 11553–11558 CrossRef Medline
13. Schauer, K., Rodionov, D. A., and de Reuse, H. (2008) New substrates for TonB-dependent transport: do we only see the 'tip of the iceberg'? *Trends Biochem. Sci.* **33,** 330 –338 CrossRef Medline
14. le Coutre, J., and Kaback, H. K. (2000) Structure-function relationships of integral membrane proteins: membrane transporters vs. channels. *Biopo- lymers* **55,** 297–307 CrossRef Medline
15. Saier, M. H., Jr. (2000) Families of proteins forming transmembrane chan- nels. *J. Membr. Biol.* **175,** 165–180 CrossRef Medline
16. Zhai, Y. F., Heijne, W., and Saier, M. H., Jr. (2003) Molecular modeling of the bacterial outer membrane receptor energizer, ExbBD/TonB, based on homology with the flagellar motor, MotAB. *Biochim. Biophys. Acta* **1614,** 201–210 CrossRef Medline
17. Rutz, J. M., Liu, J., Lyons, J. A., Goranson, J., Armstrong, S. K., McIntosh, M. A., Feix, J. B., and Klebba, P. E. (1992) Formation of a gated channel by a ligand-specific transport protein in the bacterial outer membrane. *Sci- ence* **258,** 471– 475 CrossRef Medline
18. Nikaido, H., and Rosenberg, E. Y. (1983) Porin channels in *Escherichia coli*: studies with liposomes reconstituted from purified proteins. *J. Bacteriol.* **153,** 241–252 CrossRef Medline
19. Luckey, M., and Nikaido, H. (1980) Specificity of diffusion channels produced by '1 phage receptor protein of *Escherichia coli*. *Proc. Natl. Acad. Sci. U.S.A.* **77,** 167–171 CrossRef Medline
20. Noinaj, N., Guillier, M., Barnard, T. J., and Buchanan, S. K. (2010) TonB-dependent transporters: regulation, structure, and function. *Annu. Rev. Microbiol.* **64,** 43– 60 CrossRef Medline
21. Eisenbeis, S., Lohmiller, S., Valdebenito, M., Leicht, S., and Braun, V. (2008) NagA-dependent uptake of *N*-acetyl-glucosamine and *N*-acetyl-chitin oligosaccharides across the outer membrane of *Caulobacter cres- centus*. *J. Bacteriol.* **190,** 5230 –5238 CrossRef Medline
22. Lohmiller, S., Hantke, K., Patzer, S. I., and Braun, V. (2008) TonB-dependent maltose transport by *Caulobacter crescentus*. *Microbiology* **154,** 1748 –1754 CrossRef Medline
23. Neugebauer, H., Herrmann, C., Kammer, W., Schwarz, G., Nordheim, A., and Braun, V. (2005) ExbBD-dependent transport of maltodextrins through the novel MalA protein across the outer membrane of *Caulobac- ter crescentus*. *J. Bacteriol.* **187,** 8300 – 8311 CrossRef Medline
24. Fetherston, J. D., Kirillina, O., Bobrov, A. G., Paulley, J. T., and Perry, R. D. (2010) The yersiniabactin transport system is critical for the pathogenesis of bubonic and pneumonic plague. *Infect. Immun.* **78,** 2045–2052 CrossRef Medline
25. Larson, J. A., Higashi, D. L., Stojiljkovic, I., and So, M. (2002) Replication of *Neisseria meningitidis* within epithelial cells requires TonB-dependent ac- quisition of host cell iron. *Infect. Immun.* **70,** 1461–1467 CrossRef Medline
26. Nairn, B. L., Eliasson, O. S., Hyder, D. R., Long, N. J., Majumdar, A., Chakravorty, S., McDonald, P., Roy, A., Newton, S. M., and Klebba, P. E. (2017) Fluorescence high-throughput screening for inhibitors of TonB action. *J. Bacteriol.* **199,** e00889-16 CrossRef Medline
27. Moynié, L., Milenkovic, S., Mislin, G. L. A., Gasser, V., Malloci, G., Baco, E., McCaughan, R. P., Page, M. G. P., Schalk, I. J., Ceccarelli, M., and Naismith, J. H. (2019) The complex of ferric-enterobactin with its trans- porter from *Pseudomonas aeruginosa* suggests a two-site model. *Nat. Commun.* **10,** 3673 CrossRef Medline
28. Smallwood, C. R., Jordan, L., Trinh, V., Schuerch, D. W., Gala, A., Hanson, M., Hanson, M., Shipelskiy, Y., Majumdar, A., Newton, S. M., and Klebba, P. E. (2014) Concerted loop motion triggers induced fit of FepA to ferric enterobactin. *J. Gen. Physiol.* **144,** 71– 80 CrossRef Medline
29. Chakravorty, S., Shipelskiy, Y., Kumar, A., Majumdar, A., Yang, T., Nairn, B. L., Newton, S. M., and Klebba, P. E. (2019) Universal fluorescent sensors of high affinity iron transport, applied to ESKAPE(yen) pathogens. *J. Biol. Chem.* **294,** 4682– 4692 CrossRef Medline
30. Di Masi, D. R., White, J. C., Schnaitman, C. A., and Bradbeer, C. (1973) Transport of vitamin B12 in *Escherichia coli*: common receptor sites for vitamin B12 and the E colicins on the outer membrane of the cell envelope.

    J. Bacteriol. **115,** 506 –513 CrossRef Medline
31. Josts, I., Veith, K., and Tidow, H. (2019) Ternary structure of the outer membrane transporter FoxA with resolved signalling domain provides insights into TonB-mediated siderophore uptake. *Elife* **8,** e48528 CrossRef Medline
32. Newton, S. M., Trinh, V., Pi, H., and Klebba, P. E. (2010) Direct measurements of the outer membrane stage of ferric enterobactin transport: postuptake binding. *J. Biol. Chem.* **285,** 17488 –17497 CrossRef Medline
33. Pawelek, P. D., Croteau, N., Ng-Thow-Hing, C., Khursigara, C. M., Moiseeva, N., Allaire, M., and Coulton, J. W. (2006) Structure of TonB in complex with FhuA, *E. coli* outer membrane receptor. *Science* **312,** 1399 –1402 CrossRef Medline
34. Shultis, D. D., Purdy, M. D., Banchs, C. N., and Wiener, M. C. (2006) Outer membrane active transport: structure of the BtuB:TonB complex. *Science* **312,** 1396 –1399 CrossRef Medline
35. Gumbart, J., Wiener, M. C., and Tajkhorshid, E. (2007) Mechanics of force propagation in TonB-dependent outer membrane transport. *Biophys. J.* **93,** 496 –504 CrossRef Medline
36. Ma, L., Kaserer, W., Annamalai, R., Scott, D. C., Jin, B., Jiang, X., Xiao, Q., Maymani, H., Massis, L. M., Ferreira, L. C., Newton, S. M., and Klebba, P. E. (2007) Evidence of ball-and-chain transport of ferric enterobactin through FepA. *J. Biol. Chem.* **282,** 397– 406 CrossRef Medline
37. Cao, Z., and Klebba, P. E. (2002) Mechanisms of colicin binding and transport through outer membrane porins. *Biochimie* **84,** 399 – 412 CrossRef Medline
38. Smallwood, C. R., Marco, A. G., Xiao, Q., Trinh, V., Newton, S. M., and Klebba, P. E. (2009) Fluoresceination of FepA during colicin B killing: effects of temperature, toxin and TonB. *Mol. Microbiol.* **72,** 1171–1180 CrossRef Medline
39. Scott, D. C., Cao, Z., Qi, Z., Bauler, M., Igo, J. D., Newton, S. M., and Klebba, P. E. (2001) Exchangeability of N termini in the ligand-gated

porins of *Escherichia coli*. *J. Biol. Chem.* **276,** 13025–13033 CrossRef Medline

1. Liu, J., Rutz, J. M., Klebba, P. E., and Feix, J. B. (1994) A site-directed spin-labeling study of ligand-induced conformational change in the ferric enterobactin receptor, FepA. *Biochemistry* **33,** 13274 –13283 CrossRef Medline
2. Wayne, R., Frick, K., and Neilands, J. B. (1976) Siderophore protection against colicins M, B, V, and Ia in *Escherichia coli*. *J. Bacteriol.* **126,** 7–12 CrossRef Medline
3. Annamalai, R., Jin, B., Cao, Z., Newton, S. M., and Klebba, P. E. (2004) Recognition of ferric catecholates by FepA. *J. Bacteriol.* **186,** 3578 – 3589 CrossRef Medline
4. Cao, Z., Qi, Z., Sprencel, C., Newton, S. M., and Klebba, P. E. (2000) Aromatic components of two ferric enterobactin binding sites in *Esche- richia coli* fepA. *Mol. Microbiol.* **37,** 1306 –1317 CrossRef Medline
5. Noel, D., Nikaido, K., and Ames, G. F. (1979) A single amino acid substitution in a histidine-transport protein drastically alters its mobility in sodium dodecyl sulfate-polyacrylamide gel electrophoresis. *Biochemistry* **18,** 4159 – 4165 CrossRef Medline
6. Bardwell, J. C. (1994) Building bridges: disulphide bond formation in the cell. *Mol. Microbiol.* **14,** 199 –205 CrossRef Medline
7. Gleiter, S., and Bardwell, J. C. (2008) Disulfide bond isomerization in pro- karyotes. *Biochim. Biophys. Acta* **1783,** 530 –534 CrossRef Medline
8. Goldstone, D., Haebel, P. W., Katzen, F., Bader, M. W., Bardwell, J. C., Beckwith, J., and Metcalf, P. (2001) DsbC activation by the N-terminal domain of DsbD. *Proc. Natl. Acad. Sci. U.S.A.* **98,** 9551–9556 CrossRef Medline
9. Mamathambika, B. S., and Bardwell, J. C. (2008) Disulfide-linked protein folding pathways. *Annu. Rev. Cell Dev. Biol.* **24,** 211–235 CrossRef Medline
10. Tapley, T. L., Eichner, T., Gleiter, S., Ballou, D. P., and Bardwell, J. C. (2007) Kinetic characterization of the disulfide bond-forming enzyme DsbB. *J. Biol. Chem.* **282,** 10263–10271 CrossRef Medline
11. Cao, Z., Warfel, P., Newton, S. M., and Klebba, P. E. (2003) Spectroscopic observations of ferric enterobactin transport. *J. Biol. Chem.* **278,** 1022–1028 CrossRef Medline
12. Buckling, A., Harrison, F., Vos, M., Brockhurst, M. A., Gardner, A., West, S. A., and Griffin, A. (2007) Siderophore-mediated cooperation and viru- lence in *Pseudomonas aeruginosa*. *FEMS Microbiol. Ecol.* **62,** 135–141 CrossRef Medline
13. Cornelissen, C. N., and Hollander, A. (2011) TonB-dependent transporters expressed by *Neisseria gonorrhoeae*. *Front. Microbiol.* **2,** 117 CrossRef Medline
14. Dhople, A. M., Ibanez, M. A., and Poirier, T. C. (1996) Role of iron in the pathogenesis of *Mycobacterium avium* infection in mice. *Microbios* **87,** 77– 87 Medline
15. Furman, M., Fica, A., Saxena, M., Di Fabio, J. L., and Cabello, F. C. (1994) *Salmonella typhi* iron uptake mutants are attenuated in mice. *Infect. Im- mun.* **62,** 4091– 4094 CrossRef Medline
16. Konings, A. F., Martin, L. W., Sharples, K. J., Roddam, L. F., Latham, R., Reid, D. W., and Lamont, I. L. (2013) *Pseudomonas aeruginosa* uses multiple pathways to acquire iron during chronic infection in cystic fibrosis lungs. *Infect. Immun.* **81,** 2697–2704 CrossRef Medline
17. Mortensen, B. L., and Skaar, E. P. (2013) The contribution of nutrient metal acquisition and metabolism to *Acinetobacter baumannii* survival within the host. *Front. Cell Infect. Microbiol.* **3,** 95 CrossRef Medline
18. Schoolnik, G. K. (2002) Microarray analysis of bacterial pathogenicity.

    Adv. Microb. Physiol. **46,** 1– 45 CrossRef Medline
19. Smith, K. D. (2007) Iron metabolism at the host pathogen interface: lipocalin 2 and the pathogen-associated iroA gene cluster. *Int. J. Biochem. Cell Biol.* **39,** 1776 –1780 CrossRef Medline
20. Torres, A. G., Redford, P., Welch, R. A., and Payne, S. M. (2001) TonB-dependent systems of uropathogenic *Escherichia coli*: aerobactin and heme transport and TonB are required for virulence in the mouse. *Infect. Im- mun.* **69,** 6179 – 6185 CrossRef Medline
21. Torres, V. J., Pishchany, G., Humayun, M., Schneewind, O., and Skaar, E. P. (2006) *Staphylococcus aureus* IsdB is a hemoglobin receptor required for heme iron utilization. *J. Bacteriol.* **188,** 8421– 8429 CrossRef Medline
22. Cobessi, D., Celia, H., and Pattus, F. (2005) Crystal structure at high resolution of ferric-pyochelin and its membrane receptor FptA from *Pseudomonas aeruginosa*. *J. Mol. Biol.* **352,** 893–904 CrossRef Medline
23. Cobessi, D., Celia, H., Folschweiller, N., Schalk, I. J., Abdallah, M. A., and Pattus, F. (2005) The crystal structure of the pyoverdine outer membrane receptor FpvA from *Pseudomonas aeruginosa* at 3.6 angstroms resolution.

    J. Mol. Biol. **347,** 121–134 CrossRef Medline
24. Lukacik, P., Barnard, T. J., Keller, P. W., Chaturvedi, K. S., Seddiki, N., Fairman, J. W., Noinaj, N., Kirby, T. L., Henderson, J. P., Steven, A. C., Hinnebusch, B. J., and Buchanan S. K. (2012) Structural engineering of a phage lysin that targets Gram-negative pathogens. *Proc. Natl. Acad. Sci.*

    U.S.A. **109,** 9857–9862 CrossRef Medline
25. Payne, M. A., Igo, J. D., Cao, Z., Foster, S. B., Newton, S. M., and Klebba, P. E. (1997) Biphasic binding kinetics between FepA and its ligands. *J. Biol. Chem.* **272,** 21950 –21955 CrossRef Medline
26. Takeshita, S., Sato, M., Toba, M., Masahashi, W., and Hashimoto-Gotoh, T. (1987) High-copy-number and low-copy-number plasmid vectors for lacZ a-complementation and chloramphenicol- or kanamycin-resistance selection. *Gene* **61,** 63–74 CrossRef Medline
27. Klebba, P. E., McIntosh, M. A., and Neilands, J. B. (1982) Kinetics of biosynthesis of iron-regulated membrane proteins in *Escherichia coli*. *J. Bac- teriol.* **149,** 880 – 888 CrossRef Medline
28. Neidhardt, F. C., Bloch, P. L., and Smith, D. F. (1974) Culture medium for enterobacteria. *J. Bacteriol.* **119,** 736 –747 CrossRef Medline
29. Smit, J., Kamio, Y., and Nikaido, H. (1975) Outer membrane of *Salmonella typhimurium*: chemical analysis and freeze-fracture studies with lipopo- lysaccharide mutants. *J. Bacteriol.* **124,** 942–958 CrossRef Medline
30. Hancock, R. E., and Braun, V. (1976) The colicin I receptor of *Escherichia coli* K-12 has a role in enterochelin-mediated iron transport. *FEBS Lett.* **65,** 208 –210 CrossRef Medline
31. Lugtenberg, B., Meijers, J., Peters, R., van der Hoek, P., and van Alphen, L. (1975) Electrophoretic resolution of the "major outer membrane protein" of *Escherichia coli* K12 into four bands. *FEBS Lett.* **58,** 254 – 258 CrossRef Medline
32. Murphy, C. K., Kalve, V. I., and Klebba, P. E. (1990) Surface topology of the *Escherichia coli* K-12 ferric enterobactin receptor. *J. Bacteriol.* **172,** 2736 –2746 CrossRef Medline
33. Schneider, C. A., Rasband, W. S., and Eliceiri, K. W. (2012) NIH Image to ImageJ: 25 years of image analysis. *Nat. Methods* **9,** 671– 675 CrossRef Medline
34. Newton, S. M., Igo, J. D., Scott, D. C., and Klebba, P. E. (1999) Effect of loop deletions on the binding and transport of ferric enterobactin by FepA. *Mol. Microbiol.* **32,** 1153–1165 CrossRef Medline
35. Hashimoto-Gotoh, T., Franklin, F. C., Nordheim, A., and Timmis, K. N. (1981) Specific-purpose plasmid cloning vectors. I. Low copy number, temperature-sensitive, mobilization-defective pSC101-derived contain- ment vectors. *Gene* **16,** 227–235 CrossRef Medline
36. Hollifield, W. C., Jr., Fiss, E. H., and Neilands, J. B. (1978) Modification of a ferric enterobactin receptor protein from the outer membrane of *Esch- erichia coli*. *Biochem. Biophys. Res. Commun.* **83,** 739 –746 CrossRef Medline